Holocene sea ice-ocean-climate variability from Adélie Land, East Antarctica

Thomas R. Gregory

2012

Thesis submitted for the degree of

Doctorate of Philosophy

Summary

Marine sedimentation from the Adélie Land continental margin of East Antarctica provides unique high resolution records of Holocene environmental change. The sub-annually resolved sediment cores MD03-2601 (66°03.07'S, 138°33.43'E) and IODP-318-U1357B (66°24.7990′S, 140°25.5705′E) from the Dumont d'Urville Trough, Adélie Land, document atmospheric and oceanic processes impacting on biogenic sedimentation on the Adélie Land continental shelf during the Holocene.

Resin embedded, continuous polished thin sections from each core were analysed for diatom content and sediment microfabric using scanning electron microscope back-scattered electron imagery. The sediments contained repeating sequences of seasonal diatom-rich laminae which enabled multi-taper method time series analysis. Time series analysis shows that in the Hypsithermal there appears to have been an external (solar) control on interannual sedimentation as well as internal controls (e.g. the southern annular mode, SAM, and El Nino-southern Oscillation, ENSO); whilst in the Neoglacial internal climatic modes exerted a much stronger control. Quasi-biennial (2 – 3 year) peaks commonly occurred in analysis of both Hypsitherml and Neoglacial sequences. The distribution of resting spore-rich laminae in these sections suggests that a multidecadal (>50-years) variation between phasing of the SAM and ENSO systems may exert an important control on interannual environmental variability in the sections analysed.

The distribution of diatom-derived biomarker proxies, namely C_{25} highly branched isoprenoid (HBI) alkenes, was compared to the diatom lamina-based record in core MD03-2601. At the Holocene scale, HBI diene and triene molecules have a positive association to sea ice associated diatom-rich laminae, with greater abundances of both HBI molecules and sea ice associated diatom laminae in the Neoglacial interval. However, at a sub-annual resolution there is no strong association between lamina type and HBI concentrations. This is attributed to a combination of: (i) the HBI alkenes recording a different signal to that of the diatom-rich laminae; (ii) interannual variation in HBI export that is greater than inter-seasonal variation, for which there is little modern data for comparison; (iii) possible diagenetic alteration of the HBI signal.

Acknowledgements

First and foremost, I wish to thank my supervisor Jenny Pike. Jenny's enthusiasm, knowledge and patience have collaborated to keep me inspired and motivated throughout the course of my PhD. I truly could not have had a better supervisor! I also wish to thank my co-supervisors Xavier Crosta, Guillaume Massé and Ian Hall. Xavier's expertise and friendly, insightful discussion has greatly helped me during the course of my PhD and I would also like to thank him for accommodating me at his home when I was on a visit to Université Bordeaux. Guillaume encouraged me to do a PhD when I was a Masters student and subsequently has provided expertise on HBIs during my PhD, as well as allowing me to spend 3 months working at the LOCEAN laboratory in Paris which was a fantastic experience. Ian's knowledge of climate and oceanography has been particularly helpful throughout my PhD and he has greatly aided my understanding of these systems.

For technical support I wish to thank Ian Thomas who provided assistance with processing satellite-derived sea ice concentration data and who provided Python coding for reproducing wavelet analyses. I would also like to thank Pete Fisher of Cardiff University for SEM training and technical assistance, and Vincent Klein of Université Pierre et Marie Curie, Paris, for training and assistance with HBI extraction and analysis.

I would also like to thank Lewis Collins for frequently providing me with free accommodation and lots of discussion on HBIs, diatoms and football during my time in Paris and at many conferences. Further thanks to all of my friends in Cardiff for keeping me sane and entertained, particularly Pete, Griffiths, Paola and Laura. Thank you also Pauline for supporting me and putting up with my grumpiness/gallivanting off to the southern hemisphere. Finally, I wish to thank my family for moral and financial support over the entire 8-year duration of my academic career to date. Cheers!

This work was funded by NERC small grant NE/I01537X/1.

Table of contents

Chapter 3. Proxies used in this study.

Chapter 4. Materials and methods.

Chapter 5. Diatom analysis of laminated sediments.

Chapter 6. HBI analysis of sediments.

Chapter 7. Conclusions.

Appendices

List of Figures

Chapter 5. Diatom analysis of laminated sediments

Chapter 6. HBI analysis of sediments

Appendix 4. Additional wavelet analyses

Appendix 5. HBI data

List of Tables

Appendix 2. Lamina thickness measurements

Appendix 3. Qualitative diatom assemblage counts

Appendix 5. HBI data

Chapter 1. Introduction

This thesis investigates interannual environmental variability in Adélie Land, East Antarctica, during the Holocene by examining sections of seasonally laminated marine sediment cores. Time series of lamina thicknesses are constructed from continuously laminated sections of cores that occur during: (i) the warm Hypsithermal climatic interval (ca. 8 – 3.9 ka), (ii) the cool Neoglacial climatic interval (ca. 3.9 ka – present), and (iii) the transition between these intervals (ca. 3.9 ka). Furthermore, diatom-derived highly branched isoprenoid (HBI) biomarkers are tested as a geochemical proxy of sea ice cover versus annually resolved diatom records.

1.1 Antarctic seasonally laminated sediments

Laminated diatomaceous sediments accumulate in many inner shelf basins around the Antarctic margin and can provide ultra-high-resolution records of palaeoclimatic variability at different times since the last deglaciation (Leventer et al., 2002; Bahk et al., 2003; Stickley et al., 2005; Maddison et al., 2005; Stickley et al., 2006; Denis et al., 2006; Maddison et al., 2006; Maddison et al., 2012). Mean sedimentation rates in these sequences may be up to 46 mm/year (Denis et al., 2006), and individual laminae representing discrete seasonal flux events up to 75 mm thick have been reported from deglacial sediments (Stickley et al., 2005). These high sedimentation rates, combined with the often excellent preservation of diatom frustules, provide an insight into past climatic processes from sub-annual to millennial timescales (Maddison et al., 2005; Denis et al., 2009; Maddison et al., 2006).

Where seasonally laminated sediments are preserved they represent a valuable climate archive that can be used to investigate changes in diatom productivity related to seasonal and interannual changes in sea ice concentration, wind stress and temperature during different climatic states, as well as changes in regional glacial activity inferred from the relative terrigenous content of the laminae (Denis et al., 2006; Pike et al., 2009). Previous studies using laminated sediments from the Dumont d'Urville Trough, Adélie Land, East Antarctica, have: (i) provided snapshots of seasonal variability during the Holocene Hypsithermal (30 cm of laminated sediments) and Neoglacial (30 cm of laminated sediments) (Denis et al., 2006); and (ii) highlighted changes in seasonal

deposition throughout the Neoglacial period related to changes in the timing of the spring ice retreat and autumnal ice advance (Maddison et al., 2012). Despite these studies, little is currently known about the magnitude of interannual variability recorded in these sediments under the evolving climatic regimes of the Holocene and notably the transition from the warm Hypsithermal to the cool Neoglacial has not been investigated with interannual resolution. This thesis provides the first annually resolved multidecadal records obtained from selected sections of continuously laminated marine sediments from the Antarctic margin, and presents evidence for changes in interannual productivity related to changing sea ice and meteorological conditions in the different climatic phases of the Holocene.

1.2 Aims of the thesis

This thesis aims to address the following research questions:

1) Can the influence of oscillatory climate modes (e.g. Southern Annular Mode, SAM, and El Niño-Southern Oscillation, ENSO) be detected in the seasonally laminated Adélie Land sediment records during the Holocene?
2) If so, is this relationship similar under different climate states during the Holocene?

This will be achieved by reconstructing ultra-high-resolution records of diatom species succession during the Holocene by using scanning electron microscope (SEM) back scattered electron imagery (BSEI) analysis of resin embedded thin sections of selected sediments from cores MD03-2601 and IODP-318-U1357B. The SEM-derived descriptions of lamina types will be complimented by the calculation of diatom concentrations and assemblages to complement in order to produce a seasonal model of lamina deposition. The seasonal deposition model will be used to reconstruct multidecadal time series from each core, which will be subjected to multi-taper method spectral analysis to determine any significant periodicities occurring within the records. This will permit assessment of the likely forcing mechanisms controlling diatom productivity in Adélie Land during the Holocene. Finally, the diatom lamina thickness data will be compared to the records of HBI biomarker concentration from core MD03-

2601 and investigate the potential utility of this technique to reconstruct past sea ice conditions at ultra-high-resolution.

1.3 Thesis structure

This thesis has seven chapters and 5 appendices, composed of:

Introductory chapters: Chapter 1 provides an outline of the thesis. Chapter 2 details the geological, oceanographic and glaciological history of the Antarctic continent and Southern Ocean and provides information on the major climatic modes of interannual variability of interest. A regression analysis of satellite-derived sea ice concentration compared to the Southern Annular Mode and Southern Oscillation Index is presented (upon which several research hypotheses for diatom lamina distribution are proposed for testing in Chapter 5) along with other relevant modern environmental data for the region. Chapter 3 introduces the use of diatoms and highly branched isoprenoids as proxies for sea ice and climatic variability on the Antarctic margin and discusses their modern environmental distributions. The known environmental associations of HBIs are used to provide hypotheses for HBI distribution that are tested in Chapter 6. Chapter 4 presents the details of core collection and the methodologies used in this thesis.

Results and discussion: Chapters 5 – 6 address the thesis research questions outlined in Section 1.2. Chapter 5 presents and discusses the results of sediment lamina and diatom analysis of cores MD03-2601 and IODP-318-U1357B. Chapter 6 presents the results of highly branched isoprenoid analyses of three core sections from MD03-2601 and compares them to the diatom record presented in Chapter 5.

Synthesis: Chapter 7 presents the key conclusions of this thesis, addresses the hypotheses outlined in Chapters 3 and 4, and suggests the potential future work.

Appendices: Appendix 1 contains plates of key diatom taxa recorded in this study, Appendices 2 and 3 contain the data that was analysed in Chapters 5, Appendix 4 contains additional wavelet analyses that were conducted, but not presented in Chapter 5 and Appendix 5 contains the data presented in Chapter 6.

2. The Southern Ocean, Sea Ice, and Teleconnections

This chapter outlines the role of the Southern Ocean in the global climate and the importance of the annual expansion and retreat of sea ice around the Antarctic margin. The influence of large-scale climatic modes (namely the El Niño-Southern Oscillation, ENSO, and the Southern Annular Mode, SAM) on sea ice in the Adélie Land region are discussed. The statistical relationship between the available published indices of these climate modes and the seasonal variations in sea ice as derived from satellite observations is presented. Additionally, the modern environmental setting is outlined for the Adélie Land region, including local bathymetry and oceanography, of which both have a large impact on sediment accumulation at the core sites used within this study.

2.1 The geological history of Antarctica

Antarctica is a landmass of ~14.2 million km^2 and consists of two distinct continental blocks separated by the Transantarctic Mountains (Figure 2.01). West Antarctica is an archipelago formed of several microplates composed of different Mesozoic – Cenozoic aged volcanic and metamorphic terranes. In contrast, East Antarctica consists of a large stable continental craton of principally Precambrian metamorphic basement rocks and granitic igneous intrusions formed between the Archaean and the early Cambrian, unconformably overlain by sedimentary successions (Anderson, 1999). East Antarctica was formerly located in the centre of the supercontinent Gondwana (Figure 2.02), connected to what would become Africa, India and Australia. Significant break-up of Gondwana began during the Jurassic, with Africa separating from East Antarctica between 200 and 130 Ma; India between 130 and 118 Ma; and Australia detaching by 80 Ma, with the accretion of West Antarctica onto East Antarctica also occurring during this time (Lawver et al., 1992; Anderson, 1999). This gradual rifting and break-up of Gondwana resulted in the formation of the Southern Ocean and the isolation of the Antarctic continent in its modern position. The Wilkes Land/Adélie Land margin of Antarctica was formed during the rifting of Australia from Antarctica (Veevers, 1986; Scotese, 1991), forming a basement that transitions from oceanic crust off the shelf

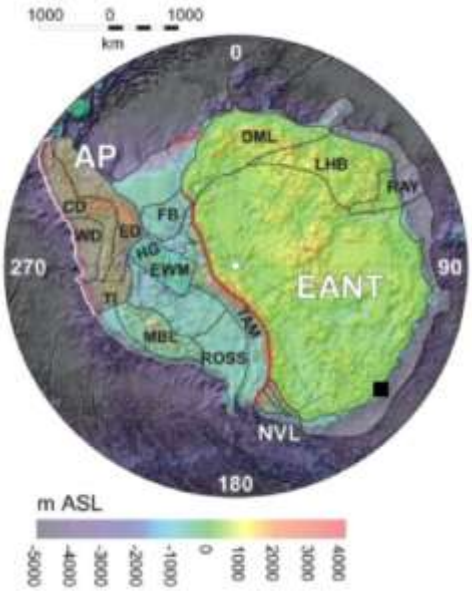

Figure 2.01. Antarctic major continental blocks, topography and bathymetry. East Antarctic terranes are: Dronning Maud Land (DML); Lützom-Holm Bay (LHB); Raynor Terrane (RAY) and the remaining undivided East Antarctica (EANT). Major West Antarctic terranes are: Antarctic Peninsula (AP) (including Eastern-Western-Central domains: ED-CD-WD); Thurston Island (TI); Filchner Block (FB); Marie Byrd Land (MBL); Haag (HG); and Ellsworth-Whitmore Mountains (EWM). Northern Victoria Land (NVL), in East Antarctica, comprises of three terranes grouped together. ROSS = extended continental crust between MBL and EANT; TAM = Transantarctic Mountains. (Source: Torsvik et al., 2008). Black square in EANT represents approximate location of core sites for this study.

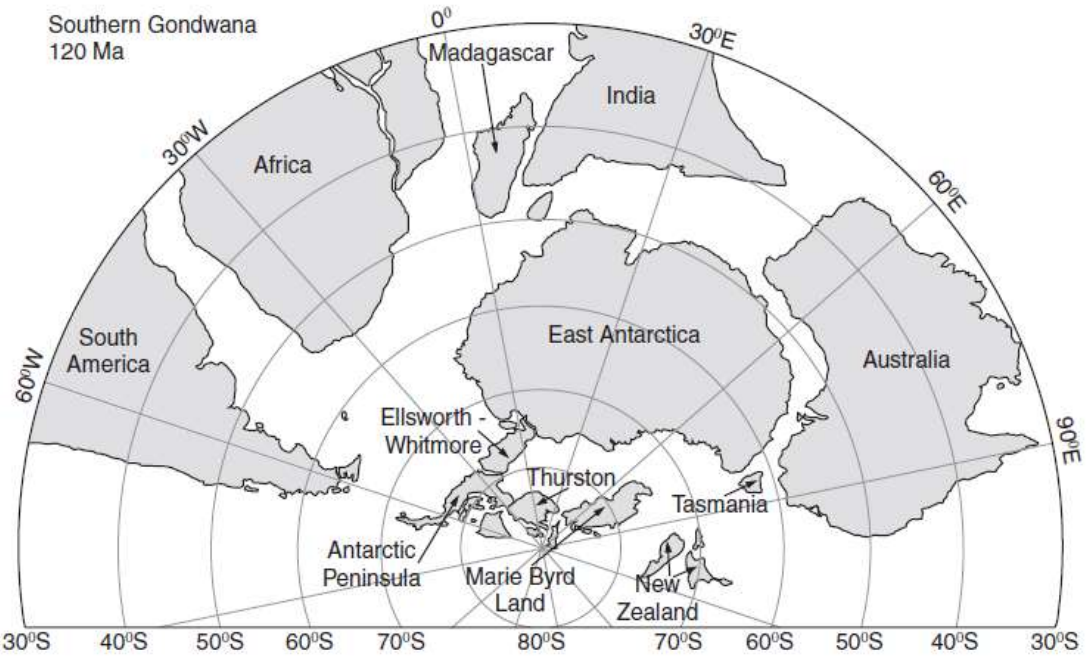

Figure 2.02. Location of Antarctica within the supercontinent of Gondwana. Figure shows position of continents during break up at ~120 Ma (Source: Jamieson and Sugden, 2008).

break, across a transitional region of rifted rocks with many igneous intrusions, to the continental rocks of Wilkes Land (Figure 2.03) (Eittreim, 1994; Miller et al., 2002; De Santis et al., 2010). The rift basins along the Wilkes Land margin form significant sites of sediment accumulation, with maximum sedimentary thicknesses up to 8 km (Escutia et al., 2005).

2.2 The glacial history of the Antarctic ice sheets

2.2.1 Cenozoic history of Antarctic glaciation

The first appearance of significant permanent ice sheets on Antarctica occurred at the Eocene/Oligocene boundary (~34 Ma), coincident with the transition from global greenhouse to icehouse conditions (Kennett and Shackleton, 1976; Zachos, 1996). This transition was associated with a ~2.5°C sea surface temperature (SST) decrease in the tropics (Lear et al., 2008), a ~5°C SST drop in the polar regions (Liu et al., 2009) and an estimated maximum ice volume increase of 25 x 10^6 km^3 (Miller et al., 2008). Evidence for this transition comes from many marine and terrestrial records, including deep sea benthic foraminiferal $\delta^{18}O$ records (e.g. Kennett and Shackleton, 1976; Miller et al., 1991; Zachos, 1996; Coxall et al., 2005; Coxall and Wilson, 2011), changes in the Mg/Ca ratio (a palaeotemperature indicator) in benthic foraminifera tests (Lear et al., 2004; Lear et al., 2008), glacial sediments deposited on the Antarctic continental margin (Ivany et al., 2006), and terrestrial remains of fossil plants (Francis et al., 2008; Francis and Poole, 2002). The trigger mechanism for the transition from greenhouse to icehouse conditions remains controversial. It occurred during a period of summer cooling related to orbital cycles (Coxall et al., 2005; DeConto and Pollard, 2003) and has been linked to: (1) the thermal isolation of Antarctica following the tectonic opening of Southern Ocean gateways and the formation of the Antarctic Circumpolar Current (Kennett and Shackleton, 1976); and (2) declining global atmospheric CO_2 (DeConto and Pollard, 2003). Recent modelling studies (Haywood et al., 2010) have suggested that the strength of the ACC was not sufficient at the opening of the Drake Passage to produce a thermal isolation of Antarctica, and only played a later secondary role in glaciation once the passage had deepened to >500 m. Instead, models broadly support a decline in atmospheric CO_2 coupled with orbitally driven changes in seasonality as a major factor driving the onset of glaciation (Haywood et al., 2010; DeConto and Pollard, 2003). Direct evidence for declining atmospheric CO_2 prior to the growth of an

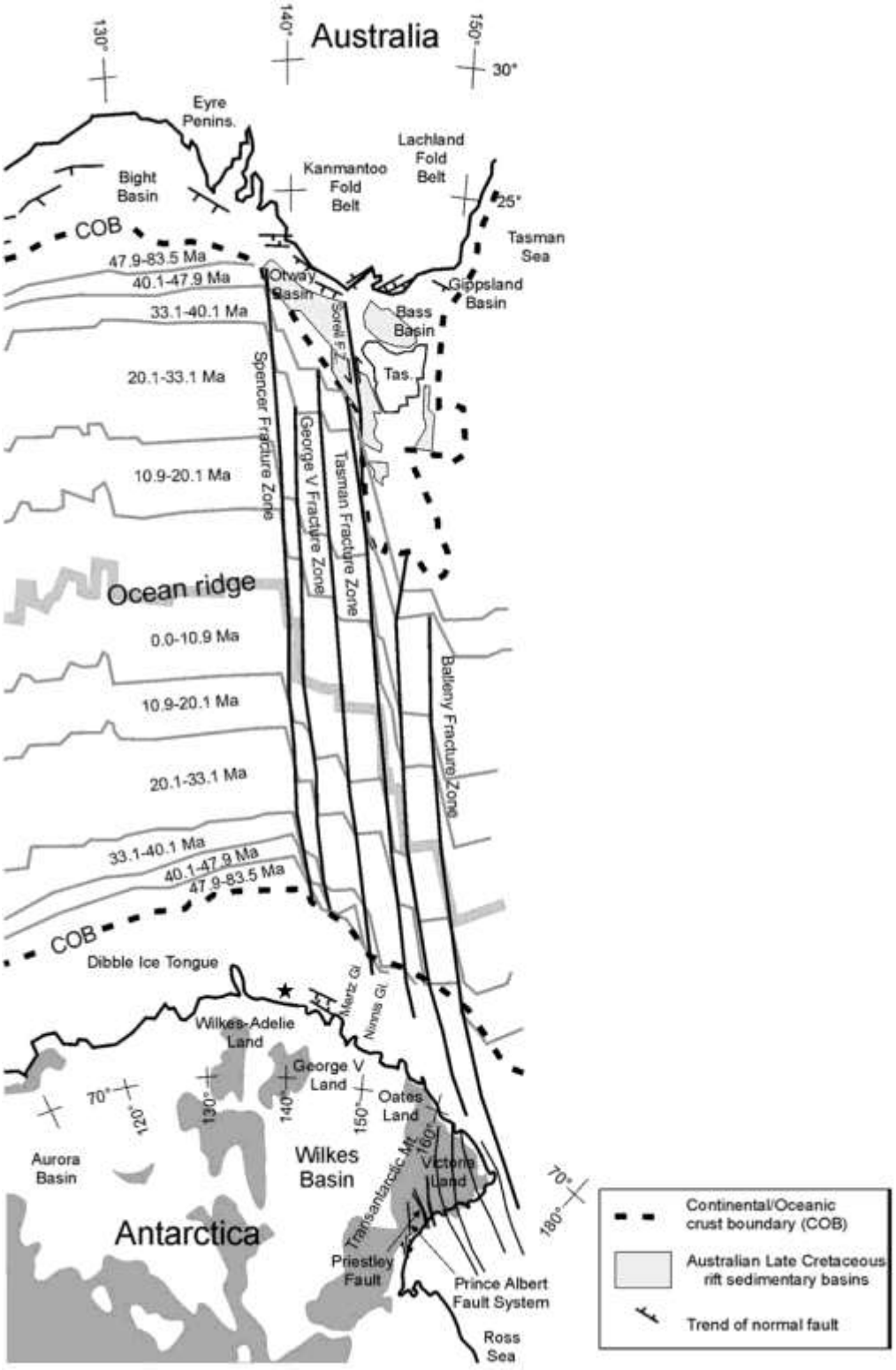

Figure 2.03. Schematic section of the Indian Ocean sector between Antarctica and Australia showing ages of sea floor rocks and the continental/oceanic crust boundary (COB). The Dumont d'Urville Trough is located by the black star. Adapted from De Santis et al. (2010); ages, COB and Australian Late Cretaceous rift location are from Miller et al. (2002).

Antarctic ice sheet comes from changes in boron isotopes within foraminifera tests in Tanzanian sediment cores (Pearson et al., 2009) and stable $\delta^{13}C$ from a suite of marine sediment cores (Pagani et al., 2005). Regardless, it is clear that as ice on Antarctica grew, it became a significant driver of global climate and has also been linked to changes in ocean circulation and chemistry (Kennett and Shackleton, 1976; Miller et al., 2008).

Between 34 and ~26 Ma a permanent East Antarctic Ice Sheet (EAIS) existed (Zachos, 1996); however, a warming trend between 26 and ~15 Ma reduced Antarctic and global ice volume, although there were brief periods of glacial re-advance during this interval (Zachos, 1996; Wright and Miller, 1993). Major growth of the EAIS commenced around 14 Ma and it has remained a significant feature of the Antarctic continent since this time (Flower and Kennett, 1994, 1995). In contrast, the West Antarctic Ice Sheet (WAIS) consisted of isolated ice caps between ~34 and 14 Ma, which linked up at ~11 Ma and has shown oscillations in extent from 11 to 0.1 Ma (Anderson and Shipp, 2001). In the Wilkes Land region, the first significant glaciation occurred around 33 – 30 Ma, with the ice sheet remaining ephemeral until ~ 14 Ma. Between 14 and 10 Ma, a permanent ice sheet was established at the Wilkes Land coast which remains until the present day with oscillations in overall extent (Escutia et al., 2005).

2.2.2 Last Glacial Maximum to Holocene glacial history

The Last Glacial Maximum (LGM), around 23-19 ka BP (Mix et al., 2001), represents the interval during which the global ice sheets reached their maximum volume. The exact spatial extent of the Antarctic ice sheet at the LGM is not presently well constrained, however, there is evidence for a lack of synchroneity in behaviour and extent of the WAIS and the EAIS (Mix et al., 2001; Anderson et al., 2002). The WAIS in the Antarctic Peninsula region is believed to have reached the shelf edge during the LGM (Sugden et al., 2006; Heroy and Anderson, 2005) whilst diamictons deposited on shelves around East Antarctica suggest a similar expansion, although some regions demonstrate little evidence for expansion beyond the current ice edge location (e.g. eastern Queen Maud Land, Anderson et al., 2002). The pan-Antarctic timing of the deglacial onset of retreat also differs, with deglaciation beginning as early as 22 ka BP in Prydz Bay, East Antarctica (Domack et al., 1998), and between 18 ka BP in the

western Antarctic Peninsula, lasting until ca. 9 ka BP (Heroy and Anderson, 2007). The timing of deglaciation across the EAIS is also diachronous (Berkman et al., 1998), and may have occurred prior to the LGM in some areas (Anderson et al., 2002).

During the last glacial, evidence from glacial marine deposits (Domack, 1982), side scan sonar observations (Barnes, 1987) and seismic straigraphy (Eittreim et al., 1995) indicate that the ice sheet edge in the Wilkes Land/Adélie Land region advanced to the continental shelf edge, grounding at approximately the modern 500 m isobath. Furthermore, modelling studies suggest that the Law Ice Dome (western Wilkes Land) expanded to the continental shelf edge (~65 km north of its present location; Goodwin and Zweck, 2000) and air content measurements from a Law Dome ice core provide an estimated elevation approximately 135 – 345 m higher than present (Delmotte et al., 1999). The minimum age of deglaciation of the Wilkes Land region is indicated from the onset of post-glacial marine sedimentation at around 10.5 ka BP in the Windmill Islands, west of Adélie Land (Verleyen et al., 2011; Hodgson et al., 2003) and prior to 13,267 ^{14}C years BP (uncalibrated) in the Mertz-Ninnis Trough, east of Adélie Land (Maddison et al., 2006). In the Dumont d'Urville Trough, glacial diamicts are overlain by a transitional sand and silt-bearing diatom ooze (IODP Expedition 318 Scientists, 2010) that indicates the deglaciation started from ca. 11 – 12 ka BP (R. Dunbar, pers comm., 2011) or ca. 11 ka BP (Crosta et al., 2007). This sand and silt bearing ooze is, in turn, overlain by Holocene (<11 ka BP) diatomaceous oozes (Crosta et al., 2007; IODP Expedition 318 Scientists, 2010).

2.2.3 The modern Antarctic ice sheet

The present ice sheet on Antarctica is estimated to contain 25.4 million km^3 of ice (Lythe and Vaughan, 2001) which represents up to 90% of freshwater on Earth (Vaughan and Spouge, 2002). The EAIS is seated on a high plateau and is considered to be relatively stable in comparison to the WAIS that rests on land that is below sea level and has faster outlet glaciers. As such, the WAIS is considered a greater contributor to contemporary sea level changes than the EAIS (Vaughan and Spouge, 2002; Lythe and Vaughan, 2001).

2.3 The Southern Ocean

The circum-Antarctic Southern Ocean is bounded to the south by the Antarctic continent and is unrestricted by landmasses to the north, apart from southernmost Australasia and South America. One of the most significant features of the Southern Ocean is the eastwards flowing Antarctic Circumpolar Current (ACC), which is the only current to encircle the globe and serves to thermally isolate the Antarctic continent (Tchernia, 1980; Orsi et al., 1995).

2.3.1 Broad features of the Southern Ocean

The Southern Ocean may be separated into two regions, the Antarctic region closer to the continent and the sub-Antarctic region further north (Figure 2.04). These regions are separated by the Polar Frontal Zone (PFZ, formerly called the Antarctic Convergence) which is a broad band of mixing that forms the fastest flowing part of the ACC (Carter et al., 2009; Cunningham, 2005). The modern PFZ is located at approximately 50°S in the Atlantic and Indian Oceans and 60°S in the Pacific Ocean, its southern boundary is the Polar Front and its northern boundary is the Sub-Antarctic Front (Figure 2.04). The Antarctic region contains relatively cooler and lower salinity surface waters than the sub-Antarctic region (Cunningham, 2005). The Antarctic region extends southwards to the Antarctic Divergence where it is bound by the westward flowing Antarctic Coastal Current, whilst the sub-Antarctic region extends northwards to the Sub-Tropical Convergence (Figure 4; Open University Course Team, 2001; Anderson, 1999; Cunningham, 2005).

2.3.2 The Antarctic region and continental margin

The ACC is the longest and largest oceanic current in the world, encompassing the entire Antarctic margin and connecting to all of the world's major oceans (Figure 2.05) with an estimated volume of 137 – 147 Sverdrups ($1Sv = x10^6\ m^3\ s^{-1}$) (Carter et al., 2009). The eastward flow of the ACC is largely driven by the direct effect of wind stress on the ocean surface (Carter et al., 2009) with a northward component resulting from the effects of the Coriolis force (Figure 2.04) (Open University Course Team, 2001; Cunningham, 2005). At the edge of the Antarctic continent flows the Antarctic Coastal Current (AcoastC; also known as the East Wind Drift), a broadly

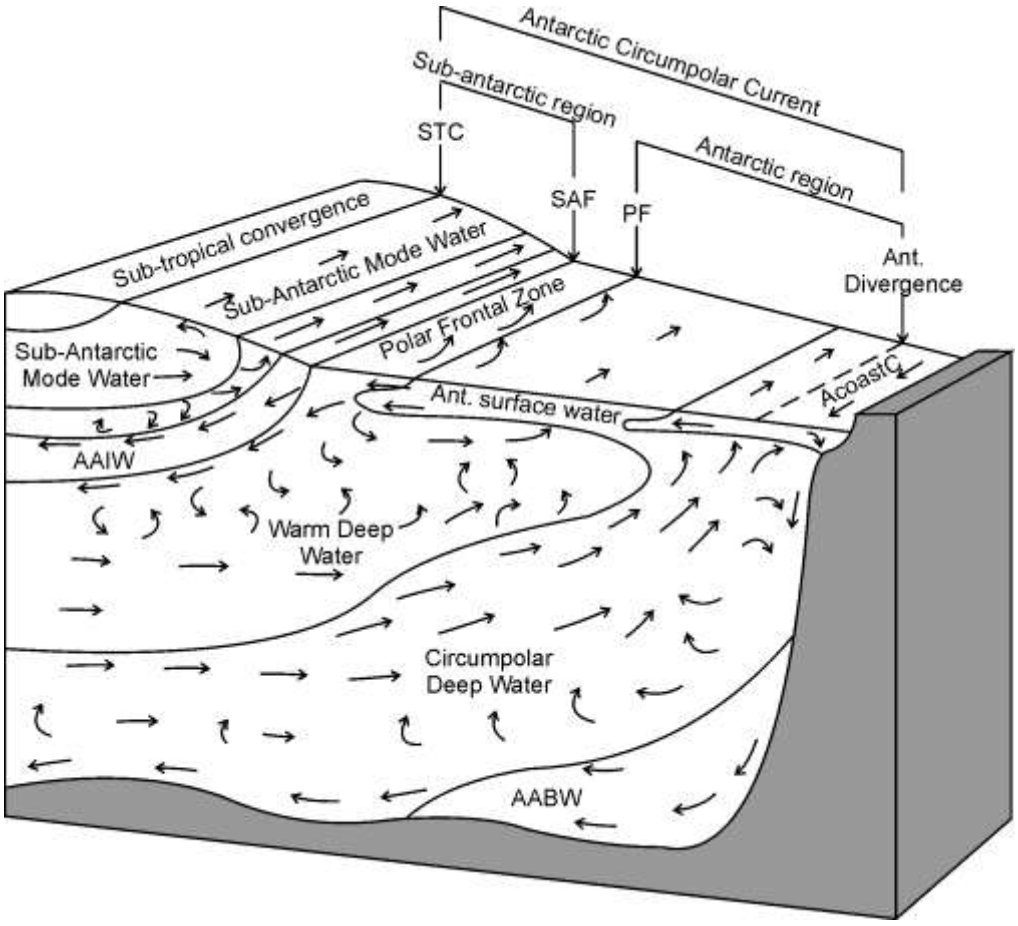

Figure 2.04. Schematic block diagram showing water masses and currents in the Southern Ocean southwards of 45°S. Fronts are: STC - Sub-Tropical Convergence; SAF - sub-Antarctic Front; PF - Polar Front. Abbreviated water masses are: AAIW - Antarctic Intermediate Water; AABW - Antarctic Bottom Water; AcoastC - Antarctic coastal current. Adapted from Cunningham (2005) and Anderson (1999).

westward flowing current that follows the coastline and is strongest towards the coast (Anderson, 1999). Waters within the AcoastC may be re-circulated within regions south of the ACC by several large cyclonic gyres (Figure 2.05) that form major features of the circulation at the continental margin (Orsi et al., 1995; Carter et al., 2009).

The volumetrically largest water mass within the ACC is the Circumpolar Deep Water (CDW; Figure 2.04), which is a relatively warm and saline water mass that upwells towards the continent (Sievers and Nowlin Jr, 1984; Orsi et al., 1995). The CDW forms from a mixture of Antarctic waters and Warm Deep Water (WDW) that enters from the Atlantic, Pacific and Indian Oceans, and within the ACC is divided into two distinct components. Upper CDW is characterised by low oxygen and high nutrient levels, whilst Lower CDW is characterised by high salinities (Orsi et al., 1995). Modified

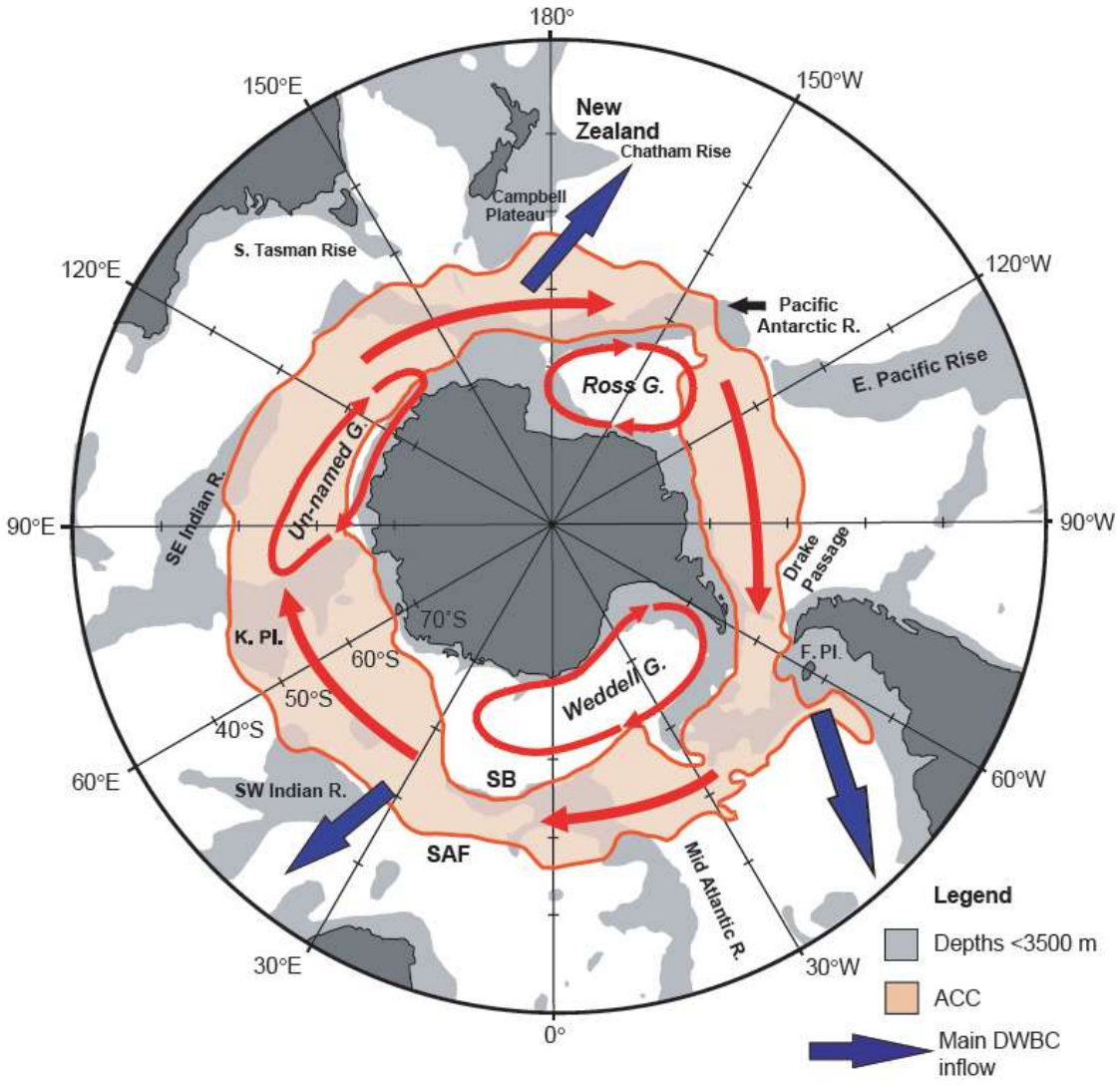

Figure 2.05. Flow of the Antarctic Circumpolar Current (ACC), major Deep Western Boundary Currents (DWBC) and circulation of major atmospheric gyres around Antarctica. (Source: Carter et al., 2009)

CDW (MCDW) forms from the vertical mixing of CDW at the shelf edge and is often found upwelling over the Antarctic continental shelf (Bindoff et al., 2000; Dinniman et al., 2011; Prézelin et al., 2000). Upwelled MCDW mixes with high salinity shelf waters (formed by brine rejection during sea ice formation) and upwelled WDW to form the dense down-slope flowing Antarctic Bottom Water (AABW; Orsi et al., 1995; Jacobs et al., 1970). Significant brine production occurs in coastal polynyas, with sea ice production up to 10 times faster than surrounding regions (Cavalieri, 1985; Zwally et al., 1985; Rintoul, 1998; Massom et al., 1998) and regions of high brine production are linked to significant AABW production (Orsi et al., 1995). AABW plays a significant role in global thermohaline circulation, ventilating the deepest regions of the Atlantic,

Indian and Pacific Oceans (Orsi et al., 1999). AABW formation occurs within the Weddell Sea (e.g. Fofonoff, 1957; Deacon, 1937), the Ross Sea (Jacobs et al., 1970; Jacobs, 2004; Bindoff et al., 2000) and along the Wilkes Land margin (Rintoul, 1998; Orsi et al., 1999; Gordon and Tchernia, 1972; Bindoff et al., 2000; Williams et al., 2008).

2.3.3 The sub-Antarctic region

North of the PFZ, the sub-Antarctic region of the ACC incorporates waters from both the sub-tropics and from the Antarctic region. The upper 500 m of the water column consists of Sub-Antarctic Mode Water (SAMW; Figure 2.04) which has a northward surface flow and a slightly deeper southward flow (Anderson, 1999). Below this, sinking of Antarctic region waters in the PFZ forms the northward flowing Antarctic Intermediate Water (AAIW; Figure 2.04) which flows northwards at depths up to 1000 m (Cunningham, 2005).

2.4 Sea ice and the Southern Ocean

Sea ice forms one of the most significant features of Antarctica, effectively doubling the size of the continental area during the winter season, reaching a maximum sea ice extent of 19 x 10^6 km^2 in September before retreating to 3 x 10^6 km^2 by March (Budd, 1991; Gloersen et al., 1992). Unlike the extent of Arctic sea ice which has shown a dramatic recent decline of 7.8 ± 0.6% per decade since the 1970s related to anthropogenic warming (Cavalieri et al., 2003; Stroeve et al., 2007; Comiso, 2006), the sea ice extent around the majority of the Antarctic margin appears to be relatively stable, with a minor increase in the annual sea ice extent of 0.4% ± 0.5% per decade (NSIDC, 2009). However, recent investigations have shown that the summer sea ice concentrations in the Bellingshausen and Amundsen seas have declined over recent decades (Jacobs and Comiso, 1993; Ozsoy-Cicek et al., 2009; Cavalieri and Parkinson, 2008) suggesting that the apparent stability of the sea ice system may be declining.

2.4.1 The annual sea ice cycle

Annual variation in solar insolation is the primary driver of the seasonal advance and retreat of the sea ice edge. At high latitudes seasonal changes in insolation are

particularly significant due to high variation between the winter months (June-July-August) during which insolation is minimal, and the summer months (December-January-February) when insolation reaches its maximum. In the Antarctic region there is no northern constraint on sea ice production by landmasses, and therefore the autumn and winter advance of sea ice is relatively unrestricted. The position of the winter sea ice limit mainly depends upon the interplay between northward advection of newly formed ice by winds and melting of the ice edge in warmer waters (Pezza et al., 2012). In spring sea ice retreats from its maximum extent (55°S in the Atlantic and Indian Oceans, 60°S in the Pacific Ocean) to the coast of Antarctica in the majority of areas, with little perennial ice being present around the continent (Ackley, 1981; Comiso, 1999, updated 2008). The winter expansion of southern hemisphere sea ice is therefore of great importance for global oceanographic circulation due to associated seasonal variations in salinity. It is also important for regional atmospheric processes as it effectively doubles the surface area of Antarctic ice that interacts with the atmosphere and limits heat exchange from the ocean to the atmosphere (Tchernia, 1980). Interannual variability in the timing and extent of the sea ice edge is largely controlled by changes in atmospheric processes such as the Southern Annular Mode and the El Niño-Southern Oscillation (Section 2.5).

Important controls on the formation of sea ice include seasonal insolation, sea surface temperature (which must be colder than around -1.86°C for sea ice to form), and surface wind speed, which controls ice advection away from the site of formation (PolarGroup, 1980; Pezza et al., 2012). On a hemispheric scale, the presence of sea ice is important as it provides an insulation layer that effectively prevents exchange of heat from the ocean to the atmosphere (Bentley, 1984; Nihashi et al., 2011), and the high albedo of ice and snow relative to sea water reflects up to 70% of incoming solar radiation (PolarGroup, 1980; Marshall and Plumb, 2008). Sea ice conditions also play a role in determining regional climatic and weather systems. For instance, in the southern hemisphere sea ice has been shown to exert control on the frequency of cyclogenesis (the formation or enhancement of cyclonic, or low pressure, weather systems), with the most significant correlations being observed in the Antarctic Peninsula region where increased sea ice extent is positively correlated with an increased formation rate of cyclones (Godfred-Spenning and Simmonds, 1996). Due to this role in modulating regional and global climate, the relationships between the atmosphere and the

cryosphere are increasingly being studied. However, the majority of studies upon sea ice are limited to the use of instrumental era records and shipping records, with the best data being available from the comparatively short period of satellite observations.

2.4.2 Sea ice and CO_2

At the glacial-interglacial time scale increases/decreases in sea ice are considered to provide an important climatic feedback mechanism by limiting/increasing the ventilation of the Southern Ocean during glacials/interglacials (e.g. Sigman and Boyle, 2000; Moore et al., 2000; Sigman et al., 2010; Keeling and Stephens, 2001; Toggweiler, 1999). The increased ventillation effect is further enhanced by greater aeolian deposition of iron to the surface ocean during glacial periods which increased the export efficiency (i.e. the rate at which it is removed from the water column and preserved in sediments) of phytoplankton productivity within the seasonal ice zone, increasing biological CO_2 sequestration (Moore et al., 2000; Martin, 1990; Bopp et al., 2003; Kohfeld et al., 2005). In the modern Southern Ocean, the waters of the seasonal ice zone contribute to the outgassing of CO_2 to the atmosphere as CO_2 builds up under winter ice to concentrations greater than atmospheric levels. This occurs as a result of respiration under the ice and ventilation of deep waters (Takahashi et al., 2009). Conversely, continental shelf waters also contribute significantly to the drawdown of CO_2 from the atmosphere during the spring and summer due to high biological productivity (Takahashi et al., 1997; Nicol et al., 2000; Ishii et al., 2002; Arrigo et al., 2008b). As a consequence of these seasonal processes, the net annual flux of CO_2 between the atmosphere and oceans is virtually zero for most regions (Takahashi et al., 2002). Recent estimates of CO_2 drawdown in Ross Sea shelf waters by Arrigo et al. (2008a) suggest this region may provide a particularly strong sink for anthropogenic CO_2 due in part to the high biological productivity and high formation rates of Ross Sea Bottom Water. It is estimated that the Ross Sea alone may account for 27% of the recent estimates for CO_2 drawdown in the entire Southern Ocean (Takahashi et al., 2009).

2.5 Major modes of interannual climatic variability in the southern hemisphere

Large-scale atmospheric processes cause secondary variations in the seasonal pattern of sea ice advance and retreat that is primarily dictated by the annual cycle of solar insolation. In the southern hemisphere, the two principal modes of atmospheric variability are the Southern Annular Mode (SAM; also known as the Antarctic Oscillation), and the El Niño-Southern Oscillation (ENSO). Studies of the influence of ENSO and SAM on interannual variability in the extent of sea ice around Antarctica are mostly limited to the relatively short instrumental period (~34 years, e.g. Simmonds and Jacka, 1995; Carleton, 1988; Yuan and Martinson, 2000; Kwok and Comiso, 2002; Stammerjohn et al., 2008; Yuan and Li, 2008), although this can be extended back to just over 100 years ago by use of qualitative shipboard and shore observations (see Mayewski et al., 2004). Recent studies have also indicated that there is a link between southern hemisphere atmospheric variations (Roscoe and Haigh, 2007; Labitzke, 2004), oceanic variability (Hibbert et al., 2010) and the quasi-biennial oscillation (QBO) in the tropical stratosphere.

2.5.1 The Southern Annular Mode

The SAM is a measure of the pressure difference between the mid and high latitudes of the southern hemisphere (Figure 2.06a and b), with positive phases equating to relatively low pressure over Antarctica, compared to the mid latitudes, and negative phases the opposite (Marshall, 2003). The SAM is the principal mode of atmospheric variability in the southern hemisphere (Thompson and Wallace, 2000). During positive phases of the SAM the westerly circumpolar winds that flow around Antarctica are strengthened, and during negative phases they are weakened (Marshall, 2003; Liu et al., 2004). Antarctic sea ice extent is consequently impacted by the strengthening (weakening) of westerly winds during positive (negative) phases, which increases (decreases) via coriolis force, northerly drift of sea ice, and consequently increases (decreases) sea ice extent (Figure 2.06d) (Hall and Visbeck, 2010; Pezza et al., 2012). Positive (negative) SAM further influences the Antarctic region by decreasing (increasing) poleward heat flux (Figure 2.06c) (Yuan and Yonekura, 2011; Hall and Visbeck, 2010). A link also exists between the SAM and the Antarctic Dipole, the dominant interannual variance structure in the sea ice edge, which is organized as a

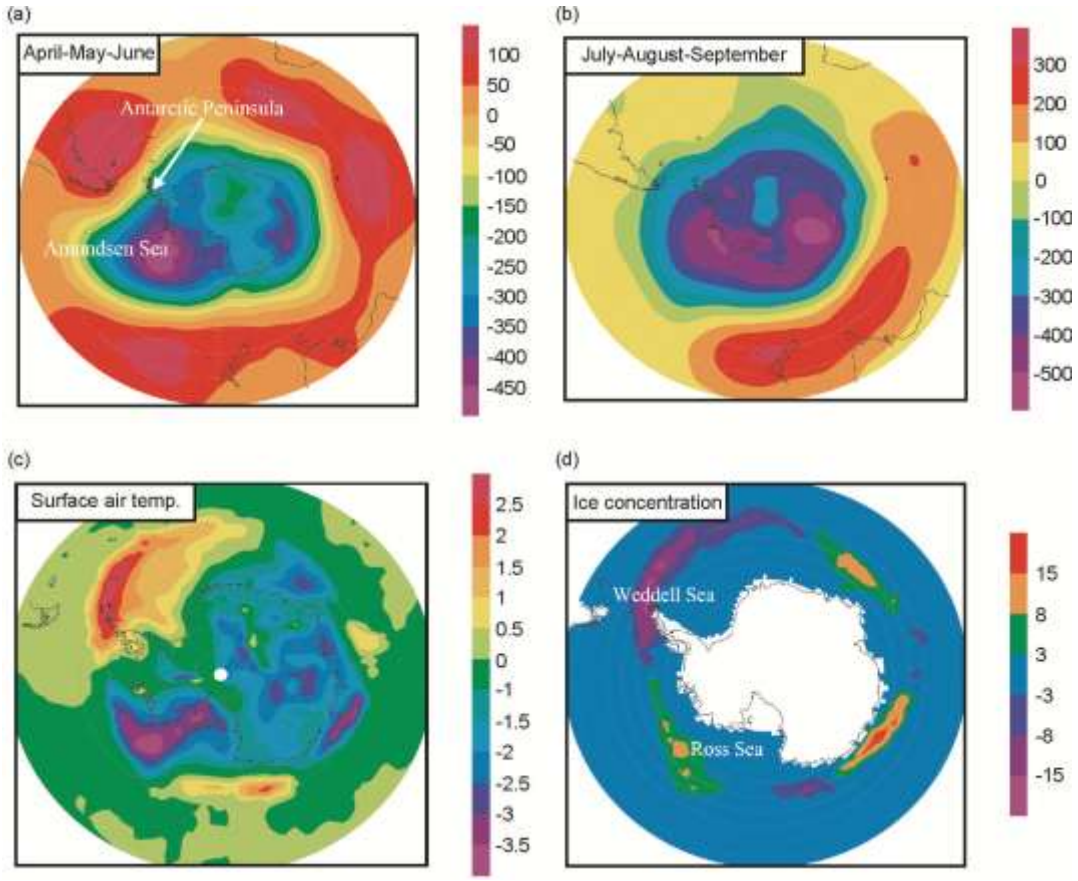

Figure 2.06. Atmospheric signature of the SAM and associated sea ice and surface air temperature anomalies. (a) Regression between atmospheric air pressure and the SAM index 1980 – 1999 in Pa for months April-May-June using reanalysis of NCEP-NCAR data showing difference in air pressure between the mid- and high latitudes; (b) same as for (a) but for July-August-September; (c) regression between surface air temperature and the SAM index; (d) regression between % sea ice concentration and the SAM index. Adapted from Goosse et al. (2010). Original data for (a – c) from Kalnay et al. (1996); original data for (d) from Rayner et al. (2003).

quasi-stationary wave in each of the basins ice fields (Yuan and Martinson, 2001). This variance results in anti-phase temperature and sea ice extent anomalies between the Ross Sea and Bellingshausen/northern Weddell Sea regions (Figure 2.06d) of ~3 – 7% cover and ~0.5 – 2°C respectively. This occurs due to the development of anomalously strong cyclonic circulation in the southeast Pacific Ocean during positive phases of the SAM causing an equatorward displacement of heat due to northward shifting of jet streams in the Ross Sea region that promotes sea ice growth. At the same time, there is a poleward flux of heat in the Bellingshausen/Weddell Sea region that serves to inhibit sea ice growth (Liu et al., 2004; Yuan, 2004; Yuan and Li, 2008).

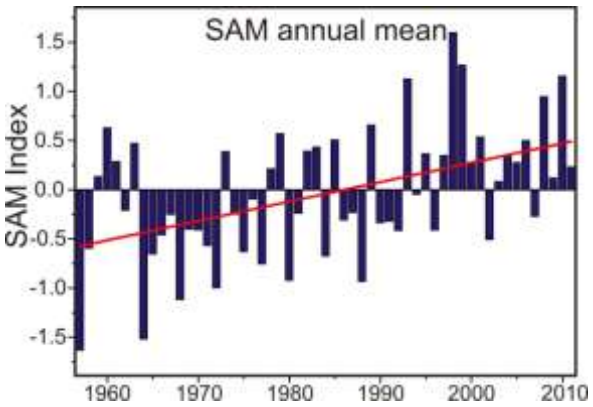

Figure 2.07. Annual mean SAM index values 1955-2011 (blue bars) and linear regression of SAM index (red line, r = 0.47, y = 0.0197x - 0.5949). Data from Marshall (2003).

Variations in surface pressures due to the SAM occur on a variety of timescales from low frequency (interdecadal - Kidson, 1999) to very high frequency (daily - Baldwin, 2001). A multidecadal trend towards positive values in the SAM index (SAMI), a measure of the mean normalised sea level pressure data between the mid- and high-southern latitudes, has been observed in modern sea level pressure (SLP) records (Figure 2.07)(Marshall, 2003). Analysis of this trend suggests that it is largely attributable to ozone-depletion over Antarctica as a consequence of anthropogenic production of ozone-depleting aerosols (Thompson and Solomon, 2002; Roscoe and Haigh, 2007) and partly to anthropogenic warming due to increased greenhouse gas emissions (Marshall et al., 2004). Seasonally, this long term trend is most apparent in the austral summer, with slightly smaller trends in autumn and winter data, and no trend in spring values (Marshall, 2003). Shorter-period variations in the SAM have been associated with combined quasi-biennial oscillation-solar forcing (Roscoe and Haigh, 2007; Labitzke, 2004). Variations in the SAMI are statistically linked to seasonal variations in sea ice concentration in Adélie Land (section 2.6.3).

2.5.2 The El Niño-Southern Oscillation

The Southern Oscillation is a major see-saw of air pressure and rainfall patterns (Walker circulation, Figure 2.08) over the Pacific Ocean (Philander, 1983), and results from the pressure difference measured between Darwin, Australia, and Tahiti, French Polynesia (King and Turner, 1997). Strong links exist between the Southern Oscillation and El Niño, an oceanic phenomenon that consists of aperiodic warming across the central and eastern Pacific Ocean and the two are referred to as a combined phenomena, the El

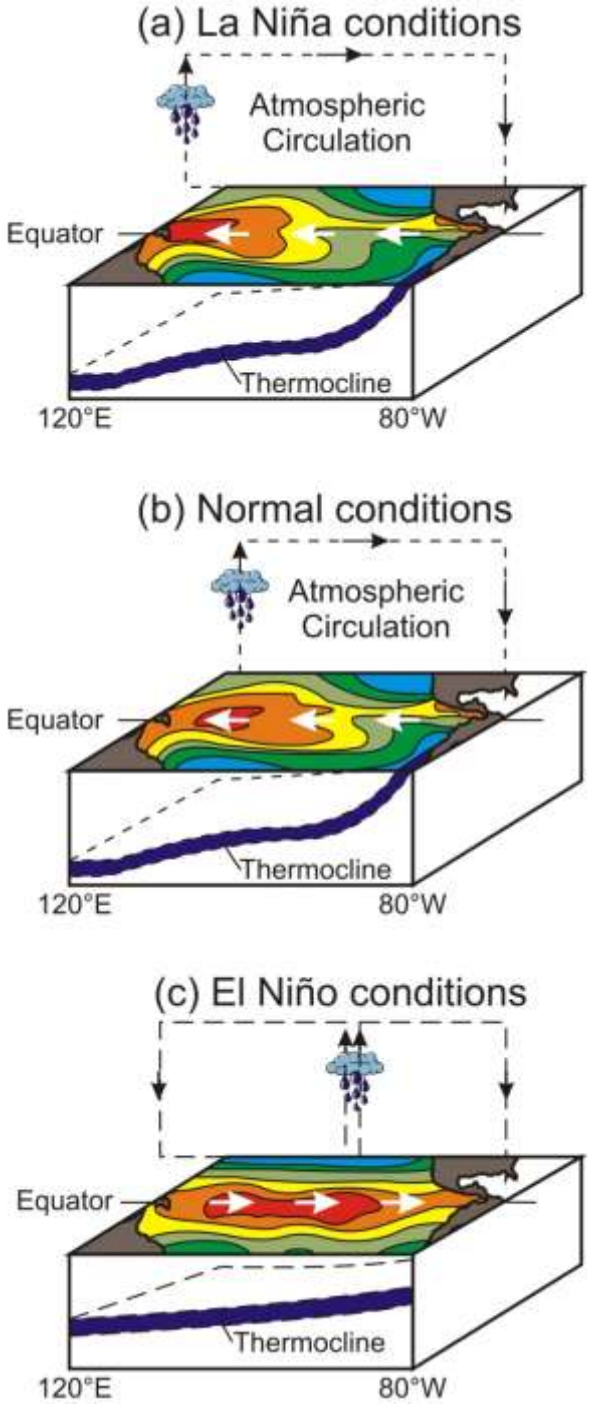

Figure 2.08. Schematic diagram of the Pacific Ocean under (a) La Niña conditions; (b) normal conditions; (c) El Niño conditions. The colour gradient indicates relative sea surface temperatures (SSTs), with red equating to warmest SSTs and blue coolest SSTs. Adapted from (McPhaden, accessed 2010).

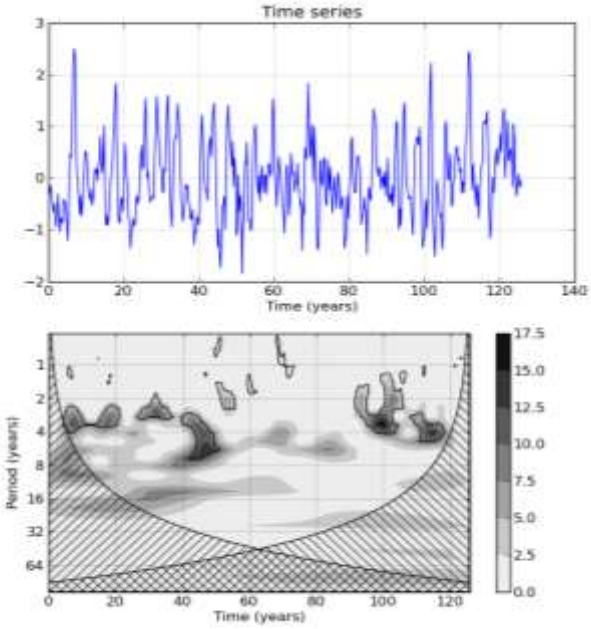

Figure 2.09. Wavelet analysis of the Niño 3 time series demonstrating the non-stationarity (irregularity) of the ENSO phenomenon and observed periods of 2 – 7 years. Recreated from Torrence and Compo (1998).

Niño-Southern Oscillation (Trenberth, 1991). The El Niño-Southern Oscillation (ENSO) is an irregular climatic phenomenon in the tropical-subtropical Pacific and Indian Oceans, which occurs with an average periodicity of 2 – 7 years (Figure 2.09), and is internally modulated over decadal timescales (Timmermann and Jin, 2002; Torrence and Compo, 1998; Kirtman and Schopf, 1998). ENSO events alternate between two extremes, warm El Niño (Figure 2.08c) and cool La Niña events (Figure 2.08a), with each event in modern records lasting for an average of 18-24 months (Allan, 2000) and warm-ENSO events usually of a greater intensity than cool-ENSO events (An and Jin, 2004).

Under normal conditions in the Pacific Ocean (Figure 2.08b), atmospheric pressure is higher in the east (by South America) than the west (Indonesia) resulting in strong westerly trade winds and a westward flow of ocean surface currents at the equator (King and Turner, 1997). This typically results in wetter conditions in the western Pacific due to higher evaporation and dryer conditions in the eastern Pacific. Warm-ENSO events occur when there is a weakening of the Walker circulation and a consequent reduction in the east-west pressure gradient of the Pacific Ocean resulting in warming of the

central and eastern Pacific Ocean, eastwards redistribution of rainfall and reduced upwelling of deep nutrient-rich waters in the eastern Pacific due to deepening of the thermocline (Figure 2.08c) (King and Turner, 1997). Cool-ENSO events (Figure 2.08a) are essentially extreme normal conditions, with warmer conditions and higher rainfall in the western Pacific Ocean. Whilst strongly enhanced by an extreme SO (high pressure in Darwin, low in Tahiti), El Niño oceanic events may occur independently of the SO, although they are a restricted phenomenon along the coast of South America (Trenberth, 1991).

Correlations between ENSO indices and the Antarctic sea ice edge show that approximately 34% of the southern hemisphere variation in sea ice concentration observed from satellites can be attributed to a teleconnection with ENSO, with the strongest connections being present in the regions of the Bellingshausen, Amundsen and Ross Seas via the Antarctic Dipole (Yuan and Martinson, 2000; Kwok and Comiso, 2002), although the changes in sea ice distribution differ regionally. During warm-ENSO events, an anomalously high pressure centre develops over the Amundsen Sea region which causes opposite sign temperature and sea ice anomalies in the Ross Sea and the Antarctic Peninsula (Figure 2.10) (Kwok and Comiso, 2002; Yuan, 2004; Bertler et al., 2006). In the Adélie Land region it can be seen that a statistical link between cool-ENSO and increased spring sea ice extent exists (section 2.6.3).

2.5.3 The quasi-biennial oscillation

The quasi-biennial oscillation (QBO) is the dominant mode of equatorial stratospheric variability (~16 – 50 km altitude). The QBO occurs as downward propagating easterly and westerly wind regimes within the stratosphere, with an average periodicity of approximately 2.3 years (Baldwin et al., 2001). Although it is a tropical stratospheric phenomenon, the effects of the QBO are transmitted to the troposphere and the mesosphere, and have an influence on polar regions by modulation of extratropical planetary (Rossby) waves (Baldwin et al., 2001). Modulation of the QBO by ENSO has been shown to increase the rate of downward propagation of QBO winds during warm-ENSO events, resulting in a shorter QBO period of 2.1 years, and to slow the propagation of QBO winds during cool-ENSO events, resulting in a longer QBO period of 2.7 years (Taguchi, 2010).

Figure 2.10. Size and position of the Amundsen Sea Low (LAS) and wind strength (red arrows = warm air, blue arrows = cooler air) during cool-ENSO (La Niña) and warm-ENSO (El Niño) events. Cooling (warming) of the Ross and Amundsen Sea for cool (warm) events is indicated in the lower images. Grey arrows indicate katabatic wind flow (Bertler et al., 2006). Black square in top left map indicates approximate location of Adélie Land core site.

Evidence exists for a link between the QBO and November conditions in the polar vortex of the southern hemisphere stratosphere (Baldwin and Dunkerton, 1998; Garfinkel and Hartmann, 2007). During the winter, a strong polar vortex inhibits influence of the QBO on the southern polar stratosphere as a strong circumpolar wind-flow inhibits the activity of planetary waves. However, during the late winter/early spring (particularly during November) the polar vortex breaks down and a downward propagating pressure anomaly occurs in the polar stratospheric pressure fields (Thompson et al., 2005; Thompson and Solomon, 2002; Baldwin and Dunkerton, 1998). Anomalies in polar stratospheric pressure are subsequently transmitted to the troposphere (Thompson et al., 2005). On an interannual time scale, it has been shown that QBO forcing of southern hemisphere climate may occur if a coupled QBO-solar index is considered (Labitzke, 2004; Roscoe and Haigh, 2007). Recently it has been shown that QBO-related changes in Southern Ocean sea level may occur due to altered surface wind patterns as stratospheric anomalies propagate into the troposphere (Hibbert et al., 2010); however, little work has been done on the regional identification of QBO forcing in meteorological and oceanographic datasets outside of the Antarctic Peninsula region.

2.6 Adélie Land environmental setting

The Adélie Land margin (136°E to 142°E) is located between Wilkes Land (100°E to 136°E) and George V Land (142°E to 153°E) sectors of the East Antarctic continental shelf, in the eastern Indian Ocean sector of the Southern Ocean, and is influenced by local glaciers, the largest of which are the Zélée, Astrolabe and Français glaciers (Figure 2.11) as well as some of the strongest Antarctic katabatic winds (Periard and Pettre, 1993). A strong seasonal cycle of sea ice formation and retreat promotes high diatom productivity due to high nutrient levels in a stratified water column during the spring period (Arrigo and van Dijken, 2003; Arrigo et al., 2008c). Strong seasonality in surface water salinity and temperature combined with high productivity produces a high export production rate (Berger and Wefer, 1990), and the exported material is focussed

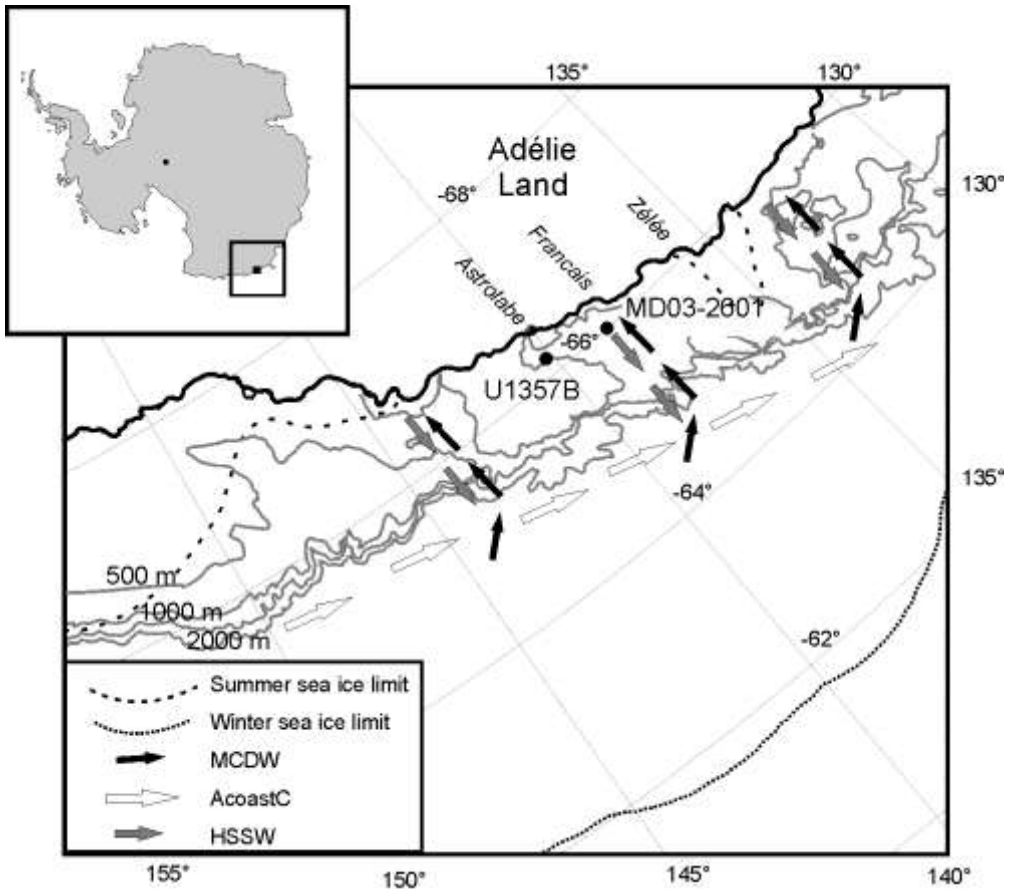

Figure 2.11. Map of the Adélie Land region showing location of cores MD03-2601 and IODP-318-U1357B; location of glaciers mentioned in text (Massom et al., 1998; Escutia et al., 2003); summer and winter sea ice limits (Schweitzer, 1995) and major oceanographic features of the region (Harris and Beaman, 2003). MCDW = Modified Circumpolar Deep Water; AcoastC = Antarctic coastal current; HSSW = High salinity shelf water. Adapted from Denis et al. (2006).

into deep troughs (IODP Expedition 318 Scientists, 2010) which leads to the ultra-high sedimentation rates of the sediments used in this study.

2.6.1 Bathymetry

The Adélie Land shelf is approximately 130 km wide and, as is common for Antarctic shelves, deepens landwards as a result of glacial erosion and loading of grounded ice. Large banks on the mid to outer shelf range between 200 to 400 m water depth, whereas large troughs produced by ice stream erosion during the last glacial interval reach depths >1000 m on the inner shelf (Ten Brink and Cooper, 1992; Domack, 1982; Eittreim et al., 1995). The Dumont d'Urville Trough trends obliquely across the Adélie Land shelf, reaching a maximum depth of 1300 m, and is flanked to the northeast by the Adélie Bank (Figure 2.12) (Eittreim et al., 1995; Beaman et al., 2010).

2.6.2 Adélie Land oceanography

Ocean circulation in the Adélie Land region is largely dominated by upwelling Modified Circumpolar Deep Water (MCDW), northwards flowing High Salinity Shelf Water (HSSW) and the westward flowing Antarctic Coastal Current (ACoastC; Figure 2.11) (Harris and Beaman, 2003). MCDW upwells onto the shelf via the deep glacial troughs, mixes with HSSW and very cold ice shelf water (a relatively low salinity, cold water formed during late spring melting) to form a descending northward flowing current that contributes to the formation of Adélie Land Bottom Water (ALBW; Harris and Beaman, 2003; Rintoul, 1998; Williams et al., 2008). ALBW is an important component of AABW, with approximately 30% of AABW formation occurring in the Wilkes Land region, although there is no direct evidence for formation of ALBW in the Dumont d'Urville Trough (Carter et al., 2009; Jacobs, 2004). The influence of katabatic winds is particularly important in the generation of the Mertz Polynya, situated over the George V Basin (Massom et al., 1998; Tamura et al., 2008), which is a significant source of HSSW and varies seasonally in areal extent. Seasonal variations in the salinity and temperature of ALBW have also been recorded, and since 1969 ALBW has shown a trend towards decreased salinity unrelated to seasonal changes, and most likely associated with increased glacial melting at 140°E (Aoki et al., 2005).

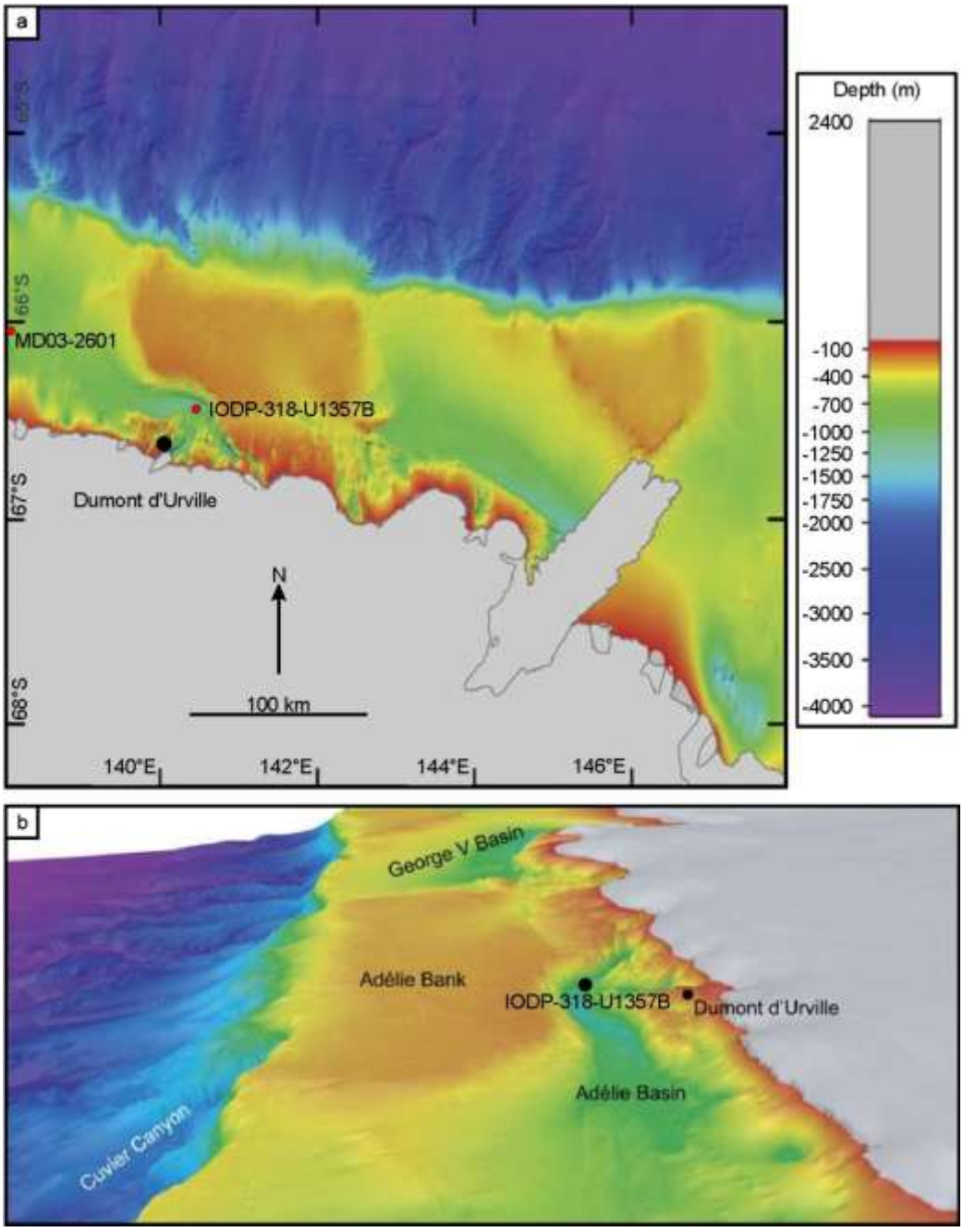

Figure 2.12. Detailed bathymetry of the Adélie Land region. (a) Mercator projection of bathymetry showing location of cores; (b) 3D oblique view of the Adélie Basin facing east, core MD03-2601 (not shown) lies slightly further west (bottom edge of b). Adapted from Beaman et al. (2010).

2.6.3 Sea ice cover

Interannual variations in the extent and concentration of sea ice are an important control on the environments of the Adélie Land coast and, subsequently, exert an important control on variations in phytoplankton biomass and composition (e.g. Riaux-Gobin et

al., 2003; Riaux-Gobin et al., 2011; Beans et al., 2008). In this section, the satellite-derived sea ice concentration data (November 1978 – December 2008; Comiso, 1999, updated 2008) are analysed for seasonal and interannual trends that may be helpful in the interpretation of lamina and HBI records produced from cores MD03-2601 and IODP-318-U1357B (Chapters 5 and 6). These data show that sea ice covers the Dumont d'Urville Trough for most of the year, with two to three months of open water Typically, sea ice retreats between November and December, with open water in January and February. A rapid advance of sea ice occurs during March and in the majority of years the trough experiences >80% sea ice concentration from April to October (Table 2.01). The open water period (defined as <20% sea ice concentration) is extremely variable, ranging between zero and four months (Table 2.02). The greatest interannual variability in sea ice cover observed in the satellite record occurs during the spring ice break-up period, whilst the lowest interannual variability occurs during the sea ice formation and winter periods (Comiso, 1999, updated 2008).

There is strong statistical evidence for links between ENSO, the SAM and the extent/concentration of Antarctic sea ice from cross comparison of satellite-derived sea ice data and climatological indices (Simmonds and Jacka, 1995; Yuan, 2004; Yuan and Martinson, 2000; Yuan and Li, 2008; Kwok and Comiso, 2002; Stammerjohn et al., 2008). The Southern Oscillation Index (SOI) provides an estimate of the strength of the SO and is computed from fluctuations in the surface air pressure difference between Tahiti and Darwin, Australia (John, 2004). Comparing the lead periods between changes in the SOI and SAM with changes in sea ice concentration in the Adélie Land region demonstrates differences in the significance of each index and differences in the

Table 2.01. Number of years in satellite record (November 1978 – December 2008; Comiso, 1999, updated 2008) in which sea ice parameters first occur for a given month.

Month of sea ice first occurrence in satellite record	<80% sea ice concentration	<20% sea ice concentration	>80% sea ice concentration
Doesn't occur	-	3	-
November	8	-	-
December	8	4	-
January	9	11	-
February	2	10	-
March	1	-	-
April	-	-	23
May	-	-	5

Table 2.02. Number of years in satellite record (November 1978 – December 2008; Comiso, 1999, updated 2008) in which sea ice concentrations are <20% for a given number of months.

Number of months <20% sea ice concentration	Number of occurrences in satellite record
0	3
1	6
2	13
3	4
4	2

seasons which they influence. The SOI data (Figure 2.13a) demonstrates a negative correlation ($r = -0.3$, $p < 0.1$, $n = 31$) between the SOI and sea ice concentration in the spring period (Figure 2.13a), with a 10-15 month lead in the SOI. The SAMI correlation with Adélie Land sea ice concentration exists in the autumn interval and is stronger than that of the SOI ($r = 0.37$, $p < 0.05$, $n = 30$; Figure 2.13b). The SAMI data demonstrates a short period response of 0-5 months in the spring and autumn sea ice concentration as well as a longer response of autumn sea ice ~11-16 months after observed changes in the SAMI. Considering a combined SOI – SAMI (achieved by subtracting SAM values from SOI values; Figure 2.13c) provides further useful insight as the two are known to reinforce each other when in phase (negative SAM and positive SOI, and vice versa), strengthening the impact of ENSO events on the Antarctic region (Stammerjohn et al., 2008; Fogt and Bromwich, 2006). This approach demonstrates a significant (95% confidence) negative correlation ($r = -0.368$, $n = 30$) between the SOI - SAMI and sea ice concentration (i.e. negative SAM and positive SOI values correlate to

Table 2.03. Table summarising the statistical analysis presented in this chapter demonstrating the influence of phasing in the SAM and ENSO climatological indices and changes in satellite-derived sea ice concentration in Adélie Land.

	Increased sea ice concentration	
Season	**SAM phase**	**ENSO phase**
Spring (S-O-N-D)	+ve ($r = 0.368$, $p < 0.05$, $n = 31$)	-ve (El Niño) ($r = -0.3$, $p < 0.1$, $n = 31$)
Autumn (M-A-M)	+ve ($r = 0.368$, $p < 0.05$, $n = 30$)	N/A
Winter (J-J-A)	+ve ($r = 0.368$, $p < 0.05$, $n = 30$)	N/A

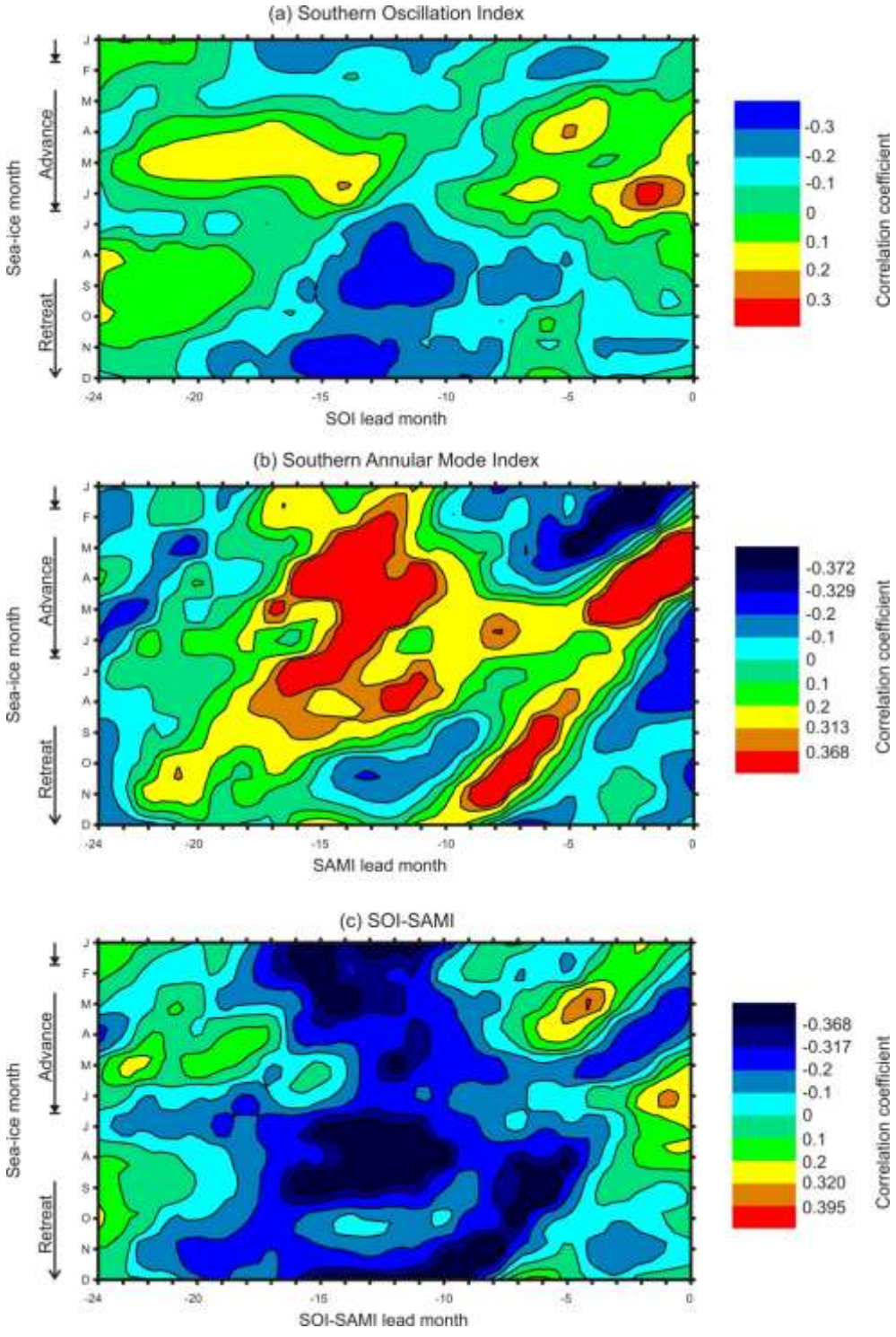

Figure 2.13. Correlation of lead periods in climatological indices with a 3-month running mean for a given month against sea ice concentration in the Adélie Land region (Figure 2.14) for the period November 1978 – December 2007. (a) The Southern Oscillation Index (90% confidence limits = 0.3 and -0.3); (b) the Southern Annular Mode Index (95% confidence limits = 0.395 and -0.368; 90% confidence limits = 0.313 and -0.329); (c) the Southern Oscillation Index - the Southern Annular Mode Index (95% confidence limits = 0.395 and -0.368; 90% confidence limits = 0.320 and -0.317). SOI data available from http://iridl.ldeo.columbia.edu/docfind/databrief/ cat-index.html. SAM index data available from http://www.antarctica.ac.uk/met/gjma/sam.html (Marshall, 2003). Raw satellite sea ice data from Comiso (1999, updated 2008), processed by Ian Thomas.

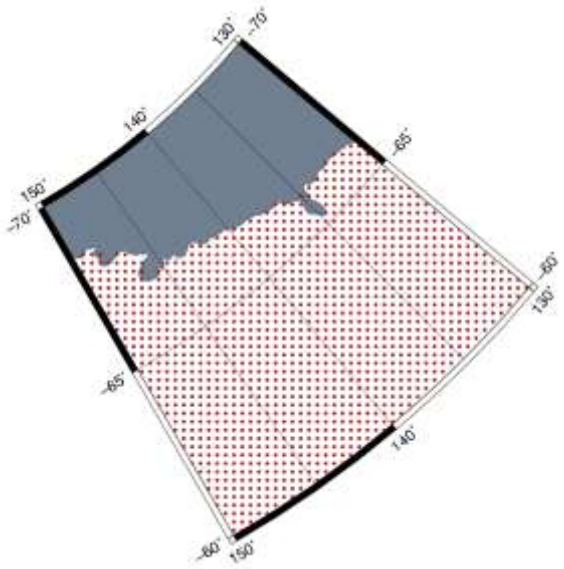

Figure 2.14. Sampling region and distribution of sampling points within satellite data used in Figure 2.13. Figure produced by Ian Thomas.

reduced sea ice); which is particularly evident within the winter and spring period. This relationship has been demonstrated at a broad scale in southern hemisphere satellite-derived sea ice records (Stammerjohn et al., 2008) and multidecadal modulation of the signal is governed by phase changes in the SAM (Fogt and Bromwich, 2006).

2.6.3.1 Hypotheses for diatom lamina distribution

Given the demonstrated statistical relationship between seasonal sea ice concentration and SAM and ENSO indices presented above, and the known sensitivity of diatoms to changes in sea ice (see also Chapter 3), several hypotheses are proposed here for testing in Chapter 5. The working hypotheses for the distribution of lamina that are rich in particular genera/species in cores MD03-2601 and IODP-318-U1357B are:

1) The distribution of spring laminae should be sensitive to ENSO forcing, based on the negative correlation between modern spring sea ice concentration and ENSO.
2) The distribution of autumn laminae should be sensitive to SAM forcing, and possibly combined SAM-ENSO forcing, based on the positive correlation between modern autumn sea ice concentration and SAM, and a combined SAM-ENSO index.
3) As a response to both the increased sea ice (Crosta et al., 2007) and ENSO intensity that occurred during the late Holocene (Moy et al., 2002; Donders et

al., 2008) ENSO-frequencies should be observed more strongly in the lamina-time series records during the Neoglacial compared to the Hypsithermal.

2.5 Summary

This chapter has introduced the geological and oceanographic history of Antarctica to explain the presence of the cryosphere and its importance within global cycles in oceanography and climate. In particular, the importance of the strongly seasonal sea ice cycle has been presented along with its impacts on biological productivity, sedimentation and nutrient cycling, as well as producing high salinity bottom waters, a major feature of global thermohaline circulation. The connectivity between sea ice and global atmospheric/climatic processes has also been demonstrated, highlighting the statistical connection between ENSO and spring sea ice concentrations in Adélie Land and the SAM and autumnal/spring sea ice concentrations. Based on this data, and known changes in the ENSO system, three hypotheses have been proposed and will be tested in Chapter 5.

Chapter 3 – Proxies used in this study

This chapter introduces Antarctic marine diatoms describing their distribution, ecology, preservation and uses in palaeoenvironmental reconstruction. Similarly, background information on the distribution, formation, preservation and palaeoenvironmental uses of highly branched isoprenoids (HBIs) are presented, along with a revised analysis of previously published data for core MD03-2601 (Denis et al., 2010). The latter is included in order to highlight the association between HBI di- and tri-unsaturated molecules and the presence of sea ice-associated diatoms in core MD03-2601.

3.1 Diatoms of the Southern Ocean

Diatoms are unicellular microscopic (typically ~2 – 200 µm, although some genera such as *Thalassiothrix* may reach lengths of up to 2 mm) algae (classes Diatomophyceae and Bacillariophyceae) which occur individually or in colonies, have a cell wall (frustule) composed of silica and exhibit a wide range of forms (Round et al., 1990). Colonies are held together by interlocking spines, ridges, mucilage pads or chitinous threads, and aggregation of colonies leads to sedimentation of large (several mm) particles that contribute to marine snow (Priddle, 1990). Diatoms are the dominant primary producers in the Southern Ocean, accounting for up to 75% of primary production in this region and are consequently of great importance in the marine and global silicic acid and carbon cycles (Treguer et al., 1995).

Sedimentary deposition of diatomaceous ooze around Antarctica occurs in a broad continuous belt which is located between the Polar Front and the winter sea ice edge (Hays, 1965; Burckle and Cirilli, 1987). To the south of this belt occurs a mix of diatomaceous and silty sediments, and to the north more carbonate-rich sediments (Burckle and Cirilli, 1987). Diatomaceous ooze also forms more sporadically at sites of high deposition rates closer to the coast such as Adélie Land (e.g. Leventer et al., 2001; Crosta et al., 2005a; IODP Expedition 318 Scientists, 2010; Maddison et al., 2012), the Mertz-Ninnis Trough (Harris and Beaman, 2003), Prydz Bay (Taylor et al., 1997), the Ross Sea (Leventer et al., 1993) and the Antarctic Peninsula (Leventer et al., 2002; Bahk et al., 2003) among others. The elevated sedimentation rates at these coastal sites

(up to 75 mm in a single season; Stickley et al., 2005) often allow for ultra-high resolution (seasonal to sub-seasonal) reconstructions of palaeoenvironments.

3.1.1 The ecology of Southern Ocean diatoms

The distribution of diatoms in the surface waters of the Southern Ocean is controlled by a variety of environmental factors. Light intensity, salinity, sea surface temperature, nutrient availability, water column stability and sea ice concentration have all been shown to exert control on the distribution of diatoms (Holm-Hansen and El-Sayed, 1975; Neori and Holm-Hansen, 1982; Jacques, 1983; Burckle et al., 1987; Leventer, 1991; Cunningham and Leventer, 1998; Beans et al., 2008; Riaux-Gobin et al., 2011). Sea ice in particular exerts an important control on diatom productivity and export, suppressing productivity when present (Hart, 1942; Whitaker, 1982) and enhancing diatom productivity as it retreats (Arrigo et al., 2010). Here the ecology of diatoms is considered in two groups: (i) sea ice associated diatom species that are confined to south of the Polar Front (Table 3.01) (Tréguer and Jacques, 1992; Armand et al., 2005) which are dominant in the sea ice zone and marginal ice zone towards the Antarctic continent (Figure 3.01); and (ii) open ocean diatom species (Table 3.02) (Crosta et al., 2005b) which are more common in the open ocean zone beyond the winter ice limit and are of high abundance in the Polar Frontal Zone (PFZ).

3.1.1.1 Sea ice associated diatoms

Sea ice has a variety of habitats for diatoms due to highly variable temperature and salinity characteristics and also providing a stable platform with adequate irradiance to promote microalgal growth within the ice and/or attached below (Arrigo et al., 2010). Land-fast ice (Figure 3.02a), which may account for only 10% of Antarctic sea ice (Lizotte and Sullivan, 1991), is formed of a layer of vertically grown columnar ice and may have a bottom layer of highly porous (approx. 20% ice and 80% sea water) platelet ice which often contains high microalgal biomasses (Arrigo et al., 2010). In contrast, pack ice (Figure 3.02b) forms from a series of processes operating on the water column. Initially dense concentrations of frazil ice crystals form in the water column and float to the surface where they form grease, nilas and pancake ice (Ackley and Sullivan, 1994).

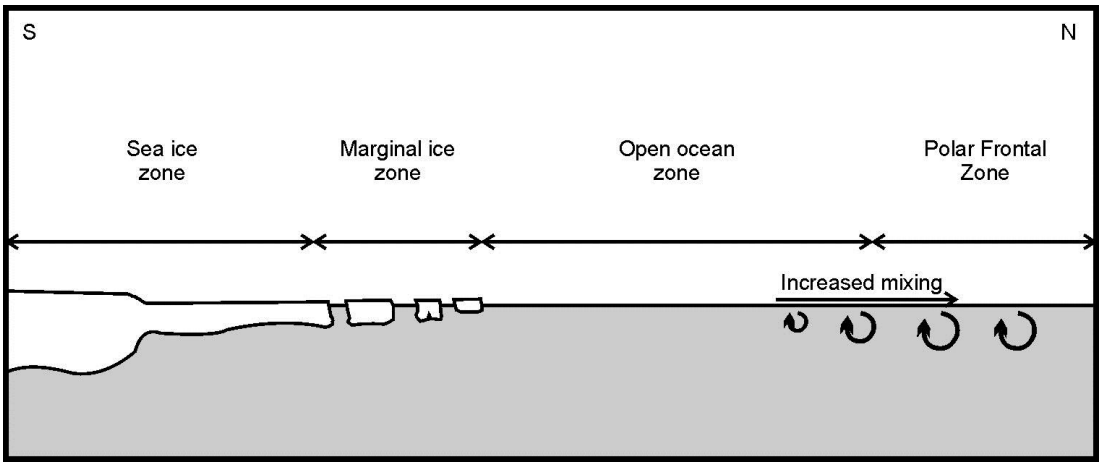

Figure 3.01. Schematic representation of the oceanic zones referred to in the text.

During this process, frazil ice crystals scavenge particles, including diatoms, from the water column and concentrate them in the lower layers of forming sea ice (Garrison et al., 1990) up to 50-times relative to the underlying sea water (Arrigo et al., 2010). Following consolidation of frazil ice, ice growth occurs vertically to form columnar ice, the lowest layer of which (the skeletal layer) is highly porous permitting infiltration of sea water and the growth of microalgal communities in the bottom 20 cm of this layer (Arrigo and Sullivan, 1992). Microalgae may also be found growing within pack ice, particularly during the late winter and early spring seasons when the ice may provide stable access to solar irradiance (Lizotte and Sullivan, 1991) and protect microalgae from grazers. They are typically associated with the upper frazil ice layer (Figure 3.02b), particularly when heavy snow layers induce flooding-freezing of the pack ice surface (Kattner et al., 2004). Incorporation of diatoms into sea ice during the autumn requires the species to be able to switch from a planktonic life mode to a "kryohaline" life mode (Eicken, 1992) and several studies have recorded a reduction from >100 species incorporated in new ice to <20 species remaining during ice melting (Krebs et al., 1987; Gleitz et al., 1996; Gleitz et al., 1998) indicating that relatively few species are able to adapt to living within the sea ice.

Land fast ice communities are commonly dominated by pennate diatom species such as *Amphiprora* spp., *Navicula* spp. and *Nitzschia* spp. that do not contribute significantly to phytoplankton standing stock and are rarely recorded in the fossil record

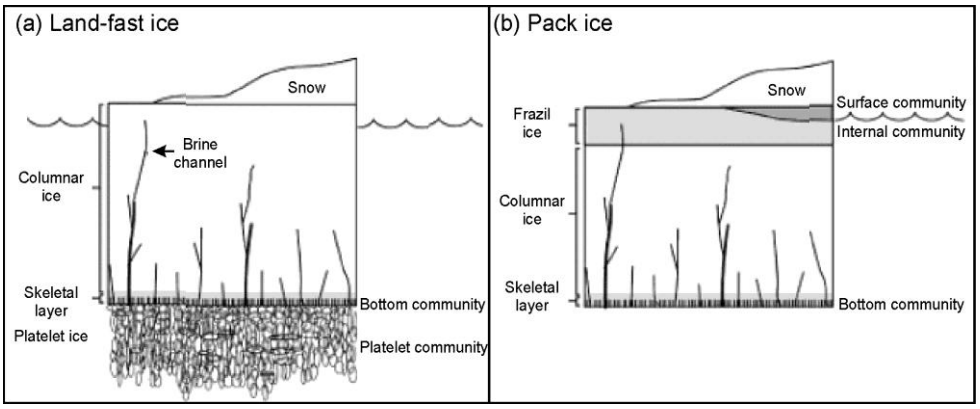

Figure 3.02. Highly idealised schematic illustration of (a) pack ice and (b) land-fast ice ecosystems in the Antarctic showing the location of major ice algal communities. Adapted from Arrigo et al. (2010).

(Riaux-Gobin et al., 2003). Species of *Fragilariopsis*, notably *F. curta* and *F. cylindrus*, may be common in fast ice communities as well as adjacent water (e.g. Smetacek et al., 1992; Grossmann et al., 1996; Gunther and Dieckmann, 2001; Thomas et al., 2001; Riaux-Gobin et al., 2003). In contrast, the more prevalent pack ice contains diatom assemblages that are more similar to the surrounding water column (Garrison et al., 1987). Pack ice may be solely dominated by *F. curta* (Scott et al., 1994) but also commonly contains other cryophilic diatoms, such as various *Fragilariopsis* spp. and *Thalassiosira antarctica* (summarised in Table 3.01) that are associated with both pack ice and the water column in the marginal ice zone. For many of these species it has been hypothesised that they are directly seeded into the water column from the sea ice (e.g. Horner, 1985; Garrison et al., 1987; Krebs et al., 1987; Garrison and Buck, 1989; Gleitz et al., 1996; Riaux-Gobin et al., 2011).

Significant phytoplankton productivity within the coastal Southern Ocean is restricted to the ice-free austral summer months, with up to 95% of annual biogenic export occurring between December and January (Wefer et al., 1988; Abelmann and Gersonde, 1991; Langone et al., 2000; Leventer, 2003). High phytoplankton biomass and export occurs at the retreating ice edge in the marginal ice zone (MIZ), due to the formation of a stable meltwater lens at the ice edge which benefits from high irradiance relative to sub-sea ice waters (Smith and Nelson, 1986). High surface water nutrient loads result from upwelling waters and release of important minerals, principally iron, from sea ice and snow cover (Fischer et al., 2002; Lannuzel et al., 2007). It has been estimated that

Table 3.01 (next three pages). Summary of ecological information from sea ice, water and surface sediment samples for common sea ice associated species observed in this study. Plates of key diatom taxa are presented in Appendix 1.

Species	Ecological information
Hyalochaeate Chaetoceros resting spores (CRS)	Vegetative cells often observed as sub-dominant within pack ice (Gleitz et al., 1998) and broadly distributed in Adélie Land surface waters (Beans et al., 2008). Resting spore formation occurs as a response to depleted nitrogen or iron levels, or reducing light during vertical mixing of the water column or as a result of reduced seasonal insolation during the autumn (Crosta et al., 1997). Sedimentary distribution of CRS is associated with high nutrient levels and strong spring stratification (Leventer, 1991; Crosta et al., 1997). Highest sedimentary abundances occur in the Antarctic Peninsula with ~7 months/year sea ice cover, although elsewhere they occupy a broad range of seasonal sea ice cover and appear to peak in areas with relatively icy summer conditions (Armand et al., 2005).
Eucampia antarctica var *recta* (Castracane) Mangin	Highest abundances in coastal zones near to ice and found in high abundance proximal to melting ice in more open ocean areas (Burckle, 1984). Often dominant in glacial sediments and most common sedimentary occurrences are towards the Antarctic coast (Burckle, 1984).
Fragilariopsis curta (van Huerck) Hustedt	Commonly reported in coastal areas and may be dominant or common within sea ice communities and waters proximal to a melting ice edge (Garrison and Buck, 1989; Tanimura et al., 1990; Smetacek et al., 1992; Kang and Fryxell, 1993; Scott et al., 1994; Gleitz et al., 1996; Leventer and Dunbar, 1996; Goffart et al., 2000; Lizotte, 2001; Riaux-Gobin et al., 2003; Riaux-Gobin et al., 2011). Sedimentary distribution confined to areas south of the winter sea ice edge, peaking in regions with 9 – 11 months per year of sea ice cover (Armand et al., 2005).
F. cylindrus (Grunow) Krieger	Dominant in sea ice meltpools/crackpools in the Weddell Sea and commonly found within pack ice (Gleitz et al., 1996). May be present within platelet ice but also does well in open ocean conditions after ice melting (Lizotte, 2001; Mangoni et al., 2009; Riaux-Gobin et al., 2011) and dominant relative to *F. curta* in water (Burckle et al., 1987) and has been considered an indicator of cold coastal waters (von Quillfeldt, 2004). One of the most common diatoms found in the Adélie Land MIZ (Kang and

Species	Ecological information
	Fryxell, 1992; Riaux-Gobin et al., 2011). Peak sedimentary abundance in regions with winter sea ice concentrations of >70 – 90%, with >7.5 months per year sea ice cover (Tanimura et al., 1990; Armand et al., 2005). May be less well preserved in sediments than *F. curta* due to smaller size resulting in preferential dissolution and greater winnowing (Leventer, 1998).
F. obliquecostata (van Huerck) Heiden	Common beneath pack ice and found in areas where winter sea ice concentrations are 65 – 90%, with >7 months per year sea ice cover. Sedimentary occurrences appear to be confined to regions south of the maximum summer sea ice extent in the South Atlantic (Gersonde and Zielinski, 2000). Confined to sediments beneath the winter sea ice limit (Armand et al., 2005).
F. rhombica (O'Meara) Hustedt	Observed in fast and pack ice samples (Garrison et al., 1983; Krebs et al., 1987; Garrison and Buck, 1989). Occur in sediments near the coast or ice shelves (Taylor et al., 1997; Zielinski and Gersonde, 1997; Cunningham and Leventer, 1998), maximum sedimentary occurrence beneath winter sea ice concentrations 65 – 90% in areas with 7-9 months of sea ice per year. Optimum February temperature range of -1°C to 1°C (Armand et al., 2005).
F. ritscheri Hustedt	Observed in fast ice and pack ice samples (Garrison and Buck, 1989; Tanimura et al., 1990), but occurs at higher abundances in water column next to sea ice than in the sea ice itself (Garrison et al., 1983; Garrison et al., 1987). Greatest sedimentary abundances in areas beneath winter ice conditions >70%, and an optimum of 9 months/year sea ice cover, but found from 2 to 10.5 months/year. Optimum sea surface temperature 0 - 3°C (Armand et al., 2005).
F. separanda Hustedt	Higher abundances at slightly offshore locations rather than inshore (Leventer, 1992; Taylor et al., 1997; Cunningham and Leventer, 1998), but may be confined to south of the Polar Front (Zielinski and Gersonde, 1997). Maximum sedimentary abundances in areas with 4.5 – 9 months/year sea ice cover and a temperature range of -1 to 8°C. Distribution may be linked to transportation of frustules (Armand et al., 2005).
F. sublinearis (van Huerck)	Reported in fast ice samples (Garrison et al., 1983; Garrison and Buck, 1989; Tanimura et al., 1990).

Species	Ecological information
Heiden	Similar sedimentary distributions to *F. obliquecostata* and *F. ritscheri* (Zielinski and Gersonde, 1997; Armand et al., 2005). Sedimentary occurrences highest where February SSTs are -1.3 to 2.5°C and with highest February sea ice concentrations (Armand et al., 2005).
Porosira glacialis (Grunow) Jörgensen	Found in sea ice samples (Krebs et al., 1987) and extremely coastal waters with high ice concentrations (Hasle, 1976). Found in sediments that have >7.5 months/year sea ice cover, sea ice <30% during the summer and with winter ice concentrations of 65 – 85%. Maximum sedimentary abundances occur linked to February SST of 0 – 0.5°C (Armand et al., 2005; Pike et al., 2009).
Stellarima microtrias (Ehrenberg) Hasle and Sims	Found at high abundances in sea ice (Garrison et al., 1987; Krebs et al., 1987; Tanimura et al., 1990). Found in sediments that have >7.5 months/year sea ice cover, sea ice <30% during the summer and with winter ice concentrations of >65%. Maximum sedimentary abundances occur linked to February SST of -0.5 – 0.5°C (Armand et al., 2005).
Thalassiosira antarctica Comber	Dominant in meltpools/crackpools and in platelet ice communities underlying drift ice in the Weddell Sea (Smetacek et al., 1992; Gleitz et al., 1996) and seeded from sea ice (Gleitz et al., 1996). Commonly linked to low SST and sea surface salinity associated with the presence of sea ice (Villareal and Fryxell, 1983), but requires open waters to bloom (Barcena et al., 1998) and may be a major phytoplankton component in poorly- or non-stratified waters (Cremer et al., 2005). Maximum sedimentary abundances in regions with >6 months per year sea ice cover, winter sea ice >70% concentration and February SSTs of 0 to 0.5°C (Armand et al., 2005).

Table 3.02. Summary of ecological information from sea ice, water and surface sediment samples for common open ocean diatom species observed in this study. Plates of key diatom taxa are presented in Appendix 1.

Species	Ecological information
Corethron pennatum (Grunow) Ostenfeld in van Heurck	Commonly found in the PFZ associated with mixed surface waters and is able to migrate vertically within a mixed water column to take advantage of light near the surface and deeper nutrients (Fryxell et al., 1971; Crawford et al., 1997; Beans et al., 2008). Periods of sexual reproduction in surface waters are associated with rapid sedimentation of *C. pennatum* (Crawford, 1995). Sedimentary occurrences are typically associated with late spring mixing of surface waters (Fryxell et al., 1971; Bahk et al., 2003; Stickley et al., 2005; Maddison et al., 2006; Denis et al., 2010; Maddison et al., 2012).
Fragilariopsis kerguelensis (O'Meara) Hustedt	Dominates assemblages of the open ocean zone south of the Polar Front (Froneman et al., 1995), with its northern oceanic boundary occurring at the Sub-Tropical Front (Hasle, 1976). Maximum sedimentary occurrence is in the circum-Antarctic diatom ooze belt, where it may be the main component. Occurs in sediments in regions where February surface waters are 1 – 8°C and in sea ice-influenced areas that experience open water (<20% ice cover) conditions during the summer (Crosta et al., 2005b).
Phaeoceros Chaetoceros dichaeta Ehrenberg	Most common in the PFZ but also found in coastal wind mixed surface waters during the summer (Assmy et al., 2008; Beans et al., 2008). Increased sedimentary abundance in Adélie Land during the Holocene linked to increased wind strength (Denis et al., 2010).
Rhizosolenia antennata (Ehrenberg) Brown	Reported from waters in the sea ice zone through to the sub-Antarctic zone, with maximum occurrences in the cool open ocean waters of the PFZ (Fenner et al., 1976; Froneman et al., 1995). Maximum sedimentary occurrences north of the winter sea ice edge (Crosta et al., 2005b), with isolated occurrences in the sea ice zone (Maddison et al., 2006).
Thalassiosira gracilis (Karsten) Hustedt	Common in open ocean samples in the Weddell Sea, absent beneath sea ice or in crack pools (Gleitz et al., 1996). Widely distributed in sediments from the Antarctic coast northwards, with traces found north of the Polar Front. Maximum occurrences between the winter sea ice edge and the Antarctic coast, with a preference for open ocean conditions in the summer (Zielinski and Gersonde, 1997; Crosta et

Species	Ecological information
	al., 2005b) and maximum February temperatures of 1 – 2°C (Crosta et al., 2005b).
T. lentiginosa (Janisch) Fryxell	Common occurrences in the Southern Ocean south of the Polar Front (Johansen and Fryxell, 1985; Theriot and Fryxell, 1985; Priddle et al., 1986; Kopczyńska et al., 1998). Most commonly reported from sediments of the permanently open ocean zone and PFZ (Crosta et al., 2005b and references therein). Maximum sedimentary occurrences between the winter sea ice edge and the Sub-Antarctic Front, with a preference for 0 – 4 months per year sea ice cover and a notably similar distribution to *F. kerguelensis* (Crosta et al., 2005b). Has been found in high concentrations in sediments from the George Vth Coast (Leventer, 1992).

50 – 60% of total Southern Ocean productivity occurs in the MIZ (Smith and Nelson, 1986; Legendre et al., 1992); 4 – 5 times greater than that which occurs under sea ice (Burckle et al., 1987). When there is a strong influence of sea ice melting during the spring, high phytoplankton biomass characterised by high abundances of *Fragilariopsis curta, F. cylindrus* or *Hyalochaete Chaetoceros* occurs (Kang and Fryxell, 1992; Dunbar et al., 1998; Beans et al., 2008; Riaux-Gobin et al., 2011). In coastal areas, diatoms species typically associated with sea ice may be replaced during the summer by assemblages characterised by species most abundant in open ocean conditions (Crosta et al., 2005b; Crosta et al., 2008).

3.1.1.2 Open ocean diatoms

In contrast to the high diatom primary productivity of the sea ice influenced MIZ, the open ocean zone is characterised by relatively low phytoplankton productivity due to low levels of iron (Martin, 1990; Priddle et al., 1998) and high grazing pressure by zooplankton (Smetacek et al., 1997). This region is characterised by open ocean taxa including large centric diatoms and various species of *Rhizosolenia, Thalassiothrix* and *Pseudonitzschia* (Froneman et al., 1995; Selph et al., 2001; Crosta et al., 2005b). Seasonally higher primary productivity occurs north of the open ocean zone in the PFZ due to eddy-induced mixing of the surface waters which enhances the supply of nutrients (De Baar et al., 1995; Abbott et al., 2000). Spring blooms are triggered within

the PFZ by a combination of increasing irradiance and increased stratification (Abbott et al., 2000; Moore and Abbott, 2000) and have been observed to include monospecific blooms of *Fragilariopsis kerguelensis* (De Baar et al., 1995; Smetacek et al., 1997), *Corethron pennatum* and *C. inerme* (Smetacek et al., 1997). Other common diatoms observed in the PFZ include *Thalassiothrix antarctica, Thalassiosira lentiginosa, Phaeoceros Chaetoceros* spp. and *Hyalochaete Chaetoceros* spp. (Assmy et al., 2008). Ecological information for common open ocean diatom species in this study is presented in Table 3.02.

3.1.2 Diatom preservational biases

The use of diatoms as palaeoenvironmental indicators in the Antarctic region may be hindered by several environmental and taphonomic factors. Firstly, only a fraction of valves formed in the euphotic zone actually reach the sediment (potentially <1%, although it may be up to 30% on high latitude continental shelves; Ragueneau et al., 2000); further account must be taken of preferential dissolution between taxa, lateral transport of diatom tests by currents and the impact of grazers within the water column and in sediments (Leventer, 1998). Frustule size and degree of silicification also provide controls on the sedimentary distribution of diatoms. Smaller species such as *Fragilariopsis cylindrus* may be lost from sediments due to increased winnowing during periods with stronger bottom currents (Harris and Beaman, 2003), whereas lightly silicified diatoms are more prone to dissolution than those with heavier frustules, which have a higher sinking velocity and are buried more readily (Gersonde and Wefer, 1987). Large diatoms and diatom mats may also become entrained in the upper layers of the water column, increasing the time for which they are exposed to dissolution processes (Leventer, 1998) or to zooplankton grazing (Gersonde and Wefer, 1987). The presence of dissolution susceptible species such as *Corethron pennatum*, *F. cylindrus* and *Porosira glacialis* within sediments may be used to identify minimal differential preservation as a result of dissolution (Pichon et al., 1992).

Diatom species that typically occur in, or attached to, sea ice may also undergo preferential dissolution (e.g. *Amphipora* spp., *Nitzschia* spp., *Pinnularia* spp. and *Pleurosigma* spp.), resulting in few individuals reaching the sediment and rendering them unsuitable as palaeo-sea ice indicators (Riaux-Gobin et al., 2011). However, sea

ice associated species such as *F. curta* and *F. cylindrus*, and open ocean diatoms such as *Thalassiosira antarctica* and *F. kerguelensis* display better preservational tendencies and are typically considered more suitable for palaeo-reconstructions (Leventer, 1998). Despite these preservational problems, a suite of studies has demonstrated that diatom sedimentary abundances are well related to surface water hydrology (e.g. Jouse et al., 1962; Truesdale and Kellogg, 1979; Gersonde, 1986; Leventer, 1992; Pichon et al., 1992; Leventer and Dunbar, 1996; Zielinski and Gersonde, 1997; Cunningham and Leventer, 1998; Pike et al., 2008).

3.2 Highly Branched Isoprenoids

Highly branched isoprenoid (HBI) alkenes are common in many modern marine settings (Belt et al., 2000a). C_{25} HBIs (Figure 3.03) have been associated with diatoms in both the natural environment and laboratory cultures (Wraige et al., 1997; Belt et al., 2001; Grossi et al., 2004). C_{25} HBIs produced by the diatom *Haslea ostrearia* have between zero and five double bonds in the HBI structure (Wraige et al., 1997). The degree of unsaturation of HBIs produced by the species *Haslea ostrearia* is temperature, not salinity, dependent, with higher levels of unsaturation (more double bonds) occurring at relatively higher temperatures (Wraige et al., 1997; Rowland et al., 2001). This temperature dependence makes HBIs potentially useful proxy indicators of palaeotemperature.

3.2.1 Sea ice and HBIs

Brown et al. (2011) have recently reported the occurrence of an HBI monoene (IP_{25}; Figure 3.03a) and diene in sea ice samples from the Arctic Ocean, whilst Massé et al. (2011) report the occurrence of an HBI diene (Figure 3.03b) in Antarctic sea ice samples and an HBI triene (Figure 3.03c) from Antarctic MIZ phytoplankton. The high $\delta^{13}C$ signature (-5.7 to -8.5‰) of the HBI diene is consistent with its formation under the low CO_2 concentrations found within sea ice (Gibson et al., 1999; Kennedy et al., 2002; Belt et al., 2008), which contrasts with the lower $\delta^{13}C$ values of the triene (typically -38 to -41 ‰) (Massé et al., 2011). Trace amounts of $C_{25:3}$ trienes have been reported from sea ice communities (Nichols et al., 1993) and are similarly associated with diatoms, although the source species/genera are unknown. Hayakawa et al. (1996) have also reported $C_{25:1}$ and $C_{25:3}$ alkenes from sediment traps in Breid Bay (Queen

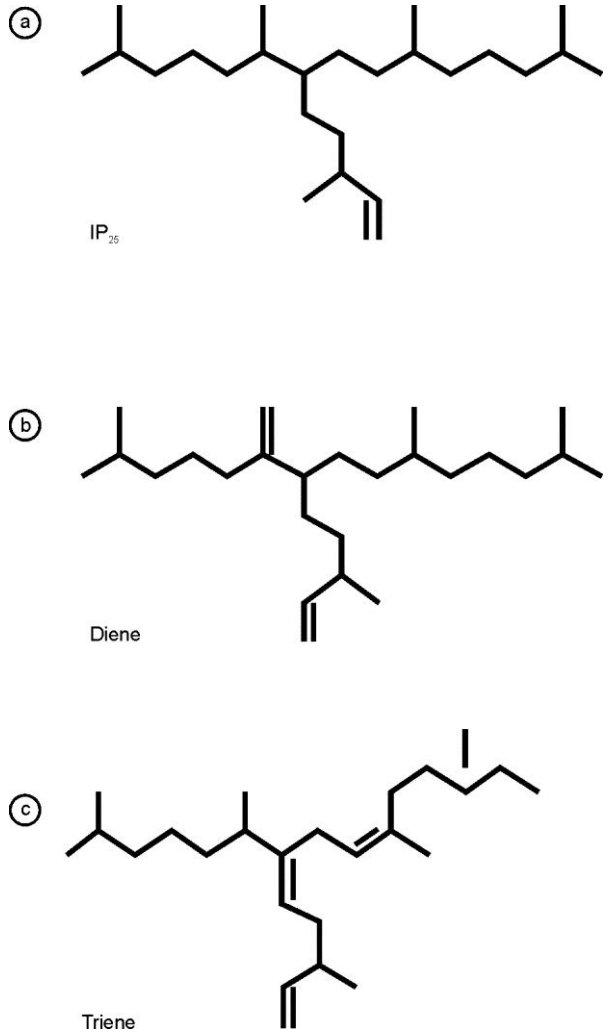

Figure 3.03. Structures of HBI hydrocarbons with 25 carbon atoms (C_{25}). (a) HBI monoene IP_{25} (Belt et al., 2007); (b) HBI diene ($C_{25:2}$), this study; (c) HBI triene ($C_{25:3}$), this study.

Maud Land) which are associated with a diatom source, noting high abundances of *Thalassiosira antarctica* in the sediment traps. Although it is uncertain as to the specific producer of HBIs in Antarctic sediments, the sea ice associated diatom *Fragilariopsis cylindrus* has been demonstrated by Damsté et al. (2004) not to be a producer of the molecules, and a similar lack of HBI production has been assumed for other *Fragilariopsis* species such as *F. curta* and *F. kerguelensis* (Massé et al., 2011).

3.2.2 HBIs as an indicator of palaeo-sea ice extent

Recently, a variety of studies have highlighted the potential of HBIs as a proxy for palaeo-sea ice extent in the Arctic (Belt et al., 2007; Massé et al., 2007; Masse et al.,

2008; Müller et al., 2009; Vare et al., 2009) and the Antarctic (Barbara et al., 2010; Denis et al., 2010; Collins et al., submitted manuscript). Initially, an HBI monoene (namely IP_{25}) was reported from sediment in samples in the Arctic (Belt et al., 2007) and has subsequently been found to be exclusively in sea ice and absent from phytoplankton samples (Brown et al., 2011). Together with a high $\delta^{13}C$ signature, consistent with formation under the low CO_2 concentrations found within sea ice (Gibson et al., 1999; Kennedy et al., 2002; Belt et al., 2008), and sedimentary concentrations that show a good correlation with historical records of sea ice extent (Masse et al., 2008), the IP_{25} monoene has been demonstrated as providing a reliable indicator of palaeo-sea ice extent on timescales ranging back to the last glacial maximum (e.g. Müller et al., 2009).

Unfortunately, the IP_{25} molecule to date has not been recorded in Antarctic sediments. However, a variety of C_{25} HBIs have been reported from Antarctic estuarine and coastal sediments, including an HBI diene which has been consistently associated with a sea ice diatom origin (Venkatesan, 1988; Nichols et al., 1989; 1993; Johns et al., 1999; Damsté et al., 2004; Massé et al., 2011) and an HBI triene found exclusively in phytoplankton. The diene is not exclusive to the Antarctic region, having been produced in laboratory cultures of the temperate diatom *Haslea ostrearia* (Johns et al., 1999) and noted in Arctic sediments (Massé et al., 2011). It has been demonstrated that the occurrence of HBI diene in Icelandic sediments reported by Massé et al. (2011) correlates very well with occurrences of IP_{25} in the same sediments, indicating a likely sea ice origin of the molecule. Given the occurrence of HBI diene in sea ice samples and triene in phytoplankton samples, it has been suggested that the ratio of diene to triene in sediments may provide an indicator of changes in sea ice versus open water over multimillenial (Holocene) timescales (Massé et al., 2011).

Denis et al. (2010) analysed changes in the diene/triene ratio throughout the Holocene from a suite of marine sediment cores collected in Adélie Land and Prydz Bay, East Antarctica, as a potential proxy for the relative input of sea ice and phytoplankton productivity to sediments. For the Prydz Bay region, a clear positive relationship between sea ice-associated diatoms (i.e. commonly preserved diatoms that are associated with the presence of sea ice, but do not necessarily live within it) and the ratio of diene/triene was observed, with both demonstrating an increase since ca. 4 cal.

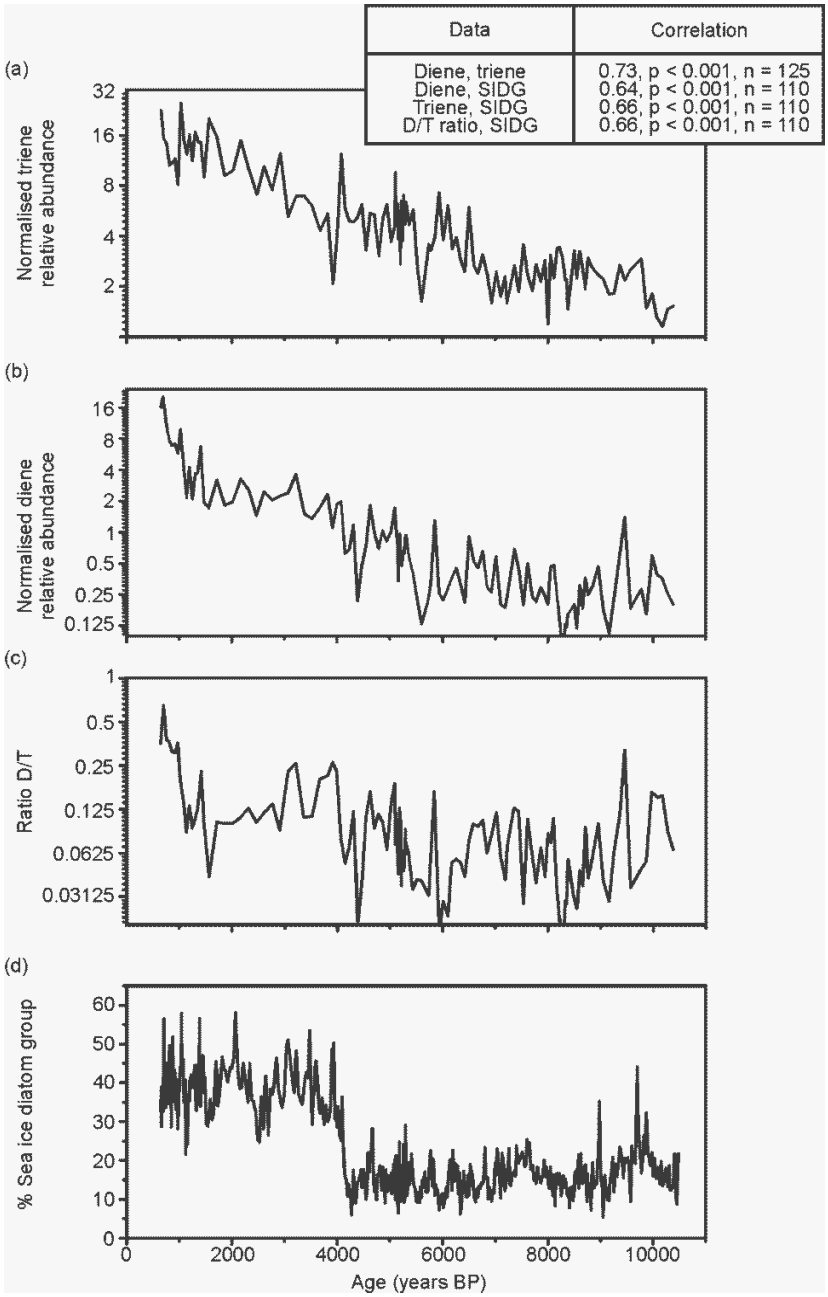

Figure 3.04. Holocene distribution of normalised relative abundances of (a) HBI diene, (b) HBI triene, (c) the ratio diene/triene and (d) the relative abundance of sea ice associated diatoms in core MD03-2601. Sea ice diatom group and Ratio D/T from Denis et al. (2010).

ka coincident with the onset of the Neoglacial. However, in Adélie Land the relationship between the ratio of HBIs and increases in sea ice associated diatoms is less clear (Figure 3.04). While the sea ice-associated diatoms sharply increase in abundance at ca. 4 cal. ka (driven by a threshold response of *F. curta* at 4 ka, the most abundant diatom within the group) the diene/triene ratio increase only slightly at ca. 4 cal. ka, and have a much more pronounced increase at ca. 1.5 cal. ka (Denis et al., 2010). Despite

the large step-wise increase in the sea ice associated diatom group, analysis of all three HBI parameters (diene, triene and the ratio D/T) demonstrates that a significant correlation exists between them and the relative abundance of sea ice associated diatoms (SIDG; Figure 3.04). It can be seen that the HBI triene increases slightly around 7 ka and increases continually from ca. 4 ka until present. In comparison, the HBI diene increases slightly at around 4 ka, followed by a more dramatic increase ca. 1.5 ka (which drives the ratio D/T; Figure 3.04). The increase in HBI diene and triene, and sea ice associated diatoms at 4 ka suggests that the sedimentary records of these molecules is linked to increases in sea ice concentrations and this can be used to infer that the ratio D/T is not recording changes in the relative contributions of sea ice diatoms versus planktonic diatoms, as suggested previously (Barbara et al., 2010; Denis et al., 2010; Massé et al., 2011). The different nature of the increases in the proxies at the mid-Holocene transition (a sharp, pronounced increase in the diatom record compared to subtler increases in HBI concentration) suggests that whilst they may both record changes in seasonal sea ice presence, the HBIs are recording an aspect of the sea ice environment (e.g. fast ice) that is not recorded by commonly preserved diatoms.

3.2.3 Stability of HBIs

Polyunsaturated HBI molecules may be unstable in sedimentary systems, particularly in the presence of sulphur species that react with the double bonds (Belt et al., 2000b; Sinninghe Damste et al., 2007). Monoene and diene molecules may be more stable in sediments compared to more unsaturated HBIs, with double bond migration and isomerisation (reorganisation of the structure but not composition of the molecule) of dienes observed by Belt et al. (2000b). Belt et al. (2000b) note that the presence of clays in sediments may act as a catalyst for isomerisation and found that although some trienes may experience both isomerisation and cyclisation (restructuring of the molecule to produce a ringed structure), the triene molecule used in this study does not experience this. A lack of sulphur molecules and HBI sulphides (c.f. Sinninghe Damste et al., 2007) in analyses of the sediments from MD03-2601 (G. Massé, pers comm., 2012) indicates that sulphurisation of HBIs is not a problem in this study. Furthermore, the study of Sinninghe Damsté et al. (2007) which suggests that sulphurisation of HBI molecules may provide a significant diagenetic control on their distribution is from an

anoxic fjordal environment, which is a strong contrast to the open ocean conditions of core site MD03-2601.

3.2.4 Hypotheses for HBI distribution in core MD03-2601

Given the known association between the HBI diene molecule and sea ice, the HBI triene molecule and MIZ conditions and the potential of these molecules as a palaeo-proxy of these outlined above, the working hypotheses for HBI distributions are:

1) Elevated HBI diene concentrations should correspond to the occurrence of spring laminae.
2) Elevated HBI triene concentrations should correspond to the occurrence of late spring/summer laminae.

3.3 Summary

This chapter has described the principal proxies used in this study. Key diatom species and their ecological associations have been introduced, as well as their use as a sedimentary proxy of past sea ice extent. The use of diatom-derived HBI biomarkers as a sedimentary proxy for sea ice occurrence in both hemispheres has also been introduced. Analysis of the data available from low-resolution observations of MD03-2601 demonstrates the significant correlation between HBI polyenes and sea ice associated diatoms over the Holocene, indicating that the sedimentary distribution of both molecules is linked to changes in the sea ice environment.

Chapter 4. Materials and methods

This chapter presents the location, description and core collection/storage details of marine sediment cores MD03-2601 and IODP Site 318-U1357B. The previously published age model for MD03-2601 (Crosta et al., 2007; Denis et al., 2009b) is presented here recalibrated using the ^{14}C calibration curves (Reimer et al., 2009) and the age model for IODP-318-U1357B is presented using the same calibration. The scanning electron microscope (SEM) methods used for sediment microfabric and qualitative diatom abundance analysis; the optical microscope methods used for quantitative diatom assemblage analysis, the gas chromatography-mass spectrometry (GC-MS) methods used for highly branched isoprenoid analyses; and the statistical analysis methods applied to these datasets are also presented in this chapter.

4.1 Core MD03-2601

Giant piston core MD03-2601 was recovered from the Dumont d'Urville Trough, East Antarctic margin (66°03.070'S, 138°33.430'E, 746 m water depth, 40.24 m long) during R.V. *Marion Dufresne II* IMAGES cruise number MD130 X- Coring of Adélie Diatom Oozes (X-CADO) in February 2003 (Crosta et al., 2005). MD03-2601 was subsampled using metal trays 1 cm deep, 7 cm wide and 155 cm long and archived at Université Bordeaux I. Trays were wrapped in cling film and stored at <4°C in order to prevent desiccation and inhibit microbial action/mould growth. Core sections with well-preserved laminae were selected for thin section analysis using positive X-ray images of trays created using the SCOPIX image-processing tool (Figure 4.02; Migeon et al., 1999; Denis et al., 2006). Intervals from previously identified contrasting climatic periods of the Holocene and the transition between them were selected for sampling (Fig. 2; Crosta et al., 2007; Pike et al., 2009). Sections XVII (2250 – 2400 cm core depth; 6.4 – 6.8 cal. ka) and IX (1200 – 1350 cm core depth; 4.8 – 5.1 cal. ka) sample the relatively warm Hypsithermal phase, which is characterised by high relative abundances of *Fragilariopsis kerguelensis* and low relative abundances of cryophilic species, in particular *F. curta*. This is exemplified by the ratio of *F. curta* : *F. kerguelensis* relative abundances (Figure 4.01; Crosta et al., 2007) that increases in core section VIII (1050 – 1200 cm; 4.4 – 4.8 cal. ka) and marks the initial transition between warm Hypsithermal and cool Neoglacial conditions. Core section III (300 – 450 cm;

1.5 – 1.8 cal. ka) is representative of the cooler Neoglacial phase as indicated by high ratios of *F. curta* : *F. kerguelensis* and high ratios of *Porosira glacialis* RS : *Thalassiosira antarctica* RS (Figure 4.01; Pike et al., 2009), in which values >0.1 are indicative of sea ice cover for >7.5 months per year. The ratio of *P. glacialis* RS : *T. antarctica* RS increases slightly later that the *F. curta* : *F. kerguelensis* ratio due to the preference of vegetative *P. glacialis* for slightly icier spring surface water conditions than *F. curta* (Armand et al., 2005; Pike et al., 2009).

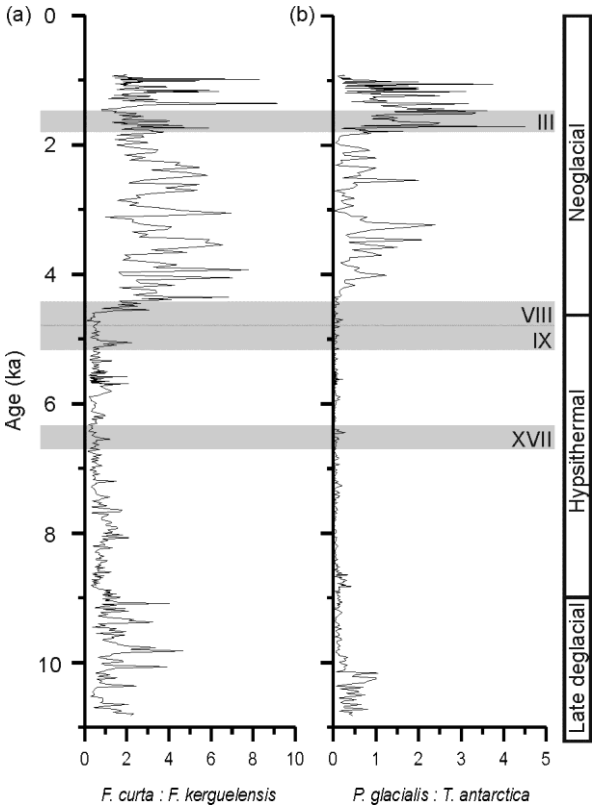

Figure 4.01. Selection of core sections (grey boxes) relative to the Hypsithermal and Neoglacial climatic intervals in, as indicated by changes in core MD03-2601 of (a) the ratio of *Fragilariopsis curta* to *F. kerguelensis* relative abundances (Crosta et al., 2007); (b) the ratio of *Porosira glacialis* RS to *Thalassiosira antarctica* RS (Pike et al., 2009).

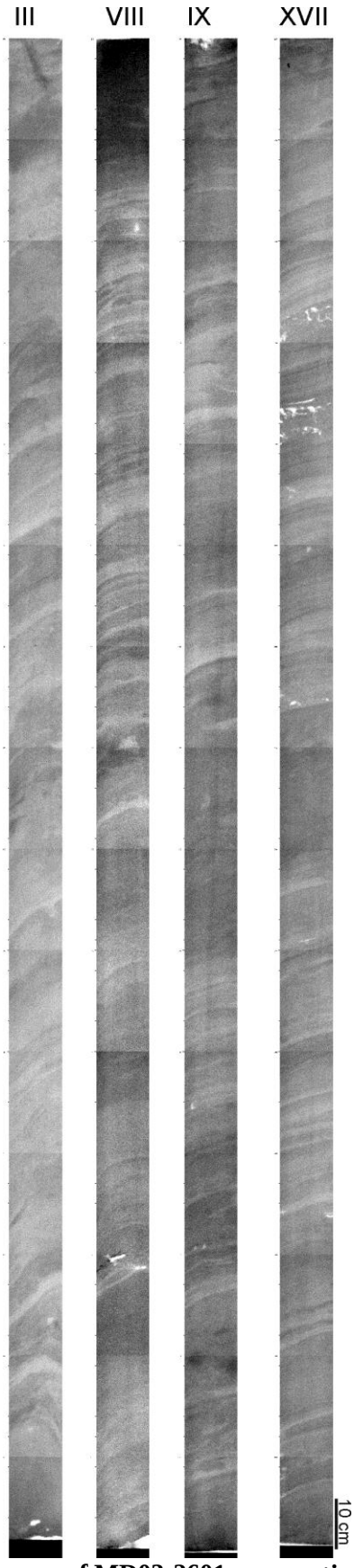

Figure 4.02. Positive X-ray images of MD03-2601 core sections used in this study. Section III (300 – 450 cm; the Neoglacial), Section VIII (1050 – 1200 cm; the mid-Holocene transition), Section IX (1200 – 1350 cm; the Hypsithermal) and Section XVII (2250 – 2400 cm; the Hypsithermal).

4.1.1 Core MD03-2601 sedimentary description

Core MD03-2601 is composed entirely of Holocene diatomaceous ooze (Crosta et al., 2007). Although homogenous to the naked eye, the sediments are observed to alternate between laminated and massive facies when viewed using positive X-ray imagery (Denis et al., 2006). Occasional macroscopic bioturbation structures are also observable in X-ray images.

4.1.2 Age model for core MD03-2601

The age model for core MD03-2601 (Figure 4.03) is based on nine radiocarbon ages on the humic acid fraction of bulk organic matter and was originally presented in Crosta et al. (2007). A variety of marine reservoir age corrections exist for Antarctic marine sediments (Ingolfsson et al., 1998 and references therein) which are commonly derived from the dating of intact moluscan shells. In order to overcome differences in age models between studies, early studies suggested using a correction age of 1300 years based upon comprehensive review of the available data (Berkman et al., 1998; Ingolfsson et al., 1998). Although slightly higher than the recently reported mean circum-Antarctic reservoir age of 1144 ± 120 years for sediments <6000 years old (Hall et al., 2010), the 1300 years ^{14}C reservoir correction is still widely applied to organic matter-rich Holocene sediments from the Adélie Land margin and the adjacent George V coast (e.g. Pudsey and Evans, 2001; Presti et al., 2003; Crosta et al., 2007). Maddison et al. (2012) applied a 1200 year correction to carbonate samples and 1600 year correction to organic matter samples in Adélie Land cores. The nine ages from core MD03-2601 (Figure 4.02) have been re-calibrated using the Marine 09 calibration curve (Reimer et al., 2009) and clam 2.1 age modelling scripts (Blaauw, 2010) in the statistical software package R 2.15.0 and assuming a total reservoir age correction of 1300 years, consistent with previous studies (Ingolfsson et al., 1998; Berkman et al., 1998). In comparison to the previously published age models for MD03-2601 (Crosta et al., 2007; Denis et al., 2010; Denis et al., 2009b), the revised age model produced in this study provides broadly similar values to those of Denis et al. (2009b, 2010) that are slightly older than those of Crosta et al. (2007) due to the up-to-date calibration curve employed here (Table 4.02).

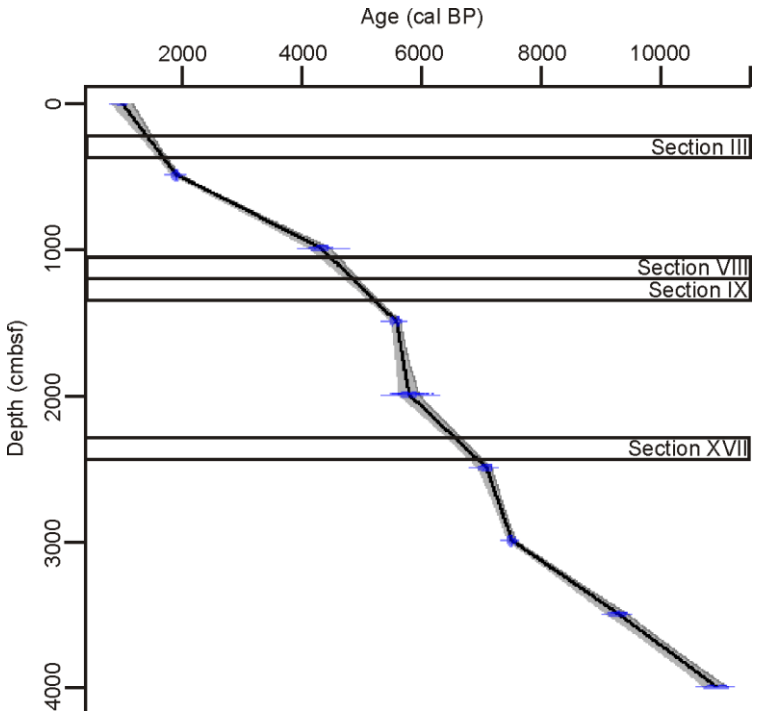

Figure 4.03. Calibrated age model for core MD03-2601 (D. Hodgson, pers. comm., 2012) showing 9 ages obtained from humic fraction of organic carbon (blue squares). Blue error bars indicate the 2 σ age range (Table 4.01). Grey envelope indicates the estimated modelled error for the interpolation between data points. Core sections sampled in this study are indicated by white boxes.

4.2 Core IODP-318-U1357B

Core IODP-318-U1357B was recovered from the Adélie Basin located on the Antarctic continental shelf off the Wilkes Land margin (66°24.7990′S, 140°25.5705′E, 1028 m water depth, total length 170.7 m) in February 2010 by IODP Wilkes Land Expedition 318 scientists (IODP Expedition 318 Scientists, 2010). The core was split in Victoria,

Table 4.01 Uncalibrated radiocarbon ages (Crosta et al., 2007) of sediment samples from core MD03-2601. Raw radiocarbon ages were calibrated using clam 2.1 (Blaauw, 2010) using the Marine 09 calibration curve (Reimer et al., 2009) and a total reservoir correction of 1300 years.

Depth (cmbsf)	Sample type	Raw age (^{14}C BP)	+/- (years)	2σ range (years)	Mean age (cal. years BP)
2	Organic carbon	2350	70	856 – 1170	1013
498	Organic carbon	3235	30	1864 – 2048	1945
998	Organic carbon	5175	60	4215 – 4558	4386.5
1498	Organic carbon	6135	35	5513 – 5690	5601.5
1998	Organic carbon	6310	100	5577 – 5986	5781.5
2498	Organic carbon	7450	40	6495 – 7186	6840.5
2998	Organic carbon	8775	40	7417 – 7557	7487
3498	Organic carbon	9570	50	9219 – 9462	9340.5
3998	Organic carbon	10855	45	10721 – 11099	10910

Table 4.02. Comparison of age models for core MD03-2601 between this study and previously published age models of Crosta et al. (2007) and Denis et al. (2009a).

Depth (cmbsf)	Raw age (^{14}C years BP)	Crosta et al. (2007) (cal. years BP)	Denis et al. (2009a) (cal. years BP)	This study (cal. years BP)
2	2350	916	1002	1013
498	3235	1871	1951	1945
998	5175	4314	4388	4386.5
1498	6135	5496	5598	5601.5
1998	6310	5703	5782	5781.5
2498	7450	6984	7069	6840.5
2998	7885	8369	8344	7487
3498	9570	9208	9348	9340.5
3998	10855	10742	10923	10910

Canada, on board the drill ship *JOIDES Resolution,* in July 2010 and subsampled, using the sediment slab cutter technique outlined in Section 4.3, to produce sediment slabs with approximate dimensions of 15 x 4 x 1 cm. The youngest material that was consolidated enough for use with the sediment slab cutter was selected for thin section analysis. The resulting sediment slabs were wrapped in cling film to prevent desiccation, then shipped to, and stored in refrigeration, Cardiff University at <4°C in order to prevent desiccation and inhibit microbial action/mould growth.

4.2.1 Core IODP-318-U1357B sedimentary description

There is no sedimentary log description of core IODP-318-U1357B currently available; however, a parallel core (IODP-318-U1357A totalling 186.6 mbsf) collected 50 m to the west of U1357B was described on the ship immediately after recovery. Core U1357A consists of three distinct lithological units. Unit III (185 – 186.6 mbsf) consists of ~1.6 m of glacial diamict; a gravelly siltstone with a carbonate cement. Unit II (170 – 185 mbsf) comprises ~15 m of sand- and silt-bearing diatom ooze. Unit I (0 – 170 mbsf) consists of continuously laminated diatom ooze of Holocene age. Unit I diatom ooze is principally composed of Antarctic diatoms, although silicoflagellates,

Figure 4.04. Core photographs of sections IODP-318-U1357B -4H-5-A (27.09 – 28.49 mbsf), -4H-6-A (28.49 – 29.88 mbsf) and -4H-7-A (29.88- 30.72 mbsf).

radiolaria and foraminifera are also present, as well as 44 discrete layers of fish bones (IODP Expedition 318 Scientists, 2010). Sediment sections sampled for this study (U1357B-4H-5, U1357B-4H-6 and U1357B-4H-7 from 27.5 – 31.4 mbsf) are composed of continuously laminated diatomaceous ooze (Figure 4.04) with alternating bands of brown-green and black sediments and are from Unit I observed in core U1357A.

4.2.2 Age model for core IODP-318-U1357B

A total of 29 radiocarbon ages are available for core IODP-318-U1357B (Figure 4.05) obtained from an acid only treatment of organic carbon (R. Dunbar, pers. comm. 2010; see section 4.2.2 for details on reservoir age and calibration). The majority of these (28 dates) fall within the deglacial to Holocene period (ca. 12 ka to present), with one value of ca. 39 ka recorded at 170.59 mbsf, presumably from Unit III. The age of 39 ka in

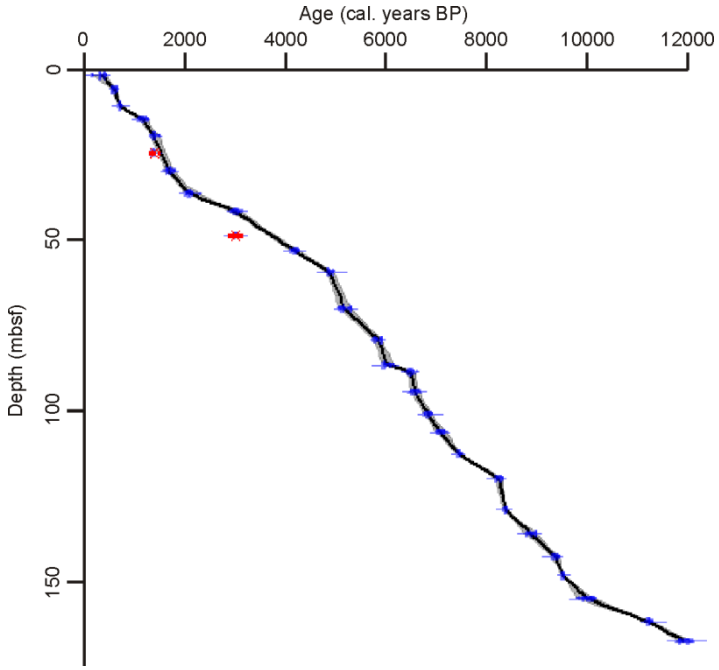

Figure 4.05. Calibrated age model for IODP-318-U1357B (black line) showing 28 radiocarbon ages (blue squares) of deglacial and Holocene data points (D. Hodgson, pers. comm., 2012). The age model was calculated using the Marine 09 calibration curve (Reimer et al., 2009) and excludes the sample dated to 40283.5 years BP (Table 4.03) that is interpreted as representing older glacial sediments. Two data points that represent small age inversions (red points) were also excluded from the age mdoel. Blue error bars indicate the 2 σ age range (Table 4.03). Grey envelope indicates the estimated modelled error for the interpolation between data points.

Unit III represents older glacial material that is not contiguous with the deglacial and Holocene sediments, suggestive of a hiatus or reduced glacial deposition at the site; hence it is excluded from the age model. Two Holocene dates (see Table 4.03 and Figure 4.05) were excluded from the age model as they represent small age inversions that may have resulted from sample contamination during sampling (R. Dunbar, pers. comm. 2012). The age vs. depth relationship was calculated from the remaining 26

Table 4.03. Uncorrected radiocarbon ages (R. Dunbar, pers. comm. 2010) and calibrated calendar ages for core IODP-318-U1357B. Raw radio carbon ages were calibrated against the Marine 09 calibration curve (Reimer et al., 2009) using clam 2.1 (Blaauw, 2010) with a total reservoir correction of 1300 years. Italicised mean calibrated ages were excluded from the age model (see text).

Top (mbsf)	Raw age (^{14}C years BP)	± (years)	2σ range	Mean age (cal. years BP)
2	1575	35	262 – 414	320.5
6.02	1890	35	517 – 638	578
10.9	2085	30	659 – 791	725
14.8	2525	30	1107 – 1266	1186.5
19.67	2805	30	1363 – 1529	*1449.5*
24.69	2795	30	1354 – 1520	1441.5
29.93	3080	30	1691 – 1860	1775.5
36.55	3410	30	2091 – 2292	2191.5
41.8	4180	30	3002 – 3228	*3125*
48.82	4180	35	2993 – 3237	3115
53.25	5100	30	4186 – 4400	4293
59.57	5610	35	4836 – 5037	4936.5
70.22	5845	30	5209 – 5419	5314
79.4	6430	30	5848 – 5991	5919.5
86.76	6535	40	5928 – 6159	6043.5
88.76	7010	30	6448 – 6630	6539
94.67	7080	45	6493 – 6731	6612
101.12	7300	35	6772 – 6980	6876
106.43	7495	30	7013 – 7216	7114.5
112.76	7835	30	7382 – 7512	7447
119.96	8705	35	8182 – 8352	8276.5
128.99	8860	30	8354 – 8503	8411
136.21	9315	30	8946 – 9118	9032
142.85	9650	30	9358 – 9501	9429.5
148.3	9845	30	9516 – 9693	9604.5
155.18	10170	30	9997 – 10200	10136.5
161.87	11125	40	11145 – 11276	11204
167.63	11535	35	11827 – 12098	11962.5
170.59	36620	1040	37891 – 42154	*40283.5*

ages using clam 2.1 (Blaauw, 2010) and the mean calibrated age range for the sediments sampled here is 1609 – 1759 cal. years BP.

4.3 Laboratory methods

4.3.1 Thin section preparation and microfabric data collection

Core MD03-2601 was sampled for polished thin section production by cutting 11 cm strips of sediment, 1 cm wide, perpendicular to the laminated sediment fabric along the length of each core section (sampled by TRG in full). Strips were taken with a 1 cm overlap relative to each other in order to provide a continuous record along the entire 1.5 m section (Figure 4.06a). Core IODP-318-U1357B was sampled using a sediment slab cutter (Schimmelmann et al., 1990) to minimise any disturbance of the sedimentary fabric (sampled by C. Riesselman and R. Dunbar). Samples were taken every 15 cm with a 1 cm overlap to allow for continuity along the sections (Figure 4.06b). The

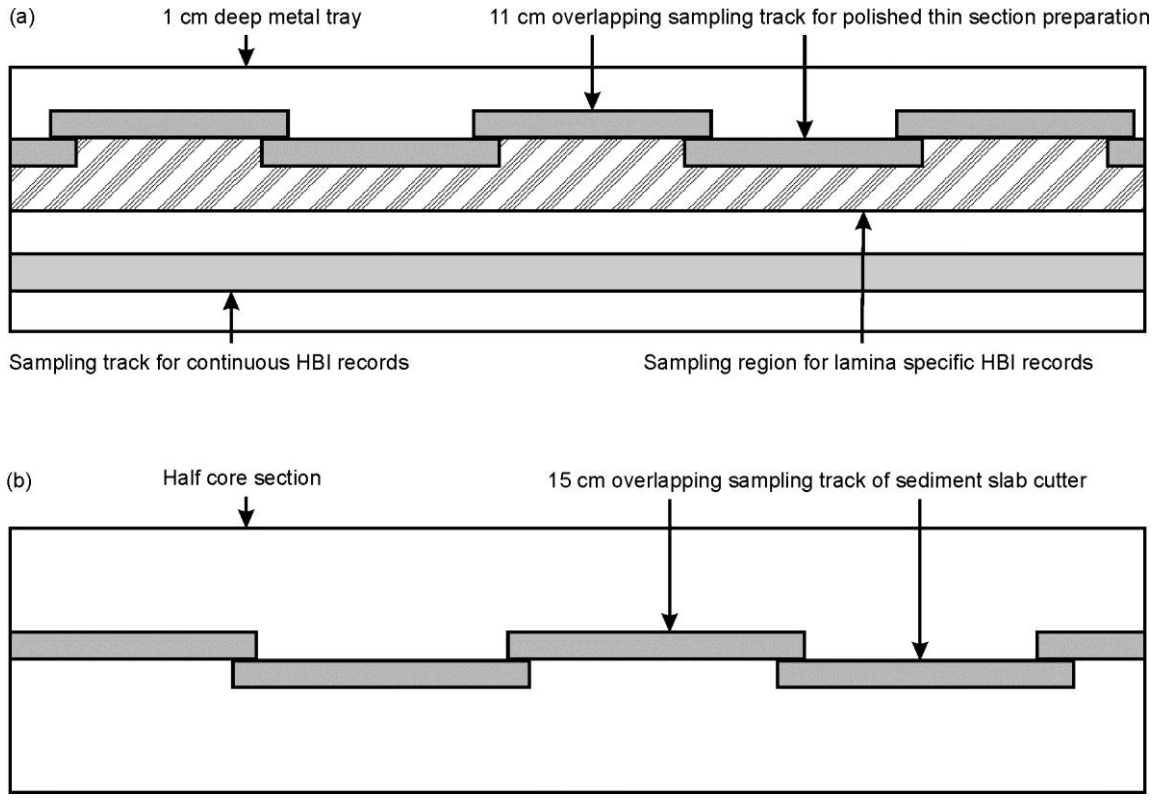

Figure 4.06. Schematic diagram of the sampling strategy for (a) producing polished thin sections and sediment samples for HBI analysis from 1 cm deep metal trays taken from core MD03-2601; (b) producing polished thin sections by sampling a half core section with a sediment slab cutter on core 318-U1357B. Images are not to scale.

sediment strips from both cores were sub-divided (by TRG) into overlapping sections 3.5 – 4 cm long (Figure 4.07) and wrapped in perforated aluminium foil in order to preserve their structure and allow penetration of acetone and resin into the sediment during fluid displacive embedding (Pike and Kemp, 1996; Pearce et al., 1998; Jim, 1985). During sampling of core MD03-2601, half of the core section was kept covered with cling film, and protective gloves were worn in order to prevent contamination of the sediments that remained for HBI analysis. The fluid displacive embedding technique allows production of highly polished thin sections that preserve the original structure of the sediment for studying with an SEM. In this study, the published technique (Pike and Kemp, 1996) was altered to include the use of TAAB® Low Viscosity Resin as an alternative to the toxic Spurr resin used in previous studies. Initially, samples were soaked in laboratory grade acetone which was exchanged three times per day for a total of nine exchanges. Next, the samples were soaked in analytical grade acetone which was exchanged three times a day for a total of six exchanges. This technique allows dehydration of the samples without causing desiccation, as water in the pore spaces of the sediment is replaced by acetone. Following pore fluid replacement by acetone, the sediment samples were soaked in TAAB® Low Viscosity Resin which was exchanged at 12 hour intervals for a total of ten exchanges. In initial exchanges, the resin was diluted with acetone but this was gradually reduced so that the final three exchanges were with pure resin (Table 4.04). After the final exchange, the samples were left to stand for three – four weeks prior to curing. The samples were cured at higher temperatures than those suggested in published methods for Spurr resin, allowing for 24 hours at each of 45°C, 60°C, 75°C and 90°C, allowing an eight hour cooling period between each temperature step. Finally, highly polished thin sections were produced by fixing cured samples to glass slides with araldite and cutting on a diamond saw so that ~0.5mm was attached to the slide. The section is then given a coarse polish for 2 minutes each at 250 rpm on 320, 800 and 1200 European grade polishing papers. Thin sections are then polished on a 6 μm diamond polishing paper for 30 minutes, then 15 minutes on 3 μm and 15 minutes on 1 μm diamond polishing papers.

Polished thin sections were examined with back scattered electron imagery (BSEI) using a Cambridge Instruments S360 SEM. A series of overlapping images were taken at a low magnification (x20) to produce a photomosaic, which served as a map of each

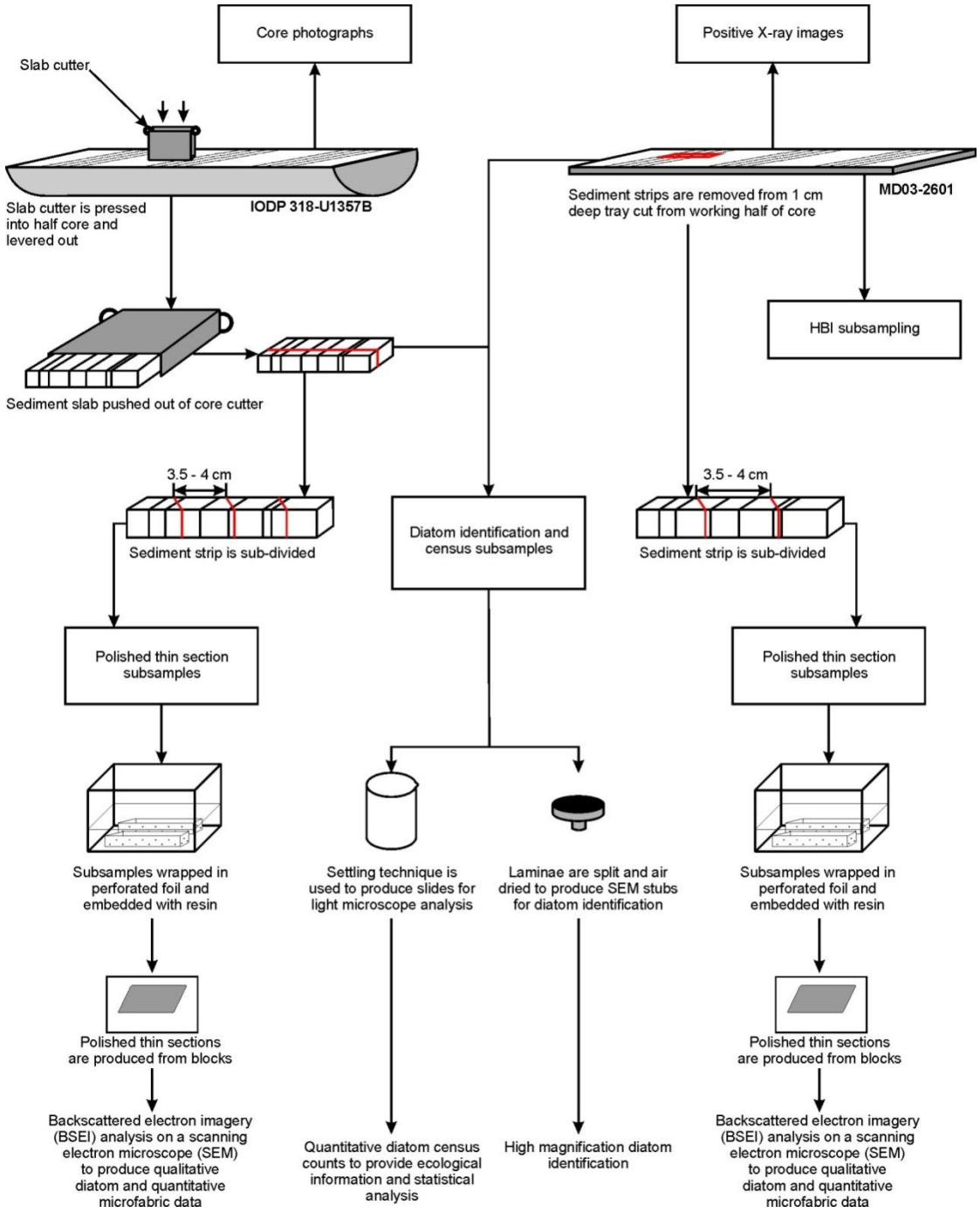

Figure 4.07. Summary of sampling methods and analysis techniques, adapted from Dean et al. (1999) and Maddison (2005).

thin section with brighter (high backscatter) images produced by laminae that contain relatively more terrigenous material and dark (low backscatter) images produced by organic-rich laminae (Figure 4.08). A qualitative analysis of visually-conspicuous diatoms was carried out using a combination of the photomosaics and higher magnification images (x100 – x850), allowing for sedimentary fabric analysis and

Table 4.04. Schedule of exchanges and ratios of chemical components for producing TAAB® Low Viscosity Resin embedded sediment blocks. The indicated resin components are TAAB® LV Resin monomer (resin), TAAB® Hardener VH2 (hardener) and TAAB® Low Viscosity Resin Accelerator (accelerator).

Resin mixture (resin: hardener : accelerator)	Resin : acetone	Exchange number
0.47 : 0.51 : 0.02	0.6 : 0.4	1-3
0.47 : 0.51 : 0.02	0.73 : 0.27	4-5
0.47 : 0.51 : 0.02	0.87 :0.13	6-7
0.47 : 0.51 : 0.02	1 : 0	8-10

identification of lamina types based upon diatom assemblage (Pike and Kemp, 1996; Maddison et al., 2006). An average of five thickness measurements per lamina (Appendix 2; mean standard error of measurements = ±0.05 mm per lamina) were taken from the thin section maps and corrected for expansion of the sediments that occurred during the resin embedding. Expansion was calculated for each thin section by

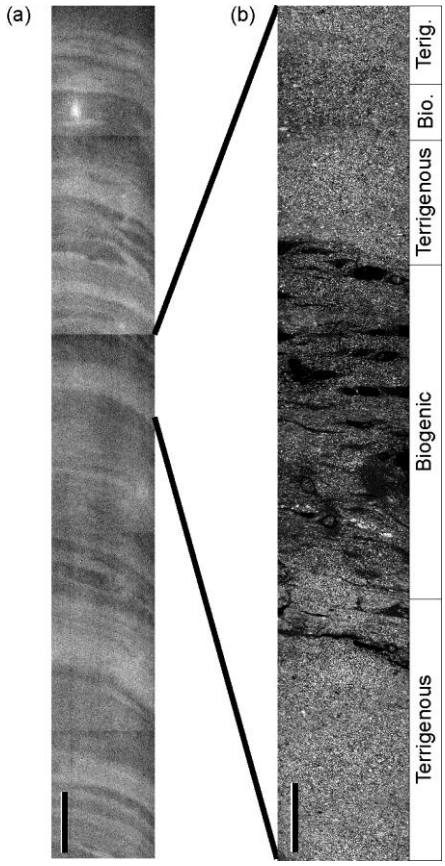

Figure 4.08. Examples of (a) X-ray image of sediment slab taken from core MD03-2601 (scale bar = 3 cm). (b) Low magnification BSEI photomosaic (scale bar = 3 mm) demonstrating alternating dark (biogenic) and light bands (higher terrigenous material).

measuring the length of the thin section before and after the resin embedding process in order to calculate the percentage by which the length of the section had changed. The measured embedded lamina thickness was then corrected back to the original lamina thickness by dividing by this mean percentage.

4.3.2 Quantitative diatom analysis

To provide a quantitative control on lamina diatom assemblages and concentrations, discrete samples were collected from each lamina type identified using BSEI analysis. A minimum of four samples per lamina type were prepared for assemblage analysis using the method of Scherer (1994) and fixed with Norland Optical Adhesive (refractive index 1.56). Samples were counted at x1000 magnification with an Olympus BX40 microscope using phase contrast. For core MD03-2601, at least 500 diatom valves were counted per sample. For core IODP 318-U1357B, which contained higher abundances of *Hyalochaeate Chaetoceros* resting spores (CRS), at least 500 valves were counted including CRS and a minimum of 250 valves were counted excluding CRS. This counting method is commonly applied in CRS-rich diatom samples from the Antarctic margin and allows ecologically important, but less abundant, species to be assessed (Leventer and Dunbar, 1996; Allen et al., 2005). Relative abundances of diatoms were calculated from MD03-2601 as a percentage of the total diatom assemblage, and for IODP 318-U1357B as a percentage of CRS-free counts. Diatom concentrations (valves/gramme dry sediment) were calculated as:

$$T = (NB/AF)/M$$

where

T = number of diatom valves per gramme dry sediment

N = total number of diatom valves counted

B = area of bottom of beaker (mm^2)

A = area per field of view (mm^2)

F = number of fields of view counted

M = dry mass of sample (g)

Diatom taxonomy followed Hasle and Syvetsen (1997) with additional references for the genera *Rhizosolenia* (Armand and Zielinski, 2001), *Thalassiosira* (Johansen and Fryxell, 1985) and *Fragilariopsis* (Cefarelli et al., 2010). Fragmented valves were included in counts following Zielinski (1993) and the criteria employed in this study are illustrated in Figure 4.09.

4.3.3 Highly Branched Isoprenoid analysis

Sediment samples 1cm^3 were collected by TRG every 1cm along core sections III, VIII and XVII of core MD03-2601, parallel to thin section samples (Figure 4.06). Further sample preparation and analysis was conducted by TRG in the LOCEAN laboratory at Université Pierre et Marie Curie, Paris, with assistance from Vincent Klein. Samples were freeze dried, weighed and then crushed using a mortar and pestle. Two internal standards (7-hexylnonadecane (7-HND) and 9-octylheptadec-8-ene (9-OHD); 0.1µg per standard) were added to the freeze-dried and crushed sediment in order to allow quantification of HBI isomers using gas chromatography-mass spectrometry (GC-MS). Lipids were extracted three times using a total of 10 ml per sample of a CH_2Cl_2/CH_4OH

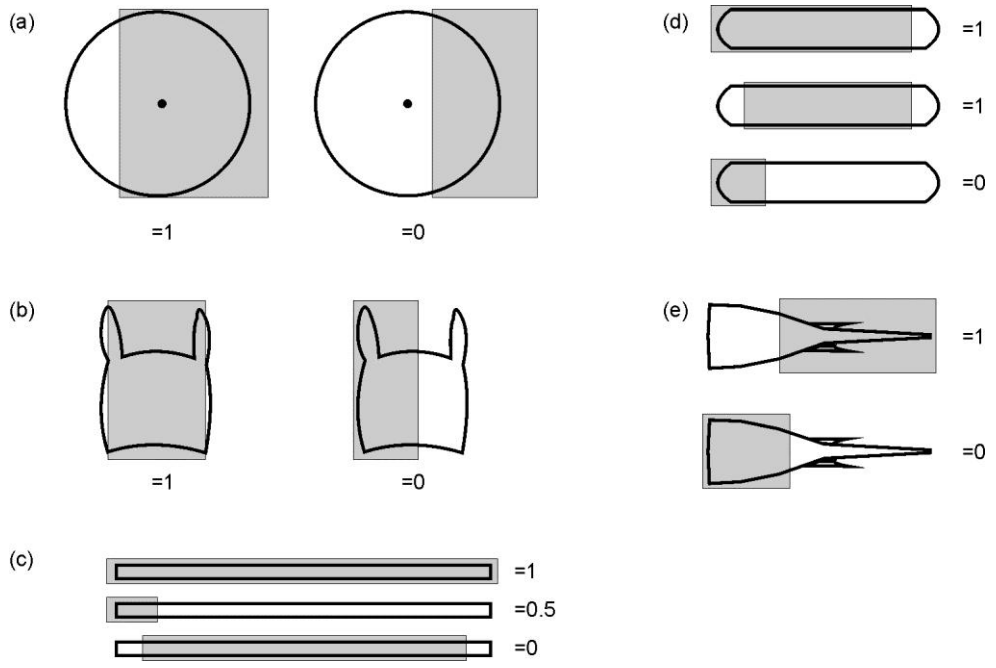

Figure 4.09. Counting method for fragmented diatom valves, adapted from Maddison (2005). Shaded area represents observed portion of diatom under microscope for (a) centric diatoms, e.g. *Thalassiosira* spp., *Porosira glacialis*; (b) *Phaeoceros Chaetoceros* vegetative cells and *Eucampia antarctica* (vegetative cells and resting spores); (c) needle-like diatoms, e.g. *Pseudonitschia* spp., *Thalassiothrix antarctica*; (d) pennate diatoms, e.g. *Fragilariopsis* spp.; (e) solenoidal diatoms, e.g. *Rhizosolenia* spp.

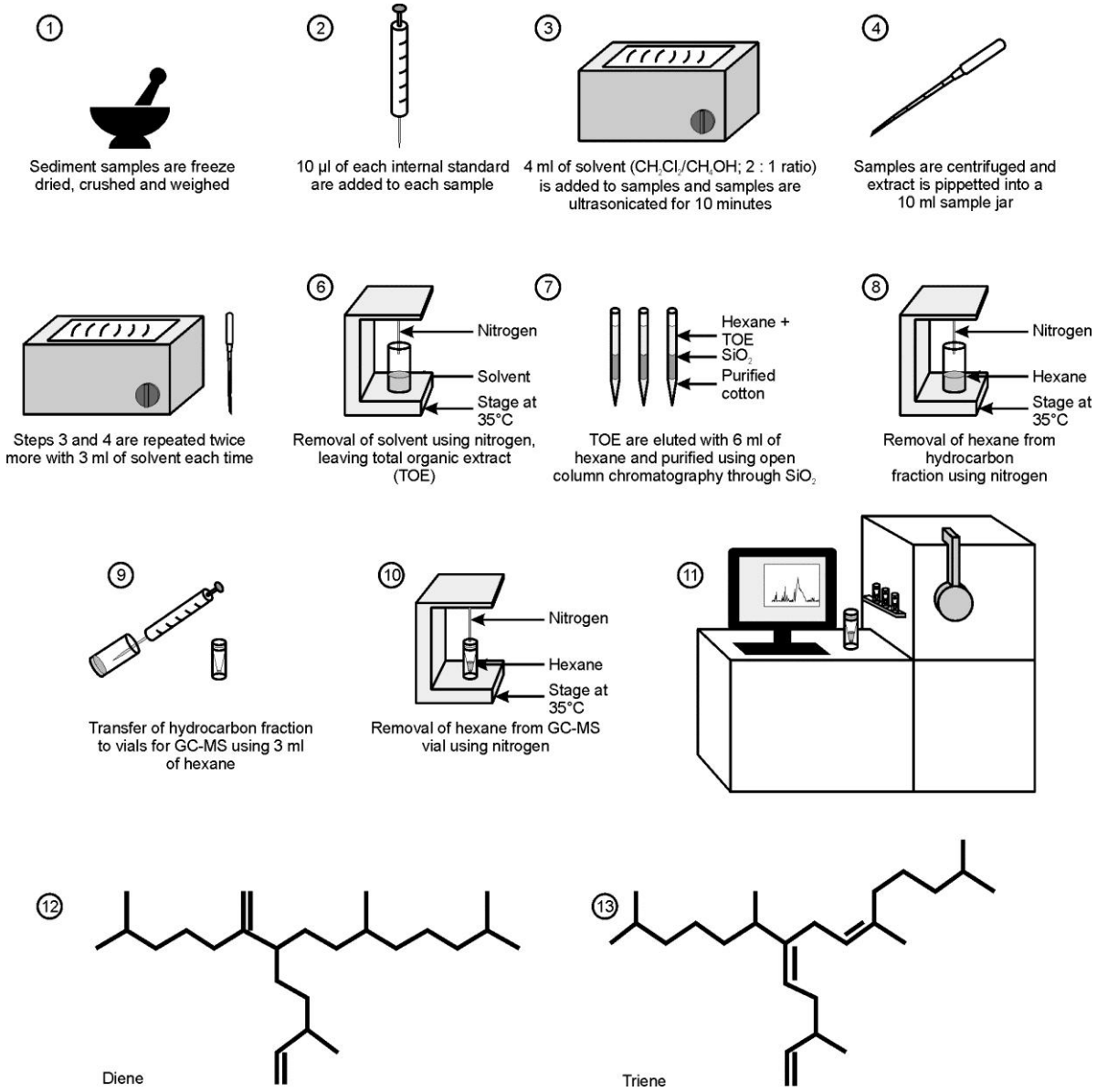

Figure 4.10. Sampling steps for HBI analysis. (1) – (6) extraction of organic material from sediment with a CH2Cl2/CH_4OH (2 : 1) mixture; (7) – (8) open column chromatography purification of TOE to obtain hydrocarbon fraction; (9) – (11) transfer of hydrocarbon fraction to GC-MS vials and analysis by GC-MS; (12) Structure of HBI diene; (13) Structure of HBI triene.

(2:1) mixture (Bligh and Dyer, 1959). Extracts were purified using open column chromatography (SiO_2) with 6 ml of hexane (Belt et al., 2007; Belt et al., 2012) (Figure 4.10). GC-MS analysis was performed on the hydrocarbon fraction using a Hewlett-Packard 5890 Series II gas chromatograph (GC) fitted with a 30 m fused silica HP-1 column (0.25 mm internal diameter, 0.25 mm film) and coupled to a 5970 Series mass selective detector (Massé et al., 2011). Identification of HBI isomers was by

comparison of their respective GC retention indices to previously published mass spectra of Antarctic HBIs (Johns et al., 1999; Massé et al., 2011). The structure of HBI diene and triene isomers used in this study is shown in Figure 4.10 (12) and (13) respectively.

4.4 Statistical analyses

4.4.1 Mann-Whitney *U* test

HBI concentrations and annual combined lamina thicknesses in continuous sediment sequences were compared using a Mann-Whitney *U* test, performed using the Paleontological Statistics Software Package (PAST; Hammer et al., 2001), to determine if variations in observed mean values were statistically significant.

4.4.2 Principal Component Analysis

The relative abundance of the diatom assemblages was analysed by principal component analysis (PCA) using the software PAST (Hammer et al., 2001). Cells of *Phaecoeros Chaetoceros* (>95% *Chaetoceros dichaeta*), and *Rhizosolenia* spp. (>95% *R. antennata*) have been grouped at the generic level for statistical analysis (Pike et al., 2008). Rare diatom taxa (those which are not >2% in any one sample) have been excluded from the PCA (Taylor et al., 1997 and references therein). Due to the large number of zero values in some samples the data have not been transformed prior to carrying out PCA (Dale and Dale, 2002). Diatom concentrations from core MD03-2601 have been analysed including CRS, whilst those from IODP-318-U1357B have been analysed using CRS-free counts due to the extremely high abundances of CRS in some samples that may mask changes in the abundance of ecologically important diatom species.

4.4.3 Time series analysis

Annual thicknesses from continuous sediment sequences were analysed using multi-taper method (MTM) single spectrum time series analysis and continuous morlet wavelet transform. MTM analysis provides a useful tool for resolving harmonic (periodic) and quasi-periodic spectral peaks from climatic (Mann and Lees, 1996) and palaeoclimatic time series data (Davies et al., 2011; Costa et al., 2007). Singular-spectrum analysis was conducted using the Singular Spectrum Analysis - MultiTaper Method (SSA-MTM) Toolkit (Ghil et al., 2002). This software uses the algorithms of

Thompson (1982) for multi-tapered spectral estimates and harmonic analysis. Resolution within the software was set to two, with three tapers which provides a suitable trade-off between frequency resolution and spectral leakage in MTM analysis of climatic time series (Mann and Lees, 1996) and is commonly applied to palaeoclimatic time series (e.g. Costa et al., 2007; Davies et al., 2011). The spectral bandwidth for each MTM analysis was calculated as the Rayleigh frequency multiplied by the number of tapers (Weedon, 2003). The Rayleigh frequency (RF) is calculated by:

$$RF = 1/N \times SI$$

where:
N = number of data points
SI = sampling interval

Wavelet analysis provides a useful tool for identifying non-stationarity of spectral signals in a climatic time series (Wang and Wang, 1996; Debret et al., 2007; Debret et al., 2009) and was conducted following the methods of Torrence and Compo (1998). For each analysis, a cone of influence (COI) was produced that indicates the region in which results are not influenced by edge effects (such as attenuation of lower frequencies due to zero padding of the dataset, Torrence and Compo, 1998). For both wavelet and SSA-MTM analysis the significance levels relative to the estimated noise background were calculated using a red noise model. A red noise model should be used in analysis of climatic time series because the system under investigation always contains longer time scales than those that are being investigated. When discriminating against a white noise model, this results in greater power at lower frequencies and may produce significant low frequency spectral peaks in the absence of a genuine signal (Ghil et al., 2002; Mann and Lees, 1996). In both instances, the red noise model is an AR(1) model (auto-regressive) that is calculated directly from the dataset (Ghil et al., 2002; Torrence and Compo, 1998).

Chapter 5. Diatom analysis of laminated sediments

This chapter presents the results of backscatter electron imagery (BSEI) analysis of thin sections produced from cores MD03-2601 and IODP-318-U1357B and quantitative diatom counts. These were both used to identify the characteristics of different lamina types. Lamina types for each core are presented first, followed by an interpretation of them with respect to seasonal fluxes in order to deduce the annual depositional cycle. Once the seasonal signal has been established for each core, the interannual record is presented by time period (the relatively warm Hypsithermal, the transition and the relatively cool Neoglacial) as the two records provide complementary data that allow a more complete understanding of Holocene interannual deposition in these time periods in the Adélie Land basin.

5.1 Lamina types and distributions in core MD03-2601

Laminae in core MD03-2601 have been classified using the diatom taxa that were visually resolved in BSEI of thin sections (Figure 5.01) and their relative position within a repeating sequence of laminae (Figure 5.02). Core MD03-2601 encompasses the warm Hypsithermal interval, cool Neoglacial interval and the transition between the two. Two categories of lamina are recorded based upon their presence in either the Hypsithermal (core sections XVII and IX – Type 1) or the Neoglacial (core section III – Type 2) with 5 sub-categories per lamina Type being recognised (categories A – E, see Table 5.01). Core section VIII contains the transition from the Hypsithermal to the Neoglacial, marked by the loss of A1 laminae in the late Hypsithermal which are replaced by A2 laminae in the early Neoglacial. Although frequently present in the early Neoglacial sediments of section VIII, B1 and E1 laminae are included as Hypsithermal

Figure 5.01 (next page). Identification of key diatom taxa and terrigenous clasts (yellow arrows i - ix) using SEM BSEI observation of highly polished thin sections. (i) CRS; (ii) *Fragilariopsis* spp.; (iii) *C. pennatum*; (iv) *Rhizosolenia* spp.; (v) *Thalassiosira* spp.; (vi) terrigenous clasts; (vii) *P. glacialis* RS; (viii) *F. kerguelensis*; (ix) *T. antarctica* RS. Lamina types shown are (a) A1 - CRS and *Fragilariopsis* spp.; (b) A2 - *Fragilariopsis* spp.; (c) B type lamina - *C. pennatum*; (d) C type lamina - *Rhizosolenia* spp.; (e) D1 - terrigenous material and mixed diatom assemblage (MDA); (f) D2 - terrigenous material and MDA with *P. glacialis* RS; (g) E1 - *T. antarctica* RS; (h) E2 - *P. glacialis* RS. Scale bars (a) and (b) 100 µm, (c) - (h) 200 µm.

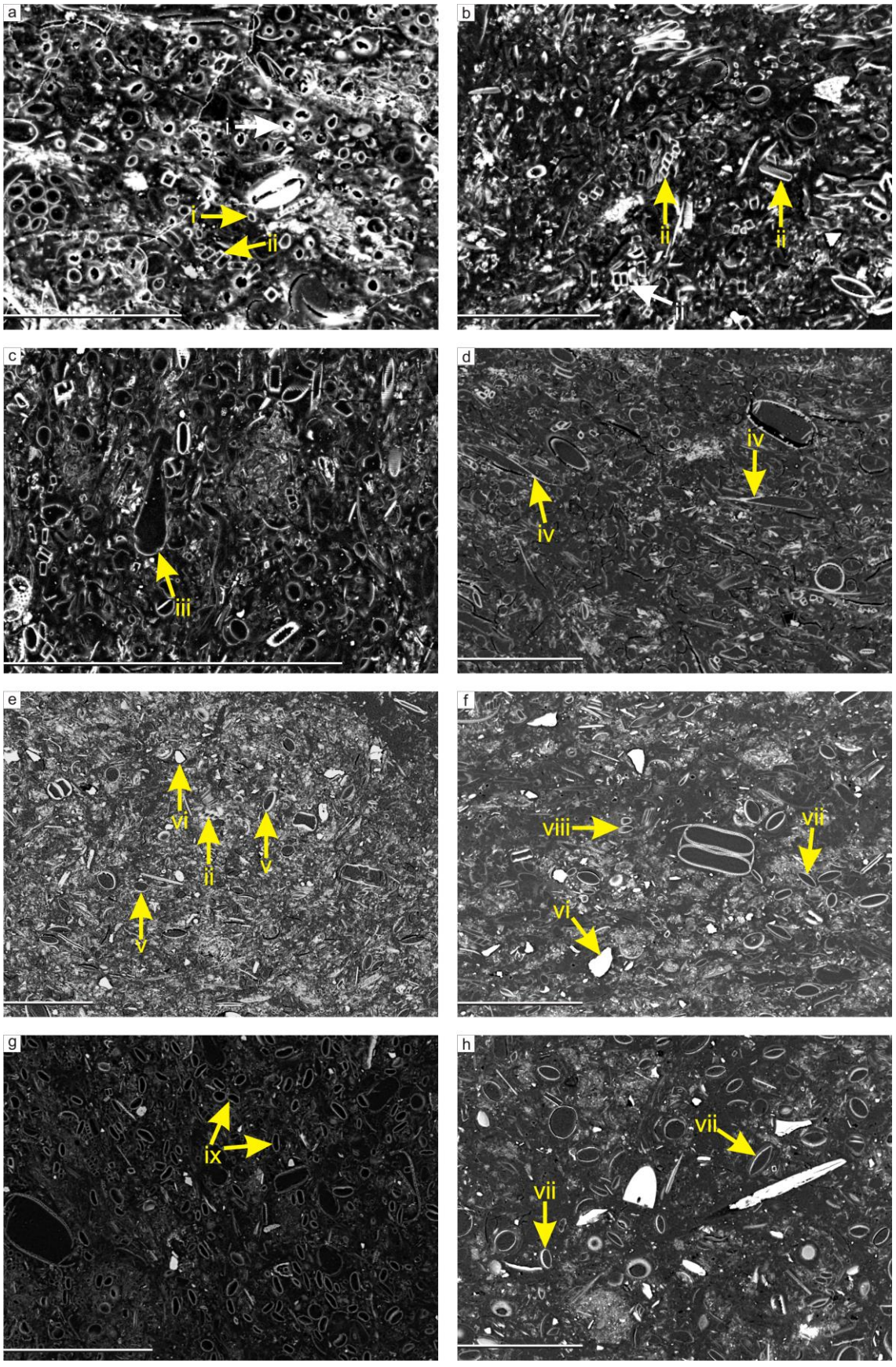
a
i
ii
b
ii
ii
ii
c
iii
d
iv
iv
e
vi
ii
v
v
f
viii
vii
vi
g
ix
h
vii
vii

Table 5.01 (next two pages). A classification of laminae and their distribution in core MD03-2601. Full diatom assemblage data is presented in Appendix 3.

Lamina type/ characteristic diatom taxa using BSEI	Number of occurrences in each core section (mean thickness; range)	Quantitative diatom assemblage description and diatom concentrations (number of diatom valves/gram of dry sediment [v/gds])
A1 – small *Fragilariopsis* spp. ± CRS	Section III: No occurrences Section VIII: 19 (5.9 mm; 1.2 – 28.9 mm) Section IX: 74 (4.0 mm; 0.4 – 15.6 mm) Section XVII: 107 (3.8 mm; 0.4 – 18.3 mm)	High relative abundances of CRS (42.5%) and small *Fragilariopsis* spp., in particular *F. rhombica* (9.4%). Additional common but variabile species in these laminae are *F. curta* and *F. kerguelensis* (between 6-18% each) and *F. ritscheri* (3-6%).*Thalassiosira antarctica* resting spores (RS) occur as 2% of valves. 9.46×10^7 v/gds.
A2 – small *Fragilariopsis* spp.	Section III: 28 (6.5 mm; 1.8 – 18.0 mm) Section VIII: 19 (3.5 mm; 0.8 – 11.1 mm) Section IX: No occurrences Section XVII: No occurrences	High relative abundances of *F. curta* (41%), and much lower CRS (15.5%) compared to other lamina types. Additional common diatoms in this lamina are *F. rhombica* (4.8%), *F. cylindrus* (4.1%) and *F. obliquecostata* (4%). 6.06×10^7 v/gds.
B1 – *Corethron pennatum* and CRS	Section III: No occurrences Section VIII: 38 (5.1 mm; 0.9 – 24.0 mm) Section IX: 7 (6.8 mm; 3.8 – 8.4 mm) Section XVII: 2 (4.0 mm; 3.6 – 4.2 mm)	High abundances of CRS (49.8%), and relatively high *F. rhombica* (9.6%). *Fragilariopsis curta* and *F. kerguelensis* are also common (8.5-11.5% each). *T. antarctica* RS make up 2.3% and *Corethron pennatum* make up 1.8% of diatom valves. 8.38×10^7 v/gds.
B2 – *Corethron pennatum* and small *Fragilariopsis* spp.	Section III: 18 (6.1 mm; 1.7 – 26.1 mm) Section VIII: No occurrences Section IX: No occurrences Section XVII: No occurrences	Characterised by relatively low CRS (25.4%) and relatively high *F. curta* (20.7%), whilst *Fragilariopsis* spp. (without *F.curta* and *F. cylindrus*) account for 31.2% within these samples. *Phaeoceros Chaetoceros* spp. make up 7.1%, *F. cylindrus* 3.3% and *C. pennatum* 2.3%. 6.83×10^7 v/gds.
C1 – *Rhizosolenia* spp., small *Fragilariopsis* spp. and CRS (CRS > *Fragilariopsis* spp.)	Section III: No occurrences Section VIII: 10 (5.1 mm; 0.6 – 14.4 mm) Section XVII: 21 (3.7 mm; 0.7 – 8.5 mm)	Dominated by CRS (33.8%) and *Fragilariopsis* spp. (49.4%), principally *F. kerguelensis* (10.9%), *F. curta* (7.5%) and *F. rhombica* (7.1%). *Phaeoceros Chaetoceros* spp. (5.5%) and *T. antarctica* RS (3%) are additional common species. Lamina type C1 have slightly higher abundances of *Rhizosolenia* spp. (1.3%), principally *R. antennata* var. *semispina*, relative to other lamina types. 9.42×10^7 v/gds.

Lamina type/ characteristic diatom taxa using BSEI	**Number of occurrences in each core section (mean thickness; range)**	**Quantitative diatom assemblage description and diatom concentrations (number of diatom valves/gram of dry sediment [v/gds])**
C2 – *Rhizosolenia* spp., small *Fragilariopsis* spp. and CRS (*Fragilariopsis* spp. > CRS)	Section III: 11 (4.9 mm; 1.5 – 17.0 mm) Section VIII: 11 (6.0 mm, 1.5 – 15.2 mm) Section IX: No occurences Section XVII: No occurrences	Dominated by CRS (36.6%) and *Fragilariopsis* spp. (50.5%), principally *F. curta* (26.4%). Sub-dominant *Fragilariopsis* spp. are *F. rhombica* (9.9%) and *F. kerguelensis* (6.1%). *Phaeoceros Chaetoceros* spp. (3.4%), *Rhizosolenia* (1.2%) and *C. pennatum* (0.9%) are also present. 5.18×10^7 v/gds
D1 – mixed diatoms and terriegnous material. Diatoms include *T. antarctica* RS and *F. kerguelensis*	Section III: No occurrences Section VIII: 78 (7.9 mm; 1.1 – 23.7 mm) Section IX: 88 (7.9 mm; 0.7 – 30.2 mm) Section XVII: 123 (5.8 mm; 0.7 – 22.2 mm)	High relative abundances of CRS (39.4%) and *F. kerguelensis* (13.7%). *F. curta*, *F. rhombica*, *F. ritscheri* and *F. seperanda* are more variable but common species, ranging between 5 and 10%. Less abundant diatoms are *T. antarctica* RS, *T. lentiginosa*, *T. gracilis* var. *gracilis* and *T. trifulta* which range between 1 and 6%. 8.39×10^7 v/gds.
D2 – mixed diatoms and terrigenous material. Diatoms include *P. glacialis* RS	Section III: 48 (8.8 mm; 1.3 – 29.9 mm) Section VIII: No occurrences Section IX: No occurrences Section: XVII: No occurrences	Moderately high relative abundances of CRS (33.6%) and *F. curta* (15.4%). *F. kerguelensis*, *F. obliquecostata* and *F. rhombica* are common but variable, ranging between 4 and 12% in each sample. *Porosira glacialis* (1.6%) and *T. gracilis* var. *gracilis* (1.5%) are commonly occurring less abundant diatoms. 5.71×10^7v/gds.
E1 – *T. antarctica* RS	Section III: No occurrences Section VII: 10 (3.8 mm; 0.6 – 13.2 mm) Section IX: 6 (1.3; 0.6 – 2.9 mm) Section XVII: 12 (2.7 mm; 0.4 – 9.3 mm)	Dominated by CRS (41.4%) whilst additional common species are *F. kerguelensis* (13.3%), *F. curta* (9.1%) and *T. antarctica* RS (8.8%). *Fragilariopsis rhombica*, *F. ritscheri* and *F. seperanda* are additional common diatoms, ranging from 4-7% per sample. 8.99×10^7 v/gds..
E2 – *P. glacialis* RS	Section III: 4 (2.8 mm; 1.9 – 3.3 mm) Section VII: No occurrences Section IX: No occurrences Section XVII: No occurrences	Dominated by high abundances of CRS (39.2%), with relatively high *F. curta* (13.9%), *F. kerguelensis* (9.1%) and *F. obliquecostata* (7.8%). The lamina are characterised by high relative abundances of *P. glacialis* (4.6%), and also have relatively high *Phaeoceros* (3.5%). 5.34×10^7 v/gds.

laminae due to their presence in core sections IX and XVII and absence from core section III (Table 5.01), and therefore are classified with the warmer climatic interval not the cooler. The seasonal interpretation of these lamina types is based upon the visually resolved species observed using BSEI and informed by the results of quantitative assemblage counts (Table 5.01) and PCA performed upon these counts (Figure 5.03). The majority of variability within the assemblage data can be explained by the first two principal component axes (PC axis 1 = 71% of variance, PC axis 2 = 11.5% of variance; see Figure 5.03). Broadly, *Hyalochaete Chaetoceros* resting spores (CRS) and *F. rhombica* plot together with positive values on PC axis 1 and negative values on PC axis 2, whilst *Phaeoceros Chaetoceros* spp., *Fragilariopsis cylindrus* and *F. obliquecostata* plot opposed to this with negative values on PC axis 1 and positive values on PC axis 2. *Fragilariopsis curta* plot orthogonally to these diatoms, with positive values on both axes, opposed to *F. kerguelensis*, *F. ritscheri* and *Thalassiosira antarctica* resting spores (RS). Additional species with influence on the distribution of samples within the PCA plot are indicated in Figure 5.03c. Hypsithermal samples have negative loadings on PC axis 1 and plot from -12 to 12 on PC axis 2 (high *F.*

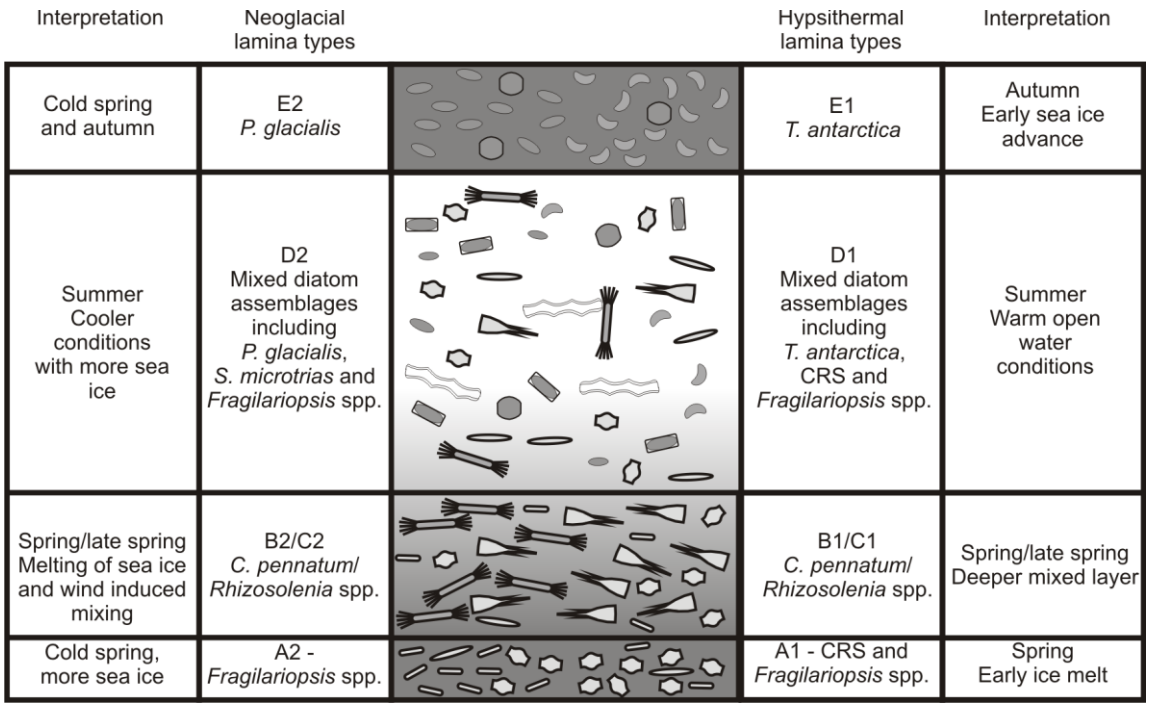

Figure 5.02. Schematic model of the annual sequence of deposition of laminae recorded in Table 5.01. Shading indicates biogenic laminae, unshaded areas indicate laminae with relatively high terrigenous material. The distribution of diatoms in each laminae is indicated in Figure 5.03.

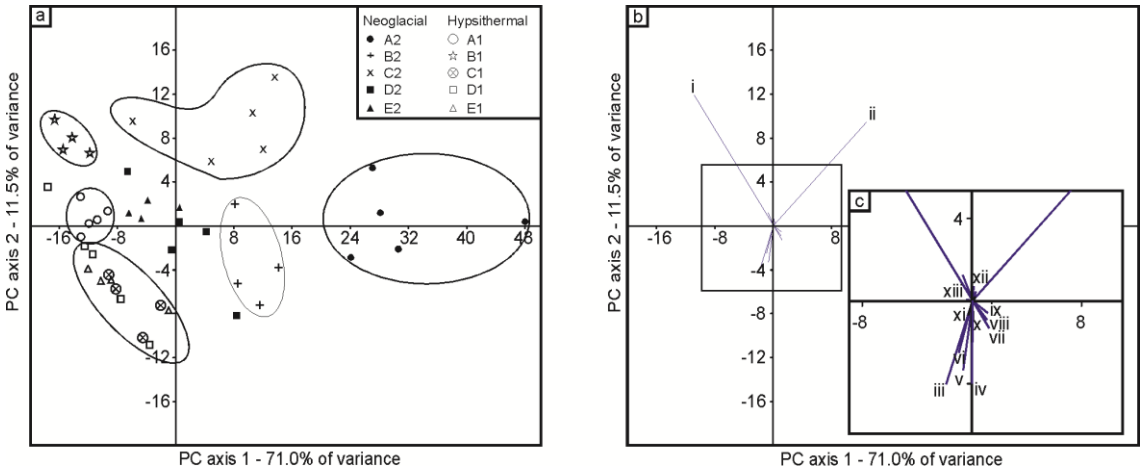

Figure 5.03. Principal component analysis of diatom lamination samples. (a) Distribution of statistically significant (Table 5.02) diatom samples on principal component axes one and two. (b) Distribution of diatom species on principal component axes one and two. (c) Detail of central area highlighted by square in (b). Diatoms indicated are (i) CRS; (ii) *Fragilariopsis curta*; (iii) *F. kerguelensis*; (iv) *F. separanda*; (v) *F. ritscheri*; (vi) *Thalassiosira antarctica* RS; (vii) *F. sublinearis*; (viii) *Phaeoceros Chaetoceros* spp.; (ix) *F. cylindrus*; (x) *T. gracilis*; (xi) *Thalassiothrix antarctica*; (xii) *F. sublinearis*; (xiii) *Thalassiosira lentiginosa*.

Table 5.02. Pearson's correlation coefficients between species analysed in the PCA of diatom assemblage data from core MD03-2601 (Figure 5.03) and eigenvalues of PC axes 1 and 2. Values in bold are statistically significant ($p < 0.05$).

Species	PC axis 1	PC axis 2
Hyalochaete Chaetoceros	-0.08	0.00
Phaeoceros Chaetoceros	**0.30**	-0.11
Chaetoceros resting spores	**-0.91**	**0.40**
Corethron pennatum	0.07	0.27
Fragilariopsis curta	**0.95**	0.29
F. cylindrus	**0.56**	-0.12
F. kerguelensis	**-0.47**	**-0.40**
F. obliquecostata	**0.31**	-0.14
F. rhombica	-0.20	0.14
F. ritscheri	-0.27	**-0.54**
F. seperanda	-0.01	**-0.66**
F. sublinearis	**0.34**	0.25
Porosira glacialis rs	0.14	0.05
Proboscia inermis	**0.44**	0.03
Pseudonitzschia sp.	0.04	-0.23
Rhizosolenia spp.	0.10	0.03
Thalassiosira antarctica rs	**-0.37**	**-0.37**
T. gracilis	0.05	**-0.54**
T. lentiginosa	**-0.37**	0.01
T. trifulta	-0.27	-0.25
Thalassiothrix antarctica	-0.10	**-0.34**

kerguelensis and *T. antarctica* RS), whilst Neoglacial samples plot from -8 to 32 on PC axis 1 and -8 to 14 on PC axis 2 (high *F. curta*; lower *F. kerguelensis* and *T. antarctica* RS).

5.1.1 Hypsithermal spring laminae: Lamina types A1, B1 and C1

A1 laminae were characterised in BSEI by the co-dominance of CRS and *Fragilariopsis* spp. In the PCA, A1 laminae form a group between -14 and -8 on PC axis 1, and from 6 to 10 on PC axis 2 (high CRS and *F. rhombica*; Figure 5.03). In assemblage counts, CRS were much more abundant than the cryophilic *Fragilariopsis* species (*F. curta*, *F. cylindrus*, *F. rhombica*, *F. obliquecostata*, *F. ritscheri*; see Armand et al., 2005) (Table 5.01). The presence of CRS within Antarctic sediments is commonly associated with stratification resulting from early spring melting of sea ice (Leventer, 1991; Crosta et al., 1997). *Fragilariopsis curta* and *F. rhombica* prefer stratified waters that are more ice-proximal than those preferred by vegetative *Hyalochaete Chaetoceros* cells (Beans et al., 2008) and are also common in A1 laminae, indicating the presence of sea ice associated with spring conditions. *Fragilariopsis rhombica* occurs in greatest abundances in A1 laminae (Table 5.01), and is typically found in sediments that lie beneath 7 – 9 months per year sea ice cover (Armand et al., 2005). Hence, A1 laminae are interpreted here as representing a relatively warm and early spring with an early sea ice melt-induced bloom of CRS and *Fragilariopsis* spp., and warmer surface waters due to a longer sea ice free period.

B1 laminae are characterised with BSEI by visually resolved *Corethron pennatum* and CRS. B1 laminae form a group from -17 to -10 on PC axis 1 and -1 to 3 on PC axis 2 (high CRS; Figure 5.03) and assemblage counts that have the highest abundances of CRS observed in core MD03-2601 (Table 5.01). *C. pennatum* is frequently found in water and sediment samples in Antarctic coastal environments and is commonly associated with late spring/early summer conditions when reported from laminated sediments (Bahk et al., 2003; Stickley et al., 2005; Maddison et al., 2006; Beans et al., 2008; Denis et al., 2010; Maddison et al., 2012). The ability of *C. pennatum* to migrate vertically within the water column allows it to take advantage of higher light levels near the surface and to acquire nutrients at a greater depth in a mixed water column (Beans et al., 2008) and the increased abundance of *C. pennatum* in the late Holocene of Adélie

Land sediments has been associated with increased spring wind strengths (Denis et al., 2009). Co-occurrences of CRS and *C. pennatum* have also been reported from late Holocene sediments in McMurdo Sound, East Antarctica and are associated with early spring sea ice retreat (Leventer et al., 1993). Hence, B1 laminae are interpreted here as representing early ice melting with stronger winds promoting a deep wind mixed layer during the spring.

C1 laminae are characterised with BSEI by visually resolved *Rhizosolenia* spp. (Table 5.01). In the PCA (Figure 5.03), C1 laminae form a group with D1 and E1 laminae between -14 to -1 on PC axis 1 and -12 to -2 on PC axis 2 (high *T. antarctica* RS, *F. kerguelensis*, *F. ritscheri* and *F. separanda*). They are distinguished from D1 and E1 laminae in assemblage counts by higher abundances of *Phaeoceros Chaetoceros* spp. and *Rhizosolenia* spp. (principally *R. antennata* forma *semispina*). *Rhizosolenia* spp. in Adélie Land have a preference for wind mixed surface waters (Assmy et al., 2008; Beans et al., 2008; Crosta et al., 2005), whilst *F. kerguelensis* and *Phaeoceros Chaetoceros* spp. are commonly found in the permanently open ocean conditions of the Polar Frontal Zone (PFZ), although they are also found in lower abundances in coastal areas which are free of sea ice during the summer. Laminae containing high abundances of *Rhizosolenia* spp. are commonly associated with oligotrophic late spring conditions that have a stable pycnocline (Stickley et al., 2005; Maddison et al., 2006), but the high abundances of *Phaeoceros Chaetoceros* spp. and *F. kerguelensis*, lower abundances of cryophilic *Fragilariopsis* spp. observed here and the modern preference of *Rhizosolenia* spp. for wind mixed surface waters in Adélie Land (Beans et al., 2008), suggest that lamina type C1 are indicative of a deeper mixed layer during the spring period, rather than stratification.

5.1.2 Hypsithermal summer and autumn: D1 and E1 lamiane

D1 laminae have the lowest mean diatom concentrations of Hypsithermal laminae (Table 5.01) and contain a visually high proportion of terrigenous material under BSEI observation (bright images relative to other Hypsithermal lamina types) and a mixed diatom assemblage (Table 5.01). D1 laminae are grouped with C1 and E1 laminae in the PCA (Figure 5.03), but are distinguished by lower absolute abundances of diatoms, lower abundances of *Phaeoceros Chaetoceros* spp. than C1 laminae and lower

abundances of *Thalassiosira antarctica* RS than E1 laminae (Table 5.01). The high concentrations of terrigenous material within these laminae likely results from the reduced dilution by diatoms after the spring bloom (Stickley et al., 2005; Denis et al., 2006; Maddison et al., 2006) and a greater lateral advection of clay particles from more coastal areas closer to glaciers following sea ice retreat (Dunbar et al., 1985; Presti et al., 2003; Maddison et al., 2012). Furthermore, the open ocean *Fragilariopsis kerguelensis* is at greatest abundance in D1 laminae and, hence, D1 laminae are interpreted here as representing relatively warm prolonged open water conditions during the summer.

E1 laminae are characterised by visually resolved *Thalassiosira antarctica* RS in BSEI and plot with C1 and D1 laminae in the PCA (Figure 5.03). E1 laminae are distinguished from this group by higher abundances of *T. antarctica* RS in quantitative counts (Table 5.01). *Thalassiosira antaractica* are found in sediments south of the winter sea ice edge and show a strong preference for >6 months per year of sea ice (Armand et al., 2005). Although a large vegetative standing stock of *T. antarctica* can also be associated with icy spring conditions as the sea ice acts as an innoculum (Krebs et al., 1987), blooms of *T. antarctica* are more commonly associated with open water conditions and low stratification (Cremer et al., 2005; Barcena et al., 1998). Formation of *T. antarctica* RS is associated with autumnal ice growth (Cunningham and Leventer, 1998) and blooms of vegetative *T. antarctica* have been observed occurring with turbulent conditions and frazil ice formation in the upper water column during the late summer season (Gleitz et al., 1998). Laminae rich in *T. antarctica* RS are usually interpreted as a resting spore formation event due to autumnal ice growth, and the distribution of laminae with high abundances of *T. antarctica* RS from around the East Antarctic margin is associated with an annual persistence of sea ice cover of ~7.5 months (Denis et al., 2006; Pike et al., 2009). E1 laminae are interpreted here as indicating years in which there is an early sea ice advance in the autumn.

5.1.3 Neoglacial spring: A2, B2 and C2 laminae

A2 laminae are characterised by the dominance of *Fragilariopsis* spp. when observed with BSEI. They form a distinct group in the PCA (Figure 5.03) from 24 to 48 on PC axis 1 and -4 to 6 on PC axis 2 (very high *F. curta*) and assemblages are dominated by

high abundances of *F. curta*, as well as high abundances of *F. cylindrus* and *F. obliquecostata* (Table 5.01). *Fragilariopsis curta* is recorded in a variety of Antarctic coastal environments and may be common or dominant within sea ice related communities (Tanimura et al., 1990; Leventer and Dunbar, 1996; Riaux-Gobin et al., 2003) and in stable stratified waters proximal to a melting ice edge (Tanimura et al., 1990; Kang and Fryxell, 1993; Goffart et al., 2000; Riaux-Gobin et al., 2003; Riaux-Gobin et al., 2011; Beans et al., 2008). *Fragilariopsis curta* appears to be confined to locations south of the winter ice edge and occurs at greatest sedimentary abundances in regions with 9 – 11 months per year sea ice cover (Armand et al., 2005), whilst *F. cylindrus* and *F. obliquecosta* are often found beneath fast and pack ice, and *F. cylindrus* is one of the most common diatoms found in the Adélie Land marginal ice zone (Armand et al., 2005; Riaux-Gobin et al., 2011; Tanimura et al., 1990). *Fragilariopsis cylindrus* and *F. curta* have also been observed in high abundances in sea ice influenced waters (greater than 37.5% sea ice cover) in a transect from New Zealand to the Ross Ice Shelf, with *F. curta* increasing southward with increased sea ice concentration (Burckle et al., 1987). Large blooms dominated by *F. curta* occur seasonally in the south western Ross Sea, and appear to be closely linked to weak winds during the early spring period that allow for a shallow wind mixed layer and late melting of sea ice during the annual December peak in insolation. This is in contrast to the central Ross Sea region where typically stronger spring winds force an earlier opening of the Ross Sea polynya, and a deeper mixed layer with a more diverse phytoplankton assemblage occurs (Dunbar et al., 1998). A2 laminae are interpreted here as representing cold spring conditions, with low average wind speeds, a high concentration of sea ice and later melting of sea ice, possibly during December or January.

B2 laminae are characterised by high abundances of *Corethron pennatum* using BSEI. They form a distinct group in the PCA from 8 to 16 on PC axis 1 and -8 to 2 on PC axis 2 (high *F. curta*, *Phaeoceros* spp., *F. cylindrus*; Figure 5.03). They are dominated by *Fragilariopsis curta* in assemblage counts, but also have relatively high abundances of *Corethron pennatum*, *Phaeoceros Chaetoceros* spp. and *F. cylindrus* (Table 5.01). As discussed above, *C. pennatum* have a preference for ice-free waters and are able to thrive in locations of strong wind-induced mixing. *Phaeoceros Chaetoceros* spp. are commonly found in open ocean waters (Kang and Fryxell, 1993; Smetacek et al., 2002;

Beans et al., 2008) and *Chaeoceros dichaeta*, which represents >95% of *Phaeoceros Chaetoceros* spp. in this study, is particularly abundant at the PFZ where high nutrient levels occur due to the upwelling of deeper waters (Assmy et al., 2008). Both *Phaeoceros Chaetoceros* spp. and *C. pennatum* increase in abundance in Adélie Land from ca. 4.5 ka to present, associated with increased wind-induced mixing during the spring period (Denis et al., 2009; 2010). Despite the presence of these species, the high abundances of *F. curta* and *F. cylindrus* indicate a proximal sea ice edge. Hence, B2 laminae are interpreted here as representing spring conditions with interplay between strong wind-induced mixing and melting of sea ice.

C2 laminae are characterised using BSEI by visually resolved *Rhizosolenia* spp. In the PCA, C2 laminae form a distinct group from 4 to 16 on PC axis 1 and 2 to 14 on PC axis 2 (high *F. curta*, moderate CRS; Figure 5.03). They contain the highest abundances of CRS of the Neoglacial spring laminae, lowest (yet still high relative to Hypsithermal lamina types) abundances of *Fragilariopsis curta* and lowest *F. cylindrus* (Table 5.01). High abundances of *F. curta* in C2 laminae indicate colder conditions than in Hypsithermal samples; however, the relatively high CRS abundances suggests warmer conditions relative to A1 and B1 laminae due to an early sea ice retreat. High abundances of *Phaeoceros Chaetoceros* spp. and *Rhizosolenia* spp. in C2 laminae are consistent with a deeper mixed layer related to stronger winds (Beans et al., 2008). Hence, C2 laminae are interpreted here as spring conditions with an early sea ice retreat that occurs due to relatively warm and windy conditions.

5.1.4 Neoglacial summer and autumn: D2 and E2 laminae

D2 laminae exhibit a relatively high proportion of terrigenous grains when observed using BSEI and have a mixed diatom assemblage which includes *P. glacialis* RS (Table 5.01). D2 and E2 laminae form a group in the centre of the PCA plot from -8 to 6 on PC axis 1 and -2 to 5 on PC axis 2 (*F. curta* higher than *F. kerguelensis*; high *Porosira glacialis* rs; low *Thalassiosira antarctica* RS; Figure 5.03), with an outlying D2 sample at 8 on PC axis 1 and -6 on PC axis 2. D2 laminae have lower total diatom abundances and lower *P. glacialis* RS relative abundances than E2 laminae (Table 5.01). Diatom assemblages from D2 laminae have higher abundances of *Fragilariopsis curta*, *F. obliquecostata* and *Porosira glacialis* rs than D1 laminae, all of which have a

preference for years with icier spring/summer conditions (Armand et al., 2005). High abundances (compared to other Neoglacial samples) of *F. kerguelensis* indicates the intrusion of oceanic waters into the region during the summer (Crosta et al., 2005), as does the presence of *P. glacialis* RS which, although it is a diatom associated with the sea ice environment, is commonly found in sediments where summer conditions have <30% sea ice concentration (Armand et al., 2005). D2 laminae are interpreted here as representing colder summer conditions than D1 laminae.

E2 laminae are characterised using BSEI by visually dominant *P. glacialis* RS and contain high abundances of *P. glacialis* RS in assemblage counts (Table 5.01). *Porosira glacialis* is ecologically similar to *Thalassiosira antarctica* and, although it is rarely found living within sea ice, its maximum occurrence is south of the winter sea ice limit, and both are common components of the summer diatom stock in areas that are icy during the spring (Armand et al., 2005; Pike et al., 2009; Krebs et al., 1987). It is not clear what induces resting spore formation in *P. glacialis*; however, the occurrence of *P. glacialis* RS in Holocene sediments around East Antarctica appears to be linked to regions that experience >7.5 months per year of sea ice cover (Pike et al., 2009). Hence, E2 laminae are interpreted here as occurring in years with both cold springs and autumns, with a later sea ice break up relative to years with E1 laminae.

5.1.5 Annual sequences in core MD03-2601

A complete annual succession of laminae (Figure 5.02) would contain an initial biogenic lamina that is high in CRS and/or *Fragilariopsis* spp. followed by a biogenic lamina visually dominated by *Corethron pennatum* or *Rhizosolenia* spp. These are succeeded by laminae that contain mixed diatom assemblages and a relative increase in terrigenous grains (Table 5.01). Terrigenous-rich laminae exhibit an up-lamina increase in *Thalassiosira antarctica* RS (D1 laminae; Hypsithermal) or *Porosira glacialis* RS (D2 laminae; Neoglacial). A final lamina visually dominated by either *T. antarctica* RS (E1; Hypsithermal) or *P. glacialis* RS (E2; Neoglacial) occurs at the end of the sequence (Figure 5.02). This complete annual sequence is rare in core MD03-2601. More commonly sequences have an initial biogenic lamina (dark under BSEI) with high CRS (A1 and B1 laminae) or high *Fragilariopsis* spp. (A2, B2 and C2 laminae) followed by a terrigenous (light under BSEI) D1 or D2 lamina, which may have a final

E1 or E2 lamina. The upper boundary of the final lamina is abrupt, representing a winter hiatus in deposition (Denis et al., 2006), whereas the visual boundary between dark and light (under BSEI) lamina in a sequence is gradual. Repeating sequences observed in BSEI are commonly interpreted as representing discrete annual deposits due to the floral succession observed within the sediments (Maddison et al., 2012; Maddison et al., 2005; Maddison et al., 2006; Stickley et al., 2005) and this interpretation is applied to core MD03-2601.

Short, non-laminated intervals, which often contain small-scale bioturbation structures (Pike et al., 2001) are also recognised. These non-laminated intervals increase in frequency and total thickness up-core, with 24.8 cm total in core section XVII, 49.8 cm total in core section IX, 35.0 cm total in core section VIII and 72.0 cm total in core section III.

The oldest Hypsithermal core section (section XVII) has the lowest occurrences of non-laminated intervals and the greatest number of preserved annual sequences (118 years; mean thickness = 10.6 mm, σ = 6.0 mm, Figure 5.04). The majority of the years (86%) are composed of an A1 lamina followed by a combination of B1, C1, D1 and E1 lamina. The remaining 14 % of years have no A1 lamina, but instead have a B1 or C1 lamina. The younger Hypsithermal section (section IX) has more non-laminated intervals (Table 5.01; Figure 5.05) and a total of 82 annual sequences (mean thickness = 12.6 mm; σ = 7.3 mm). Similarly to section XVII, 89% of annual sequences in core section IX have an initial A1 lamina, with the remaining 11% having initial B1 or C1 laminae.

Annual sequences from the transitional core section (section VIII) are considered in two intervals based upon the first occurrences of Neoglacial spring laminae; the late Hypsithermal (1200 – 1128 cm core depth) and the early Neoglacial (1128 – 1050 cm). In total, 74 years (mean thickness = 14.8 mm, σ = 8.0 mm) are recorded in core section VIII, which has several large unlaminated/bioturbated intervals (Figure 5.06). The late Hypsithermal interval has a total of 26 years (mean thickness = 19.1 mm, σ = 9.6 mm), of which 15 (58%) have an initial A1 lamina, whilst the remaining 11 have a mixture of B1 and C1 laminae at their base. The early Neoglacial interval has 48 complete years (mean thickness = 12.4 mm, σ = 6.0 mm) of which 38% have an initial A2 lamina, 35% an initial B1 lamina, 23% a C2 lamina and 4% a C1 lamina. The observed reduction in

mean annual thickness between the late Hypsithermal and the early Neoglacial sub-sections is statistically significant (n late Hypsithermal = 26, n early Neoglacial = 48, Mann-Whitney $U = 352$, $p < 0.05$).

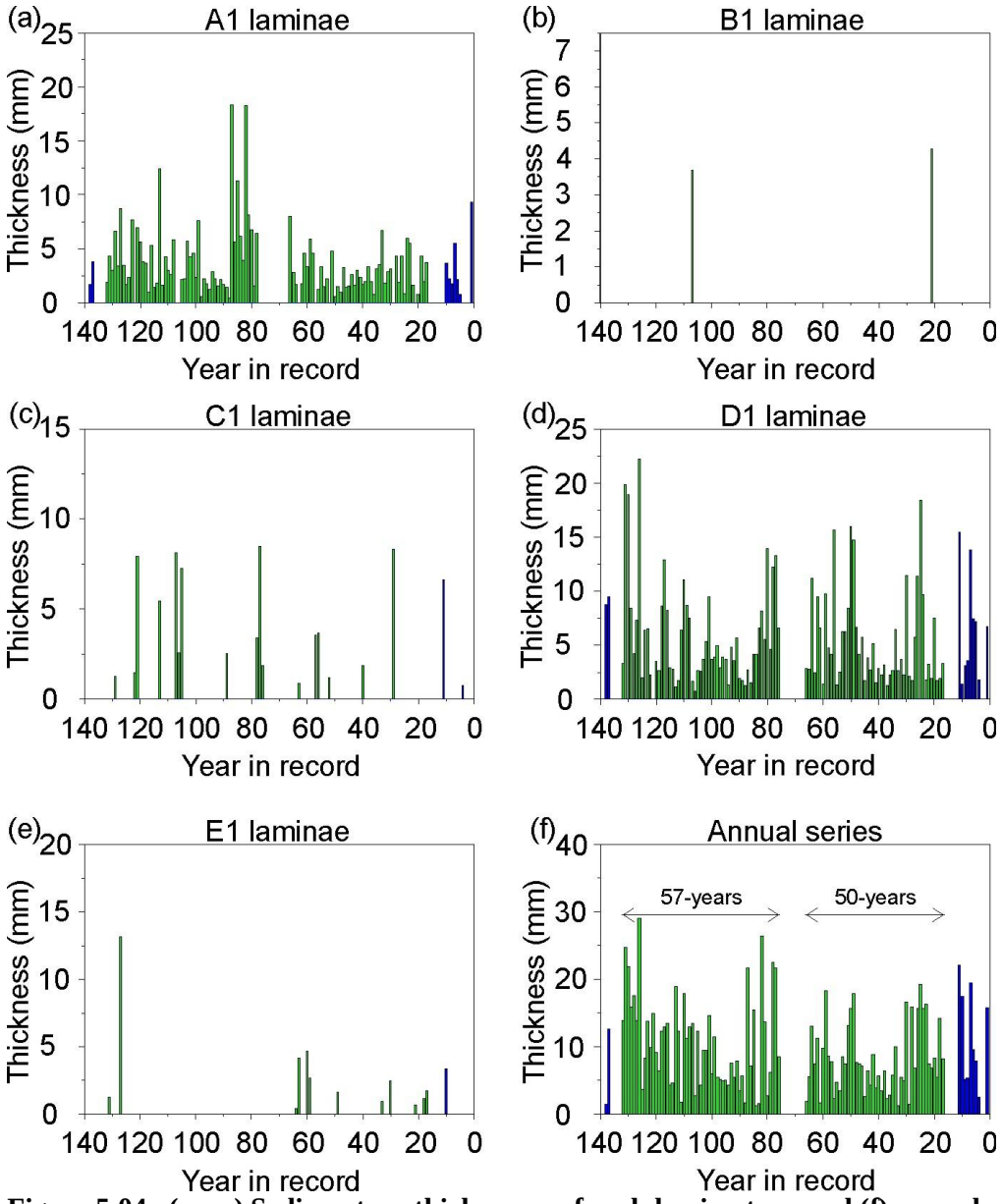

Figure 5.04. (a – e) Sedimentary thicknesses of each lamina type and (f) annual combined lamina thicknesses from all years in core MD03-2601 section XVII (Hypsithermal). Laminae/years highlighted in green contribute to the time series used in the spectral analysis in Section 6.3. The 50 and 57-year record discussed in section 6.3 are indicated on the annual time series plot (f). The time interval for bioturbation was calculated by dividing the thickness of the bioturbated intervals (mm) by the mean annual thickness (mm) from core section XVII.

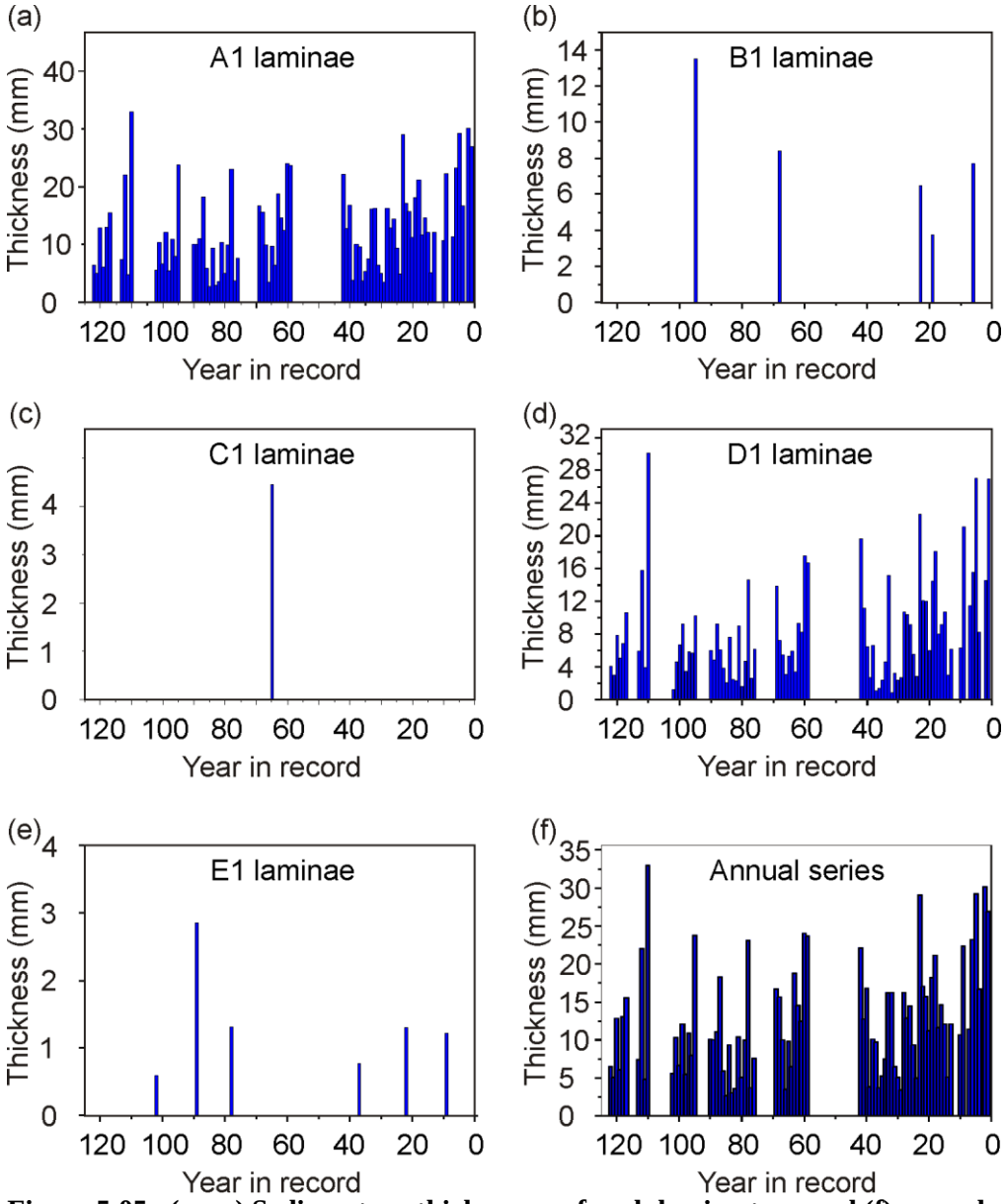

Figure 5.05. (a – e) Sedimentary thicknesses of each lamina type and (f) annual combined lamina thicknesses from all years in core MD03-2601 section IX (Hypsithermal). The time interval for bioturbation was calculated by dividing the thickness of the bioturbated intervals (mm) by the mean annual thickness (mm) from the core section IX.

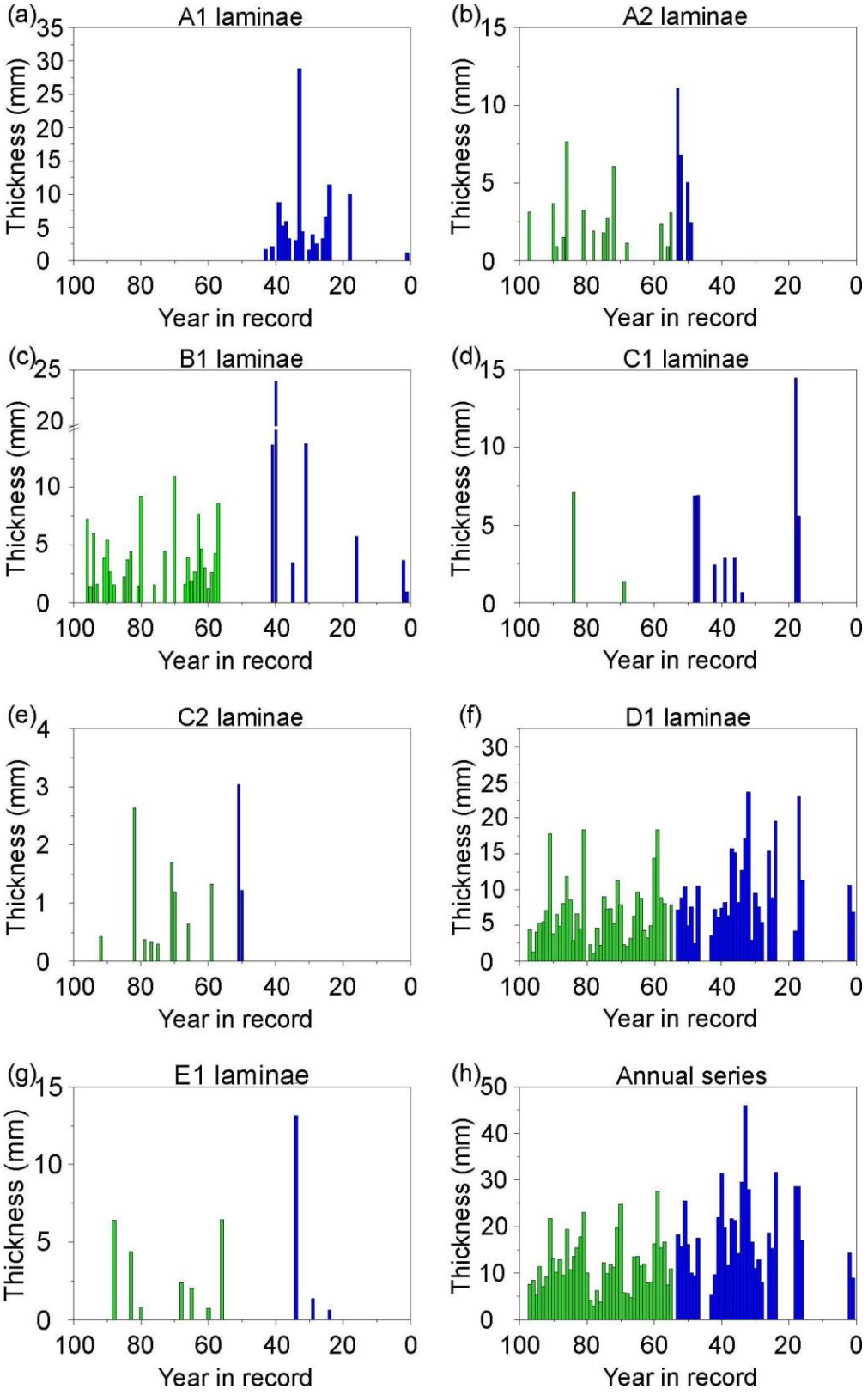

Figure 5.06. (a – e) Sedimentary thicknesses of each lamina type and (f) annual combined lamina thicknesses from all years in core MD03-2601 section VIII (transitional). Laminae/years highlighted in green contribute to the time series used in thespectral analysis in Section 6.3. The time interval for bioturbation was calculated by dividing the thickness of the bioturbated intervals (mm) by the mean annual thickness (mm) from core section VIII.

The Neoglacial section (section III; Figure 5.07) has much higher levels of bioturbation than the Hypsithermal and transitional sections of core MD03-2601. Consequently only 48 complete years of diatom succession are identified (mean thickness = 16.8 mm, σ = 18.5 mm), with the longest undisrupted sequence being 11 years. The majority of these years (44/48) consist of only two distinct laminae, whilst the remaining four also include a D1 lamina at the end of the sequence. The biogenic spring layer is most

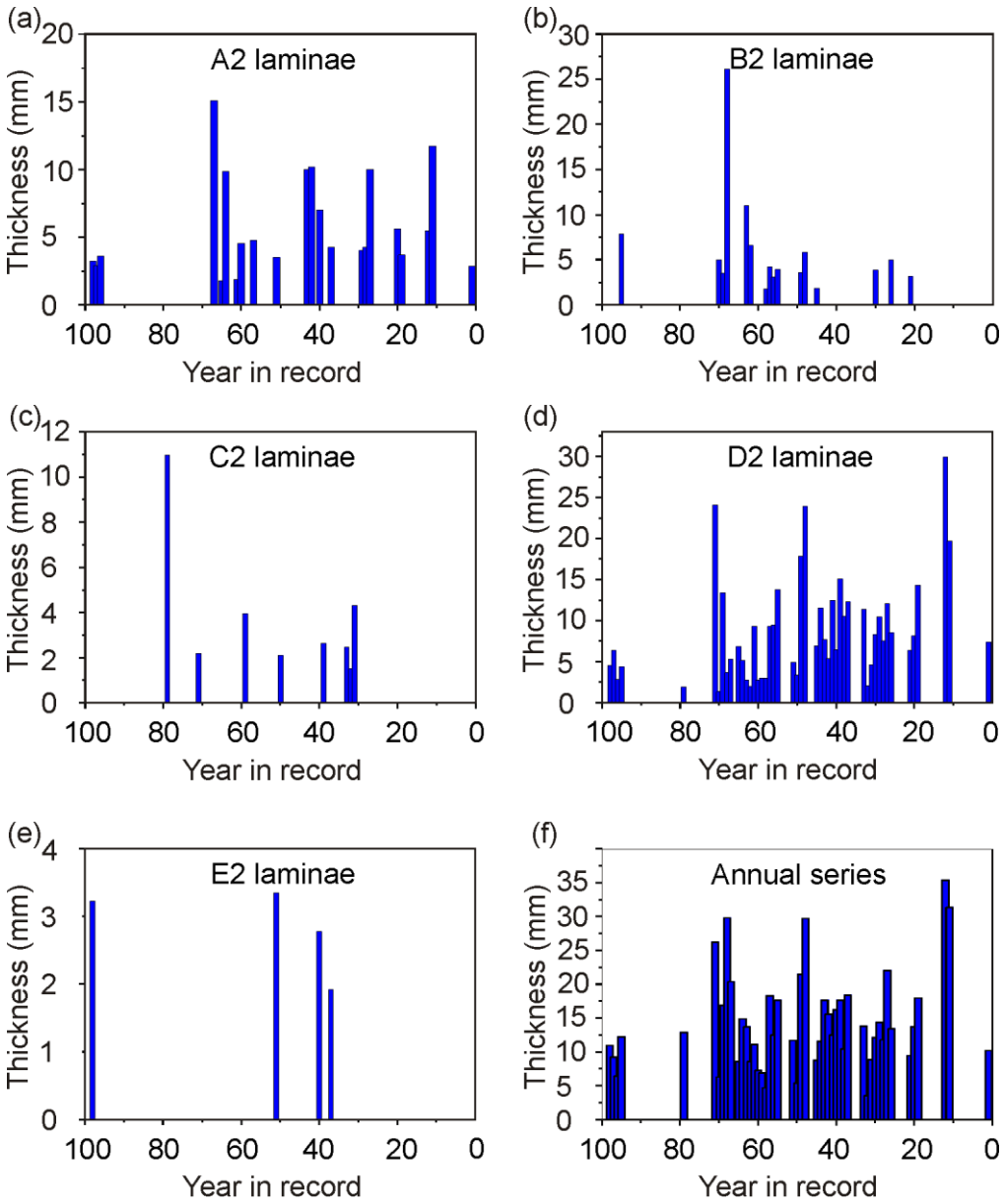

Figure 5.07. (a – e) Sedimentary thicknesses of each lamina type and (f) annual combined lamina thicknesses from all years in core MD03-2601 section III (Neoglacial). The time interval for bioturbation was calculated by dividing the thickness of the bioturbated intervals (mm) by the mean annual thickness (mm) from core section III.

commonly represented by A2 laminae (48%), but B2 laminae (29%) and C2 laminae (23%) also occur at the start of sequences, whilst the terrigenous summer layer is represented in all instances by D2 laminae.

5.2 Lamina types and distributions in core IODP-318-U1357B

Laminae in the Neoglacial sediments of core IODP-318-U1357B sections 4H-5-W, 4H-6-W and 4H-7-W (hereafter collectively referred to as "core IODP-318-U1357B") have been classified using the diatom taxa that were visually resolved in BSEI of thin sections (Figure 5.08) and their relative position within a repeating sequence of laminae (Figure 5.09; section 5.2.4). In total, five lamina categories have been identified which are broadly comparable to those from MD03-2601. However, as they have been subjected to different counting techniques (see Chapter 4, page 58) and have visual differences to their counterparts in MD03-2601 (e.g. more apparent *Phaeoceros Chaetoceros dichaeta*, see Table 5.02) they are subsequently classified as laminae A3 – E3 (Table 5.03). The seasonal interpretations of laminae A3 – E3 is based upon the visually resolved diatom species observed using BSEI and informed by the results of CRS-free quantitative assemblage counts (Table 5.03, Figure 5.11 and Figure 5.10), and PCA performed upon these counts (Figure 5.11). Broadly, *Fragilariopsis* spp. (excluding *F. kerguelensis*) have highest relative abundances within A3 laminae and lowest within E3 lamina (Figure 5.10a). *Phaeoceros Chaetoceros* spp. typically occur at ~10% relative abundance, but are much higher within B3 laminae (~25% mean relative abundance; Figure 5.10b), whilst solenoidal diatoms (Figure 5.10c) have higher relative abundances in B3, C3 and E3 laminae compared to A3 and D3 laminae. *Fragilariopsis kerguelensis* are found in highest relative abundances in C3 and D3 laminae (higher in D3 at ~15% of diatom assemblages; Figure 5.10d). *Porosira glacialis* rs (Figure 5.10e) and *Thalassiosira antarctica* rs (Figure 5.10f) have a broadly similar distribution by lamina type, with low relative abundances in A3, B3 and C3 laminae, slightly higher relative abundances in D3 laminae and maximum mean relative abundances in E3 laminae.

Table 5.03. A classification of laminae and their distribution in core IODP-318-U1357B. Full diatom assemblage data is presented in Appendix 3.

Lamina type/ characteristic diatom taxa using BSEI	Number of occurrences in recorded interval (mean thickness; range)	Mean quantitative CRS-free diatom assemblage description and CRS-free diatom concentrations given in number of diatom valves/gramme of dry sediment (v/gds)
A3 – *Fragilariopsis* spp. ± CRS	64 (10.6 mm; 0.8 – 51.4 mm)	Very high cryophilic *Fragilariopsis* spp. (69.2%), in particular *F. curta* (33.5%) and *F. rhombica* (16.3%). *Phaeoceros Chaetoceros* spp. (10.2%) are also common. 5.07×10^7 v/gds.
B3 – *Phaeoceros Chaetoceros dichaeta*, *C. pennatum*	15 (5.7 mm; 0.7 – 14.5 mm)	Moderate abundances of cryophilic *Fragilariopsis* spp. (53.6%), in particular *F. curta* (26.3%). *Phaeoceros Chaetoceros* spp. are at highest abundances (25.5%), as are the solenoidal diatom group (4.9%). 5.49×10^7 v/gds.
C3 – biogenic mixed diatom assemblages, common solenoidal diatoms	56 (11.9 mm; 1.0 – 60.4 mm)	Very high cryophilic *Fragilariopsis* spp. (60.6%), in particular *F. curta* (28.3%) and *F. rhombica* (16.5%). *Phaeoceros Chaetoceros* spp. (9.1%) and the solenoidal diatom group (4.5%) are also common. 4.30×10^7 v/gds.
D3 – mixed diatoms and terrigenous material	70 (14.1 mm; 1.7 – 53.3 mm)	Moderate abundances of cryophilic *Fragilariopsis* spp. (51.2%). High abundances of *F. kerguelensis* (13.9%) and *F. rhombica* (15.9%). *Porosira glacialis* rs (4.4%) are common. 3.61×10^7 v/gds.
E3 – *P. glacialis* RS	25 (4.3 mm; 0.9 – 20.2 mm)	40.0% cryophilic *Fragilariopsis* spp., high abundances of *P. glacialis* rs (21.0%) and the highest abundances of *T. antarctica* rs (2.8%). *Phaeoceros Chaetoceros* spp. (8.4%) are common, and *F. curta* occur in relatively low abundances (14.5%). 4.18×10^7 v/gds.

Within the PCA, the majority of variability within the assemblage data for core IODP-318-U1357B is explained by the first two PC axes (PC axis 1 = 43.9%, PC axis 2 = 21.8%). Broadly, *Phaeoceros Chaetoceros* spp. plot alone with moderate positive values on PC axis 1 and negative values on PC axis 2, whilst *Fragilariopsis kerguelensis*, *F. separanda* and *Thalassiosira antarctica* RS plot opposite to *Phaeoceros Chaetoceros* spp. with negative values on PC axis 1 and positive values on PC axis 2. *Fragilariopsis curta* and *F. rhombica* plot orthogonally to these diatoms with positive values on both axes, whilst *Porosira glacialis* RS are opposite to *F. curta* with near zero values on PC axis 1 and negative values on PC axis 2 (Figure 5.11). Additional species with influence on the distribution of samples in the PCA

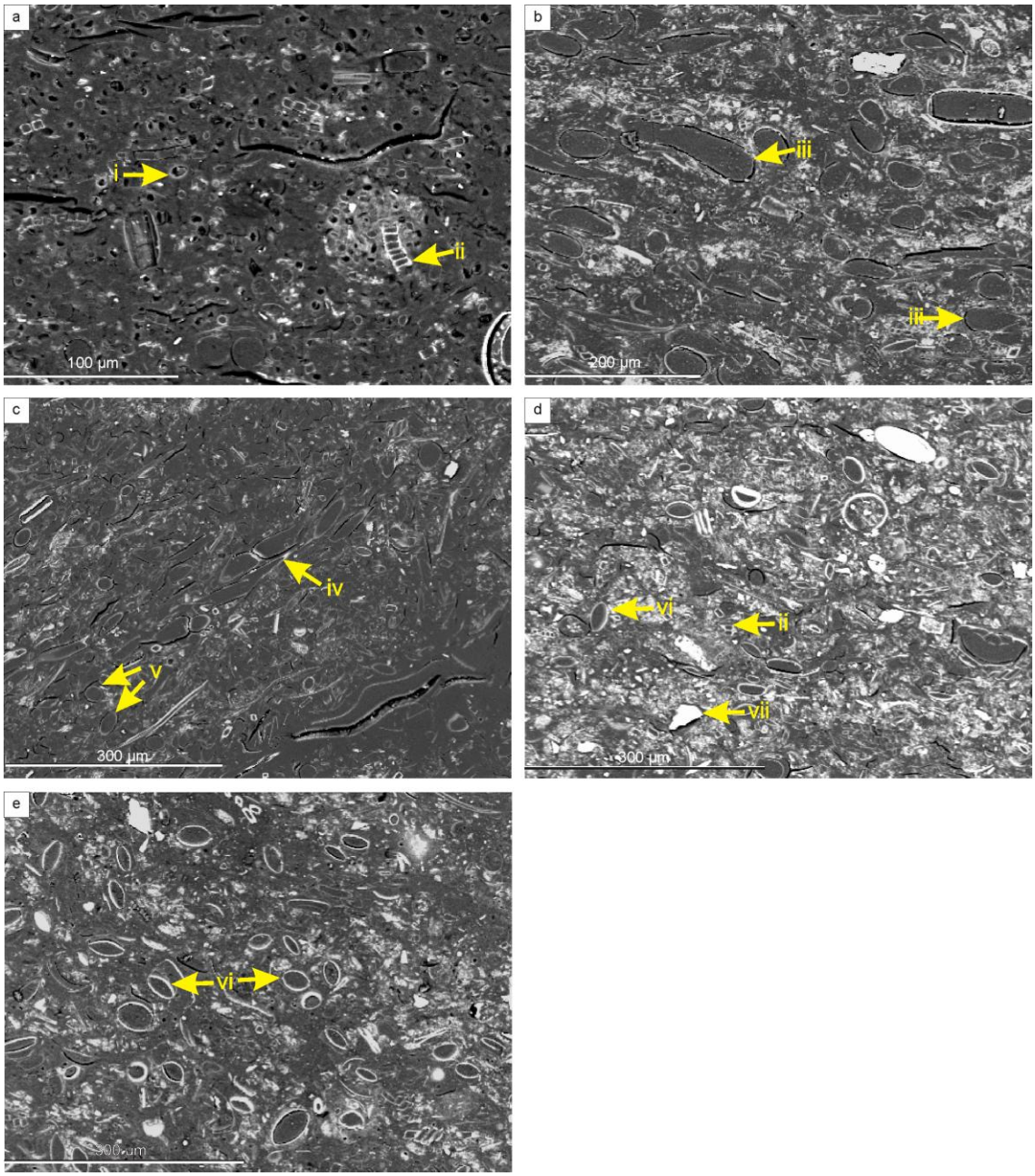

Figure 5.08. Identification of key diatom taxa and terrigenous grains (i - vii) using SEM BSEI observation of highly polished thin sections. (i) CRS; (ii) *Fragilariopsis* spp.; (iii) *C. pennatum*; (iv) *Rhizosolenia* spp.; (v) *Phaeoceros Chaetoceros* spp.; (vi) *P. glacialis* RS; (vii) terrigenous clast; Lamina types shown are (a) A3 – CRS and *Fragilariopsis* spp.; (b) B3 – *C. pennatum*; (c) C3 *Phaeoceros Chaetoceros* and solenoidal diatoms; (d) D3 – mixed diatom assemblage and terrigenous material; (e) E3 – *P.* glacialis RS.

are shown in Figure 5.11c. The solenoidal diatom group (consisting of *Rhizosolenia* spp., *Proboscia* spp. and *Corethron pennatum* which commonly occur together in laminae observed using BSEI) is used for lamina description purposes and species are not grouped in the PCA.

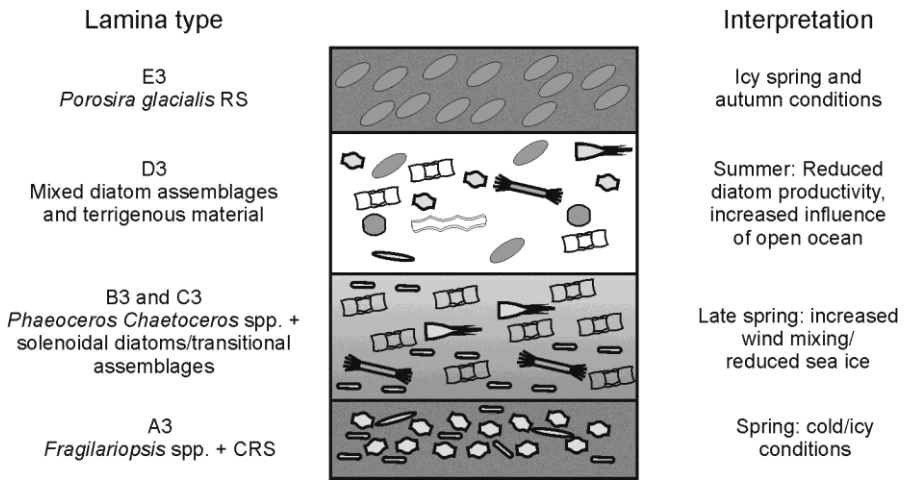

Figure 5.09. Schematic model of the annual sequence of lamina types recorded in Table 2. Shading indicates biogenic laminae, unshaded areas indicate laminae with relatively high terrigenous material. The distribution of diatoms in each lamina type is indicated in Figure 5.11, Figure 5.10 and Figure 5.12.

5.2.1 Distribution of CRS

Hyalochaete Chaetoceros resting spores (CRS) occur at higher relative abundances (21.9 – 81.0%, n = 27) and higher valve concentrations (2.87×10^{11} – 3.29×10^{11} CRS valves/g^{-1}) in core IODP-318-U1357B than MD03-2601 (5.1 – 52.5% and 7.01×10^{9} – 1.08×10^{11} CRS valves/g^{-1} respectively, n = 45) and their distribution by lamina in core IODP-318-U1357B is highly variable. CRS concentrations are high, but variable in A3 laminae, with consistently lower CRS concentrations in B3 and C3 laminae. D3 and E3

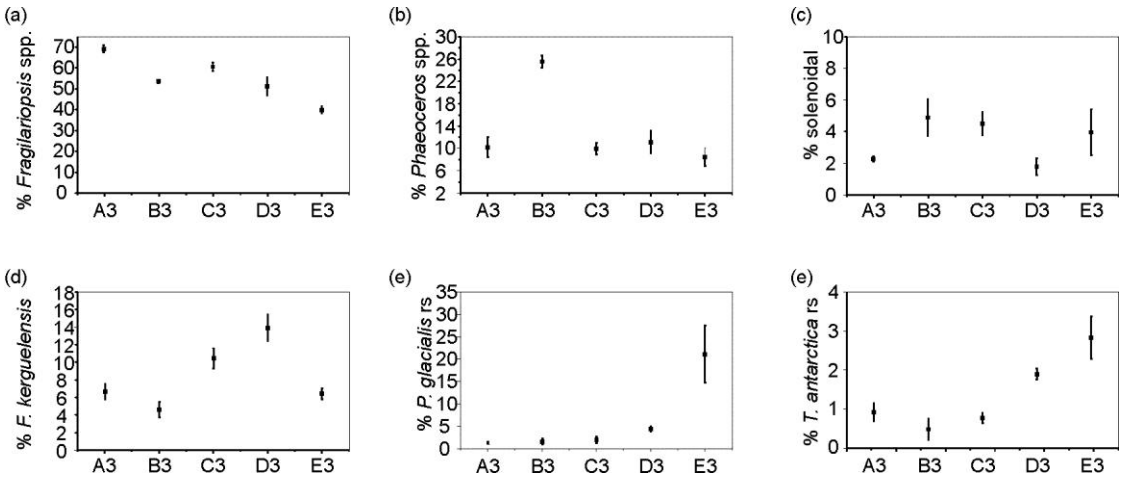

Figure 5.10. Mean relative abundance of key diatom species groups within quantitative assemblage counts by lamina type (n A3 = 7; B3 = 5; C3 = 6; D3 = 5; E3 = 4). Error bars indicate standard error for each data point.

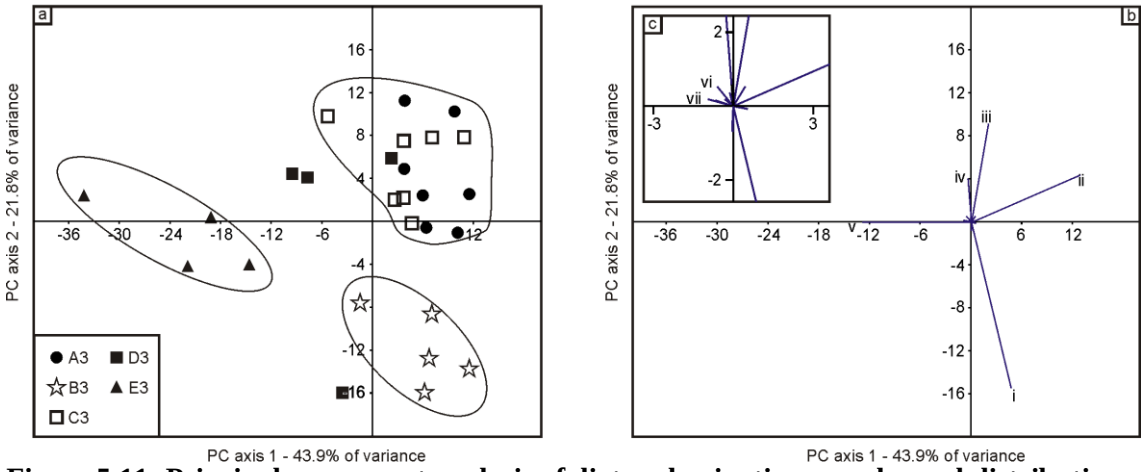

Figure 5.11: Principal component analysis of diatom lamination samples and distribution of diatom species groups that are statistically significant (see Table 5.04). (a) Distribution of diatom samples versus components one and two of the PCA. (b) Significance of diatom species versus components one and two of the PCA. (c) Detail of central area highlighted by square in (b). Diatoms indicated are (i) *Phaeoceros Chaetoceros* spp.; (ii) *F. curta*; (iii) *F. rhombica*; (iv) *F. kerguelensis*; (v) *P. glacialis* rs; (vi) *F. ritscheri*; (vii) *F. separanda*; (viii) *T. antarctica* rs; (ix) *F. cylindrus*; (x) *P. inermis*; (xi) *C. pennatum*.

laminae demonstrate the greatest variability in CRS concentrations, but have a similar mean value to A3 laminae (Figure 5.12b). The relative abundance of CRS within assemblages apparently increases from B3 to E3 laminae (Figure 5.12d) when considered in sequence (Figure 5.12d; see also section 6.2.4 and Figure 5.09), corresponding to a decrease in CRS-free diatom valves/gramme^{-1} of dry sediment (Figure 5.12a).

Chaetoceros spp. are broadly distributed in the modern surface waters of Adélie Land (Beans et al., 2008) and the occurrence of CRS in sediment traps from the Antarctic margin indicates that blooms are linked to seasonal sea ice retreat and surface water stratification (Crosta et al., 1997; Leventer, 1991), with *Hyalochaete Chaetoceros* being a common component of pack ice algal assemblages (Gleitz et al., 1998). Resting spore formation occurs due to depleted nitrogen levels or reducing light during vertical mixing of the water column or during the polar winter (Crosta et al., 1997 and references therein). The sedimentary occurrence of CRS is commonly associated with high nutrient levels and strong spring stratification and consequently resting spores may be found in high sedimentary abundances around the Antarctic margin (Crosta et al., 1997; Leventer, 1991). Generally high absolute abundances of CRS in A3 laminae (Figure 5.12b) is consistent with resting spore formation as a result of depleted nutrients

Table 5.04. Pearson's correlation coefficients between species analysed in the PCA of CRS-free diatom assemblage data from core IODP-318-U1357B (Figure 5.11) and eigenvalues of PC axes 1 and 2. Values in bold are statistically significant ($p < 0.05$).

Species	PC axis 1	PC axis 2
Phaeoceros Chaetoceros	0.38	**-0.88**
Corethron pennatum	0.24	-0.02
Eucampia antarctica	-0.37	0.07
Fragilariopsis cylindrus	-0.01	-0.07
F. curta	**0.86**	0.21
F. kerguelensis	-0.06	**0.45**
F. obliquecostata	-0.14	0.06
F. rhombica	0.20	**0.64**
F. ritscheri	0.21	0.19
F. seperanda	**-0.44**	0.30
F. sublinearis	-0.03	0.21
Porosira glacialis RS	**-0.90**	0.00
Proboscia inermis	-0.01	-0.34
Rhizosolenia semispina	0.02	0.06
Thalassiosira antarctica RS	**-0.63**	0.10
T. gracilis	-0.12	0.27
T. lentiginosa	-0.03	0.10

at the end of the spring period (Denis et al., 2006); whilst sporadically higher abundances in the summer and autumn may be indicative of mixing events (i.e. strong winds/storms) or resting spore formation in response to reducing insolation in the autumn (Crosta et al., 1997). Analysing CRS-free diatom assemblages also reveals important ecological information from other species that may be overwhelmed by the CRS signal (Leventer and Dunbar, 1996) and this approach is subsequently applied to the interpretation of laminae A3-E3.

5.2.2 Spring laminae: A3, B3 and C3 laminae

A3 laminae are characterised by the dominance of *Fragilariopsis* spp. with varying abundances of CRS when observed using BSEI. PCA shows that A3 laminae plot in a group with C3 laminae between 2 and 12 on PC axis 1, and between -1 and 12 on PC axis 2 (high *F. curta*). CRS-free assemblage counts are dominated by cryophilic *Fragilariopsis* spp. (69.2%), of which *F. curta* is the most abundant species (33.5% of total diatom valves). A3 laminae have lower abundances of solenoidal diatoms in CRS-free counts than C3 laminae (Figure 5.10). The preference of *F. curta* for a proximal ice edge (Beans et al., 2008; Riaux-Gobin et al., 2011; Riaux-Gobin et al., 2003) and

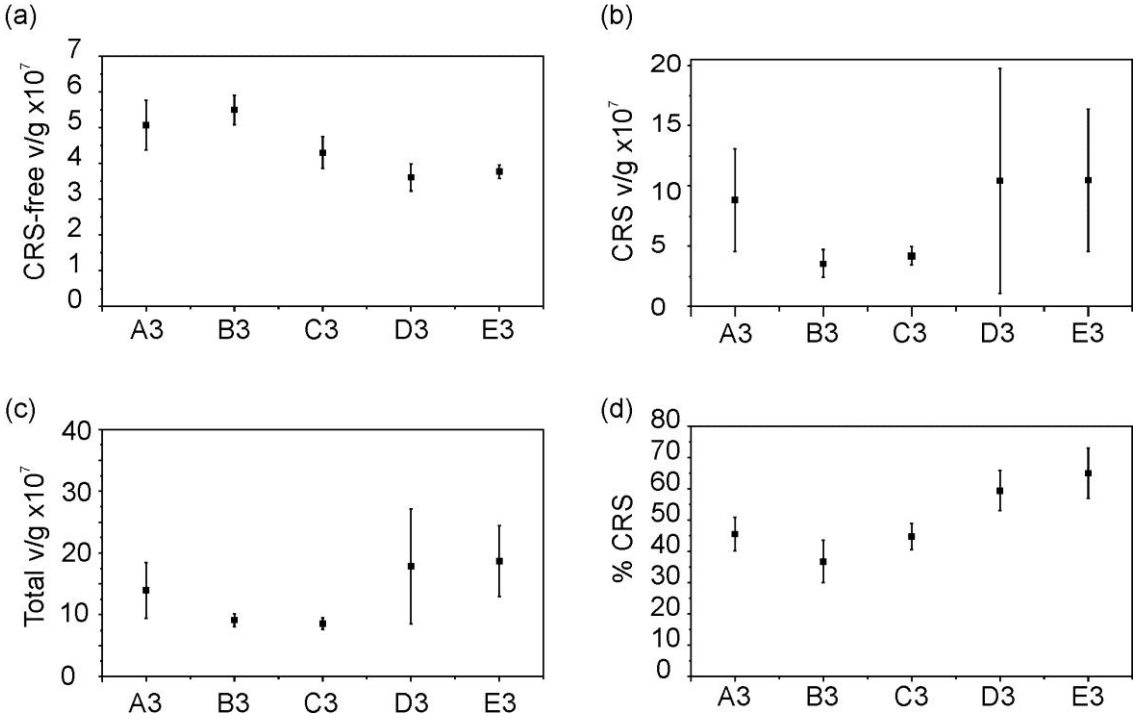

Figure 5.12. Distribution of diatom valves by lamina. (a) mean concentration of CRS-free diatom valves by lamina; (b) mean concentration of CRS valves by lamina; (c) total (CRS + other diatom species) diatom valve concentration per lamina; (d) mean relative abundance of CRS by lamina. Error bars indicated standard error of the mean (n A3 = 7; B3 = 5; C3 = 5; D3 = 6; E3 = 4).

peak sedimentary occurrences beneath 9-11 months/year sea ice cover (Armand et al., 2005) indicates that A3 laminae are associated with icy spring conditions.

B3 laminae are characterised by visually resolved *Phaeoceros Chaetoceros* spp. and solenoidal diatoms (in particular *Corethron pennatum*) when observed using BSEI. B3 laminae form a group from – 2 to 12 on PC axis 1 and -8 to -16 on PC axis 2 (high *Phaeoceros Chaetoceros* spp.). CRS-free assemblage counts are dominated by cryophilic *Fragilariopsis* spp. (53.6%) and B3 laminae have the highest abundances of *Phaeoceros Chaetoceros* spp. (25.5%) observed in this study. *Phaeoceros Chaetoceros* spp. thrive in open ocean waters (Kang and Fryxell, 1993; Smetacek et al., 2002), and their increased abundance in Adélie Land sediments since ca. 4.5 ka has been linked to increased wind-induced mixing of surface waters during the spring (Denis et al., 2010). *Corethron pennatum* in Adélie Land have a preference for ice free, wind-mixed surface

waters (Beans et al., 2008), and have also increased in sedimentary abundance since ca. 4.5 ka, linked to increased wind-induced mixing of surface waters (Denis et al., 2010).

C3 laminae are characterised by visually dominant *Fragilariopsis* spp. with centric and solenoidal diatoms also common when observed using BSEI. C3 laminae form a group with A3 laminae in the PCA, but tend to have lower values on PC axis 1 (slightly lower *F. curta*). When occurring at the end of a spring layer, C3 laminae exhibit a gradual increase in terrigenous matter, solenoidal diatoms and centric diatoms upcore, with a decrease in *Fragilariopsis* spp. in BSEI observations. Assemblages are similar to those of A3 laminae, with high abundances of cryophilic *Fragilariopsis* spp. (60.6%; *F. curta* 28.3%), but contain higher abundances of the solenoidal diatom group (4.5%). C3 laminae are interpreted here as representing high productivity associated with spring sea ice retreat, with a greater influence of oceanic waters than A3 laminae and weaker winds compared to B3 laminae.

5.2.3 Summer/autumn laminae: D3 and E3 laminae

D3 laminae are characterised using BSEI as having a mixed diatom assemblage and a relatively high proportion of terrigenous material. D3 laminae have the highest abundances of *Fragilariopsis kerguelensis* (13.9%) observed from laminae in IODP-318-U1357B, the lowest CRS-free diatom concentrations (Figure 5.12), relatively high abundances of *P. glacialis* RS (4.4%, Table 2) and do not form a distinct group in the PCA (Figure 5.11). Relatively high abundances of cryophilic *Fragilariopsis* spp. (51.2%) in D3 laminae are consistent with icy conditions, but the higher abundance of *F. kerguelensis* indicates a stronger influence of open oceanic waters (Crosta et al., 2005). Similarly, *P. glacialis* RS are found preferentially in sediments in regions where summer sea ice concentrations are <30% (Armand et al., 2005). The high concentrations of terrigenous material observed using BSEI indicates reduced dilution by diatoms following the spring bloom, and lateral advection of clay particles from more coastal areas following sea ice retreat (Denis et al., 2006; Dunbar et al., 1985; Presti et al., 2003; Maddison et al., 2012). D3 laminae are interpreted here as representing cool summer conditions with varying sea ice and meteorological conditions playing an important role in determining diatom composition.

E3 laminae are characterised by visually dominant *Porosira glacialis* RS with common *Stellarima microtrias* when observed using BSEI. E3 laminae form a distinct group in the PCA from -7 to -35 on PC axis 1 and -5 to 4 on PC axis 2 (high *P. glacialis* RS). CRS-free assemblage counts contain the lowest abundances of cryophilic *Fragilariopsis* species observed in core IODP-318-U1357B (40.0%), very high *P. glacialis* RS (21.0%) and high *T. antarctica* rs (2.8%). The presence of *P. glacialis* RS and *T. antarctica* RS in sediments is associated with a pulsed resting spore formation event due to autumnal ice growth in regions with >7.5 months/year sea ice cover (Pike et al., 2009). The greater abundances of *P. glacialis* RS relative to *T. antarctica* RS is consistent with the presence of *P. glacialis* RS laminae in the Neoglacial sediments of MD03-2601, and E3 laminae are interpreted here as representing years with both cold springs and autumns.

5.2.4 Annual sequences in core IODP-318-U1357B

A complete succession of repeating laminae in core IODP-318-U1357B contains an initial biogenic lamina (dark under BSEI) visually dominated by *Fragilariopsis* spp. ± CRS (A3 laminae), followed by a layer in which there is an increase in larger diatoms such as *Phaeoceros Chaetoceros* spp. and *Corethron pennatum* (B3 and C3 laminae), as well as an increase in centric diatoms. C3 laminae often show an increase in terrigenous material towards the upper boundary and are succeeded by a lamina with relatively high terrigenous material (light under BSEI), mixed diatom assemblage and reduced concentrations of *Fragilariopsis* spp. (D3 lamina). A final lamina which is visually dominated by *Porosira glacialis* RS (E3) occurs at the end of the sequence (Figure 5.09). There are commonly 3 – 5 lamina types per complete annual sequence; however, repetition of lamina types within the spring layer is common and up to 14 discrete laminae may be present in one year (Figure 5.13). The end of an annual sequence is defined by a sharp transition from either a mixed assemblage with relatively high *P. glacialis* RS and terrigenous material (D3), or a biogenic layer rich in *P. glacialis* RS (E3), to a lamina with much higher concentrations of *Fragilariopsis* spp. (A3). As with annual sequences in MD03-2601 (section), the contact between the final lamina of one year and the initial lamina of the following year is sharp. Repeated lamina sequences within the spring layer, in which there are no sharp transitions in floral succession, are

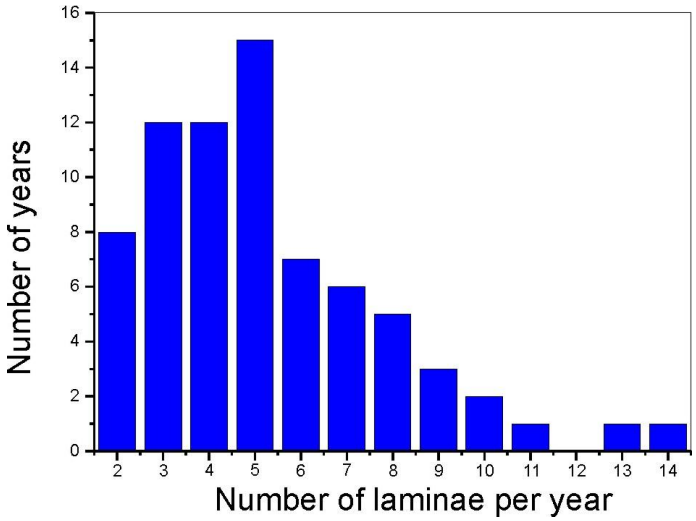

Figure 5.13. Histogram showing variations in the frequency of discrete laminae per year.

interpreted as representing single spring seasons in which there may be repeated lateral fluxes of diatoms or terrigenous material to the core site.

In total, 73 annual sequences (mean thickness = 35.0 mm, σ = 19.6 mm; Figure 5.14) are recorded in the core IODP-318-U1357B study interval, the majority of which (82%) have an initial A3 lamina, whilst the remaining 18% have an initial B3 or C3 lamina. This is in contrast to the Neoglacial section of core MD03-2601 which has greater variability in both the thickness (MD03-2601 has a lower mean annual thickness, but a standard deviation [σ] of ~ 110% of the mean, whereas IODP-318-U1357B σ = ~55% of the mean) and initial lamina type of annual sequences (48% of MD03-2601 have an initial A2 lamina, in comparison to the 82% of IODP-318-U1357B with an initial A3 lamina). The difference in the degree of variability is potentially due to preservational biases between the two cores that may reflect changes in oxidation. Multi-annual sequences in section III of MD03-2601 are limited to short snapshots disrupted by bioturbation (indicating short periods of anoxia that permits preservation of lamina), whereas the Neoglacial sediments of IODP-318-U1357B show a multidecadal, continuously laminated sequence with minimal sediment fabric disruption (suggesting a more continuously anoxic environment).

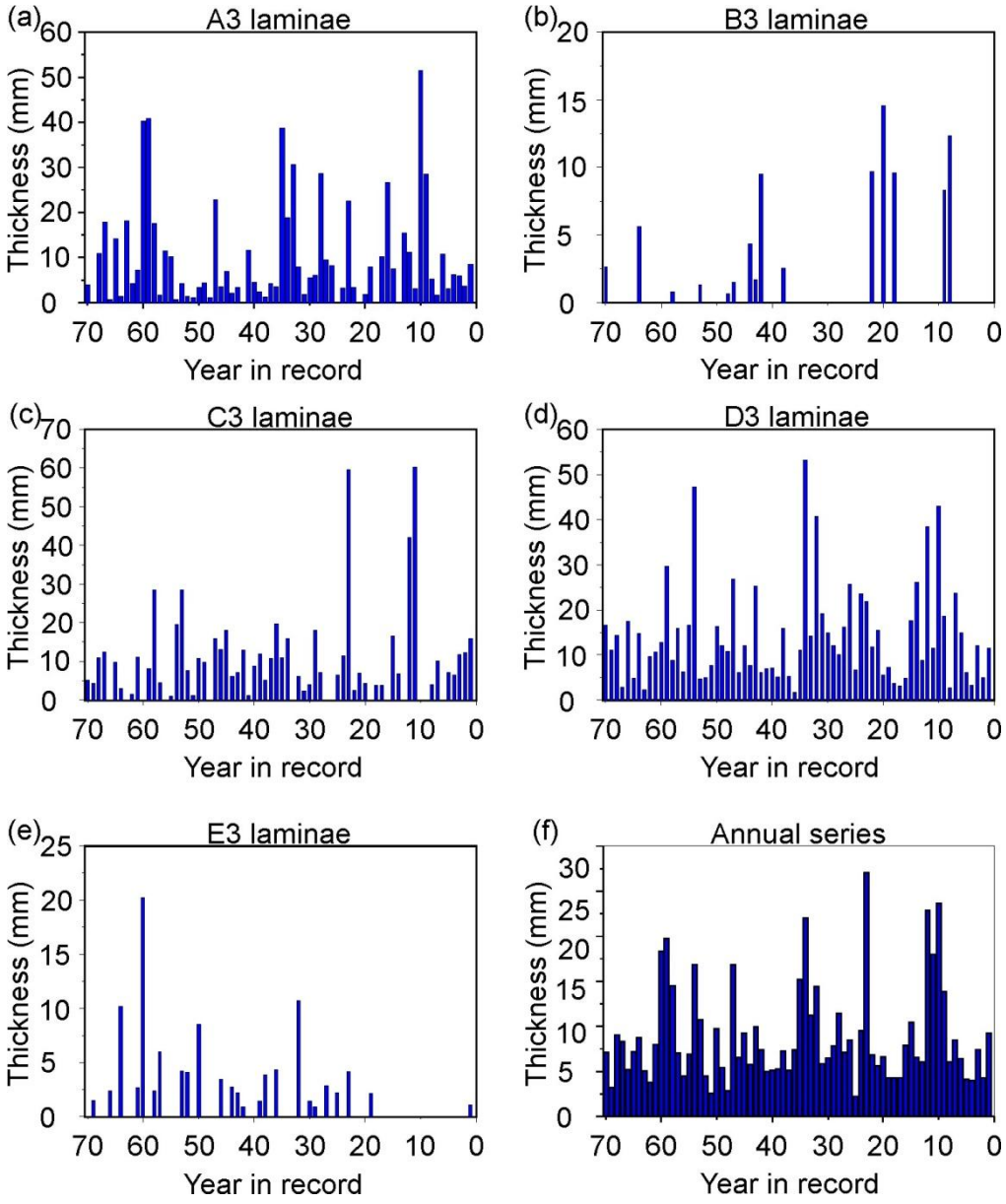

Figure 5.14. (a – e) Sedimentary thicknesses of laminae and (f) annual thicknesses from all years in sections examined from core IODP-318-U1357B (Neoglacial, ca. 1.8 – 1.6 cal ka BP).

5.3 Interannual variability

Changes in the interannual variability of diatom productivity can be compared between the investigated sections of cores MD03-2601 and IODP-318-U1357B. Sections from core MD03-2601 provide snapshots of continuously laminated, multidecadal records from the warm Hypsithermal (core section XVII and IX; 6.8 – 6.4 cal. ka BP and 5.2 – 4.8 cal. ka BP, respectively) and the mid-Holocene transition (core section VIII). MD03-2601 core section III provides snapshots of the interannual variability in the cool Neoglacial, whilst the sections analysed from core IODP-318-U1357B provides a 73-

year snapshot of a continuously laminated multidecadal record that is comparable in length to the multidecadal Hypsithermal and transitional records of MD03-2601.

Multi-taper method (MTM; Chapter 4) spectral analysis of the annual thickness and lamina type thickness time series from core section XVII and VIII of MD03-2601, and the record from IODP-318-U1357B has been used to statistically evaluate these records for significant cyclicities. The results of MTM are subsequently grouped into three categories related to climatic phenomena that have an influence on meteorology and climatology in the Antarctic (Chapter 2). Following previous work, the bands of cyclicities discussed here are quasi-biennial (QB; 2 - 3 years; Wang and Wang, 1996), 3 – 7 years (typical El Niño-Southern Oscillation [ENSO] spectra; Torrence and Compo, 1998) and longer periodicities which may be indicative of the SAM (Thompson and Wallace, 2000) or solar variability (Roscoe and Haigh, 2007). Although a quasi-biennial signal exists in ENSO time series (Allan, 2000) evidence exists for a link between the westerly phase of the quasi-biennial oscillation (QBO) and November conditions in the stratospheric southern hemisphere polar vortex (Baldwin and Dunkerton, 1998; Garfinkel and Hartmann, 2007). Conditions in the southern hemisphere stratosphere are transmitted to the Antarctic troposphere (Thompson et al., 2005) and consequently the Southern Ocean (Hibbert et al., 2010). QB-spectra have also been detected in re-analysis of satellite-derived sea ice concentrations (Gloersen and Huang, 2003). Increasing evidence for a complex ENSO-QBO inter-relationship (Taguchi, 2010) has also been used to argue for separation of QB and ENSO-band spectral signals in annually laminated polar sediments (Davies et al., 2011). Comparison with wavelet analyses of continuous time series that demonstrate ENSO-band peaks in the MTM analysis is used to demonstrate the non-stationarity (irregularity) of the observed 3 – 7 year frequencies, which is a characteristic of ENSO frequencies in wavelet analysis (Torrence and Compo, 1998). The wavelet analyses performed badly on the less regularly occurring lamina types (i.e. E-type laminae), and these wavelet analyses are presented in Appendix 4.

5.3.1 The Hypsithermal – core MD03-2601

Multidecadal records of interannual variability during the Hypsithermal have been developed from core sections IX (ca. 5.2 – 4.8 cal. ka BP) and XVII (ca. 6.8 – 6.4 cal.

ka BP). Relatively low variability is observed in both the composition and thickness of annual deposits in the Hypsithermal climatic interval (section 5.1.5). The majority of years (86%) have an initial A1 lamina indicative of earlier sea ice retreat earlier during the Hypsithermal relative to the Neoglacial, consistent with previous studies in the Dumont d'Urville Trough (Crosta et al., 2007; Denis et al., 2006). The occurrence of C1 laminae at the start of the remaining 14% of years is interpreted as representing warm spring conditions in which sea ice clears rapidly followed by an abrupt breakdown of stratification, inhibiting the formation of the ice edge proximal laminae A1 and B1. The relatively infrequent occurrence of E1 laminae (10% of years in core section XVII; 7% of years in core section IX) and the preference of *T. antarctica* for ~7.5 months per year sea ice cover (Pike et al., 2009) is consistent with an early sea ice retreat and prolonged open water period. At a broader scale, both Hypsithermal core sections are consistent with multidecadally resolved Holocene trends in diatom abundance (Chapter 4, Figure 4.01) that indicate reduced spring sea ice during the Hypsithermal (Crosta et al., 2007).

Two continuously laminated records from core section XVII (50 and 57 years long) reveal insights into multidecadal and interannual variability during the Hypsithermal climatic interval. The shorter 50-year record differs slightly from the 57-year record as it has more frequent occurrences of E1 laminae, less frequent occurrences of C1 laminae and a slightly lower mean annual thickness (Table 5.05). Furthermore, the 57-year record contains a sequence of 51 years in which there are no occurrences of E1 laminae. The association of E1 laminae with relatively icier Hypsithermal spring/autumn conditions and C1 laminae with relatively warmer Hypsithermal spring conditions indicates that the 50-year record of MD03-2601 core section XVII represents relatively cooler conditions compared to the 57-year record. This suggests that there were multidecadal (>50 year) variations between periods of relatively more/less sea ice and

Table 5.05. Comparison of sedimentary features between the 50 (2377 – 2322 cmbsf) and 57 year (2322 -2257 cmbsf) record in MD03-2601 core section XVII (Figure 5.04).

Feature	50-year record	57-year record
Mean annual thickness	8.25mm, σ = 5.03 mm	10.78 mm, σ = 6.83 mm
Years with C1 laminae	6 (12% of total)	11 (19% of total)
Years with E1 laminae	7 (14% of total)	2 (3.5% of total)

slightly cooler/warmer spring conditions occurring during this period of the Hypsithermal. A comparable long term change has been observed in the modern SAM record (Marshall, 2003), which demonstrates a trend from more negative to more positive values over several decades related to stratospheric warming resulting from ozone depletion (Thompson and Solomon, 2002) and anthropogenic warming (Marshall et al., 2004). These observations have been confirmed by modelling studies (Roscoe and Haigh, 2007; Arblaster and Meehl, 2006) demonstrating that the SAM may be forced by multidecadal climatic changes. The SAM influences East Antarctic sea ice extent in modern records by strengthening (weakening) westerly winds during positive (negative) phases, increasing (decreasing) northerly drift of sea ice, and subsequently increasing (decreasing) sea ice extent (i.e. positive phases of the SAM result in increased sea ice extent and *vice versa*). Additionally, during positive SAM phases, poleward heat flux decreases in the circumpolar region (Yuan and Yonekura, 2011; Hall and Visbeck, 2010). It was demonstrated in Chapter 2 that a correlation exists between positive SAM index and increased autumnal sea ice concentrations in Adélie Land; consequently the multidecadal changes in the distribution of E1 laminae (which are sensitive to autumnal sea ice formation) provides evidence for multidecadal phase changes in the SAM during the Hypsithermal. Accordingly, the relatively cooler 50-year record is interpreted as representing a prolonged period of more positive values in the SAM, whilst the relatively warmer 57-year record a prolonged period of more negative values in the SAM.

MTM analysis of the multidecadal records from core section XVII (Figure 5.15 and Figure 5.16) demonstrates that significant (>95%) longer period spectral peaks (>8 years; Table 5.06) occur in the annual thicknesses (26-year peak, 99% confidence) and A1 lamina thicknesses (22-year peak, 95% confidence) time series from the 57-year record (Figure 5.16 and Table 5.06). Although these periodicities should be treated cautiously, as only two full cycles can be fully expressed within the record, they may reflect control by the 22-year solar cycle, a multiple of the 11 year Schwabe cycle, which is observed in the geochemical record of the last 2000 years in the Adélie Drift (Costa et al., 2007). A QBO modulated 11-year solar cycle has been linked to increased late winter adiabatic warming of the southern polar stratosphere during solar maxima/westerly phases of the QBO (Labitzke, 2004; Roscoe and Haigh, 2007), from which anomalies are transmitted to the troposphere (Thompson et al., 2005). This

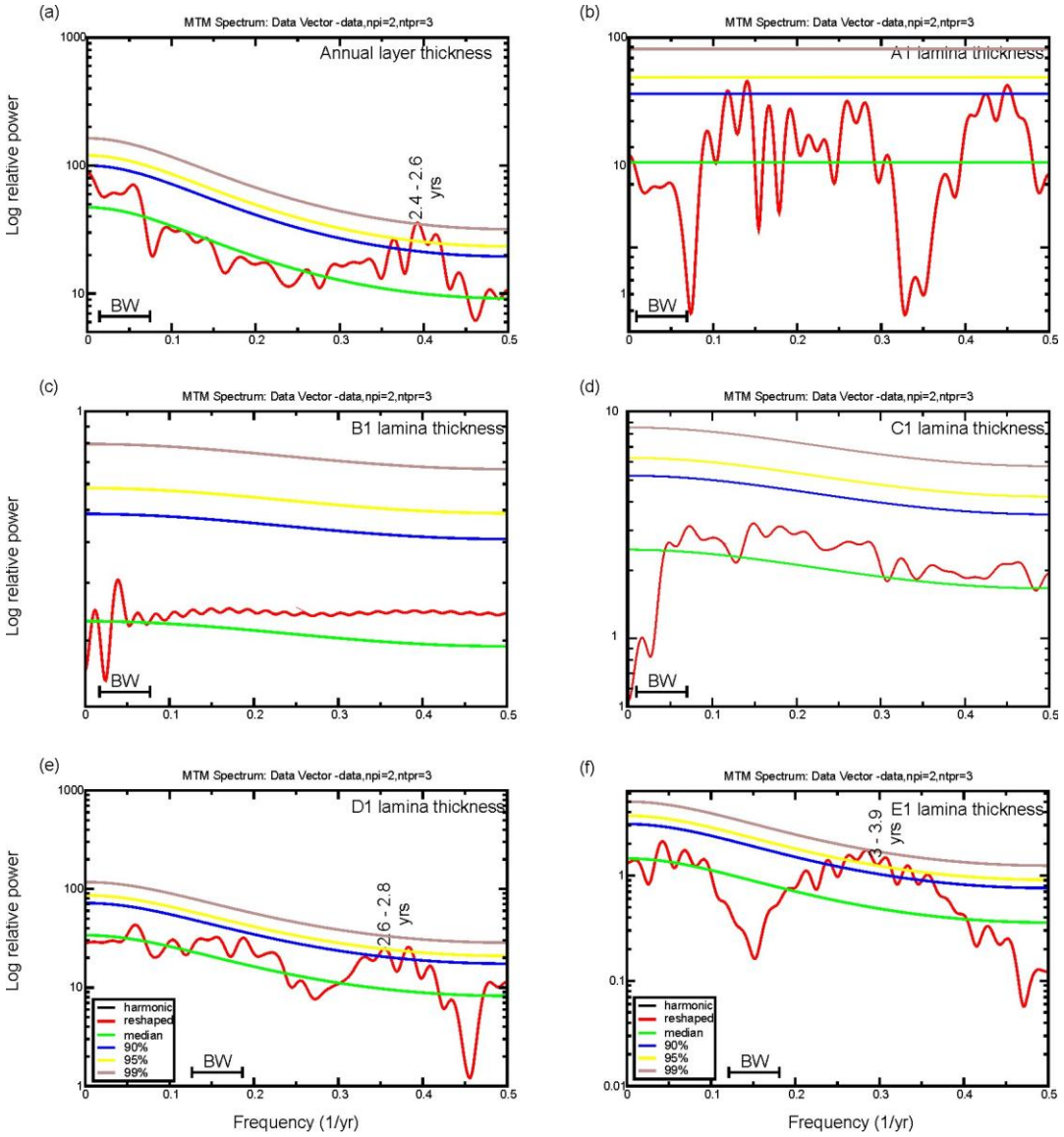

Figure 5.15. Multi-taper method (MTM) time series analyses (a) annual thicknesses and (b – f) lamina type thicknesses from a continuously laminated 50-year record (n = 50) in the MD03-2601 core section XVII (Hypsithermal ca. 6.8 – 6.4 cal. ka BP). Significant (>95% confidence) frequencies in years are indicated above spectral peaks, bandwidth (BW) = 0.06 cycles per year.

results in more negative conditions in the SAM during solar maxima/westerly QBO and positive SAM during solar minima/easterly QBO conditions. Eleven-year solar cycle periodicities linked to solar activity are present in methanesulphonic acid (MSA) concentrations from the Law Dome (Wilkes Land) ice core over the past 150 years (Curran et al., 2003). MSA is produced as a result of phytoplankton productivity in the ocean, is strongly influenced by the presence of sea ice (Curran et al., 2003; Foster et al., 2006) and provides evidence for a link between phytoplankton productivity and solar activity in recent records. It has also been shown that the solar influence on

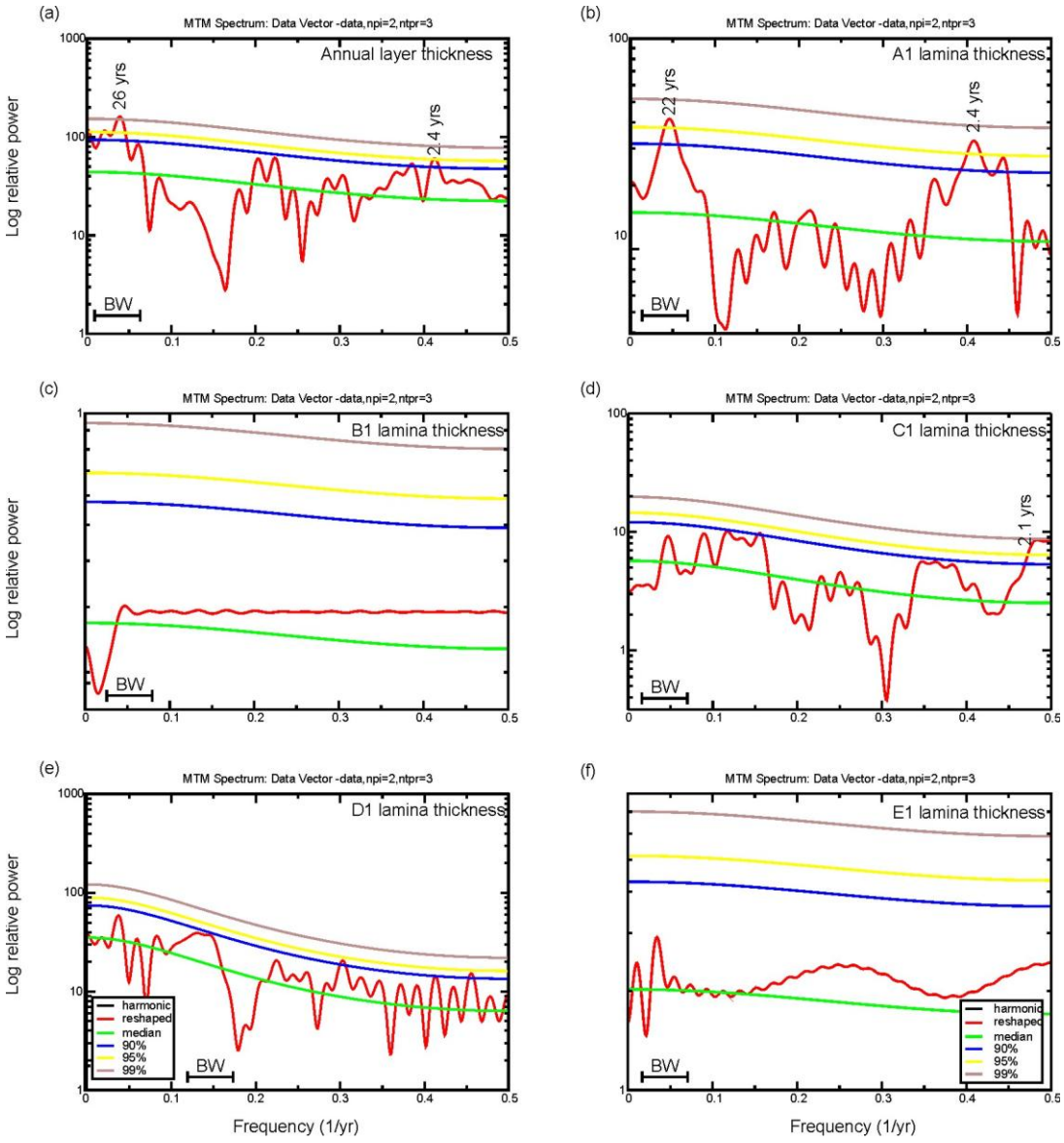

Figure 5.16. MTM time series analyses of (a) annual thickness and (b – f) lamina type thickness time series from a continuously laminated 57 year record (n = 57) in the MD03-2601 core section XVII (Hypsithermal). Significant (>95% confidence) frequencies in years are indicated above spectral peaks, bandwidth (BW) = 0.054 cycles per year.

Antarctic sea ice is stronger during the Hypsithermal climatic interval (Debret et al., 2009) and, hence, multiples of the11-year cycle may be well-expressed in Hypsithermal sea ice records (Crosta et al., 2007). Indeed, it has been suggested that a connection between longer period (centennial to millennial) solar activity and sea ice seasonality may exist in Holocene sedimentary records of the Antarctic Peninsula (Leventer et al., 1996) and the Dumont d'Urville Trough (Crosta et al., 2007). The 22-year periodicity in A1 lamina thickness may, therefore, be explained by an influence of solar variability

Table 5.06. Summary of the results of MTM spectral analyses conducted on all laminae from sequences >40 years long. Spectral peaks are significant to 95% (regular) and 99% (italic), those followed by an (h) are harmonic signals. Spectral bands are divided into QB (2.1 – 2-9 years; Wang and Wang, 1996), ENSO (3 – 8 years; Torrence and Compo, 1998) and longer period spectral peaks.

Interval (core/record length)	Time series	QB spectral peaks (2.1 – 2.9 years)	ENSO spectral peaks (3 – 8 years)	Longer period spectral peaks
1.6 ka (IODP/73 years)	Annual		4.5	
	A3 laminae		4, 3.2	
	B3 laminae	2 – 2.3		
	C3 laminae			
	D3 laminae	*2.4*	5.6	
	E3 laminae		3.7	100
4.5 ka (MD/43 years)	Annual			
	A2 laminae			
	B1 laminae			
	C1 laminae			
	C2 laminae			
	D1 laminae		*5.3 – 6 (h)*	
	E1 laminae			
6.8 ka (MD/57 years)	Annual	2.4		*26*
	A1 laminae	2.4		22
	B1 laminae			
	C1 laminae	2.1		
	D1 laminae			
	E1 laminae			
6.8 ka (MD/50 years)	Annual	*2.4 – 2.6*		
	A1 laminae			
	B1 laminae			
	C1 laminae			
	D1 laminae	2.6 – 2.8		
	E1 laminae		3.8, 3.6, 3.2, 3	

on spring sea ice concentrations (i.e. warmer springs corresponding to reduced deposition of the spring sea ice associated lamina type A1).

Significant sub-decadal frequencies in annual layer and lamina type thicknesses are also present within both the 50- and 57 year records (Figure 5.15, Figure 5.16 and Table 5.06). Within both records QB spectral peaks are the most commonly observed and are the only sub-decadal spectral peaks observed in the 57-year record (Figure 5.16). Within the57-year record, QB spectra peaks occur within the A1, C1 and combined annual lamina thickness records (Figure 5.16), whilst within the 50-year record QB spectra peaks occur within the D1 and combined annual lamina thickness records (Figure 5.15). ENSO-band peaks are observed within the E1 lamina (3 – 3.8 year

periodicities) time series of the 50-year record (Figure 5.15 and Table 5.06). E1 laminae (along with A1 laminae) show the strongest sea ice association of the Hypsithermal laminae in this study and it has been shown in Chapter 2 that a good correlation exists between spring sea ice concentrations in Adélie Land and a SAM-reinforced southern oscillation index. It is, therefore, reasonable to expect to see ENSO-associated spectral peaks within these laminae, particularly within the cooler 50-year record which indicates more positive phasing of the SAM.

5.3.2 The mid-Holocene transition – core MD03-2601

The interannual record of the late Hypsithermal in core section VIII is broadly comparable to the record of Hypsithermal core section IX (Figure 5.05), dominated by warm spring conditions with occasionally stronger spring winds indicated by the presence of B1 laminae. The continued presence of B1 laminae in the early Neoglacial is consistent with the observations of Maddison et al. (2012), and indicates that warm and windy springs were common for multi-year periods at this time; however, they are frequently interspersed by years with colder springs indicated by the presence of A2 and C2 laminae (Figure 5.05). Summer laminae throughout core section VIII are Hypsithermal in nature, with the presence of *T. antarctica* RS and absence of *P. glacialis* RS (Table 5.01). This is consistent with the 10 kyr long record of *T. antarctica* RS and *P. glacialis* RS from MD03-2601 which demonstrates an increase in absolute abundance of *P. glacialis* RS above section VIII at ~1000 cm core depth (3.7 cal. ka BP) and agrees with the distribution of E1 and E2 laminae. The increase in *P. glacialis* RS is associated with a transition to >7.5 months sea ice cover per year (Pike et al., 2009), suggesting that this boundary was not crossed during the initial transition into the Neoglacial. E1 laminae occur more frequently during the early Neoglacial interval (in 17% of years), indicating a shortening of the growing season.

The only significant spectral peak in MTM analysis of the continuous 43-year time series from core section VIII (Figure 5.17) is a 5.3 – 6 year harmonic (continuous or near-continuous oscillations in the data) spectral peak in MTM analysis of the D1 laminae (Figure 5.17 and Table 5.06). The apparent 5.3 – 6 year harmonic peak may be an artefact of the short time series considered here as harmonic signals are rare in climatic data which are commonly driven by red noise rather than white noise (which

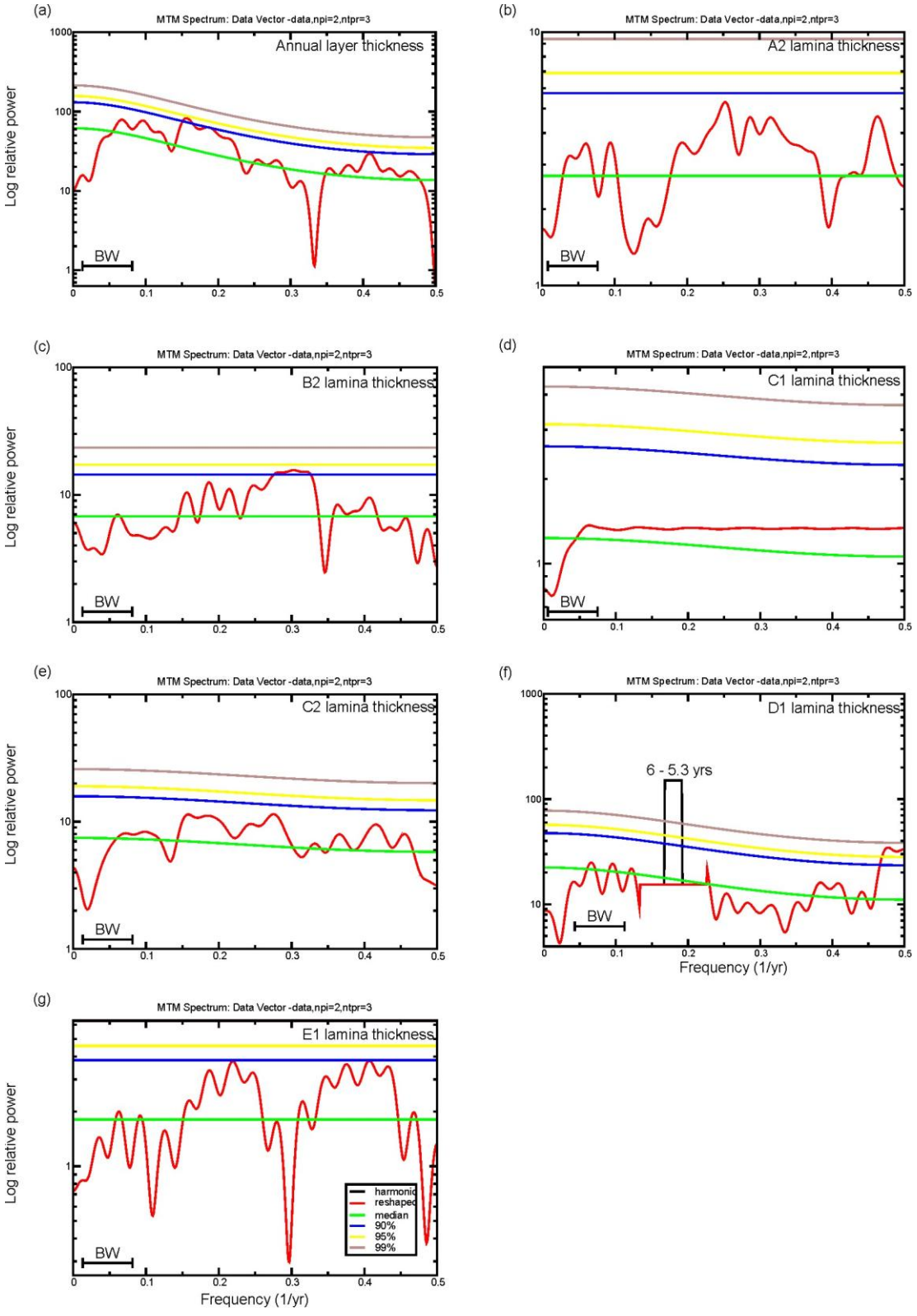

Figure 5.17. Multi-taper method (MTM) time series analyses of (a) annual thickness and (b – f) lamina type thickness time series from a continuously laminated 43-year record (n = 43) (Figure 5.06) in the MD03-2601 core section VIII (Transitional). Significant (>95% confidence) frequencies in years are indicated above spectral peaks. The black box in (f) indicates a broad harmonic signal (>99% confidence) identified by the MTM analysis, bandwidth (BW) = 0.069 cycles per year.

would be more likely to produce harmonic signals) processes (Ghil et al., 2002). Figure 5.18 demonstrates that the signal is not truly harmonic, occurring in two regions of the record but not throughout. Were the signal harmonic, a continuous band of significant (>95% that the periodicity is not produced by red noise processes) periodicity would occur across the whole time series, as opposed to the isolated peaks that occur at 5 – 10 years and (very weakly at) 30 – 35 years in the wavelet analysis of the time series. Furthermore, the spectral peak identified at 5 – 10 years in Figure 5.18 occurs largely outside the cone of influence. Periodicities outside of the cone of influence may suffer from attenuation of the signal due edge effects of the dataset and are unlikely to be statistically valid. Although not truly a harmonic signal as it is not continuous throughout the dataset, the ~5 – 6 year periodicity is consistently (although weakly) identified in both the MTM and wavelet analysis, suggesting that it may be a legitimate signal. These periodicities are within the ENSO band (Torrence and Compo, 1998) and may reflect a response of the D1 laminae to spring sea ice changes related to ENSO that are not recorded by the sporadic distributions of spring laminae A2, B1 and C2.

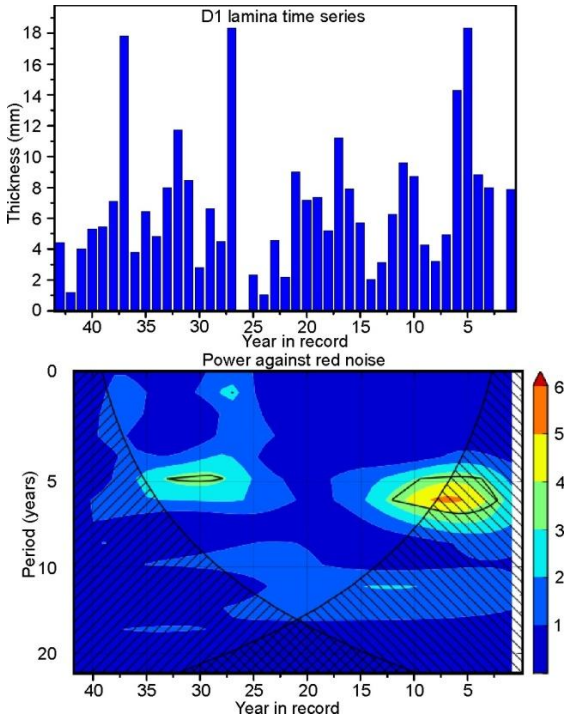

Figure 5.18. Wavelet time series analysis against a red noise model of D1 lamina thickness from the 43-year record in core section VIII. Solid lines indicate periodicities that are >95% confidence, cross hatching indicates the cone of influence, outside of which attenuation of the signal may occur due to edge effects of the data.

5.3.3 The Neoglacial

Cores MD03-2601 and IODP-318-U1357B have sharply contrasting preservation in the Neoglacial sediments examined here, but equally provide insight into longer period climatic processes during this interval. The sedimentary record of core section III from MD03-2601 has substantially higher degrees of bioturbation relative to the analysed sediments of IODP-318-U1357B, preserving brief snapshots (up to 11-year records) of Neoglacial interannual variability in sedimentation. Core IODP-318-U1357B provides a continuously laminated 73-year record of sedimentation. Both records, combined with the previously discussed Hypsithermal and transitional sections from MD03-2601, contribute to the understanding of interannual variability in Adélie Land during the Holocene.

5.3.3.1 Core MD03-2601

Increased bioturbation in core section III of MD03-2601 (Figure 5.07) makes it difficult to determine significant multi-annual trends in diatom productivity. It is possible, however, to gain some insights into the nature of interannual variability in meteorological conditions affecting sea ice break-up and diatom productivity in this climatic phase. The dominance of *Fragilariopsis curta* in all Neoglacial spring laminae indicates considerably icier spring conditions relative to Hypsithermal and early Neoglacial times. In particular, A2 laminae have very high abundances of *F. curta* and form 48% of spring laminae within the Neoglacial, suggesting that approximately half of the years in this climatic interval are characterised by low spring winds and a late sea ice melt. The remaining springs are characterised by higher relative abundances of CRS and open ocean species relative to A2 laminae; the presence of CRS suggests earlier sea ice retreat than A2 laminae. The higher abundances of *Corethron pennatum* and *Phaeoceros Chaetoceros* spp. in B2 laminae indicate that strong wind mixing during ice break up is important in these years. This strong contrast in interannual variability of meteorological conditions during the spring explains the high variability observed in multidecadal-resolution proxy records constructed from laminated sediments (e.g. Crosta et al., 2007).

Neoglacial summer laminae (D2) demonstrate the lowest consistency of diatom assemblages in core MD03-2601 (Table 5.01; Figure 5.03) most likely due to the high

variability of preceding spring conditions, as well as interannual changes in the concentration of sea ice during the summer. The common occurrence of *P. glacialis* RS in Neoglacial summer laminae likely reflects icier spring conditions relative to Hypsithermal summer laminae (Crosta et al., 2008). Particularly, *P. glacialis* RS laminae (E2) only occur following an A2 and D2 lamina, consistent with the interpretation of A2 laminae representing the coldest springs, with high sea ice concentrations that allow for a larger vegetative population of *P. glacialis* during the summer (Armand et al., 2005; Crosta et al., 2008; Pike et al., 2009). Years in which *P. glacialis* RS laminae form probably represent an early ice advance during the autumn (Maddison et al., 2012; Pike et al., 2009) and are rare within the MD03-2601 record, indicating that years in which both springs and autumns have high concentrations of sea ice were not common, consistent with modelling that suggests a later ice advance in the Neoglacial (Pike et al., 2009; Renssen et al., 2005).

The presence of well-preserved short sequences (~ten years; Figure 5.07) in core section III of MD03-2601 suggests that multi-decadal variations in preservation occurred at this core site during the Neoglacial. A similar late Holocene increase in bioturbation is observed in the Mertz Drift deposit on the George V margin (Presti et al., 2003) where sediments younger than 3 ka are characterised by high levels of bioturbation. This has been associated with increased oxygenation/ventilation of Adélie Land Bottom Water (ALBW) due to stronger brine formation in the cooler Neoglacial interval and reduced fluxes of organic matter to the sediment, consistent with the observations in core MD03-2601. Multi-decadal changes in the salinity of high salinity shelf water (HSSW – a precursor to ALBW) in the Ross Sea are correlated to multi-decadal changes observed in the SAM (Jacobs and Giulivi, 2010), which exerts an important control on Antarctic sea ice and oceanographic conditions at interannual to decadal periods (Hall and Visbeck, 2010; Stammerjohn et al., 2008; Yuan and Yonekura, 2011). Changes in preservation in core MD03-2601 may therefore be linked to long term changes in the salinity of HSSW forced by the SAM.

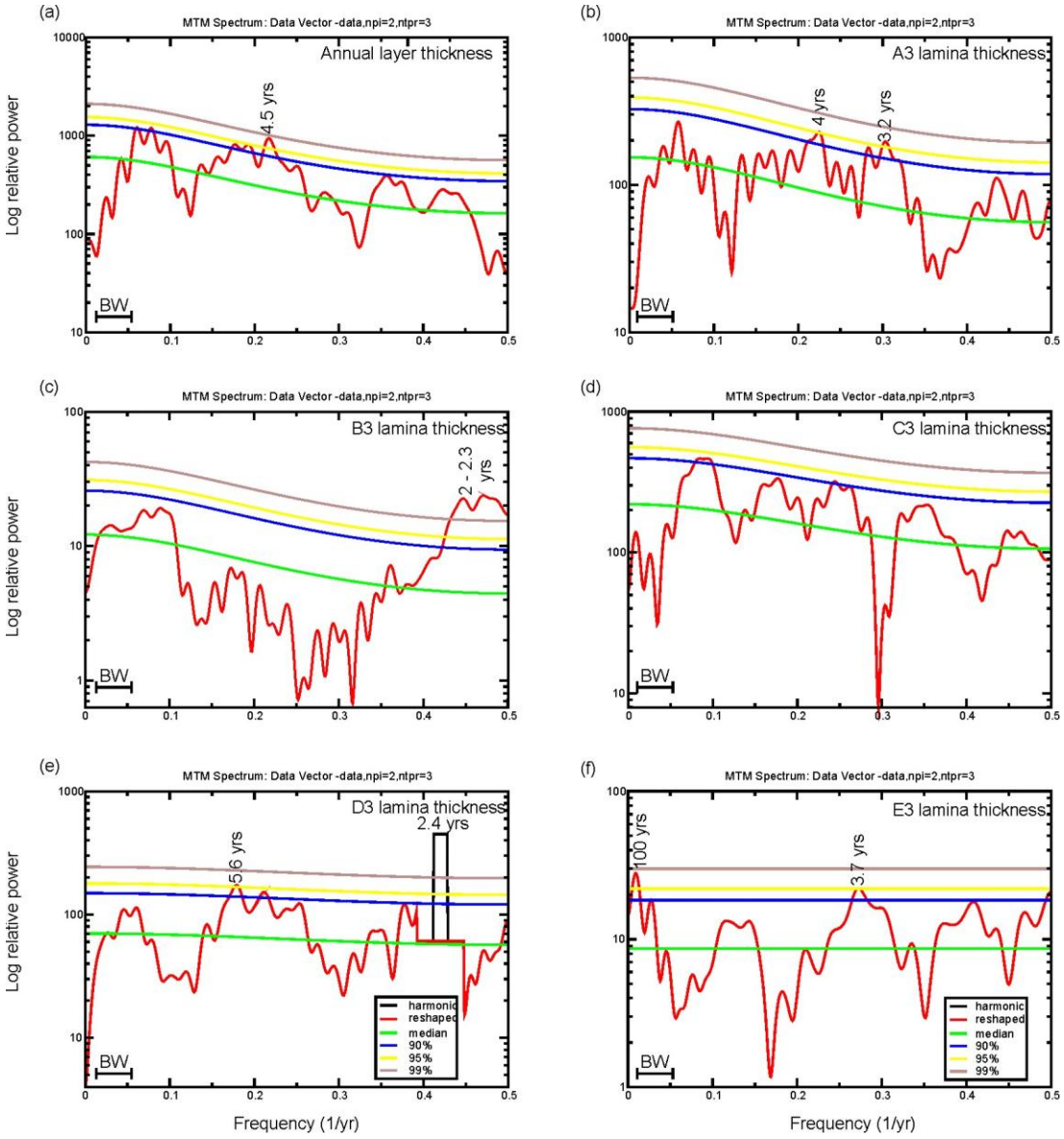

Figure 5.19. Multi-taper method (MTM) time series analyses of (a) annual thickness and (b – f) lamina type thickness time series from a continuously laminated 73-year record (n = 73) in the core sections from IODP-318-U1357B (Neoglacial). Significant (>95% confidence) frequencies in years are indicated above spectral peaks, bandwidth (BW) = 0.042 cycles per year.

5.3.3.2 Core IODP-318-U1357B

Core IODP-318-U1357B contains a 73-year record of continuous laminations, with a complex interannual variability in the total thickness and distribution of laminae. The majority of spring layers (91%) contain one or more A3 laminae, indicative of late sea ice break up during the Neoglacial and persistently icy springs. C3 laminae occur commonly in spring layers of IODP-318-U1357B (80% of spring layers), whilst B3

laminae occur less frequently (in 21% of springs). These further support the conclusion of persistent spring sea ice in the Neoglacial, whilst B3 laminae (with high abundances of *Phaeoceros Chaetoceros* spp.) indicate periods of stronger spring winds and more open conditions.

With the exception of E3 laminae, which demonstrate a 100-year spectral peak that cannot be considered valid from a 73-year time series, time series from IODP-318-U1357B do not display significant longer period spectral peaks from MTM analysis (Figure 5.19 and Table 5.06). Low frequency (3 – 4 year) ENSO band peaks occur within the A3 and E3 lamina time series whilst a slightly longer 5.6 year peak is observed in the D3 lamina time series. As with the occurrence of ENSO-band frequencies in E1 lamina time series identified at ca. 6.8 ka, the A3 and E3 laminae in core IODP-318-U1357B are those interpreted as having the strongest sea ice association (in particular, relatively high spring sea ice concentrations). ENSO-band frequencies in D3 laminae may result from changes summer sea ice (although this is not supported by the statistical analysis presented in Chapter 2) or in spring sea ice conditions altering the summer phytoplankton composition. The occurrence of these frequencies in resting spore-rich laminae in both the cooler Hypsithermal record and the Neoglacial record suggests that for longer records these species (*Thalassiosira antarctica* and *Porosira glacialis*) may provide useful information on changes in the ENSO-sensitivity of Adélie Land sea ice. Again, QB peaks have the strongest signal in MTM analysis at 99% confidence in the D3 lamina time series and are also observed in the B3 lamina time series at 95% confidence (Figure 5.19 and Table 5.06). Although the records presented here present only multidecadal snapshots of the whole Holocene, the common occurrence of QB peaks suggests that these may be a feature of both climatic intervals and is a hypothesis which requires further testing.

5.4 Summary

The results and interpretations presented here form the most detailed analysis of interannual sedimentary changes on the Antarctic margin to date and demonstrate a number of statistically significant relationships between the diatom composition and thickness of laminae in Adélie Land to external and internal forcings during the Holocene. In particular, the results demonstrate changes in the sensitivity of interannual

variations in sea ice (as indicated by A- and E- laminae) to internal climatic forcing during prolonged positive phases of the SAM and a reduced sensitivity during prolonged negative phases.

Analysis of the longer continuously-laminated (>40-years) time series by MTM for shorter period variations (see Table 5.06 for summary) demonstrates that in the warmer of the Hypsithermal records (the 57-year record ca. 6.8 ka) significant spectral peaks of 22 and 26 years, considered indicative of solar variability, occur in the A1 lamina and annual record, respectively. Given the modern connection between ice core MSA records and sea ice associated phytoplankton productivity (Curran et al., 2003; Foster et al., 2006) and evidence from around the Antarctic margin for a strong solar control on climate prior to ca. 4.5 ka (Debret et al., 2009), it is unsurprising that spectral peaks similar to the 22-year Schwabe cycle are observed in the 57-year record from ca. 6.8 ka (Table 5.06). The absence of these peaks from the 4.8 – 4.4 ka and 1.8 – 1.6 ka records the stronger influences of other factors on internal variability.

Quasi-biennial band peaks are the most commonly observed statistically significant spectral peaks throughout the sequences presented here, occurring in both the Hypsithermal and Neoglacial sections (Table 5.06). Recent observations of QB spectral peaks in in the coherent ocean mode (an oceanic equivalent to the SAM) of the Southern Ocean (Hibbert et al., 2010) demonstrates that this is a phenomena with the potential to influence polar regions. The QB band spectral peaks observed here have not previously been reported from Antarctic sediments are consistently around the 2.3 – 2.4 year mean for the phenomena (Baldwin et al., 2001). This suggests that there is no substantial change in the relationship between the QBO and biogenic sedimentation in Adélie Land during the selected Holocene periods analysed here.

5.4.1 RS-rich laminae, ENSO and SAM

The modern correlation between the SAM and autumnal sea ice (Chapter 2; Stammerjohn et al., 2008) and the known association of resting spore-rich sediments with autumnal sea ice formation (Pike et al., 2009; Maddison et al., 2012; Maddison et al., 2006; Denis et al., 2006) indicates that we should expect more frequent RS-rich laminae to be deposited during periods of positively phased SAM. This is demonstrated

by comparison of the two Hypsithermal multidecadal sequences in MD03-2601core section XVII and the 73-year sequence from core IODP-318-U1357B where it can be seen that such variations in RS-rich laminae exist and vary on multidecadal time scales greater than the records presented here (i.e. >50 years). A multidecadal change from negative to positive phasing of the SAM is broadly comparable to modern changes in SAM phasing (Figure 5.20). Although it must be bourne in mind that the modern record is forced to some extent by anthropogenic changes in ozone-depleting chemicals and greenhouse gases (Marshall et al., 2004; Thompson and Solomon, 2002), it demonstrates the sensitivity of the SAM to forcing by changes in the mean climatic state and we can reasonably speculate that such changes may be recorded in the sedimentary record. Furthermore, a connection between ENSO and SAM during the Holocene exists in the mid-latitude Pacific Ocean, alternating at a millennial scale between phases in which the reinforcing of the two climatic modes on one another is stronger or weaker (Gomez et al., 2012). The interpretations presented in this study suggest that there may be a multidecadal to centennial variability in this connection that exists in both Hypsithermal and Neoglacial periods in the records.

The distribution of E1 (*Thalassiosira antarctica* RS) laminae in core section XVII of MD03-2601, wherein there are only two occurrences of resting spore laminae in the 57-year record, but seven within the 50-year record demonstrates these potentially long term phases of cooler and warmer autumns. It can also be seen in the distribution of E3 laminae within IODP-318-U1357B that the first 23 years of the record contain only two occurrences of E3 laminae, whilst the later 50 years have frequent occurrences of E3 laminae (Figure 5.20), again suggesting multidecadal changes in RS-sedimentation. The sedimentary distribution of *T. antarctica* RS and *Porosira glacialis* RS is highly sensitive to subtle variations in the annual persistence and concentration of sea ice (Pike et al., 2009) and RS-rich laminae form (E1 and E3) as a consequence of autumnal ice formation (Pike et al., 2009; Maddison et al., 2012; Denis et al., 2006). In the modern record (Figure 5.20b – d) there is a strong association between positive values in the SAM and increased autumnal (March-April-May) sea ice concentration in Adélie Land (see also Chapter 2). Given that it is known that RS-rich laminae are sensitive to changes in autumnal sea ice, and that autumnal sea ice in the modern record is closely linked to the SAM, it can reasonably be assumed that RS-rich lamina distribution in Adélie Land may therefore be linked to multi-decadal phase changes in the SAM, with

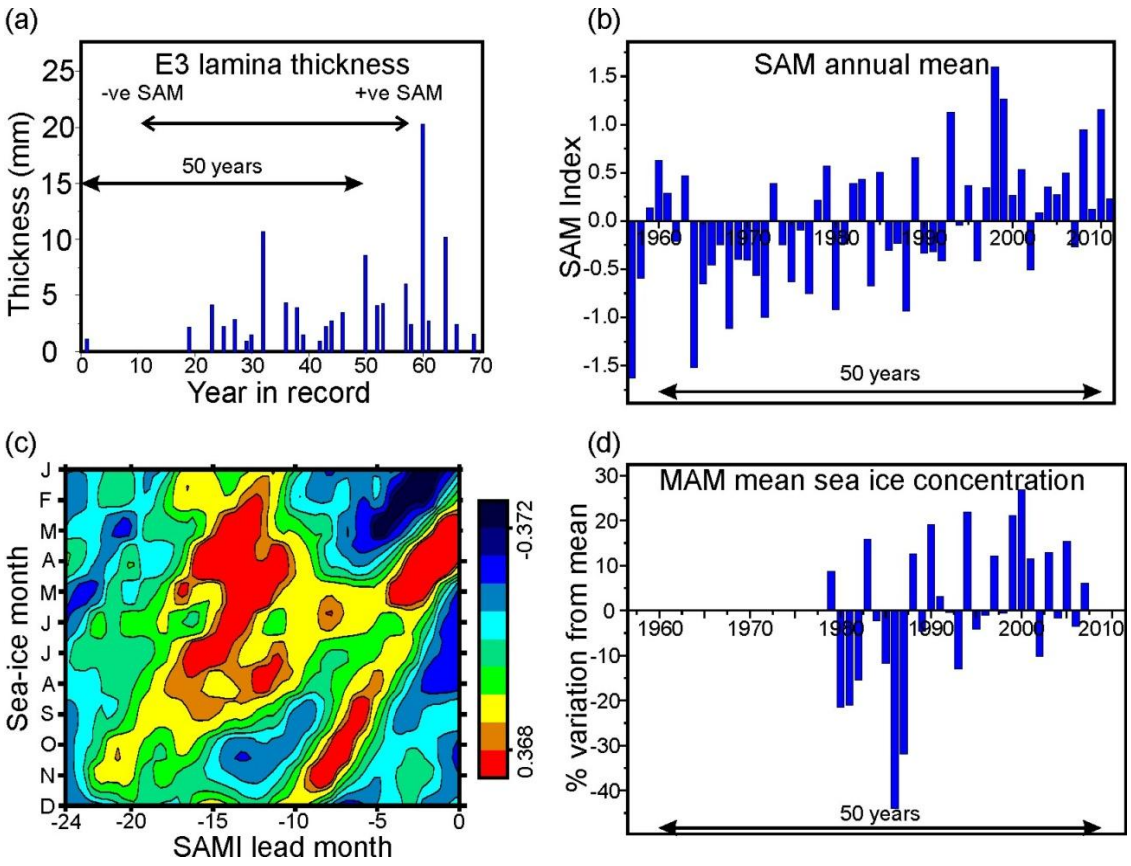

Figure 5.20. Comparison of (a) E3 lamina distribution in core IODP-318-U1357B (ca. 1.2 ka) and (b) annual mean values of the SAM 1955 – 2011; (c) cross comparison of monthly mean sea ice concentration (Comiso, 1999, updated 2008) versus lead time in the SAM Index with a 3 month running mean (Chapter 2; Marshall, 2003), 95% confidence limits are r = 0.368 and r = -0.372 (shown on legend); (d) the trend in autumnal (March-April-May) sea ice concentrations versus mean values for the period 1979 – 2007, derived from satellite data (Comiso, 1999, updated 2008) and plotted on a comparable scale to (b). Note that the axis on (a) has been inverted relative to the occurrence of the same data on Figure 5.14e for easier comparison to modern data.

RS-rich laminae occurring more frequently during positive phases of the SAM (i.e. during periods of higher autumnal sea ice; Figure 5.20a). Wavelet analysis of the more complete (A3 and D3 laminae; Figure 5.21) time series demonstrates that the ENSO-band frequencies occur more frequently in the latter half of the two records, coincident with cooler conditions as indicated by the distribution of E3 laminae (Figure 5.20) and as would be expected for changes in productivity related to increased sea ice during warm ENSO events reinforced by positive mode SAM. It was similarly shown (Section 5.3.1) that the occurrence on ENSO-band frequencies in the analysed Hypsithermal sediments (ca. 6.8 – 6.4 ka) was in the E1 lamina record interpreted as representing a positive phase of the SAM. These preliminary observations and interpretations provide

the hypothesis that phasing between the influence of ENSO and SAM on Adélie Land sea ice may occur at multidecadal to centennial timescales and would be testable on longer sequences of continuously-laminated Adélie Land sediments.

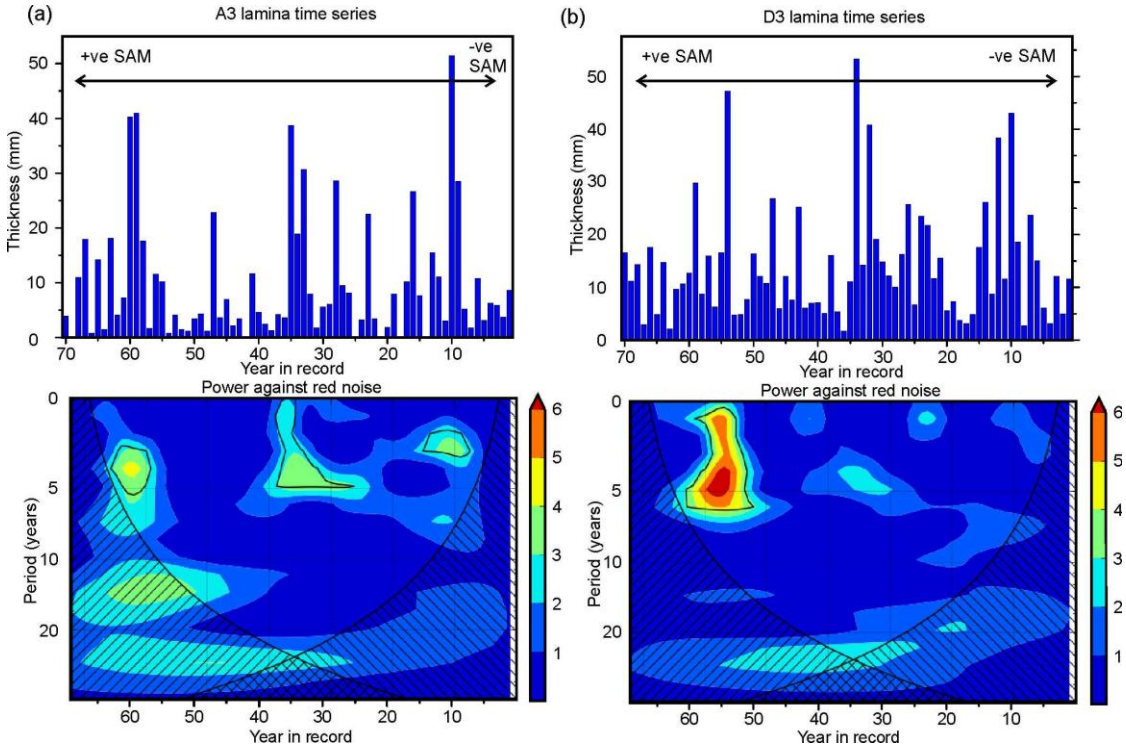

Figure 5.21. Wavelet time series analyses of sedimentary thicknesses from the continuously laminated 73 year record in core IODP-318-U1357B (Neoglacial) relative to a red noise model. (a) A3 lamina time series; (b) D3 lamina time series. Solid lines indicate >95% confidence limits and cross hatching indicates areas outside the cone of influence in which edge effects of the dataset may become important. SAM modes from Figure 5.20a.

Chapter 6. HBI analysis of sediments

Results from analysis of highly branched isoprenoid (HBI) alkenes in sediments from core MD03-2601 are presented. Attempts to directly target individual laminae for HBI analysis were ultimately unsuccessful, due to the difficulty of sampling the often very thin laminae from sediments in which obvious colour changes had been lost due to oxidation. Consequently, these lamina-scale results are not discussed further but are contained in Appendix 5. HBI analysis of the lower resolution sampling, of continuous 1 cm samples from core sections III, VIII and XVII, are discussed in detail below. The results are considered in two ways. First, trends in HBI distribution are investigated in selected sediment sections, with a focus on the mid-Holocene transition, which provides the strongest contrast in diatom lamina type distribution (Chapter 5). Second, the distribution of HBIs from the continuous 1 cm samples relative to lamina distribution in each core section is considered, in order to determine if a quasi-seasonal signal can be detected in the HBI record.

6.1 Holocene trends in HBI concentrations

The concentration of both HBI diene and triene shows an increase from the Hypsithermal (core section XVII) to the Neoglacial (core section III), as does the ratio of diene/triene (D/T; Figure 6.01). The HBI diene is only present in three of 141 samples from core section XVII; it occurs in low relative abundances between 1200 and 1110 cm (mean relative abundance = 0.4) and with increased frequency and concentrations between 1110 and 1050 cm (mean relative abundance = 1.5; Table 6.01) in core section VIII, a statistically significant increase (Mann-Whitney U = 693, n 1200 – 1110 cm = 86, n 1110 – 1050 cm = 57, $p < 0.001$). Higher, although variable, diene concentrations are observed in the majority of samples from core section III (mean relative abundance = 3.8; Table 6.01). In contrast, HBI triene was present in most of the samples analysed. HBI triene occurs in relatively low concentrations in core section XVII (mean relative abundance = 13.6; Table 6.01), slightly (yet statistically significant) higher concentrations in core section VIII (mean relative abundance = 18.3; Mann-Whitney U = 6084, section XVII n = 141, section VIII n = 143, $p < 0.001$) and highest concentrations in core section III (mean relative abundance = 51.9). The ratio of D/T is dominated by the presence, absence and relative concentrations of HBI diene

versus the more stable values of HBI triene within the sediments of core MD03-2601 (Figure 6.01).

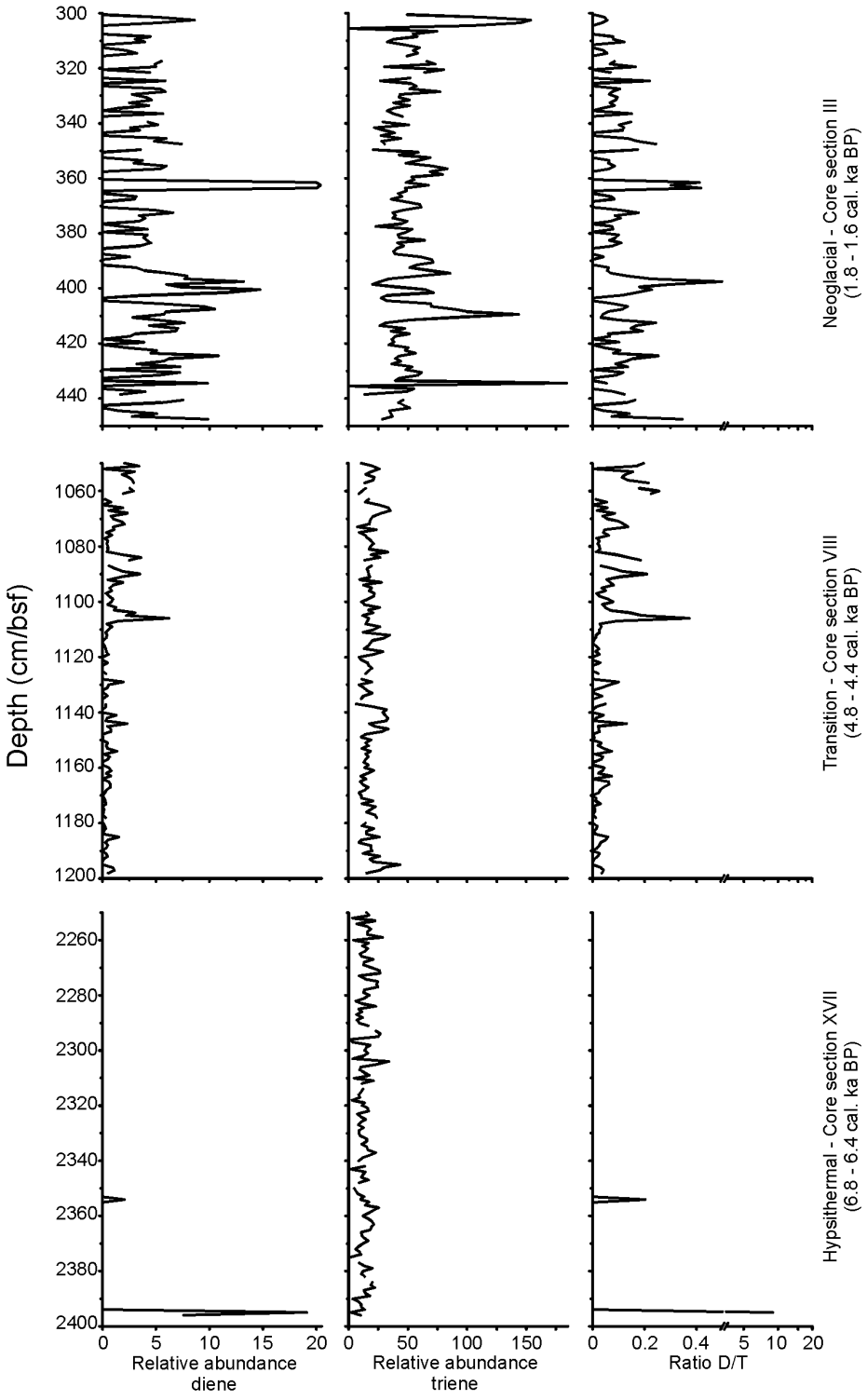

Figure 6.01. Holocene trends in relative abundances of HBI diene, HBI triene and the ratio D/T in core MD03-2601.

Table 6.01. Mean relative abundance data of HBI diene and triene in all core sections.

Core section (sample depths)	Number of samples measured	Mean diene relative abundance (1σ standard deviation)	Mean triene relative abundance (1σ standard deviation)
III (300 – 450 cm)	143	3.79 (3.96)	51.94 (25.40)
VIII (1050 – 1110 cm)	56	1.51 (1.18)	18.26 (7.23)
VIII (1110 – 1200 cm)	87	0.39 (0.43)	18.31 (6.09)
VIII (all data)	143	0.83 (0.98)	18.28 (6.79)
XVII (2250 – 2400 cm)	141	0.20 (1.74)	13.60 (6.09)

Pearson correlation coefficients between all of the HBI diene and all of the HBI triene data presented here suggests that there is a moderately strong correlation between the two at the millennial time scale ($r = 0.463$, $p < 0.001$, $n = 429$). However, Figure 6.02 shows that no consistent relationship between HBI diene and triene concentrations exists at shorter timescales (i.e. when considered within an individual core section). It should be noted that comparisons in core section XVII are compromised due to an absence of HBI diene from the majority of samples.

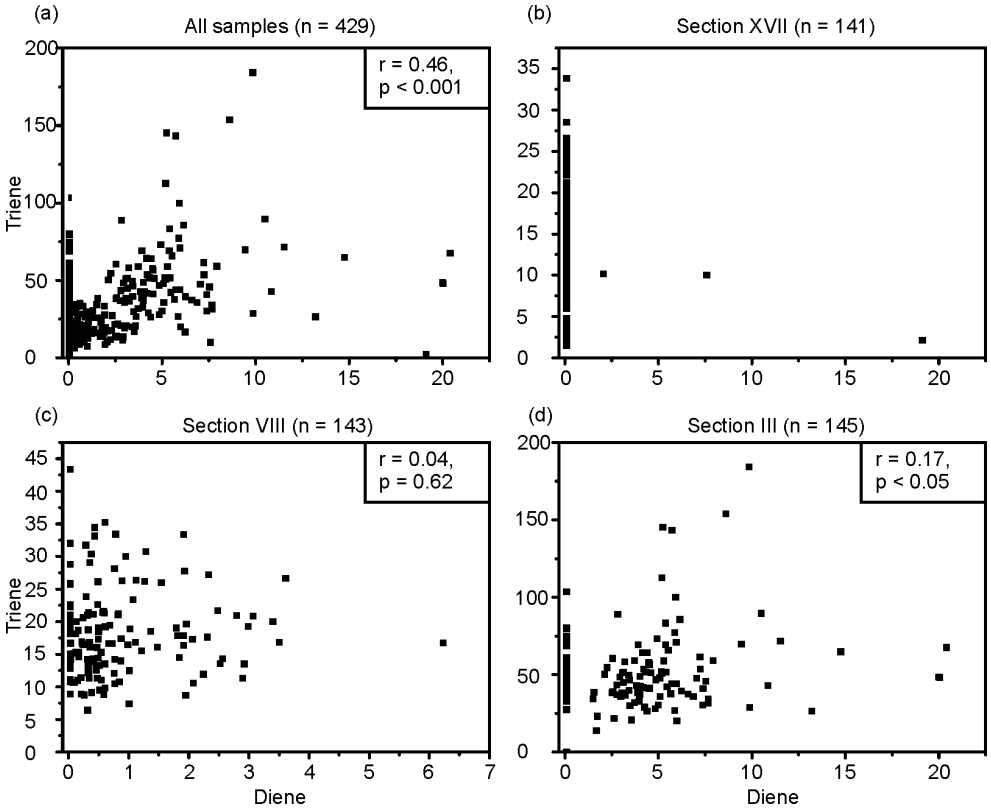

Figure 6.02. Pearson correlation between relative abundances of HBI diene and triene values in (a) all samples shown in Figure 6.01; (b) all samples from core section XVII; (c) all samples from core section VIII; (d) all samples from core section III.

The statistically significant increase in HBI diene across the mid-Holocene transition (Table 6.01; Figure 6.03) is broadly consistent with the changes in diatom lamina distribution (Chapter 5). A large increase in HBI diene at 1110 cm occurs ~20 cm above the mid-Holocene transition identified from the first occurrences of Neoglacial spring laminae (Chapter 5). However, the diatom lamina record of this study demonstrates that the early Neoglacial interval contains many Hypsithermal-like laminae and is gradual in nature, therefore a sharp increase in HBI biomarkers may not occur coincident with the threshold required to produce the initial Neoglacial spring laminae. This reflects that HBI diene is produced by diatoms that exclusively live within sea ice and are poorly preserved in the sedimentary record (Belt et al., 2008; Brown et al., 2011), in contrast to those diatom species widely employed by micropalaeontologists to infer the presence of sea ice, that are commonly found in open waters as well as within sea ice (e.g. von Quillfeldt, 2004; Beans et al., 2008; Riaux-Gobin et al., 2011). Given this, it is not too surprising that the HBI concentrations do not exactly follow the lamina-derived record of seasonal changes in sea ice presented here.

Unfortunately, the intermittent presence of bioturbated sediments (section 6.2.2 and Chapter 5) across the Hypsithermal – Neoglacial boundary prevents us from estimating the relative timing of changes in diatom lamina type and HBI concentrations. However, the HBI diene demonstrates a good similarity to the sea ice associated diatom group record (Figure 6.03) (*Fragilariopsis curta, F. cylindrus, F. sublinearis, F. obliquecostata, F. vanheurkii, Porosira glacialis*; Denis et al., 2009), which increases from ~12% at 1136 cm to >25% above 1120 cm. In contrast, relative abundances of CRS and *F. kerguelensis* decrease above the 1128 cm boundary. CRS form following nutrient depletion at the end of a sea ice melt-induced bloom and are indicative of relatively earlier sea ice melt in the Hypsithermal compared to the Neoglacial (Chapter 5). *Fragilariopsis kerguelensis* is an open ocean species that may enter coastal areas during the summer when sea ice cover has reduced and its sedimentary Holocene distribution is generally inverse to sea ice duration (Crosta et al., 2008). The reduction of both these taxa above 1128 cm (Figure 6.03) potentially supports later spring melting of sea ice, which would permit a longer growing period for the sea ice taxa that produce the elevated sedimentary HBI diene concentrations.

Due to the occurrence of HBI diene exclusively within sea ice and the presence of HBI triene in phytoplankton samples (Massé et al., 2011) it has been suggested that the use of the D/T ratio in sedimentary records provides an indication of the relative contribution of sea ice and open water productivity (Barbara et al., 2010; Denis et al., 2010; Massé et al., 2011). The definition of open water conditions often varies widely between studies (e.g. Barbara et al., 2010; Denis et al., 2010; Massé et al., 2011) hence the relationship between triene and open water production is not clear, however, comparison of the individual diene and triene trends may provide information about changes in the sea ice and marginal ice zone environments (i.e. seasonal sea ice duration and concentrations) (Collins et al., submitted manuscript). The reasonable correlation between the two HBI alkenes at lower temporal resolution recorded in core MD03-2601 ($r = 0.463$, $p < 0.001$, $n = 429$) suggests that they both reflect similar elements of the sea ice environment and therefore increases in their concentrations may provide a good proxy for increased duration of sea ice on millennial timescales (i.e. between distinct climatic phases). If this is the case then changes in the D/T ratio may not clearly reflect changes in the relative input of sea ice versus open water biomass to sedimentation as has been previously suggested (Barbara et al., 2010; Denis et al., 2010; Massé et al., 2011). At higher resolution (annual to sub-annual) the poor correlation between the HBI diene and triene (Figure 6.02) shows that the longer time scale relationship

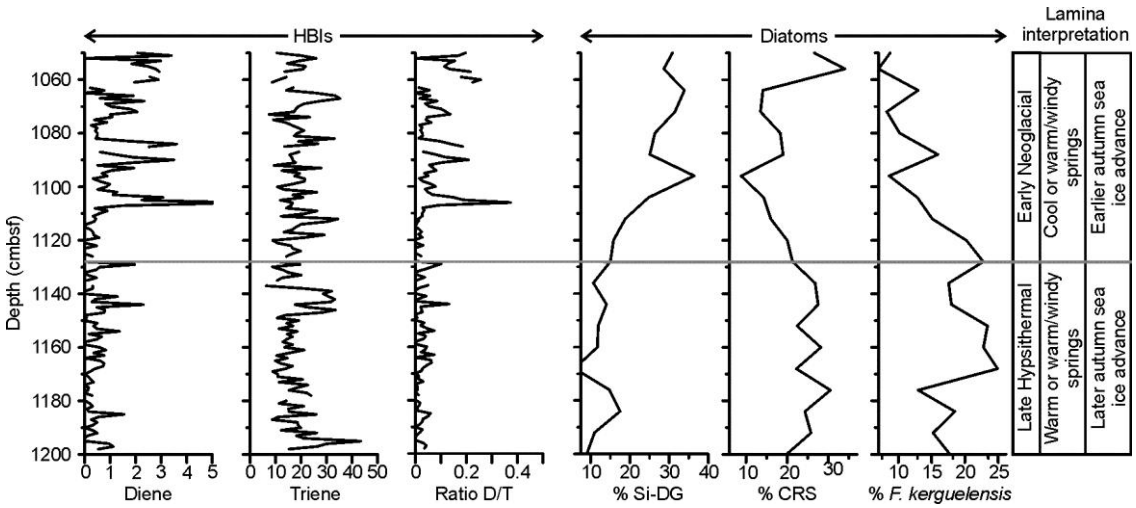

Figure 6.03. The mid-Holocene transition in core MD03-2601 section VIII as indicated by HBIs, low resolution diatom counts of the sea ice diatom group (Si-DG; Denis et al., 2009), relative abundances of CRS and *Fragilariopsis kerguelensis* (Crosta et al., 2007) and summarised seasonal changes in temperature and sea ice cover (Chapter 5, this study). The grey line indicates the mid-Holocene transition as defined in Chapter 5 by the first occurrence of Neoglacial-type spring laminae.

between the two breaks down; potentially due to their different concentrations in individual laminae.

6.2 High resolution analysis of HBIs

The 1 cm resolution HBI record (Figure 6.01) demonstrates a large degree of high frequency variability and here these data are considered in comparison to the diatom-lamina data presented in Chapter 5 (Figure 6.04 – 6.05).

6.2.1 Core section XVII (the Hypsithermal)

Section XVII of core MD03-2601 is dated at ca. 6.8 – 6.4 ka BP and records warm conditions with reduced annual sea ice presence during this part of the Holocene climatic optimum (Chapter 5). The HBI triene occurs in all samples from core section XVII with many peaks apparently coincident with samples that contain A1 laminae or A1 laminae mixed with other lamina types (e.g. at 2306 and 2296 cm). However, this is not consistent throughout the core section and not all A1 laminae are associated with high triene relative abundances (e.g. at 2291 and 2320 cm core depth there are large A1 laminae but low relative abundances of triene). Comparison of the mean relative abundance of triene between the intervals identified by lamination analysis (Chapter 5) as slightly cooler (earlier autumnal ice advance, lower annual deposition; 2377 – 2332 cm, n = 43) and slightly warmer (later autumnal ice advance, higher annual deposition, more frequent warm springs; 2322 – 2257 cm, n = 64) reveals that there is no significant variation in triene relative abundances across core section XVII (Mann-Whitney U = 1247, n 2377 – 2332 cm = 43, n 2322 – 2257 cm = 64, p = 0.41). This may indicate a lack of sensitivity of the HBI triene proxy to subtle interannual variations in marginal ice zone (MIZ) conditions during warmer periods due to an overall reduced duration of the MIZ. Only two HBI diene peaks are observed in core MD03-2601 section XVII indicating that the HBI diene is not common in climatic intervals with relatively warm spring conditions.

Figure 6.04 (next three pages). Relative abundances of diene, triene and the ratio D/T at a 1 cm resolution in core section XVII, compared to stratigraphic log of lamina distribution. Note, particularly thin C1 laminae are represented by grey bars rather than a symbol (see key, p 119).

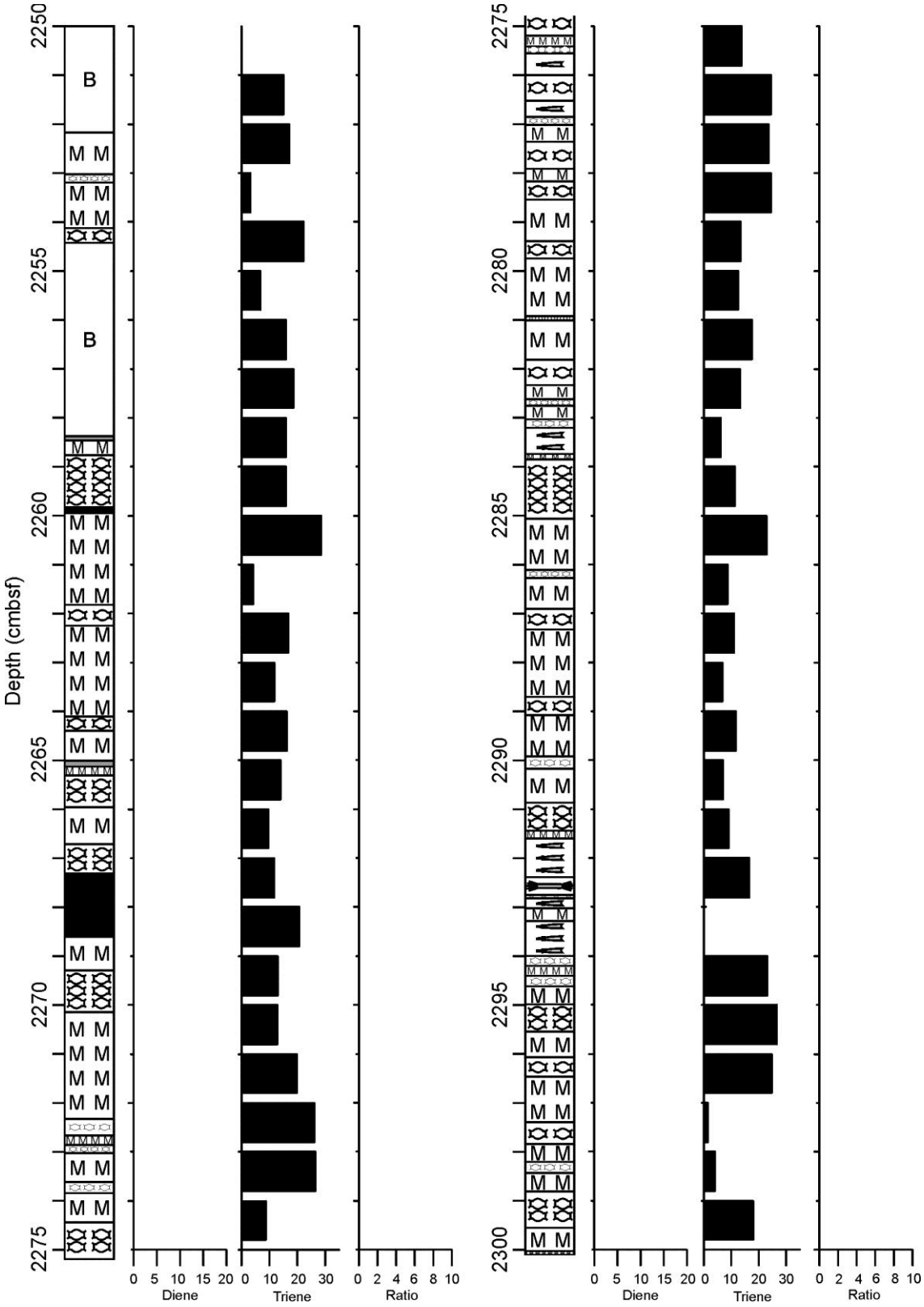

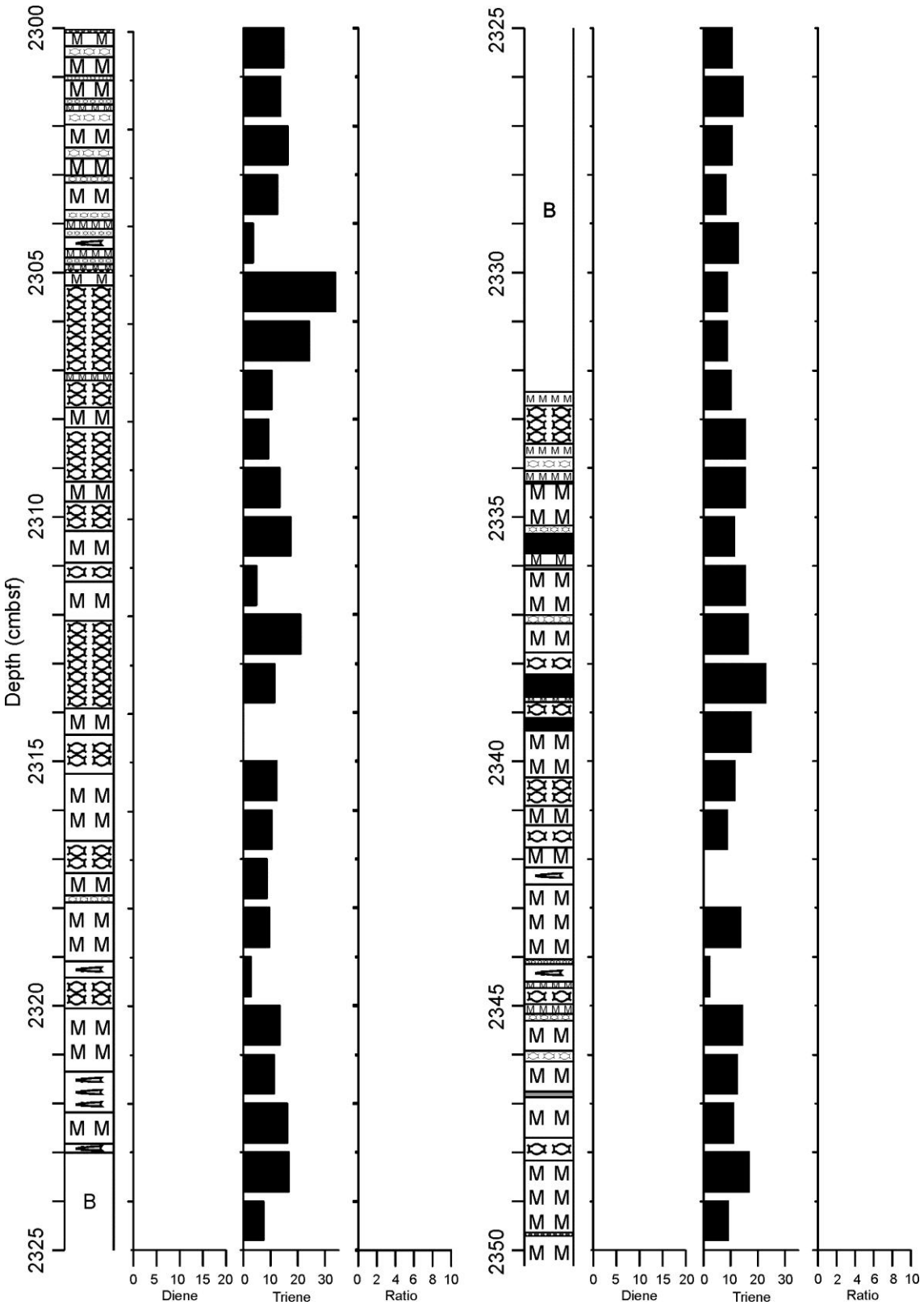
Depth (cmbsf)
2300
2305
2310
2315
2320
2325
2330
2335
2340
2345
2350
B
B
0 5 10 15 20
Diene
0 10 20 30
Triene
0 2 4 6 8 10
Ratio
0 5 10 15 20
Diene
0 10 20 30
Triene
0 2 4 6 8 10
Ratio

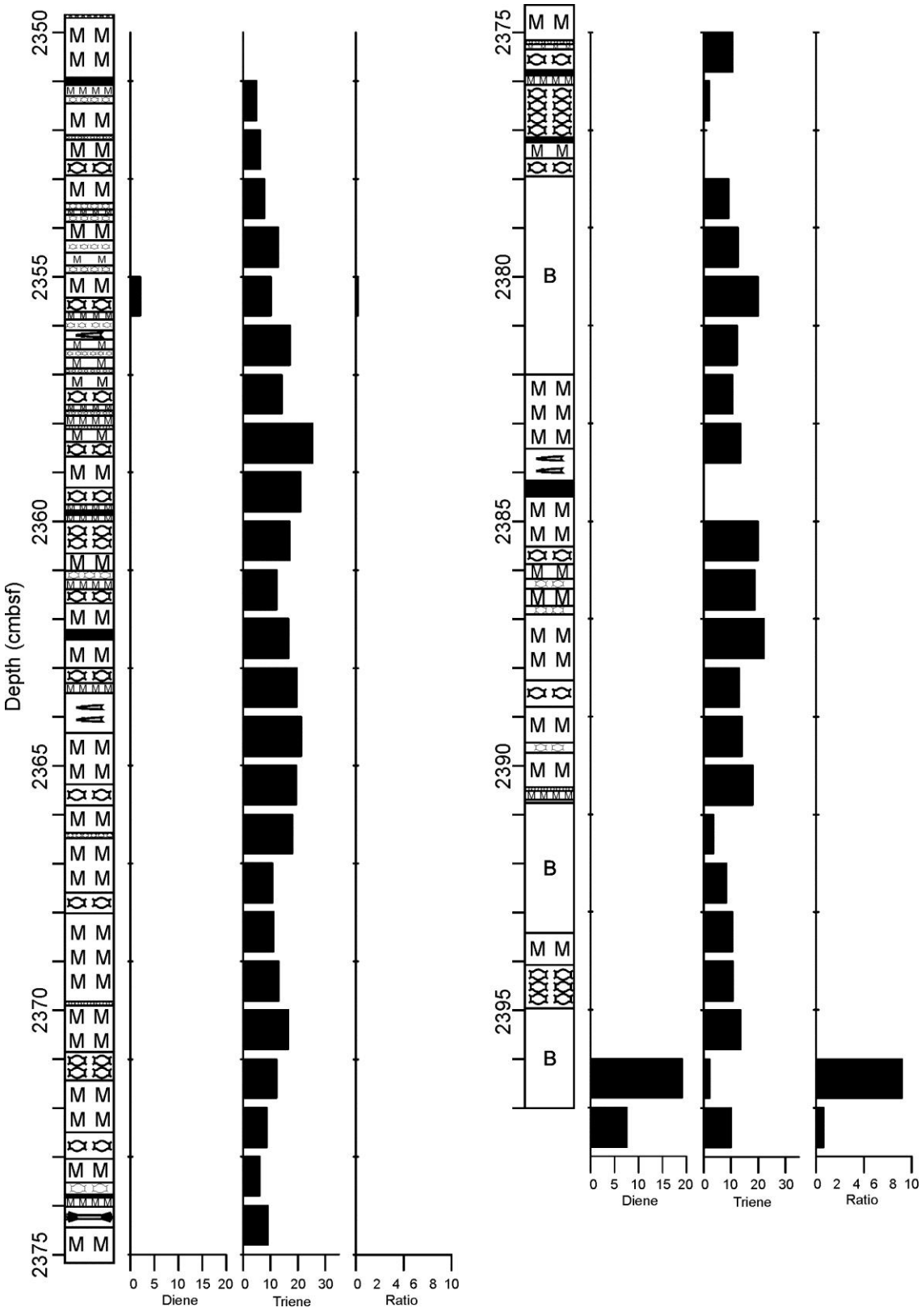
Depth (cmbsf)
2350
2355
2360
2365
2370
2375
2380
2385
2390
2395
M
B
0 5 10 15 20
Diene
0 10 20 30
Triene
0 2 4 6 8 10
Ratio

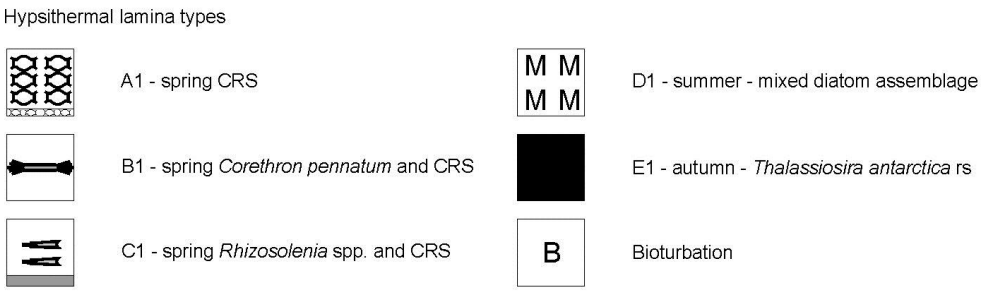

6.2.2 Core section VIII (the mid-Holocene transition)

Core section VIII can be divided into two sub-sections based upon the last occurrence of A1 laminae and increased frequency of A2 laminae; the late Hypsithermal and the early Neoglacial (Chapter 5). The early Neoglacial sediments between 1137 cm and 1050 cm core depth contain frequent Hypsithermal type laminae and indicate a gradual transition into the Neoglacial. Similarly to the triene distribution in core section XVII, there is a lack of consistency between lamina distribution and the sedimentary relative abundance of HBI diene. However, higher mean abundances of HBI diene occur between 1137 and 1064 cm (mean diene relative abundance = 1.0, n = 70; see Figure 6.05 and Table 6.02) than in the latest Hypsithermal sediments between 1200 and 1137 cm (mean diene relative abundance = 0.4, n = 61; see Figure 6.05 and Table 6.02). This is a statistically significant increase (Mann-Whitney U = 1331, n 1137 – 1064 cm = 70, n 1200 – 1137 cm = 61, $p < 0.01$) that is broadly coincident with the spring cooling (identified using BSEI lamina analysis; Chapter 5) associated with the transition. A further significant increase in HBI diene relative abundances occurs within the heavily bioturbated section at the top of core section VIII (1064 – 1050 cm core depth; mean diene relative abundance = 2.2, n = 12) compared to mean HBI diene abundances between 1137 and 1164 cm (Mann-Whitney U = 180.5, n 1064 – 1050 cm = 12, n 1137 – 1164 cm = 70, $p < 0.001$; see Table 6.02). This could suggest that there is a link between HBI diene concentrations and bioturbated intervals in the early Neoglacial that may result from better oxygenation of sea floor sediments during cooler periods due to a strengthened sinking of high salinity shelf waters (Chapter 5). However, the gradually increasing HBI diene concentrations in the early Neoglacial also supports the interpretation of the diatom laminae that the transition from Hypsithermal to Neoglacial conditions is more gradual than the large step-wise change suggested by previously reported relative abundances of sea ice associated diatoms (Crosta et al., 2007; Denis et

Table 6.02. Summary of Mann-Whitney *U* tests conducted on mean relative diene abundances in core section VIII.

	1050 – 1064 cm (mean = 2.2; n = 12)	1137 – 1200 cm (mean = 0.4; n = 61)
1064 – 1137 (mean = 1. 0; n = 70)	$U = 180.5$; $p < 0.001$	$U = 1331$; $p < 0.001$

al., 2009). The increased HBI diene concentrations may, therefore, be recording gradually cooling ocean surface conditions that are coincidental with bioturbated sediments at the top of core section VIII (see also Section 6.2.3).

The HBI triene is present in all samples of core section VIII and again shows no consistent distribution relative to laminae (Figure 6.05). Comparing the relative abundance of triene above and below the transition (taken as 1137 cm core depth) reveals no significant difference in mean values (Mann-Whitney $U = 2496$, n above =82, n below = 61, $p = 0.99$). It can be seen in Figure 6.05 that there is no increase in triene abundances in the bioturbated interval that would be comparable with the observed increased diene abundances.

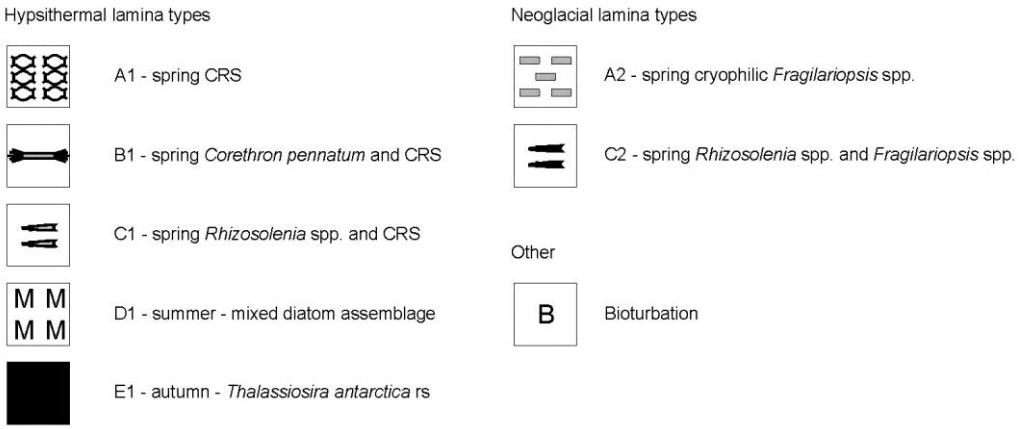

Figure 6.05 (next three page). Relative abundances of diene, triene and the ratio D/T at a 1 cm resolution in core section VIII, compared to stratigraphic log of lamina distribution.

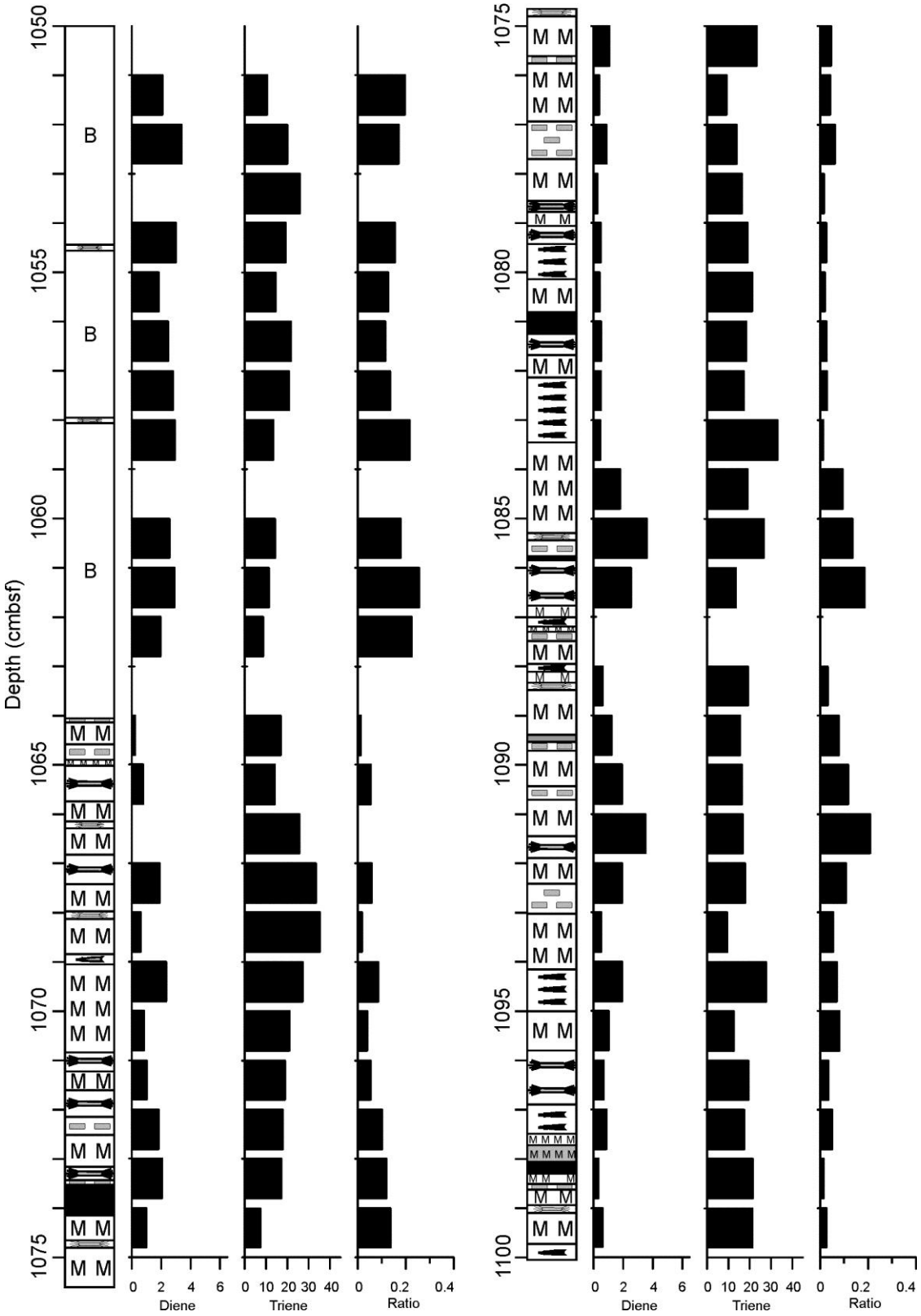
Depth (cmbsf)
1050
1055
1060
1065
1070
1075
1080
1085
1090
1095
1100
B
M
Diene
Triene
Ratio
0 2 4 6
0 10 20 30 40
0 0.2 0.4

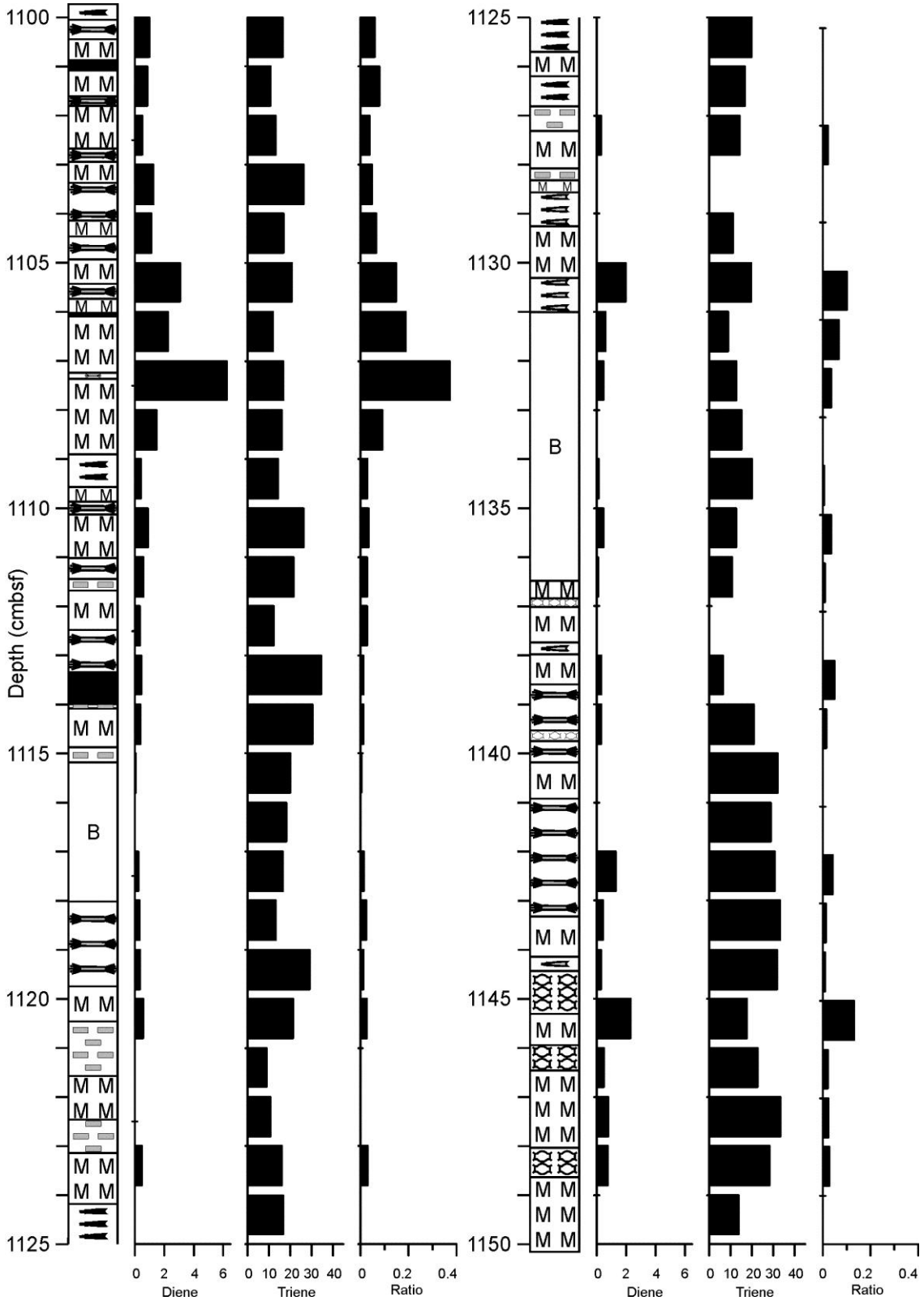
Depth (cmbsf)
1100
1105
1110
1115
1120
1125
1130
1135
1140
1145
1150
M M
B
0 2 4 6
Diene
0 10 20 30 40
Triene
0 0.2 0.4
Ratio

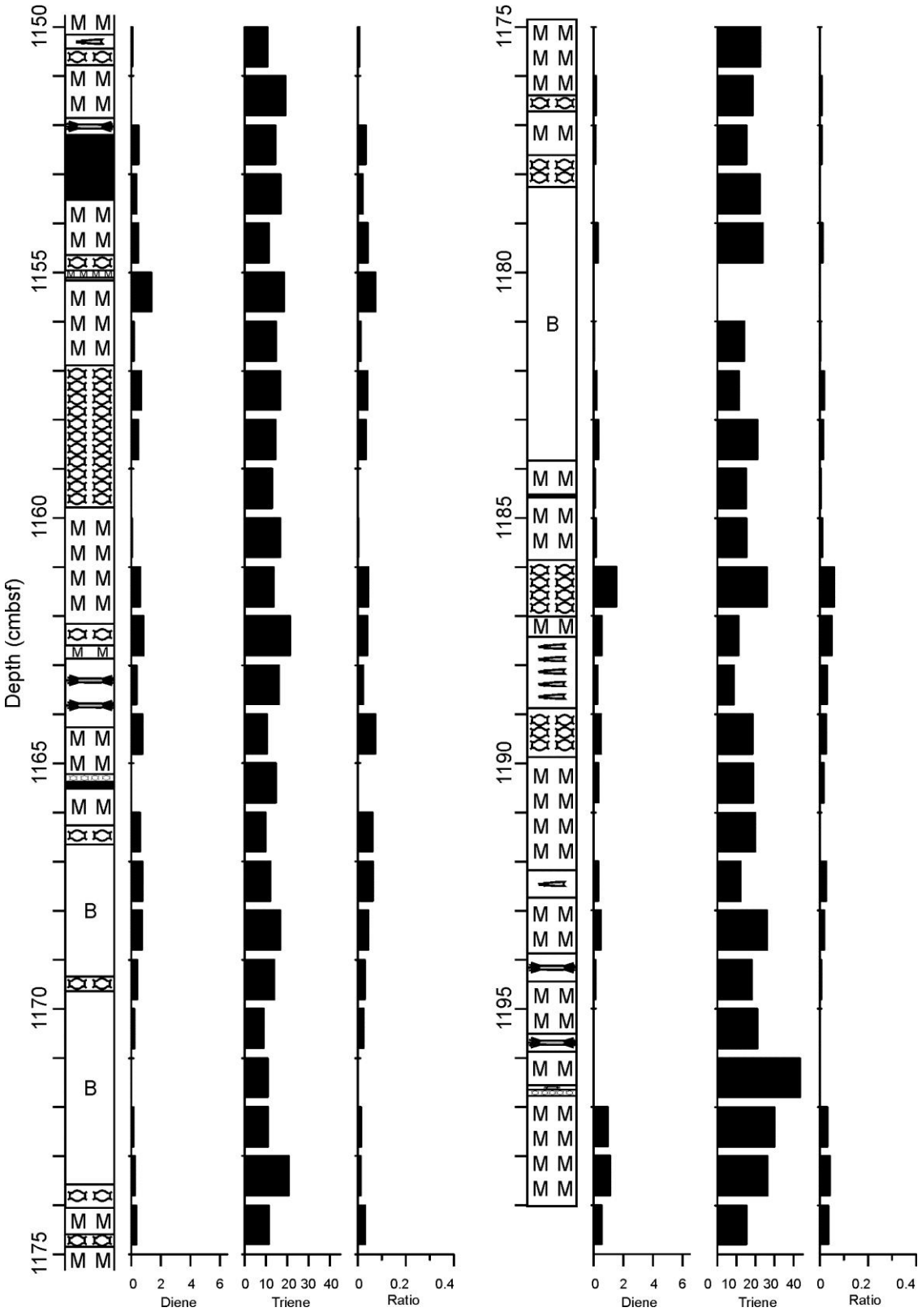
Depth (cmbsf)
1150
1155
1160
1165
1170
1175
1180
1185
1190
1195
M
B
0 2 4 6
Diene
0 10 20 30 40
Triene
0 0.2 0.4
Ratio

6.2.3 Core section III (the Neoglacial)

Both HBI alkenes are present in high abundances in the majority of samples in MD03-2601 core section III (Figure 6.01), deposited during the Neoglacial (ca. 1.6 ka BP). As with core sections XVII and VIII, there is no clear association between the significant HBI concentration peaks and lamina type, even with the larger mean lamina thickness in core section III (Figure 6.06). Unlike that observed at the top of core section VIII, there is no apparent association between high diene concentrations and bioturbated intervals (e.g. in the bioturbated interval at ca. 390 cm core depth there are very low HBI diene abundances, whilst in the bioturbated interval ca, 365 cm core depth there are high HBI diene abundances; Figure 6.06). This suggests that the association between HBI diene and bioturbated sediments in core section VIII is a spurious and supports the interpretation of gradually increasing HBI diene abundances associated with the onset of the Neoglacial.

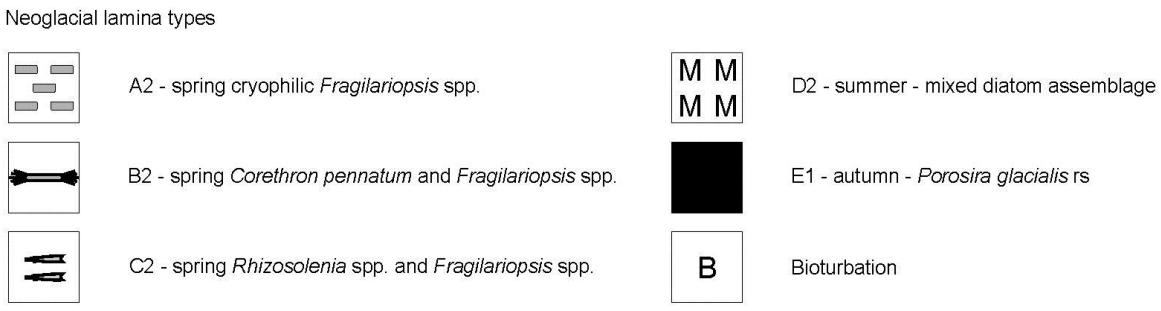

Figure 6.06. Relative abundances of diene, triene and the ratio D/T at a 1 cm resolution in core section III, compared to stratigraphic log of lamina distribution.

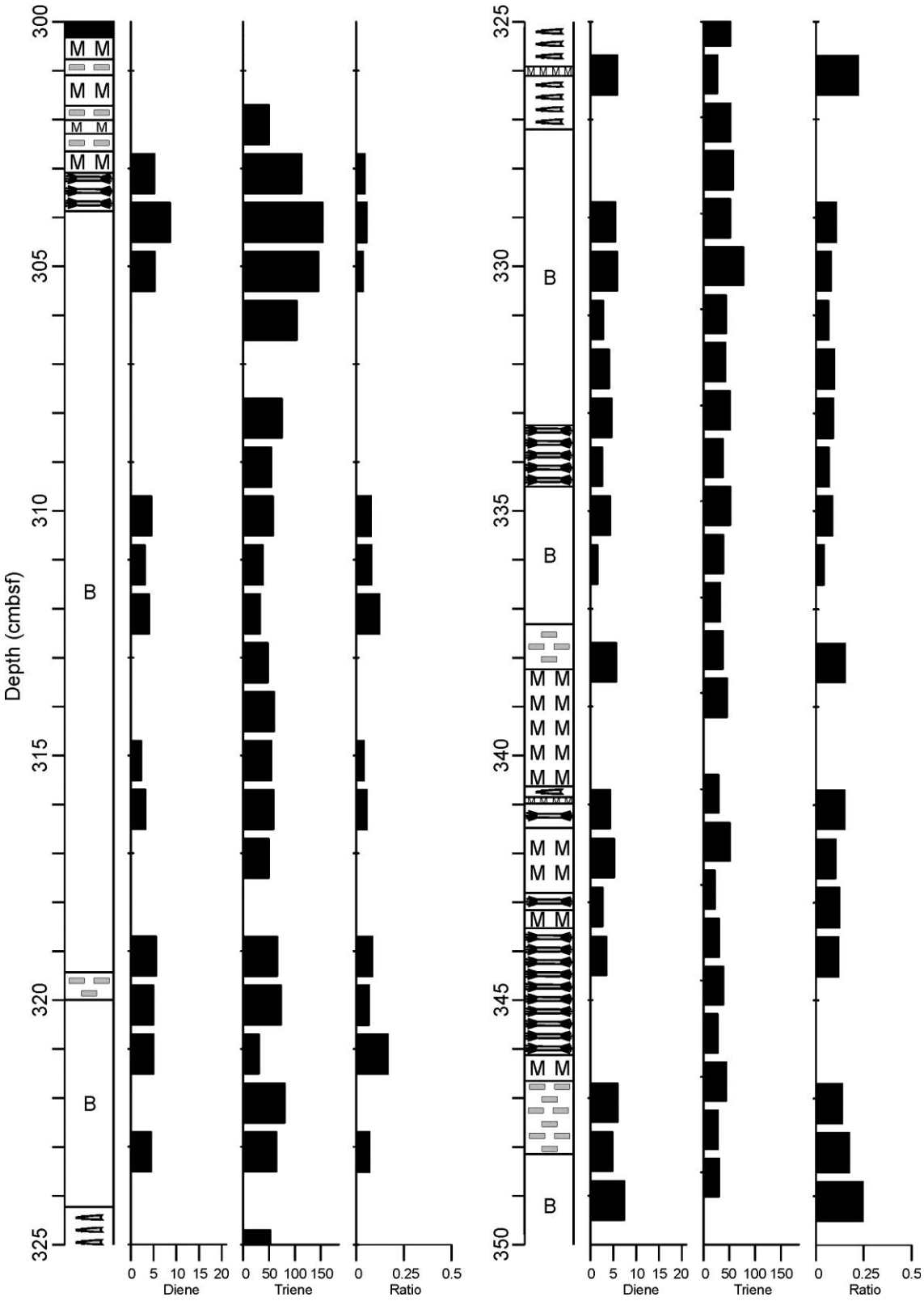
Depth (cmbsf)
300
305
310
315
320
325
330
335
340
345
350
M
B
0 5 10 15 20
Diene
0 50 100 150
Triene
0 0.25 0.5
Ratio

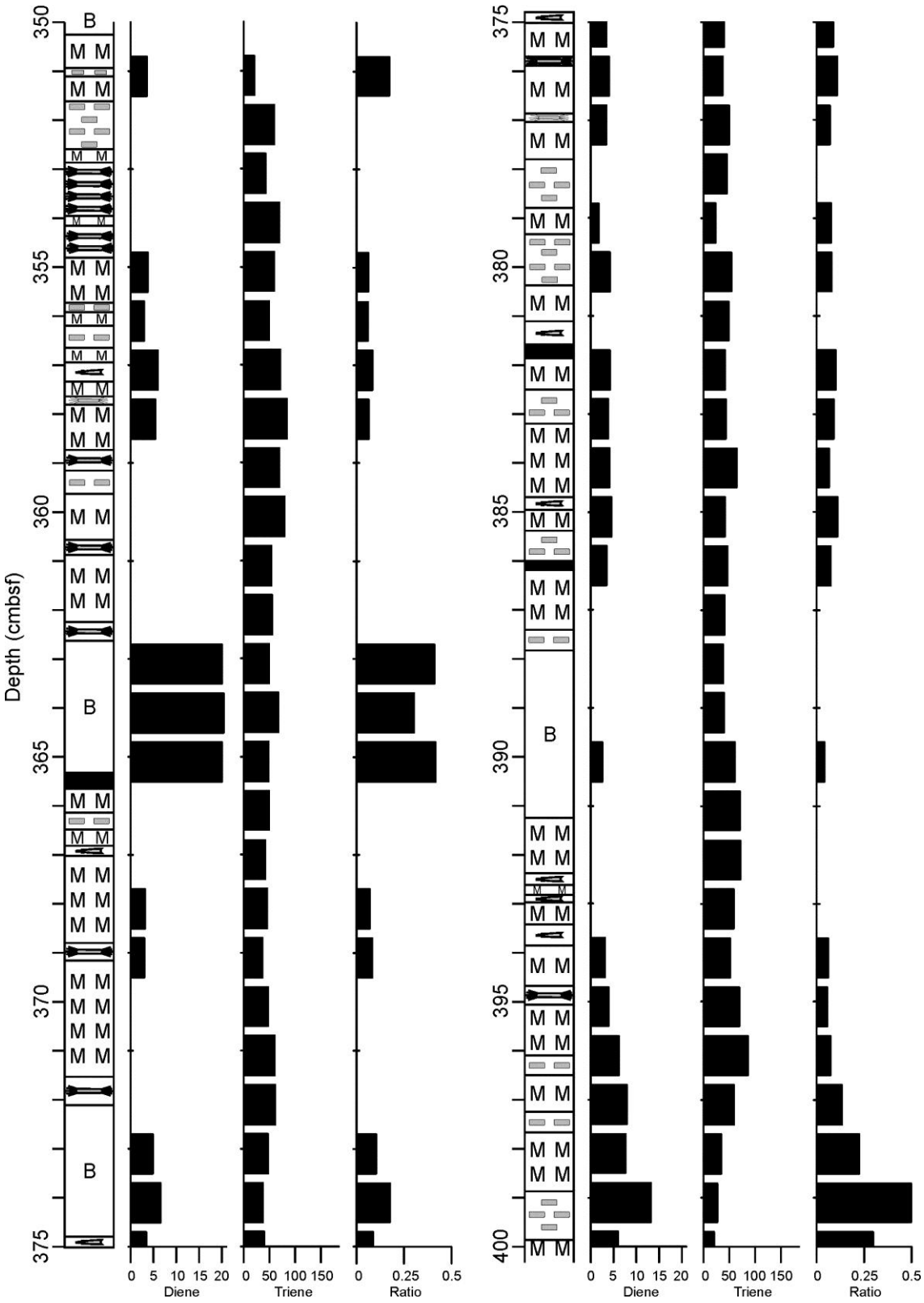
Depth (cmbsf)
350
355
360
365
370
375
380
385
390
395
400
B
M
0 5 10 15 20
Diene
0 50 100 150
Triene
0 0.25 0.5
Ratio

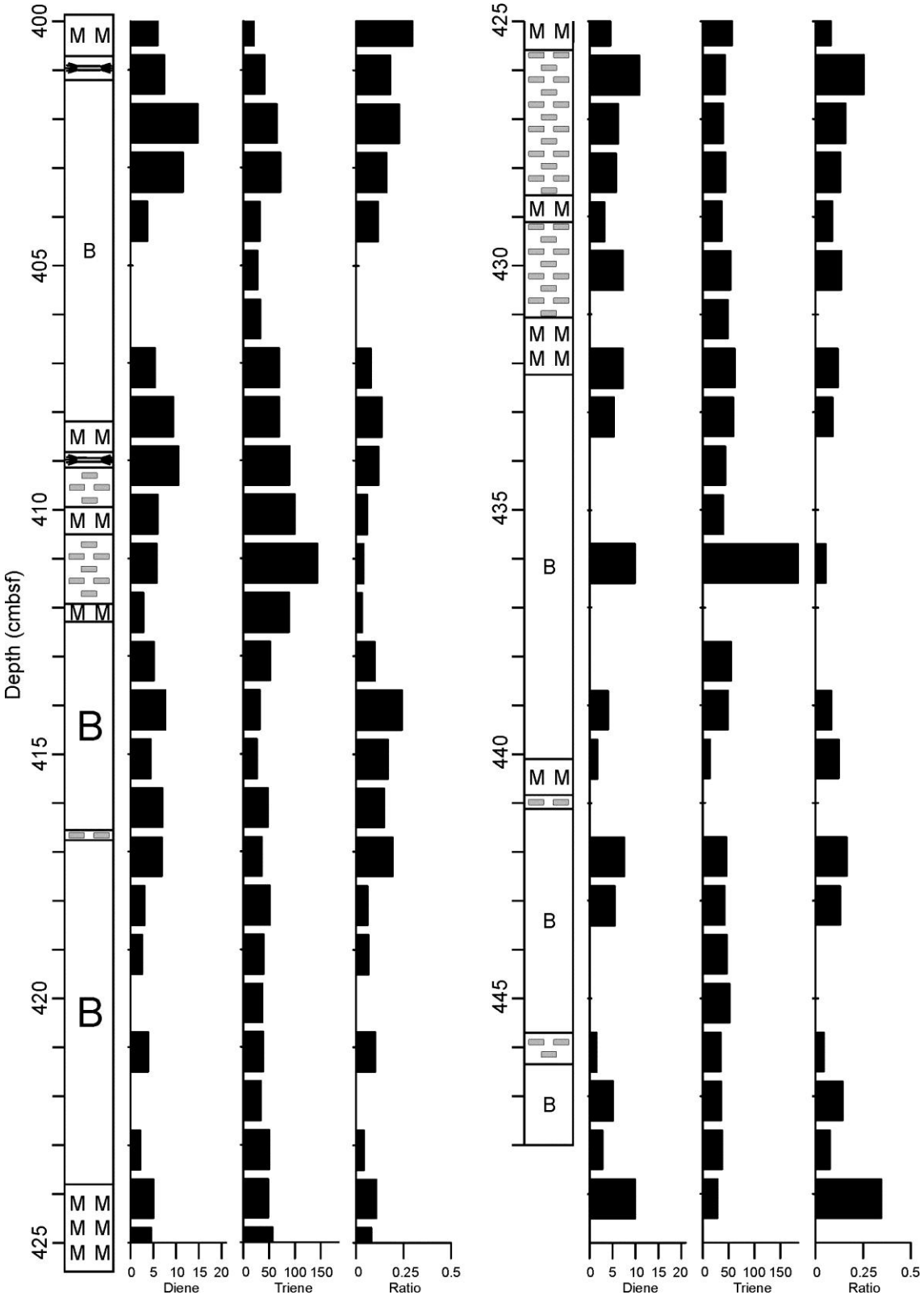
Depth (cmbsf)
400
405
410
415
420
425
430
435
440
445
M M
B
0 5 10 15 20
Diene
0 50 100 150
Triene
0 0.25 0.5
Ratio

6.3 The distribution of HBIs in core MD03-2601

The HBI data presented in this chapter provides equivocal results about the nature of HBI distribution in laminated sediments. HBIs, in particular HBI diene, may potentially provide a proxy of changes in the sea ice environment at longer timescales (section 6.1); however, when compared to the lamina reconstructions presented in Chapter 5, there is no obvious coeval pattern in HBI distribution (section 6.2) at these fine scales. The demonstrated inconsistency of HBI distribution with regards to a given lamina type suggests that it is not an issue of sampling resolution. Consequently, three alternative hypotheses are considered in this section (1 – 3 below), with particular focus on the HBI diene, which has the stronger modern environmental association (being produced only within sea ice rather than in waters proximal to melting sea ice which may display a range of hydrographic conditions, Massé et al., 2011):

1) HBI diene and triene abundances are not responding to the same environmental forcing as recorded by the changing lamina types identified by diatom assemblages;
2) interannual variability in HBI production is greater than the interseasonal variability of a given year;
3) alteration of the HBI signal may occur during sedimentary and early diagenetic processes.

Hypothesis (1) must be taken into account when comparing the record of HBI alkenes to diatom distributions, particularly when considering changes in the relative abundance of HBI diene. As the HBI diene is synthesised by sea ice biota (Belt et al., 2008; Brown et al., 2011; Massé et al., 2011) it is recording a signal that is not commonly preserved in sedimentary diatom assemblages, as sea ice diatoms are highly susceptible to dissolution processes and are only infrequently observed in the sedimentary record (Matsuda et al., 1990). Diatom-based inferences of the presence of sea ice are made by particular comparison to the *Fragilariopsis* genus (in particular *F. curta* and *F. cylindrus* which are associated with the presence of sea ice, but do not necessarily form high biomass within it), of which *F. curta* has been shown not to synthesise HBIs (Damsté et al., 2004) and the same is likely for other members of the genus (Massé et al., 2011). Cryophilic *Fragilariopsis* species are indicators of the presence of sea ice or cold water, but are not indicators of primary production within sea ice itself (von

Quillfeldt, 2004; Beans et al., 2008; Riaux-Gobin et al., 2011). In an ultra-high-resolution analysis of a sediment water interface core, Massé et al. (2011) showed that peaks in HBI concentrations were offset (HBI slightly lagged) from peaks in sea ice associated diatoms.

Currently there is little information available about interannual variations in HBI production within the ocean surface and sea ice (Hypothesis [2]) and subsequent export from the water column. Given that there is substantial variation in the total extent and timing of the break-up of sea ice cover in the modern environment (Chapter 2; Comiso, 1999, updated 2008) there is the potential for large interannual variability in primary production related to sea ice, hence delivery of HBIs to sediments. Additionally, the exact species make-up of a sea ice community is influenced by a large variety of factors including time of ice formation, type of sea ice, duration of sea ice and snow cover (Arrigo et al., 2010), all of which may vary year-on-year. This combined with the lack of an identified genus/species of diatoms that is producing HBIs within Antarctic sea ice and the MIZ makes it difficult to assess production rates of HBIs within the modern environment.

Processes controlling the flux rate of HBIs to the sediment and subsequent sedimentary distribution are also poorly constrained (Hypothesis [3]). Given that it is presumed that Antarctic HBIs are produced from a sea ice diatom source that is rarely preserved itself (Denis et al., 2010; Barbara et al., 2010; Massé et al., 2011) we cannot assume that HBIs (or, indeed, any geochemical proxy) within a given horizon have followed the same sedimentary pathway as the preserved diatoms, despite high sedimentation rates (Rosell-Melé and McClymont, 2007; Zonneveld et al., 2010). At present, very little work has been conducted on assessing the biological pathways through which HBIs may enter the sedimentary environment, although Brown et al. (2011) have observed high concentrations of the IP_{25} HBI biomarker within Arctic macrofauna, demonstrating the potential for a non-direct (i.e. HBIs may not rain out from the ocean surface directly to sediments) transport route. Massé et al. (2011) have presented data from a seawater/sediment interface core that is tentatively interpreted as spanning the latter half of the 2001/2002 summer season and the first half of the 2002/2003 summer season that suggests that at very high accumulation rates (>10 cm per year sedimentation) peaks in HBI diene may occur associated with spring biogenic sedimentation. However, little is

known about the effects of early diagenesis (Chapter 3) and diffusion of the HBI molecules within the sediment. Whilst the HBI signal for core MD03-2601 has not been altered by sulfuristation (a degradational problem for HBIs in certain environments; G. Massé pers. comm., 2012), there is still little understanding of the mobility of HBIs within the sediment (i.e. whether or not they enter "bound" to other molecules, or if they become bound to a horizon shortly after sedimentation). Certainly, the data presented here indicate that a seasonal signal in the HBI proxy is not preserved in the sediments of MD03-2601, regardless of the underlying cause(s) of the loss of this signal.

6.4 Summary

When considered over selected intervals in the Holocene, HBI diene and triene are reasonably correlated with each other in the data presented here from core MD03-2601 ($r = 0.437$, $p < 0.001$, $p = 429$; Figure 6.02) and well correlated ($r = 0.73$, $p < 0.001$, $n = 125$) in the MD03-2601 data from Denis et al. (2010; see Chapter 3). This demonstrates that at longer timescales (i.e. between relatively warm and cool climatic intervals) the record of the two alkenes may be recording two linked aspects of the sea ice system (i.e. sea ice productivity and MIZ productivity; Massé et al., 2011). However, when considered within each core section independently (Figure 6.02) it has been demonstrated that the relationship between HBI diene and triene is not present at annual to sub-annual timescales. HBI diene appears to be more closely related to changes in sea ice cover inferred from the diatom records, showing a small, yet significant (n above = 61, n below = 82, Mann-Whitney $U = 1331$, $p < 0.001$), increase in relative abundance at the mid-Holocene transition. This slow increase in HBI diene in the early Neoglacial of core section VIII supports the interpretation of the diatom lamina data that the transition from Hypsithermal to Neoglacial conditions is slow in nature. In the data presented here, there is a lack of consistency between HBI abundances and lamina distribution that is not linked to sampling resolution (i.e. one may pick a lamina type and find instances of both high and low HBI abundances corresponding with it). This lack of consistency at a high- temporal resolution may be linked to differences in what the two proxies are recording, large interannual variations in the production of HBIs, or diagenetic processes affecting their distribution in sediments.

Chapter 7 – Conclusions

This thesis has presented the most detailed analysis of interannual sedimentary changes in diatoms and HBIs on the Antarctic margin to date. It has demonstrated changes in the sensitivity of diatom productivity to internal and external forcing during the Holocene (section 7.1) and has compared high resolution analysis of highly branched isoprenoid (HBI) alkenes against diatom lamina-derived time series (section 7.2). Furthermore, this research has successfully addressed all of the hypotheses posed in section 1.3 as discussed in sections 7.1.1 and 7.2.1 below. This chapter concludes by suggesting further avenues of research (section 7.3).

7.1 Lamina-based reconstructions

Ultra-high resolution analysis of Antarctic diatom-rich laminated sediments provides insight into the processes that have exerted an influence on Adélie Land sea ice dynamics during the different climatic intervals of the Holocene. A typical repeating sequence of diatom-rich laminae has been identified which is interpreted as representing the seasonal diatom succession, an increase of terrigenous material later in the year and a sharp winter hiatus. The complete sequence, when observed using backscatter electron imagery (BSEI), has an initial lamina rich in *Hyalochaete Chaetoceros* resting spores (CRS) and/or cryophilic *Fragilariopsis* spp. which is indicative of high diatom productivity in nutrient-rich waters following the spring sea ice retreat. This is followed by a lamina that is visually dominated by *Corethron pennatum*, *Rhizosolenia* spp. or *Phaeoceros Chaetoceros* spp and indicates late spring nutrient depletion and mixing of the surface water. In turn, these laminae are followed by a lamina with a mixed diatom assemblage and relatively high terrigenous content indicative of summer input of sediments from nearer the coast. Finally, a layer visually dominated by *Thalassiosira antarctica* resting spores (rs) or *Porosira glacialis* rs completes the sequences and indicates autumnal sea ice formation.

The identification of this annual cycle has allowed the first compilation of annually-resolved multi-decadal records from the sedimentary sections analysed in different Holocene climatic intervals. Two continuously laminated sequences of 50- and 57-years are identified in core MD03 2601 core section XVII (Hypsithermal, ca. 6.8 – 6.4

ka BP) and are interpreted as representing relatively cooler and warmer conditions, respectively. This interpretation is based upon the greater frequency of *T. antarctica* RS-rich laminae (cooler autumns) and lower frequency of *Rhizosolenia* spp. laminae (warmer springs) in the 50-year record. Given the sensitivity of RS-rich laminae to autumn ice formation and the statistical association of Southern Annular Mode (SAM) indices with satellite-derived sea ice concentrations, the cooler 50-year record is interpreted as responding to a positive phase of the SAM (which strengthens the westerlies around Antarctica and enhances sea ice production), whilst the warmer 57-year record is interpreted as representing a negative phase of the SAM. The data suggests that multidecadal (>50-year) trends in the SAM were a feature of the southern hemisphere atmospheric circulation during this phase of the Hypsithermal. Multi-taper method (MTM) analysis of lamina thickness time series reveals a 22-year frequency in the 57-year record spring A1 type lamina thickness (Hypsithermal spring) and is consistent with a stronger solar influence on the climate during the Hypsithermal climatic interval (Debret et al., 2007). El Nino – Southern Oscillation (ENSO)-band frequencies in the E1 lamina (Hypsithermal autumn) thickness time series of the 50-year record (see section 7.1.1) and Quasi-biennial Oscillation (QBO)-band frequencies in both the 50- and 57-year records were also found.

A continuously laminated 43-year record from the early Neoglacial (core MD03 2601, section VIII, ca. 4.8 – 4.4 ka BP) indicates highly variable spring conditions during this interval, with multiannual periods in which warm and windy conditions prevailed, alternating with multiannual periods in which relatively icier spring conditions prevailed. MTM analysis of lamina thicknesses reveals a 5.3 – 6 year frequency in the D1 lamina thickness (Hypsithermal summer laminae which continue into the early Neoglacial) time series that may indicate a possible ENSO-influence on summer diatom assemblage composition from a delayed start to the summer season due to increased spring sea ice concentrations. However, a similar frequency is not present in the spring laminae of this interval and longer sequences are needed to test this hypothesis.

Neoglacial (ca. 1.8 – 1.6 ka) sediments from core MD03 2601 section III are disrupted by significant bioturbation. The observed upcore increase in bioturbation is interpreted as being due to increased oxygenation of bottom waters, resulting from more vigorous brine production in the cooler Neoglacial. Despite this, the presence of ~10-year

continuously laminated sequences in this core section suggests that there is a multidecadal variation in oxygenation resulting from brine formation and that there may, therefore, be multidecadal variations in the formation of high salinity shelf waters (HSSW). Multidecadal variations in HSSW production in the modern Ross Sea have been linked to multidecadal variations in the SAM (Jacobs and Giulivi, 2010) and the data presented here indicates that a similar process may be recorded in the sediments of MD03 2601. In contrast, the Neoglacial sediments of core IODP-318-U1357B (ca. 1.8 – 1.6 ka) benefit from better preservation related to the position of the core site at the centre of the Dumont d'Urville Trough, where sedimentation rates are higher. This thesis has demonstrated for the first time the seasonal nature of the laminae in core IODP-318-U1357B, from which a 73-year continuously-laminated record has been obtained. In contrast to the Hypsithermal, no lamina thickness time series contained solar frequencies in MTM analysis, interpreted as a stronger internal forcing of Adélie Land climate during the Neoglacial. ENSO-band frequencies were observed in the A3 (spring), D3 (summer) and E3 (autumn) lamina thickness time series, indicating the potential sensitivity of sediments from this core to changes in the ENSO system. As with the Hypsithermal sediments analysed from core MD03-2601, QB-band frequencies were the most commonly observed in core IODP-318-U1357B, indicating a potential connection between the QBO and Adélie Land sedimentation during the Holocene that has not previously been observed. A multidecadal (>50-years) trend in the distribution of E3 laminae (*Porosira glacialis* RS, Neoglacial autumn laminae; see Section 5.4, Figure 5.20) is comparable to the trends observed in the distribution of Hypsithermal RS-rich laminae from core MD03 2601 (Section 5.3.1, Table 5.03). From these observations, and the known association between SAM and modern autumnal sea ice concentrations, it is proposed that multidecadal (>50-year) changes in phasing were a feature of the SAM during the Neoglacial and Hypsithermal intervals analysed here.

7.1.1 Hypotheses

Hypothesis 1: The distribution of spring laminae should be sensitive to ENSO forcing, based on the negative correlation between modern sea ice concentration and ENSO.

MTM time series analysis of spring lamina type A3 thickness in the sediments analysed from core IODP-318-U1357B revealed ENSO-band frequencies that are not present in spring laminae from the analysed Hypsithermal sections of core MD03-2601. Hypothesis 1 for lamina-based reconstructions is, therefore, valid for the Neoglacial climatic interval but not the Hypsithermal climatic interval. This difference reflects the greater sensitivity to ENSO of spring sea ice conditions in the Neoglacial relative to the Hypsithermal climatic intervals.

Hypothesis 2: The distribution of autumn laminae should be sensitive to SAM forcing, and possibly combined SAM-ENSO forcing, based on the positive correlation between modern autumn sea ice concentration and SAM, and a combined SAM-ENSO index.

The distribution of lamina types E1 (core MD03 2601 core section XVII) and E3 (sediments from core IODP-318-U1357B), which are sensitive to autumnal ice formation, demonstrate multidecadal variations in their presence/absence. Furthermore, a statistically valid positive association can be demonstrated between a multidecadal increase in the modern SAM index and satellite-derived sea ice concentrations (Chapters 2 and 5). This suggests that longer term (>50 years) increases and decreases in sea ice have occurred throughout the Holocene in relation to phase changes in the SAM. Furthermore, lamina types E1 and E3 also display ENSO-band frequencies in MTM time series analysis, which occur in periods of the record interpreted from the distribution of different laminae (Section 5.3.1, Table 5.03) as representing more positive SAM values, indicating a coupling between the SAM and ENSO. The evidence indicates that Hypothesis 2 for lamina-based reconstructions is valid.

Hypothesis 3: As a response to both the increased sea ice and ENSO intensity that occurred during the late Holocene, ENSO-frequencies should be observed more strongly in the lamina-time series records during the Neoglacial compared to the Hypsithermal.

ENSO-frequencies of 3 – 4 years are recorded in the Hypsithermal E1 laminae (autumn) and Neoglacial A3 (spring) and E3 (autumn) laminae, whilst slightly longer ENSO-band frequencies of 5 – 6 years are recorded in the early Neoglacial (ca. 3.9 ka; core MD03 2601 section VIII) D1 laminae and later Neoglacial (ca. 1.2 ka; sediments from IODP-318-U1357B) D3 laminae. The data does not suggest a change in ENSO intensity (i.e. there is no change in the signal to noise ratio, with ENSO-band frequencies being significant at 95% in both intervals) or periodicity between the Hypsithermal and Neoglacial. Thus from the results of this research hypothesis 3 for lamina-based reconstructions is falsified.

7.2 HBI biomarker distribution in laminated sediments

At the Holocene scale, this research has demonstrated that both HBI diene and triene are positively correlated to long term increases in sea ice concentration interpreted from the distribution of diatom lamina types, consistent with the lower resolution HBI reconstructions of Denis et al. (2010). This provides good evidence for the two molecules being linked to the presence of sea ice and supports their use as a proxy for changes in the sea ice and marginal ice zones during the Holocene period. There was no evidence that the diene/triene (D/T) ratio provided an indication of sea ice (diene) versus open water productivity (triene) (Massé et al., 2011). Rather, it is more likely that diatoms producing the triene molecule (e.g. *Rhizosolenia* spp.) benefit from the stratification that occurs at a retreating sea ice edge, consequently more HBI diene and triene are deposited when there is a greater concentration of sea ice during the spring. However, there was no correlation between the diene and triene at annual to sub-annual resolution, suggesting potentially different factors affect their production, export and preservation at an inter-annual resolution, such as the influence of temperature, light and nutrient availability that have not previously been considered. From the data presented here, HBIs do not provide a proxy for past annual variations in sea ice cover and surface oceanography that is comparable to the diatom lamina-derived record.

7.2.1 Hypotheses

Hypothesis 1: Elevated HBI diene concentrations should correspond to the occurrence of spring laminae.

Due to the origin of HBI diene within sea ice it was hypothesised that HBI diene concentrations should be highest in spring associated laminae, which have the strongest sea ice association. However, this trend is not evident in the data presented here, with a notable lack of consistency in lamina type versus HBI diene concentration. This most likely results from a combination of sedimentary biases (i.e. interannual variations in HBI export and possible diagenetic effects) and the contrast between the processes that produce HBIs and laminations. HBI diene is exclusively produced by diatoms living within sea ice, whilst the diatom-rich sea ice-related laminae are typically composed of an assemblage of diatoms that may be living within the sea ice but also blooming in cold open water conditions at the ice edge and, subsequently, laminae are amalgamating signals from different parts of the environment. HBI hypothesis 1 is, therefore, rejected.

Hypothesis 2: Elevated HBI triene concentrations should correspond to the occurrence of late spring/summer laminae.

Due to the phytoplankton origin of HBI triene it was hypothesised that HBI triene concentrations should be highest in late spring/summer laminae which have the strongest phytoplankton/open water association. As with HBI diene, there is a lack of consistency between lamina type and HBI triene concentration, suggesting that HBIs do not provide a useful proxy for understanding annual variability in palaeoclimate reconstructions. Again, this may be due to substantial interannual variability in HBI triene export linked to changes in diatom community composition in a given year, diagenetic alteration of the recorded signal, or HBIs being forced by other factors than solely sea ice (e.g. temperature or light availability). HBI hypothesis 2 is, therefore, rejected.

7.3 Future work

7.3.1 Time series analysis of laminated sediments

This thesis presents selected multidecadal annually resolved records from Adélie Land sediments. These results and analysis are particularly relevant to guide future research using core IODP-318-U1357B. Potentially, the seasonal banding which is visible to the eye may be used to construct additional long (multidecadal to centennial) records using other microfossil and geochemical palaeoclimate proxies. New records will shed further light on natural phase changes in the SAM and their impact of the coastal East Antarctic environment. They will also facilitate further testing of the phasing observed in this study between ENSO and SAM at multidecadal to centennial timescales, allowing us to test the impact of these large climatic modes on sea ice fields throughout the Holocene. In particular, the data presented here has also highlighted the potential use of laminae rich in *Thalassiosira antarctica* RS and *Porosira glacialis* RS to record long term changes in the SAM. This can be further tested by quantitative counts that can be directly sampled from the annual layering observed here and would provide a quantitative dataset for further time series analyses. Lower resolution multi-proxy studies on IODP-318-U1357B may also demonstrate millennial phase changes in the SAM and the influence of the SAM on Adélie Land sea ice distribution and oceanography (e.g. increases or decreases in bottom water production) throughout the Holocene.

7.3.2 Understanding the distribution of HBIs

The HBI data from core MD03-2601 indicates a complicated relationship between the HBI diene and triene molecules and environmental conditions at different time scales (i.e. they are poorly correlated with each other and diatom inferred changes at a near annual timescale, but well correlated at millennial time scales). This thesis has shown that, at both timescales, HBIs are recording aspects of the sea ice environment that differs from the record of the diatom lamina-based reconstructions. This highlights a significant gap in our understanding of HBIs in terms of their source species/genera, their function and activity within the cell, their response to environmental variables and biases in their sedimentation/deposition and taphonomy. Our understanding of the distribution of HBIs in sediments may be enhanced by further high resolution

comparison of HBIs to quantitative proxies (i.e. diatom assemblage counts) that were beyond the scope of this study. In particular, *Rhizosolenia antennata* and *R. hebetata* (L. Collins, unpublished data; L. Barabara, unpublished data) may show a good association with HBI triene concentrations in lower resolution studies (G. Massé, pers comm.) and ultra-high resolution laminated sediments provide an excellent opportunity to test this against a seasonally constrained timescale. The study of sea floor sediment-water interface cores with well constrained chronologies will also help provide constraints on the interannual variations in HBI export in the modern environment versus long term instrumental data and biological monitoring programmes (e.g. Long Term Ecological Research; LTER). Additionally, multiannual interface cores have the potential to demonstrate whether the large variations in HBI concentration over a short sedimentary interval (1 – 2 cm) observed in this study are due to interannual variability in HBI export from the water column, rather than diagenetic changes within ancient sediments.

References

ABBOTT, M. R.; RICHMAN, J. G.; LETELIER, R. M. & BARTLETT, J. S. 2000. The spring bloom in the Antarctic Polar Frontal Zone as observed from a mesoscale array of bio-optical sensors. *Deep Sea Research Part II: Topical Studies in Oceanography,* 47**,** 3285-3314.

ABELMANN, A. & GERSONDE, R. 1991. Biosiliceous particle flux in the Southern Ocean. *Marine Chemistry,* 35**,** 503-536.

ACKLEY, S. F. 1981. A review of sea-ice weather relationships in the Southern Hemisphere. *Sea Level, Ice, and Climatic Change***,** 127-159.

ACKLEY, S. F. & SULLIVAN, C. W. 1994. Physical controls on the development and characteristics of Antarctic sea ice biological communities--a review and synthesis. *Deep Sea Research Part I: Oceanographic Research Papers,* 41**,** 1583-1604.

ALLAN, R. J. 2000. ENSO and Climatic Variability in the Past 150 Years. *In:* DIAZ, H. F. A. M., V. (ed.) *El Niño and the Southern Oscillation.* Cambridge: Cambridge University Press.

ALLEN, C. S.; PIKE, J.; PUDSEY, C. J. & LEVENTER, A. 2005. Submillennial variations in ocean conditions during deglaciation based on diatom assemblages from the southwest Atlantic. *Paleoceanography,* 20**,** PA2012.

AN, S. I. & JIN, F. F. 2004. Nonlinearity and Asymmetry of ENSO. *Journal of Climate,* 17**,** 2399-2412.

ANDERSON, J. B. 1999. *Antarctic marine geology,* Cambridge Univ Press.

ANDERSON, J. B. & SHIPP, S. S. 2001. Evolution of the West Antarctic ice sheet. *Antarctic Research Series,* 77**,** 45-57.

ANDERSON, J. B.; SHIPP, S. S.; LOWE, A. L.; WELLNER, J. S. & MOSOLA, A. B. 2002. The Antarctic Ice Sheet during the Last Glacial Maximum and its subsequent retreat history: a review. *Quaternary Science Reviews,* 21**,** 49-70.

AOKI, S.; RINTOUL, S. R.; USHIO, S.; WATANABE, S. & BINDOFF, N. L. 2005. Freshening of the Adélie Land Bottom Water near 140 E. *Geophysical Research Letters,* 32.

ARBLASTER, J. M. & MEEHL, G. A. 2006. Contributions of external forcings to southern annular mode trends. *Journal of Climate,* 19**,** 2896-2905.

ARMAND, L. K.; CROSTA, X.; ROMERO, O. & PICHON, J.-J. 2005. The biogeography of major diatom taxa in Southern Ocean sediments: 1. Sea ice related species. *Palaeogeography, Palaeoclimatology, Palaeoecology,* 223**,** 93-126.

ARMAND, L. K. & ZIELINSKI, U. 2001. Diatom species of the genus *Rhizosolenia* from Southern Ocean sediments: distribution and taxonomic notes. *Diatom Research,* 16**,** 259-294.

ARRIGO, K. R.; MOCK, T. & LIZOTTE, M. P. 2010. Primary Producers and Sea Ice. *In:* THOMAS, D. N. & DIECKMANN, G. (eds.) *Sea Ice.* 2 ed. Chichester: Wiley-Blackwell.

ARRIGO, K. R. & SULLIVAN, C. W. 1992. The influence of salinity and temperature covariation on the phoyophysiological characteristics of Antarctic sea ice microalgae 1. *Journal of Phycology,* 28**,** 746-756.

ARRIGO, K. R.; VAN DIJKEN, G. & LONG, M. 2008a. Coastal Southern Ocean: A strong anthropogenic CO2 sink. *Geophysical Research Letters,* 35.

ARRIGO, K. R.; VAN DIJKEN, G. & PABI, S. 2008b. Impact of a shrinking Arctic ice cover on marine primary production. *Geophysical Research Letters,* 35**,** L19603.

ARRIGO, K. R. & VAN DIJKEN, G. L. 2003. Phytoplankton dynamics within 37 Antarctic coastal polynya systems. *Journal of Geophysical Research,* 108**,** 3271.
ARRIGO, K. R.; VAN DIJKEN, G. L. & BUSHINSKY, S. 2008c. Primary production in the Southern Ocean, 1997 – 2006. *Journal of Geophysical Research,* 113**,** C08004.
ASSMY, P.; HERNÁNDEZ-BECERRIL, D. U. & MONTRESOR, M. 2008. Morphological variability and life cycle traits of the type species of the diatom genus Chaetoceros, C. dichaeta. *Journal of Phycology,* 44**,** 152-163.
BAHK, J.; YOON, H.; KIM, Y.; KANG, C. & BAE, S. 2003. Microfabric analysis of laminated diatom ooze (Holocene) from the eastern Bransfield Strait, Antarctic Peninsula. *Geosciences Journal,* 7**,** 135-142.
BALDWIN, M. P. 2001. Annular modes in global daily surface pressure. *Geophysical Research Letters,* 28**,** 4115-4118.
BALDWIN, M. P. & DUNKERTON, T. J. 1998. Quasi-biennial modulation of the southern hemisphere stratospheric polar vortex. *Geophysical Research Letters,* 25**,** 3343-3346.
BALDWIN, M. P.; GRAY, L. J.; DUNKERTON, T. J.; HAMILTON, K.; HAYNES, P. H.; RANDEL, W. J.; HOLTON, J. R.; ALEXANDER, M. J.; HIROTA, I. & HORINOUCHI, T. 2001. The quasi-biennial oscillation. *Reviews of Geophysics,* 39**,** 179-230.
BARBARA, L.; CROSTA, X.; MASSÉ, G. & THER, O. 2010. Deglacial environments in eastern Prydz Bay, East Antarctica. *Quaternary Science Reviews,* 29**,** 2731-2740.
BARCENA, M. A.; GERSONDE, R.; LEDESMA, S.; FABRES, J.; CALAFAT, A. M.; CANALS, M.; SERRO, F. J. & FLORES, J. A. 1998. Record of Holocene glacial oscillations in the Bransfield Basin as revealed by siliceous microfossil assemblages. *Antarctic Science-Institutional Subscription,* 10**,** 269-285.
BARNES, P. W. 1987. Morphologic studies of the Wilkes Land continental shelf, Antarctica-Glacial and iceberg effects. *The Antarctic Continental Margin: Geology and Geophysics of offshore Wilkes Land. Houston, Circum-Pacific Council for Energy and Mineral Resources. Earth Science Series,* 5**,** 175-194.
BEAMAN, R. J.; O'BRIEN, P. E.; POST, A. L. & DE SANTIS, L. 2010. A new high-resolution bathymetry model for the Terre Adélie and George V continental margin, East Antarctica. *Antarctic Science,* 23**,** 95.
BEANS, C.; HECQ, J. H.; KOUBBI, P.; VALLET, C.; WRIGHT, S. & GOFFART, A. 2008. A study of the diatom-dominated microplankton summer assemblages in coastal waters from Terre Adélie to the Mertz Glacier, East Antarctica (139 E–145 E). *Polar Biology,* 31**,** 1101-1117.
BELT, S. T.; ALLARD, W. G.; MASSE, G.; ROBERT, J. M. & ROWLAND, S. J. 2000a. Highly branched isoprenoids (HBIs): Identification of the most common and abundant sedimentary isomers. *Geochimica Et Cosmochimica Acta,* 64**,** 3839-3851.
BELT, S. T.; ALLARD, W. G.; RINTATALO, J.; JOHNS, L. A.; VAN DUIN, A. C. T. & ROWLAND, S. J. 2000b. Clay and acid catalysed isomerisation and cyclisation reactions of highly branched isoprenoid (HBI) alkenes: implications for sedimentary reactions and distributions. *Geochimica et Cosmochimica Acta,* 64**,** 3337-3345.
BELT, S. T.; BROWN, T. A.; RODRIGUEZ, A. N.; SANZ, P. C.; TONKIN, A. & INGLE, R. 2012. A reproducible method for the extraction, identification and quantification of the Arctic sea ice proxy IP25 from marine sediments. *Anal. Methods,* 4**,** 705-713.
BELT, S. T.; MASSÉ, G.; ALLARD, W. G.; ROBERT, J.-M. & ROWLAND, S. J. 2001. Identification of a C25 highly branched isoprenoid triene in the freshwater diatom Navicula sclesvicensis. *Organic Geochemistry,* 32**,** 1169-1172.

BELT, S. T.; MASSE, G.; ROWLAND, S. J.; POULIN, M.; MICHEL, C. & LEBLANC, B. 2007. A novel chemical fossil of palaeo sea ice: IP_{25}. *Organic Geochemistry,* 38**,** 16-27.

BELT, S. T.; MASSÉ, G.; VARE, L. L.; ROWLAND, S. J.; POULIN, M.; SICRE, M. A.; SAMPEI, M. & FORTIER, L. 2008. Distinctive ^{13}C isotopic signature distinguishes a novel sea ice biomarker in Arctic sediments and sediment traps. *Marine Chemistry,* 112**,** 158-167.

BENTLEY, C. R. 1984. Some aspects of the cryosphere and its role in climatic change. *Geophysical Monograph,* 29**,** 207-220.

BERGER, W. H. & WEFER, G. 1990. Export production: seasonality and intermittency, and paleoceanographic implications. *Global and Planetary Change,* 3**,** 245-254.

BERKMAN, P. A.; ANDREWS, J. T.; BJORCK, S.; COLHOUN, E. A.; EMSLIE, S. D.; GOODWIN, I. D.; HALL, B. L.; HART, C. P.; HIRAKAWA, K. & IGARASHI, A. 1998. Circum-Antarctic coastal environmental shifts during the Late Quaternary reflected by emerged marine deposits. *Antarctic Science,* 10**,** 345-362.

BERTLER, N. A. N.; NAISH, T. R.; MAYEWSKI, P. A. & BARRETT, P. J. 2006. Opposing oceanic and atmospheric ENSO influences on the Ross Sea Region, Antarctica. *Advances in Geosciences,* 6**,** 83-86.

BINDOFF, N. L.; ROSENBERG, M. A. & WARNER, M. J. 2000. On the circulation and water masses over the Antarctic continental slope and rise between 80 and 150°E. *Deep Sea Research Part II: Topical Studies in Oceanography,* 47**,** 2299-2326.

BLAAUW, M. 2010. Methods and code for 'classical'age-modelling of radiocarbon sequences. *Quaternary Geochronology,* 5**,** 512-518.

BLIGH, E. G. & DYER, W. J. 1959. A rapid method of total lipid extraction and purification. *Canadian journal of biochemistry and physiology,* 37**,** 911-917.

BOPP, L.; KOHFELD, K. E.; LE QUÉRÉ, C. & AUMONT, O. 2003. Dust impact on marine biota and atmospheric CO_2 during glacial periods. *Paleoceanography,* 18**,** 1046.

BROWN, T. A.; BELT, S. T.; PHILIPPE, B.; MUNDY, C. J.; MASSÉ, G.; POULIN, M. & GOSSELIN, M. 2011. Temporal and vertical variations of lipid biomarkers during a bottom ice diatom bloom in the Canadian Beaufort Sea: further evidence for the use of the IP_{25} biomarker as a proxy for spring Arctic sea ice. *Polar Biology,* 34**,** 1857-1868.

BUDD, W. F. 1991. Antarctica and global change. *Climatic Change,* 18**,** 271-299.

BURCKLE, L. H. 1984. Ecology and paleoecology of the marine diatomEucampia antarctica (Castr.) Mangin. *Marine Micropaleontology,* 9**,** 77-86.

BURCKLE, L. H. & CIRILLI, J. 1987. Origin of diatom ooze belt in the Southern Ocean; implications for late Quaterary paleoceanography. *Micropaleontology,* 33**,** 82-86.

BURCKLE, L. H.; JACOBS, S. S. & MCLAUGHLIN, R. B. 1987. Late austral spring diatom distribution between New Zealand and the Ross Ice Shelf, Antarctica; hydrographic and sediment correlations. *Micropaleontology,* 33**,** 74-81.

CARLETON, A. M. 1988. Sea Ice–Atmosphere Signal of the Southern Oscillation in the Weddell Sea, Antarctica. *Journal of Climate,* 1**,** 379-388.

CARTER, L.; MCCAVE, I. N. & WILLIAMS, M. J. M. 2009. Circulation and Water Masses of the Southern Ocean: A Review. *In:* FLORINDO, F. & SIEGERT, M. (eds.) *Antarctic Climate Evolution.* The Netherlands: Elsevier.

CAVALIERI, D. J. 1985. A passive microwave study of polynyas along the Antarctic Wilkes Land coast. *Oceanology of the Antarctic Continental Shelf, Antarct. Res. Ser.,* 43**,** 227-252.

CAVALIERI, D. J. & PARKINSON, C. L. 2008. Antarctic sea ice variability and trends, 1979–2006. *Journal of Geophysical Research,* 113**,** C07004.

CAVALIERI, D. J.; PARKINSON, C. L. & VINNIKOV, K. Y. 2003. 30-year satellite record reveals contrasting Arctic and Antarctic decadal sea ice variability. *Geophysical Research Letters,* 30**,** 1970.

CEFARELLI, A. O.; FERRARIO, M. E.; ALMANDOZ, G. O.; ATENCIO, A. G.; AKSELMAN, R. & VERNET, M. 2010. Diversity of the diatom genus *Fragilariopsis* in the Argentine Sea and Antarctic waters: morphology, distribution and abundance. *Polar Biology,* 33**,** 1-22.

COLLINS, L. G.; ALLEN, C. S.; PIKE, J.; HODGSON, D.; WECKSTRÖM, K. & MASSÉ, G. submitted manuscript. Highly branched isoprenoid (HBI) biomarkers as a new Antarctic sea-ice proxy in deep ocean glacial age sediments. *Earth and Planetary Science Letters*.

COMISO, J. C. 1999, updated 2008. Bootstrap sea ice concentrations from NIMBUS-7 SMMR and DMSP SSM/I, [November 1978 - December 2007]. Boulder, Colorado USA: National Snow and Ice Data Centre.

COMISO, J. C. 2006. Abrupt decline in the Arctic winter sea ice cover. *Geophysical Research Letters,* 33**,** L18504.

COSTA, E.; DUNBAR, R. B.; KRYC, K. A.; MUCCIARONE, D. A.; BRACHFELD, S.; ROARK, E. B.; MANLEY, P. L.; MURRAY, R. W. & LEVENTER, A. 2007. Solar forcing and El Niño-Southern Oscillation (ENSO) influences on productivity cycles interpreted from a late-Holocene high-resolution marine sediment record, Adélie Drift, East Antarctic Margin. *U.S Geological Survey and The National Academies,* USGS OF-2007-1047.

COXALL, H. K. & WILSON, P. A. 2011. Early Oligocene glaciation and productivity in the eastern equatorial Pacific: Insights into global carbon cycling. *Paleoceanography,* 26**,** PA2221.

COXALL, H. K.; WILSON, P. A.; PÄLIKE, H.; LEAR, C. H. & BACKMAN, J. 2005. Rapid stepwise onset of Antarctic glaciation and deeper calcite compensation in the Pacific Ocean. *Nature,* 433**,** 53-57.

CRAWFORD, R. M. 1995. The role of sex in the sedimentation of a marine diatom bloom. *Limnology and Oceanography***,** 200-204.

CRAWFORD, R. M.; HINZ, F. & RYNEARSON, T. 1997. Spatial and temporal distribution of assemblages of the diatom Corethron criophilum in the Polar Frontal region of the South Atlantic. *Deep Sea Research Part II: Topical Studies in Oceanography,* 44**,** 479-496.

CREMER, H.; ROBERTS, D.; MCMINN, A.; GORE, D. & MELLES, M. 2005. The Holocene diatom flora of marine bays in the Windmill Islands, East Antarctica. *Botanica marina,* 46**,** 82-106.

CROSTA, X.; CRESPIN, J.; BILLY, I. & THER, O. 2005a. Major factors controlling Holocene $d^{13}C$ org changes in a seasonal sea-ice environment, Adélie Land, East Antarctica. *Global Biogeochem. Cycles,* 19**,** GB4029, 9 PP.

CROSTA, X.; DEBRET, M.; DENIS, D.; COURTY, M. A. & THER, O. 2007. Holocene long- and short-term climate changes off Adelie Land, East Antarctica. *Geochemistry Geophysics Geosystems,* 8**,** Q11009, 15 PP.

CROSTA, X.; DENIS, D. & THER, O. 2008. Sea ice seasonality during the Holocene, Adelie Land, East Antarctica. *Marine Micropaleontology,* 66**,** 222-232.

CROSTA, X.; PICHON, J.-J. & LABRACHERIE, M. 1997. Distribution of Chaetoceros resting spores in modern peri-Antarctic sediments. *Marine Micropaleontology,* 29**,** 283-299.

CROSTA, X.; ROMERO, O.; ARMAND, L. K. & PICHON, J.-J. 2005b. The biogeography of major diatom taxa in Southern Ocean sediments: 2. Open ocean related species. *Palaeogeography, Palaeoclimatology, Palaeoecology,* 223**,** 66-92.
CUNNINGHAM, S. A. 2005. Southern ocean circulation. *Archives of natural history,* 32**,** 265-280.
CUNNINGHAM, W. L. & LEVENTER, A. 1998. Diatom assemblages in surface sediments of the Ross Sea: relationship to present oceanographic conditions. *Antarctic Science,* 10**,** 134-146.
CURRAN, M. A. J.; VAN OMMEN, T. D.; MORGAN, V. I.; PHILLIPS, K. L. & PALMER, A. S. 2003. Ice Core Evidence for Antarctic Sea Ice Decline Since the 1950s. *Science,* 302**,** 1203-1206.
DALE, A. & DALE, B. 2002. Application of ecologically based statistical treatments to micropalaeontology. *In:* HASLETT, S. (ed.) *Quaternary Environmental Micropalaeontology.* London: Arnold.
DAMSTÉ, J. S. S.; MUYZER, G.; ABBAS, B.; RAMPEN, S. W.; MASSÉ, G.; ALLARD, W. G.; BELT, S. T.; ROBERT, J. M.; ROWLAND, S. J. & MOLDOWAN, J. M. 2004. The rise of the rhizosolenid diatoms. *Science,* 304**,** 584-587.
DAVIES, A.; KEMP, A. E. S. & PÄLIKE, H. 2011. Tropical ocean-atmosphere controls on inter-annual climate variability in the Cretaceous Arctic. *Geophysical Research Letters,* 38**,** L03706.
DE BAAR, H. J. W.; DE JONG, J. T. M.; BAKKER, D. C. E.; LÖSCHER, B. M.; VETH, C.; BATHMANN, U. & SMETACEK, V. 1995. Importance of iron for plankton blooms and carbon dioxide drawdown in the Southern Ocean.
DE SANTIS, L.; BRANCOLINI, G.; DONDA, F. & O'BRIEN, P. 2010. Cenozoic deformation in the George V Land continental margin (East Antarctica). *Marine Geology,* 269**,** 1-17.
DEACON, S. G. E. R. 1937. *The hydrology of the Southern Ocean,* Cambridge University Press.
DEAN, J. M.; KEMP, A. E. S.; BULL, D.; PIKE, J.; PATTERSON, G. & ZOLITSCHKA, B. 1999. Taking varves to bits: Scanning electron microscopy in the study of laminated sediments and varves. *Journal of Paleolimnology,* 22**,** 121-136.
DEBRET, M.; BOUT-ROUMAZEILLES, V.; GROUSSET, F.; DESMET, M.; MCMANUS, J. F.; MASSEI, N.; SEBAG, D.; PETIT, J. R.; COPARD, Y. & TRENTESAUX, A. 2007. The origin of the 1500-year climate cycles in Holocene North-Atlantic records. *Climate of the Past,* 3**,** 569-575.
DEBRET, M.; SEBAG, D.; CROSTA, X.; MASSEI, N.; PETIT, J. R.; CHAPRON, E. & BOUT-ROUMAZEILLES, V. 2009. Evidence from wavelet analysis for a mid-Holocene transition in global climate forcing. *Quaternary Science Reviews,* 28**,** 2675-2688.
DECONTO, R. M. & POLLARD, D. 2003. Rapid Cenozoic glaciation of Antarctica induced by declining atmospheric CO 2. *Nature,* 421**,** 245-249.
DELMOTTE, M.; RAYNAUD, D.; MORGAN, V. & JOUZEL, J. 1999. Climatic and glaciological information inferred from air-content measurements of a Law Dome (East Antarctica) ice core. *Journal of Glaciology,* 45**,** 255-263.
DENIS, D.; CROSTA, X.; BARBARA, L.; MASSÉ, G.; RENSSEN, H.; THER, O. & GIRAUDEAU, J. 2010. Sea ice and wind variability during the Holocene in East Antarctica: insight on middle-high latitude coupling. *Quaternary Science Reviews,* 29**,** 3709-3719.
DENIS, D.; CROSTA, X.; SCHMIDT, S.; CARSON, D. S.; GANESHRAM, R. S.; RENSSEN, H.; BOUT-ROUMAZEILLES, V.; ZARAGOSI, S.; MARTIN, B. &

CREMER, M. 2009a. Holocene glacier and deep water dynamics, Adélie Land region, East Antarctica. *Quaternary Science Reviews,* 28**,** 1291-1303.
DENIS, D.; CROSTA, X.; SCHMIDT, S.; CARSON, D. S.; GANESHRAM, R. S.; RENSSEN, H.; CRESPIN, J.; THER, O.; BILLY, I. & GIRAUDEAU, J. 2009b. Holocene productivity changes off Adélie Land (East Antarctica). *Paleoceanography,* 24**,** PA3207.
DENIS, D.; CROSTA, X.; ZARAGOSI, S.; ROMERO, O.; MARTIN, B. & MAS, V. 2006. Seasonal and subseasonal climate changes recorded in laminated diatom ooze sediments, Adelie Land, East Antarctica. *Holocene,* 16**,** 1137-1147.
DINNIMAN, M. S.; KLINCK, J. M. & SMITH JR, W. O. 2011. A model study of Circumpolar Deep Water on the West Antarctic Peninsula and Ross Sea continental shelves. *Deep Sea Research Part II: Topical Studies in Oceanography,* 58**,** 1508-1523.
DOMACK, E.; O'BRIEN, P.; HARRIS, P.; TAYLOR, F.; QUILTY, P. G.; SANTIS, L. D. & RAKER, B. 1998. Late Quaternary sediment facies in Prydz Bay, East Antarctica and their relationship to glacial advance onto the continental shelf. *Antarctic Science,* 10**,** 236-246.
DOMACK, E. W. 1982. Sedimentology of glacial and glacial marine deposits on the George V-Adelie continental shelf, East Antarctica. *Boreas,* 11**,** 79-97.
DONDERS, T. H.; WAGNER-CREMER, F. & VISSCHER, H. 2008. Integration of proxy data and model scenarios for the mid-Holocene onset of modern ENSO variability. *Quaternary Science Reviews,* 27**,** 571-579.
DUNBAR, R. B.; ANDERSON, J. B. & DOMACK, E. W. 1985. Oceanographic influences on sedimentation along the Antarctic continental shelf. *In:* JACOBS, S. S. (ed.) *Oceanology of the Antarctic Shelf: Antarctic Research Series.* American Geophysical Union.
DUNBAR, R. B.; LEVENTER, A. R. & MUCCIARONE, D. A. 1998. Water column sediment fluxes in the Ross Sea, Antarctica: Atmospheric and sea ice forcing. *Journal of Geophysical Research,* 103**,** 30741-30759.
EICKEN, H. 1992. The role of sea ice in structuring Antarctic ecosystems. *Polar Biology,* 12**,** 3-13.
EITTREIM, S. L. 1994. Transition from continental to oceanic crust on the Wilkes-Adelie margin of Antarctica. *Journal of Geophysical Research,* 99**,** 24189-24,205.
EITTREIM, S. L.; COOPER, A. K. & WANNESSON, J. 1995. Seismic stratigraphic evidence of ice-sheet advances on the Wilkes Land margin of Antarctica. *Sedimentary Geology,* 96**,** 131-156.
ESCUTIA, C.; DE SANTIS, L.; DONDA, F.; DUNBAR, R. B.; COOPER, A. K.; BRANCOLINI, G. & EITTREIM, S. L. 2005. Cenozoic ice sheet history from East Antarctic Wilkes Land continental margin sediments. *Global and Planetary Change,* 45**,** 51-81.
ESCUTIA, C.; WARNKE, D.; ACTON, G. D.; BARCENA, A.; BURCKLE, L.; CANALS, M. & FRAZEE, C. S. 2003. Sediment distribution and sedimentary processes across the Antarctic Wilkes Land margin during the Quaternary. *Deep Sea Research Part II: Topical Studies in Oceanography,* 50**,** 1481-1508.
FENNER, J.; SCHRADER, H. J. & WIENIGK, H. 1976. Diatom phytoplankton studies in the southern Pacific Ocean, composition and correlation to the Antarctic Convergence and its paleoecological significance. *Initial Reports of the Deep Sea Drilling Project,* 35**,** 757-813.
FISCHER, G.; GERSONDE, R. & WEFER, G. 2002. Organic carbon, biogenic silica and diatom fluxes in the marginal winter sea-ice zone and in the Polar Front Region:

interannual variations and differences in composition. *Deep-sea Research Part II - Topical Studies in Oceanography,* 49**,** 1721-1745.
FLOWER, B. P. & KENNETT, J. P. 1994. The middle Miocene climatic transition: East Antarctic ice sheet development, deep ocean circulation and global carbon cycling. *Palaeogeography, Palaeoclimatology, Palaeoecology,* 108**,** 537-555.
FLOWER, B. P. & KENNETT, J. P. 1995. Middle Miocene deepwater paleoceanography in the southwest Pacific: Relations with East Antarctic Ice Sheet development. *Paleoceanography,* 10**,** 1095-1112.
FOFONOFF, N. P. 1957. Some properties of sea water influencing the formation of Antarctic bottom water. *Deep Sea Research (1953),* 4**,** 32-35.
FOGT, R. L. & BROMWICH, D. H. 2006. Decadal variability of the ENSO teleconnection to the high-latitude South Pacific governed by coupling with the Southern Annular Mode*. *Journal of Climate,* 19**,** 979-997.
FOSTER, A. F. M.; CURRAN, M. A. J.; SMITH, B. T.; VAN OMMEN, T. D. & MORGAN, V. I. 2006. Covariation of sea ice and methanesulphonic acid in Wilhelm II Land, East Antarctica. *Annals of Glaciology,* 44**,** 429-432.
FRANCIS, J. E.; ASHWORTH, A.; CANTRILL, D. J.; CRAME, J. A.; HOWE, J.; STEPHENS, R.; TOSOLINI, A. M. & THORN, V. 100 million years of Antarctic climate evolution: evidence from fossil plants. 2008. 19-27.
FRANCIS, J. E. & POOLE, I. 2002. Cretaceous and early Tertiary climates of Antarctica: evidence from fossil wood. *Palaeogeography, Palaeoclimatology, Palaeoecology,* 182**,** 47-64.
FRONEMAN, P. W.; PERISSINOTTO, R.; MCQUAID, C. D. & LAUBSCHER, R. K. 1995. Summer distribution of netphytoplankton in the Atlantic sector of the Southern Ocean. *Polar Biology,* 15**,** 77-84.
FRYXELL, G. A.; HASLE, G. R.; LLANO, G. A. & WALLEN, I. E. 1971. Corethron criophilum Castracane: its distribution and structure. *Biology of the Antarctic Seas IV,* 4**,** 335.
GARFINKEL, C. I. & HARTMANN, D. L. 2007. Effects of the El Nino–Southern Oscillation and the Quasi-Biennial Oscillation on polar temperatures in the stratosphere. *Journal of Geophysical Research,* 112**,** D19112.
GARRISON, D. L. & BUCK, K. R. 1989. The biota of Antarctic pack ice in the Weddell Sea and Antarctic Peninsula regions. *Polar Biology,* 10**,** 211-219.
GARRISON, D. L.; BUCK, K. R. & FRYXELL, G. A. 1987. Algal assemblages in Antarctic pack ice and in ice edge plankton. *Journal of Phycology,* 23**,** 564-572.
GARRISON, D. L.; BUCK, K. R. & SILVER, M. W. 1983. Studies of ice-algal communities in the Weddell Sea. *Antarctic JUS,* 18**,** 179-180.
GARRISON, D. L.; CLOSE, A. R. & REIMNITZ, E. 1990. Microorganisms concentrated by frazil ice. Evidence from laboratory experiments and field measurements. *Sea ice properties and processes. US Army Corps of Engineers (CRREL) Monograph***,** 90-1.
GERSONDE, R. Siliceous microorganisms in sea ice and their record in sediments in the southern Weddell Sea (Antarctica). 1986. 549-566.
GERSONDE, R. & WEFER, G. 1987. Sedimentation of biogenic siliceous particles in Antarctic waters from the Atlantic sector. *Marine Micropaleontology,* 11**,** 311-332.
GERSONDE, R. & ZIELINSKI, U. 2000. The reconstruction of late Quaternary Antarctic sea-ice distribution—the use of diatoms as a proxy for sea-ice. *Palaeogeography, Palaeoclimatology, Palaeoecology,* 162**,** 263-286.
GHIL, M.; ALLEN, M. R.; DETTINGER, M. D.; IDE, K.; KONDRASHOV, D.; MANN, M. E.; ROBERTSON, A. W.; SAUNDERS, A.; TIAN, Y. & VARADI, F. 2002. Advanced spectral methods for climatic time series.

GIBSON, J. A. E.; TRULL, T.; NICHOLS, P. D.; SUMMONS, R. E. & MCMINN, A. 1999. Sedimentation of ^{13}C-rich organic matter from Antarctic sea-ice algae: A potential indicator of past sea-ice extent. *Geology,* 27**,** 331-334.

GLEITZ, M.; BARTSCH, A.; DIECKMANN, G. & EICKEN, H. 1998a. Composition and succession of sea ice diatom assemblages in the eastern and southern Weddell Sea. *Antarctica, Antarctic sea ice Biological processes, interactions, and variability (M Lizotte, K Arrigo, eds) Antarctic Res Ser, AGU, Washingon DC,* 73,107-120.

GLEITZ, M.; BARTSCH, A.; DIECKMANN, G. S. & EICKEN, H. 1998b. Composition and succession of sea ice diatom assemblages in the eastern and southern Weddell Sea, Antarctica. *Antarctic sea ice biological processes, interactions and variability: American Geophysical Union Antarctic Research Series,* 73**,** 107–120.

GLEITZ, M.; GROSSMANN, S.; SCHAREKM, R. & SMETACEK, V. 1996. Ecology of diatom and bacterial assemblages in water associated with melting summer sea ice in the Weddell Sea, Antarctica. *Antarctic Science,* 8**,** 135-146.

GLOERSEN, P.; CAMPBELL, W. J.; CAVALIERI, D. J.; COMISO, J. C.; PARKINSON, C. L. & ZWALLY, H. J. 1992. Arctic and Antarctic sea ice, 1978–1987. *National Aeronautics and Space Administration, Washington, DC,* 290.

GLOERSEN, P. & HUANG, N. 2003. Comparison of interannual intrinsic modes in hemispheric sea ice covers and other geophysical parameters. *Geoscience and Remote Sensing, IEEE Transactions on,* 41**,** 1062-1074.

GODFRED-SPENNING, C. R. & SIMMONDS, I. 1996. An analysis of Antarctic sea-ice and extratropical cyclone associations. *International Journal of Climatology,* 16**,** 1315-1332.

GOFFART, A.; CATALANO, G. & HECQ, J. H. 2000. Factors controlling the distribution of diatoms and Phaeocystis in the Ross Sea. *Journal of Marine Systems,* 27**,** 161-175.

GOMEZ, B.; CARTER, L.; ORPIN, A. R.; COBB, K. M.; PAGE, M. J.; TRUSTRUM, N. A. & PALMER, A. S. 2012. ENSO/SAM interactions during the middle and late Holocene. *The Holocene,* 22**,** 23-30.

GOODWIN, I. D. & ZWECK, C. 2000. Glacio-isostasy and glacial ice load at Law Dome, Wilkes land, east Antarctica. *Quaternary Research,* 53**,** 285-293.

GOOSSE, H.; BARRIAT, P. Y.; LEFEBVRE, W.; LOUTRE, M. F. & ZUNZ, V. 2010. Brief history of climate: causes and mechanisms. *Introduction to climate dynamics and climate modeling.* Online textbook available at http://www.climate.be/textbook.

GORDON, A. L. & TCHERNIA, P. 1972. Waters of the continental margin off Adelie Coast, Antarctica. *Antarctic oceanology,* 2**,** 59-69.

GROSSI, V.; BEKER, B.; GEENEVASEN, J. A. J.; SCHOUTEN, S.; RAPHEL, D.; FONTAINE, M. F. & DAMSTE, J. S. S. 2004. C-25 highly branched isoprenoid alkenes from the marine benthic diatom Pleurosigma strigosum. *Phytochemistry,* 65**,** 3049-3055.

GROSSMANN, S.; LOCHTE, K. & SCHAREK, R. 1996. Algal and bacterial processes in platelet ice during late austral summer. *Polar Biology,* 16**,** 623-633.

GUNTHER, S. & DIECKMANN, G. S. 2001. Vertical zonation and community transition of sea-ice diatoms in fast ice and platelet layer, Weddell Sea, Antarctica. *Annals of Glaciology,* 33**,** 287-296.

HALL, A. & VISBECK, M. 2010. Synchronous Variability in the Southern Hemisphere Atmosphere, Sea Ice, and Ocean Resulting from the Annular Mode*. *Journal of Climate,* 15**,** 3043-3057.

HALL, B. L.; HENDERSON, G. M.; BARONI, C. & KELLOGG, T. B. 2010. Constant Holocene Southern-Ocean ^{14}C reservoir ages and ice-shelf flow rates. *Earth and Planetary Science Letters,* 296**,** 115-123.

HAMMER, Ø.; HARPER, D. A. T. & RYAN, P. D. 2001. PAST: Paleontological Statistics Software Package for Education and Data Analysis. *Palaeontologica Electronica,* 4**,** 9pp.
HARRIS, P. T. & BEAMAN, R. J. 2003. Processes controlling the formation of the Mertz Drift, George Vth continental shelf, East Antarctica: evidence from 3.5 kHz sub-bottom profiling and sediment cores. *Deep Sea Research Part II: Topical Studies in Oceanography,* 50**,** 1463-1480.
HART, T. J. 1942. *Phytoplankton periodicity in Antarctic surface waters,* Cambridge University Press.
HASLE, G. R. 1976. The biogeography of some marine planktonic diatoms. *Deep Sea Research and Oceanographic Abstracts,* 23**,** 319-IN6.
HASLE, G. R. & SYVERTSEN, E. E. 1997. Marine Diatoms. *In:* TOMAS, C. (ed.) *Identifying Marine Phytoplankton.* San Diego: Academic Press.
HAYAKAWA, K.; HANDA, N.; IKUTA, N. & FUKUCHI, M. 1996. Downward fluxes of fatty acids and hydrocarbons during a phytoplankton bloom in the austral summer in Breid Bay, Antarctica. *Organic Geochemistry,* 24**,** 511-521.
HAYS, J. D. 1965. Quaternary sediments of the Antarctic Ocean. *Progress In Oceanography,* 4**,** 117-131.
HAYWOOD, A.; VALDES, P.; LUNT, D. & PEKAR, S. 2010. The Eocene-Oligocene boundary and the Antarctic Circumpolar Current. *EGU General Assembly 2010, held 2-7 May, 2010 in Vienna, Austria, p. 5031,* 12**,** 5031.
HEROY, D. C. & ANDERSON, J. B. 2005. Ice-sheet extent of the Antarctic Peninsula region during the Last Glacial Maximum (LGM)—Insights from glacial geomorphology. *Geological Society of America Bulletin,* 117**,** 1497-1512.
HEROY, D. C. & ANDERSON, J. B. 2007. Radiocarbon constraints on Antarctic Peninsula ice sheet retreat following the Last Glacial Maximum (LGM). *Quaternary Science Reviews,* 26**,** 3286-3297.
HIBBERT, A.; LEACH, H.; WOODWORTH, P.; HUGHES, C. W. & ROUSSENOV, V. 2010. Quasi-Biennial Modulation of the Southern Ocean Coherent Mode. *Quarterly Journal of the Royal Meteorological Society,* 136**,** 755-768.
HODGSON, D. A.; MCMINN, A.; KIRKUP, H.; CREMER, H.; GORE, D.; MELLES, M.; ROBERTS, D. & MONTIEL, P. 2003. Colonization, succession, and extinction of marine floras during a glacial cycle: A case study from the Windmill Islands (east Antarctica) using biomarkers. *Paleoceanography,* 18**,** 1067.
HOLM-HANSEN, O. & EL-SAYED, S. Z. 1975. Primary production and the factors controlling phytoplankton growth in the Antarctic seas.
HORNER, R. A. 1985. Ecology of sea-ice microalgae. *In:* HORNER, R. A. (ed.) *Sea-ice biota.* Boca Raton: CRC Press.
INGOLFSSON, O.; HJORT, C.; BERKMAN, P. A.; COLHOUN, E.; GOODWIN, I. D.; HALL, B. H. K.; MELLES, M.; PRENTICE, M. L.; BJÖRCK, S. & MÖLLER, P. 1998. Antarctic glacial history since the Last Glacial Maximum: an overwiew of the record on land.
IODP EXPEDITION 318 SCIENTISTS. 2010. Wilkes Land Glacial History: Cenozoic East Antarctic Ice Sheet evolution from Wilkes Land margin sediments. *IODP Preliminary Report,* 318.
ISHII, M.; INOUE, H. Y. & MATSUEDA, H. 2002. Net community production in the marginal ice zone and its importance for the variability of the oceanic pCO2 in the Southern Ocean south of Australia. *Deep Sea Research Part II: Topical Studies in Oceanography,* 49**,** 1691-1706.

IVANY, L. C.; VAN SIMAEYS, S.; DOMACK, E. W. & SAMSON, S. D. 2006. Evidence for an earliest Oligocene ice sheet on the Antarctic Peninsula. *Geology,* 34**,** 377-380.
JACOBS, S. S. 2004. Bottom water production and its links with the thermohaline circulation. *Antarctic Science,* 16**,** 427-437.
JACOBS, S. S.; AMOS, A. F. & BRUCHHAUSEN, P. M. Ross Sea oceanography and Antarctic bottom water formation. 1970. Elsevier, 935-962.
JACOBS, S. S. & COMISO, J. C. 1993. A recent sea-ice retreat west of the Antarctic Peninsula. *Geophysical Research Letters,* 20**,** 1171-1174.
JACOBS, S. S. & GIULIVI, C. F. 2010. Large multidecadal salinity trends near the Pacific-Antarctic continental margin. *Journal of Climate,* 23**,** 4508-4524.
JACQUES, G. 1983. Some ecophysiological aspects of the Antarctic phytoplankton. *Polar Biology,* 2**,** 27-33.
JAMIESON, S. S. R. & SUGDEN, D. E. Landscape evolution of Antarctica. 2008.
JIM, C. Y. 1985. Impregnation of moist and dry unconsolidated clay samples using Spurr resin for microstructural studies. *Journal of Sedimentary Research,* 55**,** 597.
JOHANSEN, J. R. & FRYXELL, G. A. 1985. The genus *Thalassiosira* (Bacillariophyceae): studies on species occurring south of the Antarctic Convergence Zone. *Phycologia,* 24**,** 155-179.
JOHN, T. 2004. The El Niño-southern oscillation and Antarctica. *International Journal of Climatology,* 24**,** 1-31.
JOHNS, L.; WRAIGE, E. J.; BELT, S. T.; LEWIS, C. A.; MASSÉ, G.; ROBERT, J. M. & ROWLAND, S. J. 1999. Identification of a C25 highly branched isoprenoid (HBI) diene in Antarctic sediments, Antarctic sea-ice diatoms and cultured diatoms. *Organic Geochemistry,* 30**,** 1471-1475.
JOUSE, A. P.; KOROLEVA, G. S. & NAGAEVA, G. A. 1962. Diatoms in the surface layer of sediment in the Indian sector of the Antarctic. *Trudy Instituta Okeanologii Akademiya Nauk SSSR,* 61**,** 20-91.
KALNAY, E.; KANAMITSU, M.; KISTLER, R.; COLLINS, W.; DEAVEN, D.; GANDIN, L.; IREDELL, M.; SANA, S.; WHITE, G. & WOOLLEN, J. 1996. The NCEP/NCAR 40-Year Reanalysis Project III.
KANG, S.-H. & FRYXELL, G. 1992. *Fragilariopsis cylindrus* (Grunow) Krieger: The most abundant diatom in water column assemblages of Antarctic marginal ice-edge zones. *Polar Biology,* 12**,** 609-627.
KANG, S. H. & FRYXELL, G. A. 1993. Phytoplankton in the Weddell Sea, Antarctica: composition, abundance and distribution in water-column assemblages of the marginal ice-edge zone during austral autumn. *Marine Biology,* 116**,** 335-348.
KATTNER, G.; THOMAS, D. N.; HAAS, C.; KENNEDY, H. & DIECKMANN, G. S. 2004. Surface ice and gap layers in Antarctic sea ice: highly productive habitats. *Marine Ecology Progress Series,* 277**,** 1-12.
KEELING, R. F. & STEPHENS, B. B. 2001. Antarctic sea ice and the control of Pleistocene climate instability. *Paleoceanography,* 16**,** 112-131.
KENNEDY, H.; THOMAS, D. N.; KATTNER, G.; HAAS, C. & DIECKMANN, G. S. 2002. Particulate organic matter in Antarctic summer sea ice: concentration and stable isotopic composition. *Marine Ecology Progress Series,* 238**,** 1-13.
KENNETT, J. P. & SHACKLETON, N. J. 1976. Oxygen isotopic evidence for the development of the psychrosphere 38 Myr ago.
KIDSON, J. W. 1999. Principal modes of Southern Hemisphere low-frequency variability obtained from NCEP-NCAR reanalyses. *Journal of Climate,* 12**,** 2808-2830.
KING, J. C. & TURNER, J. 1997. *Anarctic Meteorology and Climatology,* Cambridge, Cambridge University Press.

KIRTMAN, B. P. & SCHOPF, P. S. 1998. Decadal variability in ENSO predictability and prediction. *Journal of Climate,* 11**,** 2804-2822.
KOHFELD, K. E.; LE QUÉRÉ, C.; HARRISON, S. P. & ANDERSON, R. F. 2005. Role of marine biology in glacial-interglacial CO2 cycles. *Science,* 308**,** 74-78.
KOPCZYŃSKA, E. E.; FIALA, M. & JEANDEL, C. 1998. Annual and interannual variability in phytoplankton at a permanent station off Kerguelen Islands, Southern Ocean. *Polar Biology,* 20**,** 342-351.
KREBS, W. N.; LIPPS, J. H. & BURCKLE, L. H. 1987. Ice diatom floras, Arthur Harbor, Antarctica. *Polar Biology,* 7**,** 163-171.
KWOK, R. & COMISO, J. C. 2002. Southern Ocean Climate and Sea Ice Anomalies Associated with the Southern Oscillation. *Journal of Climate,* 15**,** 487-501.
LABITZKE, K. 2004. On the signal of the 11-year sunspot cycle in the stratosphere over the Antarctic and its modulation by the Quasi-Biennial Oscillation (QBO). *Meteorologische Zeitschrift,* 13**,** 263-270.
LANGONE, L.; FRIGNANI, M.; RAVAIOLI, M. & BIANCHI, C. 2000. Particle fluxes and biogeochemical processes in an area influenced by seasonal retreat of the ice margin (northwestern Ross Sea, Antarctica). *Journal of Marine Systems,* 27**,** 221-234.
LANNUZEL, D.; SCHOEMANN, V.; DE JONG, J.; TISON, J.-L. & CHOU, L. 2007. Distribution and biogeochemical behaviour of iron in the East Antarctic sea ice. *Marine Chemistry,* 106**,** 18-32.
LAWVER, L. A.; GAHAGAN, L. M. & COFFIN, M. F. 1992. The development of paleoseaways around Antarctica.
LEAR, C. H.; BAILEY, T. R.; PEARSON, P. N.; COXALL, H. K. & ROSENTHAL, Y. 2008. Cooling and ice growth across the Eocene-Oligocene transition. *Geology,* 36**,** 251.
LEAR, C. H.; ROSENTHAL, Y.; COXALL, H. K. & WILSON, P. A. 2004. Late Eocene to early Miocene ice sheet dynamics and the global carbon cycle. *Paleoceanography,* 19**,** 1-11.
LEGENDRE, L.; ACKLEY, S. F.; DIECKMANN, G. S.; GULLIKSEN, B.; HORNER, R.; HOSHIAI, T.; MELNIKOV, I. A.; REEBURGH, W. S.; SPINDLER, M. & SULLIVAN, C. W. 1992. Ecology of sea ice biota. *Polar Biology,* 12**,** 429-444.
LEVENTER, A. 1991. Sediment trap diatom assemblages from the northern Antarctic Peninsula region. *Deep Sea Research Part A. Oceanographic Research Papers,* 38**,** 1127-1143.
LEVENTER, A. 1992. Modern distribution of diatoms in sediments from the George V Coast, Antarctica. *Marine Micropaleontology,* 19**,** 315-332.
LEVENTER, A. 1998. The fate of Antarctic "sea ice diatoms" and their use as paleoenvironmental indicators. *Antarctic sea ice biological processes, interactions and variability: American Geophysical Union Antarctic Research Series,* 73**,** 121-137.
LEVENTER, A. 2003. Particulate flux from sea ice in Polar waters. *In:* THOMAS, D. N. & DIECKMANN, G. S. (eds.) *Sea Ice: An introduction to its physics, chemistry, biology and geology.* Oxford: Blackwell Science.
LEVENTER, A.; BRACHFELD, S.; DOMACK, E.; DUNBAR, R.; MANLEY, P. & MCCLENNAN, C. 2001. CHAOS (Coring Holocene Antarctic Ocean Sediments).
LEVENTER, A.; DOMACK, E.; BARKOUKIS, A.; MCANDREWS, B. & MURRAY, J. 2002. Laminations from the Palmer Deep: a diatom-based interpretation. *Paleoceanography,* 17**,** 8002.
LEVENTER, A.; DOMACK, E. W.; ISHMAN, S. E.; BRACHFELD, S.; MCCLENNEN, C. E. & MANLEY, P. 1996. Productivity cycles of 200–300 years in the Antarctic

Peninsula region: understanding linkages among the sun, atmosphere, oceans, sea ice, and biota. *Geological Society of America Bulletin,* 108**,** 1626-1644.
LEVENTER, A. & DUNBAR, R. B. 1996. Factors influencing the distribution of diatoms and other algae in the Ross Sea. *Journal of Geophysical Research,* 101**,** 18489-18500.
LEVENTER, A.; DUNBAR, R. B. & DEMASTER, D. J. 1993. Diatom Evidence for Late Holocene Climatic Events in Granite Harbor, Antarctica. *Paleoceanography,* 8**,** 373-386.
LIU, J.; CURRY, J. A. & MARTINSON, D. G. 2004. Interpretation of recent Antarctic sea ice variability. *Geophysical Research Letters,* 31**,** L02205.
LIU, Z.; PAGANI, M.; ZINNIKER, D.; DECONTO, R.; HUBER, M.; BRINKHUIS, H.; SHAH, S. R.; LECKIE, R. M. & PEARSON, A. 2009. Global cooling during the Eocene-Oligocene climate transition. *Science,* 323**,** 1187-1190.
LIZOTTE, M. P. 2001. The Contributions of Sea Ice Algae to Antarctic Marine Primary Production. *Amer. Zool.,* 41**,** 57-73.
LIZOTTE, M. P. & SULLIVAN, C. W. 1991. Photosynthesis-irradiance relationships in microalgae associated with Antarctic pack ice: Evidence for in situ activity. *Marine ecology progress series. Oldendorf,* 71**,** 175-184.
LYTHE, M. B. & VAUGHAN, D. G. 2001. BEDMAP: A new ice thickness and subglacial topographic model of Antarctica. *Journal of Geophysical Research,* 106**,** 11335-11,351.
MADDISON, E. J. 2005. *Seasonally laminated late Quaternary Antarctic sediments.* Doctorate of Philosophy, Cardiff University.
MADDISON, E. J.; PIKE, J. & DUNBAR, R. 2012. Seasonally-laminated diatom-rich sediments from Dumont d'Urville Trough, East Antarctic Margin: Late Holocene Neoglacial sea-ice conditions. *The Holocene*.
MADDISON, E. J.; PIKE, J.; LEVENTER, A. & DOMACK, E. W. 2005. Deglacial seasonal and sub-seasonal diatom record from Palmer Deep, Antarctica. *Journal of Quaternary Science,* 20**,** 435-446.
MADDISON, E. J.; PIKE, J.; LEVENTER, A.; DUNBAR, R.; BRACHFELD, S.; DOMACK, E. W.; MANLEY, P. & MCCLENNEN, C. 2006. Post-glacial seasonal diatom record of the Mertz Glacier Polynya, East Antarctica. *Marine Micropaleontology,* 60**,** 66-88.
MANGONI, O.; SAGGIOMO, M.; MODIGH, M.; CATALANO, G.; ZINGONE, A. & SAGGIOMO, V. 2009. The role of platelet ice microalgae in seeding phytoplankton blooms in Terra Nova Bay (Ross Sea, Antarctica): a mesocosm experiment. *Polar Biology,* 32**,** 311-323.
MANN, M. E. & LEES, J. M. 1996. Robust estimation of background noise and signal detection in climatic time series. *Climatic Change,* 33**,** 409-445.
MARSHALL, G. J. 2003. Trends in the Southern Annular Mode from observations and reanalyses. *Journal of Climate,* 16**,** 4134-4143.
MARSHALL, G. J.; STOTT, P. A.; TURNER, J.; CONNOLLEY, W. M.; KING, J. C. & LACHLAN-COPE, T. A. 2004. Causes of exceptional atmospheric circulation changes in the Southern Hemisphere. *Geophysical Research Letters,* 31**,** L14205.
MARSHALL, J. & PLUMB, R. A. 2008. *Atmosphere, Ocean, and Climate Dynamics: An Introductory Text,* London, Elsevier.
MARTIN, J. H. 1990. Glacial-interglacial CO2 change: The iron hypothesis. *Paleoceanography,* 5**,** 1-13.
MASSÉ, G.; BELT, S. T.; CROSTA, X.; SCHMIDT, S.; SNAPE, I.; THOMAS, D. N. & ROWLAND, S. J. 2011. Highly branched isoprenoids as proxies for variable sea ice conditions in the Southern Ocean *Antarctic Science,* 23**,** 487-498.

MASSÉ, G.; BELT, S. T.; ROWLAND, S. J.; SICRE, M. A. & CROSTA, X. Highly branched isoprenoid biomarkers as indicators of sea ice diatoms: implications for historical sea ice records and future predictions. 2007. 04001.
MASSE, G.; ROWLAND, S. J.; SICRE, M. A.; JACOB, J.; JANSEN, E. & BELT, S. T. 2008. Abrupt climate changes for Iceland during the last millennium: Evidence from high resolution sea ice reconstructions. *Earth and Planetary Science Letters,* 269**,** 564-568.
MASSOM, R. A.; HARRIS, P. T.; MICHAEL, K. J. & POTTER, M. J. 1998. The distribution and formative processes of latent-heat polynyas in East Antarctica. *Annals of Glaciology,* 27**,** 420-426.
MATSUDA, O.; ISHIKAWA, S. & KAWAGUCHI, K. 1990. Seasonal variation of particulate organic matter under the Antarctic fast ice and its importance to benthic life. *Antarctic Ecosystems, Ecological Change and Conservation. Springer− Verlag, Berlin***,** 143-148.
MAYEWSKI, P. A.; MAASCH, K. A.; WHITE, J. W. C.; STEIG, E. J.; MEYERSON, E.; GOODWIN, I.; MORGAN, V. I.; VAN OMMEN, T.; CURRAN, M. A. J.; SOUNEY, J. & KREUTZ, K. 2004. A 700 year record of Southern Hemisphere extratropical climate variability. *Annals of Glaciology,* 39**,** 127-132.
MCPHADEN, M. J. accessed 2010. *Tropical Atmosphere Ocean project diagrams* [Online]. Available: http://www.pmel.noaa.gov/tao/proj_over/diagrams/index.html [Accessed 10/10/2008 2008].
MIGEON, S.; WEBER, O.; FAUGERES, J. C. & SAINT-PAUL, J. 1999. SCOPIX: a new X-ray imaging system for core analysis. *Geo-Marine Letters,* 18**,** 251-255.
MILLER, J. M. L.; NORVICK, M. S. & WILSON, C. J. L. 2002. Basement controls on rifting and the associated formation of ocean transform faults--Cretaceous continental extension of the southern margin of Australia. *Tectonophysics,* 359**,** 131-155.
MILLER, K. G.; WRIGHT, J. D. & FAIRBANKS, R. G. 1991. Unlocking the ice house: Oligocene-Miocene oxygen isotopes, eustasy, and margin erosion. *Journal of Geophysical Research,* 96**,** 6829-6848.
MILLER, K. G.; WRIGHT, J. D.; KATZ, M. E.; BROWNING, J. V.; CRAMER, B. S.; WADE, B. S. & MIZINTSEVA, S. F. A view of Antarctic ice-sheet evolution from sea-level and deep-sea isotope changes during the Late Cretaceous–Cenozoic. 2008. 55-70.
MIX, A. C.; BARD, E. & SCHNEIDER, R. 2001. Environmental processes of the ice age: land, oceans, glaciers (EPILOG). *Quaternary Science Reviews,* 20**,** 627-657.
MOORE, J. K. & ABBOTT, M. R. 2000. Phytoplankton chlorophyll distributions and primary production in the Southern Ocean. *Journal of Geophysical Research,* 105**,** 28,709-28,722.
MOORE, J. K.; ABBOTT, M. R.; RICHMAN, J. G. & NELSON, D. M. 2000. The Southern Ocean at the last glacial maximum: A strong sink for atmospheric carbon dioxide. *Global Biogeochemical Cycles,* 14**,** 455-475.
MOY, C. M.; SELTZER, G. O.; RODBELL, D. T. & ANDERSON, D. M. 2002. Variability of El Nino/Southern Oscillation activity at millennial timescales during the Holocene epoch. *Nature,* 420**,** 162-165.
MÜLLER, J.; MASSÉ, G.; STEIN, R. & BELT, S. T. 2009. Variability of sea-ice conditions in the Fram Strait over the past 30,000 years. *Nature Geoscience,* 2**,** 772-776.
NEORI, A. & HOLM-HANSEN, O. 1982. Effect of temperature on rate of photosynthesis in Antarctic phytoplankton. *Polar Biology,* 1**,** 33-38.

NICHOLS, D. S.; NICHOLS, P. D. & SULLIVAN, C. W. 1993. Fatty acid, sterol and hydrocarbon composition of Antarctic sea ice diatom communities during the spring bloom in McMurdo Sound. *Antarctic Science,* 5**,** 271-278.
NICHOLS, P. D.; PALMISANO, A. C.; RAYNER, M. S.; SMITH, G. A. & WHITE, D. C. 1989. Changes in the lipid composition of Antarctic sea-ice diatom communities during a spring bloom: an indication of community physiological status. *Antarctic Science,* 1**,** 133-140.
NICOL, S.; PAULY, T.; BINDOFF, N. L. & WRIGHT, S. 2000. Ocean circulation off east Antarctica affects ecosystem structure and sea-ice extent. *Science,* 260**,** 1617-1623.
NIHASHI, S.; OHSHIMA, K. I. & KIMURA, N. 2011. Creation of a Heat and Salt Flux Dataset Associated with Sea Ice Production and Melting in the Sea of Okhotsk. *Journal of Climate,* 25**,** 2261-2278.
OPEN UNIVERSITY COURSE TEAM. 2001. *Ocean Circulation,* Oxford, Butterworth Heinemann.
ORSI, A. H.; JOHNSON, G. C. & BULLISTER, J. L. 1999. Circulation, mixing, and production of Antarctic Bottom Water. *Progress In Oceanography,* 43**,** 55-109.
ORSI, A. H.; WHITWORTH, T. & NOWLIN, W. D. 1995. On the meridional extent and fronts of the Antarctic Circumpolar Current. *Deep Sea Research Part I: Oceanographic Research Papers,* 42**,** 641-673.
OZSOY-CICEK, B.; XIE, H.; ACKLEY, S. F. & YE, K. 2009. Antarctic summer sea ice concentration and extent: comparison of ODEN 2006 ship observations, satellite passive microwave and NIC sea ice charts. *The Cryosphere,* 3**,** 1-9.
PAGANI, M.; ZACHOS, J. C.; FREEMAN, K. H.; TIPPLE, B. & BOHATY, S. 2005. Marked decline in atmospheric carbon dioxide concentrations during the Paleogene. *Science,* 309**,** 600-603.
PEARCE, R. B.; KEMP, A. E. S.; KOIZUMI, I.; PIKE, J.; CRAMP, A. & ROWLAND, S. J. A lamina-scale, SEM-based study of a late Quaternary diatom-ooze sapropel from the Mediterranean Ridge, Site 971. 1998. Ocean Drilling Program, 349-363.
PEARSON, P. N.; FOSTER, G. L. & WADE, B. S. 2009. Atmospheric carbon dioxide through the Eocene-Oligocene climate transition. *Nature,* 461**,** 1110-1113.
PERIARD, C. & PETTRE, P. 1993. Some aspects of the climatology of Dumont d'Urville, Adélie Land, East Antarctica. *International Journal of Climatology,* 13**,** 313-327.
PEZZA, A.; RASHID, H. & SIMMONDS, I. 2012. Climate links and recent extremes in antarctic sea ice, high-latitude cyclones, Southern Annular Mode and ENSO. *Climate Dynamics,* 38**,** 57-73.
PHILANDER, S. G. H. 1983. El Nino Southern Oscillation phenomena. *Nature,* 302**,** 295-301.
PICHON, J. J.; BAREILLE, G.; LABRACHERIE, M.; LABEYRIE, L. D.; BAUDRIMONT, A. & TURON, J. L. 1992. Quantification of the biogenic silica dissolution in Southern Ocean sediments. *Quaternary Research,* 37**,** 361-378.
PIKE, J.; ALLEN, C. S.; LEVENTER, A.; STICKLEY, C. E. & PUDSEY, C. J. 2008. Comparison of contemporary and fossil diatom assemblages from the western Antarctic Peninsula shelf. *Marine Micropaleontology,* 67**,** 274-287.
PIKE, J.; CROSTA, X.; MADDISON, E. J.; STICKLEY, C. E.; DENIS, D.; BARBARA, L. & RENSSEN, H. 2009. Observations on the relationship between the Antarctic coastal diatoms *Thalassiosira antarctica* Comber and *Porosira glacialis* (Grunow) Jørgensen and sea ice concentrations during the late Quaternary. *Marine Micropaleontology,* 73**,** 14-25.
PIKE, J. & KEMP, A. E. S. 1996. Preparation and analysis techniques for studies of laminated sediments. *In:* KEMP, A. E. S. (ed.) *Palaeoclimatology and*

Palaeoceanography From Laminated Sediments. Geological Society Special Publications.
POLARGROUP 1980. Polar atmosphere-ice-ocean processes: A review of polar problems in climate research. *Reviews of Geophysics and Space Physics,* 18**,** 525-543.
PRESTI, M.; DE SANTIS, L.; BUSETTI, M. & HARRIS, P. T. 2003. Late Pleistocene and Holocene sedimentation on the George V Continental Shelf, East Antarctica. *Deep Sea Research Part II: Topical Studies in Oceanography,* 50**,** 1441-1461.
PRÉZELIN, B. B.; HOFMANN, E. E.; MENGELT, C. & KLINCK, J. M. 2000. The linkage between Upper Circumpolar Deep Water (UCDW) and phytoplankton assemblages on the west Antarctic Peninsula continental shelf. *Journal of Marine Research,* 58**,** 165-202.
PRIDDLE, J. 1990. The Antarctic planktonic ecosystem. *Polar Marine Diatom***,** 25-34.
PRIDDLE, J.; HEYWOOD, R. B. & THERIOT, E. 1986. Some environmental factors influencing phytoplankton in the Southern Ocean around South Georgia. *Polar Biology,* 5**,** 65-79.
PRIDDLE, J.; NEDWELL, D. B.; WHITEHOUSE, M. J.; REAY, D. S.; SAVIDGE, G.; GILPIN, L. G.; MURPHY, E. J. & ELLIS-EVANS, J. C. 1998. Re-examining the Antarctic Paradox: speculation on the Southern Ocean as a nutrient-limited system. *Annals of Glaciology,* 27**,** 661-668.
PUDSEY, C. J. & EVANS, J. 2001. First survey of Antarctic sub–ice shelf sediments reveals mid-Holocene ice shelf retreat. *Geology,* 29**,** 787-790.
RAGUENEAU, O.; TRÉGUER, P.; LEYNAERT, A.; ANDERSON, R. F.; BRZEZINSKI, M. A.; DEMASTER, D. J.; DUGDALE, R. C.; DYMOND, J.; FISCHER, G. & FRANCOIS, R. 2000. A review of the Si cycle in the modern ocean: recent progress and missing gaps in the application of biogenic opal as a paleoproductivity proxy. *Global and Planetary Change,* 26**,** 317-365.
RAYNER, N. A.; PARKER, D. E.; HORTON, E. B.; FOLLAND, C. K.; ALEXANDER, L. V.; ROWELL, D. P.; KENT, E. C. & KAPLAN, A. 2003. Global analyses of sea surface temperature, sea ice, and night marine air temperature since the late nineteenth century. *Journal of Geophysical Research,* 108**,** 4407.
REIMER, P. J.; BAILLIE, M. G. L.; BARD, E.; BAYLISS, A.; BECK, J. W.; BLACKWELL, P. G.; RAMSEY, C. B.; BUCK, C. E.; BURR, G. S. & EDWARDS, R. L. 2009. IntCal09 and Marine09 radiocarbon age calibration curves, 0–50,000 years cal BP.
RENSSEN, H.; GOOSSE, H.; FICHEFET, T.; MASSON-DELMOTTE, V. & KOÇ, N. 2005. Holocene climate evolution in the high-latitude Southern Hemisphere simulated by a coupled atmosphere-sea ice-ocean-vegetation model. *The Holocene,* 15**,** 951.
RIAUX-GOBIN, C.; POULIN, M.; DIECKMANN, G.; LABRUNE, C. & VÉTION, G. 2011. Spring phytoplankton onset after the ice break-up and sea-ice signature (Adélie Land, East Antarctica). *Polar Research,* 30.
RIAUX-GOBIN, C.; POULIN, M.; PRODON, R. & TRÉGUER, P. 2003. Land-fast ice microalgal and phytoplanktonic communities (Adélie Land, Antarctica) in relation to environmental factors during ice break-up. *Antarctic Science,* 15**,** 353-364.
RINTOUL, S. R. 1998. On the origin and influence of Adelie Land Bottom Water. *Ocean, ice and atmosphere: Interactions at the Antarctic continental margin,* 75**,** 151–171.
ROSCOE, H. K. & HAIGH, J. D. 2007. Influences of ozone depletion, the solar cycle and the QBO on the Southern Annular Mode. *Quarterly Journal of the Royal Meteorological Society,* 133**,** 1855-1864.

ROSELL-MELÉ, A. & MCCLYMONT, E. L. 2007. Biomarkers as Paleoceanographic Proxies. *In:* HILLAIRE-MARCEL, C. & DE VERNAL, A. (eds.) *Proxies in Late Cenozoic Paleoceanography.* Cambridge: Elsevier.

ROUND, F. E.; CRAWFORD, R. M. & MANN, D. G. 1990. *The Diatoms. Biology and Morphology of the Genera,* Cambridge, Cambridge University Press.

ROWLAND, S. J.; BELT, S. T.; WRAIGE, E. J.; MASSE, G.; ROUSSAKIS, C. & ROBERT, J. M. 2001. Effects of temperature on polyunsaturation in cytostatic lipids of Haslea ostrearia. *Phytochemistry,* 56**,** 597-602.

SCHERER, R. P. 1994. A new method for the determination of absolute abundance of diatoms and other silt-sized sedimentary particles. *Journal of Paleolimnology,* 12**,** 171-179.

SCHIMMELMANN, A.; LANGE, C. B. & BERGER, W. H. 1990. Climatically controlled marker layers in Santa Barbara Basin sediments and fine-scale core-to-core correlation. *Limnology and Oceanography***,** 165-173.

SCHWEITZER, P. N. 1995. *Monthly average polar sea-ice concentration,* US Geological Survey.

SCOTESE, C. R. 1991. Jurassic and Cretaceous plate tectonic reconstructions. *Palaeogeography, Palaeoclimatology, Palaeoecology,* 87**,** 493-501.

SCOTT, P.; MCMINN, A. & HOSIE, G. 1994. Physical parameters influencing diatom community structure in eastern Antarctic sea ice. *Polar Biology,* 14**,** 507-517.

SELPH, K. E.; LANDRY, M. R.; ALLEN, C. B.; CALBET, A.; CHRISTENSEN, S. & BIDIGARE, R. R. 2001. Microbial community composition and growth dynamics in the Antarctic Polar Front and seasonal ice zone during late spring 1997. *Deep Sea Research Part II: Topical Studies in Oceanography,* 48**,** 4059-4080.

SIEVERS, H. A. & NOWLIN JR, W. D. 1984. The stratification and water masses at Drake Passage. *Journal of Geophysical Research,* 89**,** 10489-10,514.

SIGMAN, D. M. & BOYLE, E. A. 2000. Glacial/interglacial variations in atmospheric carbon dioxide. *Nature,* 407**,** 859-869.

SIGMAN, D. M.; HAIN, M. P. & HAUG, G. H. 2010. The polar ocean and glacial cycles in atmospheric CO2 concentration. *Nature,* 466**,** 47-55.

SIMMONDS, I. & JACKA, T. H. 1995. Relationships between the Interannual Variability of Antarctic Sea Ice and the Southern Oscillation. *Journal of Climate,* 8**,** 637-647.

SINNINGHE DAMSTE, J. S.; RIJPSTRA, W. I. C.; COOLEN, M. J. L.; SCHOUTEN, S. & VOLKMAN, J. K. 2007. Rapid sulfurisation of highly branched isoprenoid (HBI) alkenes in sulfidic Holocene sediments from Ellis Fjord, Antarctica. *Organic Geochemistry,* 38**,** 128-139.

SMETACEK, V.; DE BAAR, H. J. W.; BATHMANN, U. V.; LOCHTE, K. & RUTGERS VAN DER LOEFF, M. M. 1997. Ecology and biogeochemistry of the Antarctic Circumpolar Current during austral spring: a summary of Southern Ocean JGOFS cruise ANT X/6 of RV Polarstern. *Deep Sea Research Part II: Topical Studies in Oceanography,* 44**,** 1-21.

SMETACEK, V.; KLAAS, C.; MENDEN-DEUER, S. & RYNEARSON, T. A. 2002. Mesoscale distribution of dominant diatom species relative to the hydrographical field along the Antarctic Polar Front. *Deep Sea Research Part II: Topical Studies in Oceanography,* 49**,** 3835-3848.

SMETACEK, V.; SCHAREK, R.; GORDON, L. I.; EICKEN, H.; FAHRBACH, E.; ROHARDT, G. & MOORE, S. 1992. Early spring phytoplankton blooms in ice platelet layers of the southern Weddell Sea, Antarctica. *Deep Sea Research Part A. Oceanographic Research Papers,* 39**,** 153-168.

SMITH, W. O. & NELSON, D. M. 1986. Importance of ice edge phytoplankton production in the Southern Ocean. *BioScience,* 36**,** 251-257.
STAMMERJOHN, S. E.; MARTINSON, D. G.; SMITH, R. C.; YUAN, X. & RIND, D. 2008. Trends in Antarctic annual sea ice retreat and advance and their relation to El Niño–Southern Oscillation and Southern Annular Mode variability. *Journal of Geophysical Research,* 113.
STICKLEY, C. E.; PIKE, J. & LEVENTER, A. 2006. Productivity events of the marine diatom Thalassiosira tumida (Janisch) Hasle recorded in deglacial varves from the East Antarctic Margin. *Marine Micropaleontology,* 59**,** 184-196.
STICKLEY, C. E.; PIKE, J.; LEVENTER, A.; DUNBAR, R.; DOMACK, E. W.; BRACHFELD, S.; MANLEY, P. & MCCLENNAN, C. 2005. Deglacial ocean and climate seasonality in laminated diatom sediments, Mac.Robertson Shelf, Antarctica. *Palaeogeography, Palaeoclimatology, Palaeoecology,* 227**,** 290-310.
STROEVE, J.; HOLLAND, M. M.; MEIER, W.; SCAMBOS, T. & SERREZE, M. 2007. Arctic sea ice decline: Faster than forecast. *Geophysical Research Letters,* 34**,** 9501.
SUGDEN, D. E.; BENTLEY, M. J. & COFAIGH, C. Ó. 2006. Geological and geomorphological insights into Antarctic ice sheet evolution. *Philosophical Transactions of the Royal Society A: Mathematical, Physical and Engineering Sciences,* 364**,** 1607-1625.
TAGUCHI, M. 2010. Observed connection of the stratospheric quasi-biennial oscillation with El Niño-Southern Oscillation in radiosonde data. *Journal of Geophysical Research,* 115**,** D18120.
TAKAHASHI, T.; FEELY, R. A.; WEISS, R. F.; WANNINKHOF, R. H.; CHIPMAN, D. W.; SUTHERLAND, S. C. & TAKAHASHI, T. T. 1997. Global air-sea flux of CO_2: An estimate based on measurements of sea–air pCO_2 difference. *Proceedings of the National Academy of Sciences,* 94**,** 8292.
TAKAHASHI, T.; SUTHERLAND, S. C.; SWEENEY, C.; POISSON, A.; METZL, N.; TILBROOK, B.; BATES, N.; WANNINKHOF, R.; FEELY, R. A. & SABINE, C. 2002. Global sea-air CO_2 flux based on climatological surface ocean pCO_2, and seasonal biological and temperature effects. *Deep Sea Research Part II: Topical Studies in Oceanography,* 49**,** 1601-1622.
TAKAHASHI, T.; SUTHERLAND, S. C.; WANNINKHOF, R.; SWEENEY, C.; FEELY, R. A.; CHIPMAN, D. W.; HALES, B.; FRIEDERICH, G.; CHAVEZ, F. & SABINE, C. 2009. Climatological mean and decadal change in surface ocean pCO_2, and net sea-air CO_2 flux over the global oceans. *Deep Sea Research Part II: Topical Studies in Oceanography,* 56**,** 554-577.
TAMURA, T.; OHSHIMA, K. I. & NIHASHI, S. 2008. Mapping of sea ice production for Antarctic coastal polynyas. *Geophysical Research Letters,* 35**,** L07606.
TANIMURA, Y.; FUKUCHI, M.; WATANABE, K. & MORIWAKI, K. 1990. Diatoms in water column and sea-ice in Lützow-Holm Bay, Antarctica, and their preservation in the underlying sediments. *Bulletin of the National Science Museum. Series C,* 16**,** 15-39.
TAYLOR, F.; MCMINN, A. & FRANKLIN, D. 1997. Distribution of diatoms in surface sediments of Prydz Bay, Antarctica. *Marine Micropaleontology,* 32**,** 209-229.
TCHERNIA, P. 1980. *Descriptive regional oceanography,* Oxford, Pergamon Press.
TEN BRINK, U. S. & COOPER, A. K. 1992. Modeling the bathymetry of Antarctic continental margins. *In:* YOSHIDA, Y., KAMINUMA, K. & SHIRAISHI, K. (eds.) *Recent Progress in Antarctic Earth Sciences.* Tokyo: Terra Publishing.
THERIOT, E. & FRYXELL, G. 1985. Multivariate statistical analysis of net diatom species distributions in the Southwestern Atlantic and Indian Ocean. *Polar Biology,* 5**,** 23-30.

THOMAS, D. N.; KENNEDY, H.; KATTNER, G.; GERDES, D.; GOUGH, C. & DIECKMANN, G. S. 2001. Biogeochemistry of platelet ice: its influence on particle flux under fast ice in the Weddell Sea, Antarctica. *Polar Biology,* 24**,** 486-496.

THOMPSON, D. W. J.; BALDWIN, M. P. & SOLOMON, S. 2005. Stratosphere–Troposphere Coupling in the Southern Hemisphere. *Journal of the Atmospheric Sciences,* 62**,** 708-715.

THOMPSON, D. W. J. & SOLOMON, S. 2002. Interpretation of recent Southern Hemisphere climate change. *Science,* 296**,** 895.

THOMPSON, D. W. J. & WALLACE, J. M. 2000. Annular Modes in the Extratropical Circulation. Part I: Month-to-Month Variability*. *Journal of Climate,* 13**,** 1000-1016.

THOMSON, D. J. 1982. Spectrum estimation and harmonic analysis. *Proceedings of the IEEE,* 70**,** 1055-1096.

TIMMERMANN, A. & JIN, F. F. 2002. A nonlinear mechanism for decadal El Nino amplitude changes. *Geophysical Research Letters,* 29**,** 3-1.

TOGGWEILER, J. R. 1999. Variation of Atmospheric CO_2 by Ventilation of the Ocean's Deepest Water. *Paleoceanography,* 14**,** 571-588.

TORRENCE, C. & COMPO, G. P. 1998. A practical guide to wavelet analysis. *Bulletin of the American Meteorological Society,* 79**,** 61-78.

TORSVIK, T. H.; GAINA, C. & REDFIELD, T. F. Antarctica and global paleogeography: from Rodinia, through Gondwanaland and Pangea, to the birth of the Southern Ocean and the opening of gateways. 2008.

TRÉGUER, P. & JACQUES, G. 1992. Dynamics of nutrients and phytoplankton, and fluxes of carbon, nitrogen and silicon in the Antarctic Ocean. *Polar Biology,* 12**,** 149-162.

TREGUER, P.; NELSON, D. M.; VAN BENNEKOM, A. J.; DEMASTER, D. J.; LEYNAERT, A. & QUEGUINER, B. 1995. The silica balance in the world ocean: a reestimate. *Science,* 268**,** 375-379.

TRENBERTH, K. E. 1991. General Characteristics of El Niño-Southern Oscillation. *In:* GLANTZ, M. H., KATZ, R.W. AND NICHOLLS, N. (ed.) *Teleconnections Linking Worldwide Climate Anomalies.* Cambridge: Cambridge University Press.

TRUESDALE, R. S. & KELLOGG, T. B. 1979. Ross Sea diatoms: Modern assemblage distributions and their relationship to ecologic, oceanographic, and sedimentary conditions. *Marine Micropaleontology,* 4**,** 13-31.

VARE, L. L.; MASSÉ, G.; GREGORY, T. R.; SMART, C. W. & BELT, S. T. 2009. Sea ice variations in the central Canadian Arctic Archipelago during the Holocene. *Quaternary Science Reviews,* 28**,** 1354-1366.

VAUGHAN, D. G. & SPOUGE, J. R. 2002. Risk estimation of collapse of the West Antarctic Ice Sheet. *Climatic Change,* 52**,** 65-91.

VEEVERS, J. J. 1986. Breakup of Australia and Antarctica estimated as mid-Cretaceous (95±5 Ma) from magnetic and seismic data at the continental margin. *Earth and Planetary Science Letters,* 77**,** 91-99.

VENKATESAN, M. I. 1988. Organic geochemistry of marine sediments in Antarctic region: Marine lipids in McMurdo Sound. *Organic Geochemistry,* 12**,** 13-27.

VERLEYEN, E.; HODGSON, D. A.; SABBE, K.; CREMER, H.; EMSLIE, S. D.; GIBSON, J.; HALL, B.; IMURA, S.; KUDOH, S. & MARSHALL, G. J. 2011. Post-glacial regional climate variability along the East Antarctic coastal margin—Evidence from shallow marine and coastal terrestrial records. *Earth-Science Reviews,* 104**,** 199-212.

VILLAREAL, T. A. & FRYXELL, G. A. 1983. Temperature effects on the valve structure of the bipolar diatoms Thalassiosira antarctica and Porosira glacialis. *Polar Biology,* 2**,** 163-169.

VON QUILLFELDT, C. H. 2004. The diatom *Fragilariopsis cylindrus* and its potential as an indicator species for cold water rather than for sea ice. *Vie et milieu,* 54**,** 137-143.
WANG, B. & WANG, Y. 1996. Temporal Structure of the Southern Oscillation as Revealed by Waveform and Wavelet Analysis. *Journal of Climate,* 9**,** 1586-1598.
WEEDON, G. 2003. *Time-Series Analysis and Cyclostratigraphy,* Cambridge, Cambridge University Press.
WEFER, G.; FISCHER, G.; FÜETTERER, D. & GERSONDE, R. 1988. Seasonal particle flux in the Bransfield Strait, Antartica. *Deep Sea Research Part A. Oceanographic Research Papers,* 35**,** 891-898.
WHITAKER, T. M. 1982. Primary production of phytoplankton off Signy Island, South Orkneys, the Antarctic. *Proceedings of the Royal Society of London. Series B. Biological Sciences,* 214**,** 169-189.
WILLIAMS, G. D.; BINDOFF, N. L.; MARSLAND, S. J. & RINTOUL, S. R. 2008. Formation and export of dense shelf water from the Adélie Depression, East Antarctica. *Journal of Geophysical Research,* 113.
WRAIGE, E. J.; BELT, S. T.; LEWIS, C. A.; COOKE, D. A.; ROBERT, J. M.; MASSE, G. & ROWLAND, S. J. 1997. Variations in structures and distributions of C-25 highly branched isoprenoid (HBI) alkenes in cultures of the diatom, *Haslea ostrearia* (Simonsen). *Organic Geochemistry,* 27**,** 497-505.
WRIGHT, J. D. & MILLER, K. G. 1993. Southern Ocean influences on late Eocene to Miocene deepwater circulation. *Antarctic Research Series,* 60**,** 1-25.
YUAN, X. 2004. ENSO-related impacts on Antarctic sea ice: a synthesis of phenomenon and mechanisms. *Antarctic Science,* 16**,** 415-425.
YUAN, X. & MARTINSON, D. G. 2000. Antarctic Sea Ice Extent Variability and Its Global Connectivity. *Journal of Climate,* 13**,** 1697-1717.
YUAN, X. & MARTINSON, D. G. 2001. The Antarctic dipole and its predictability. *Geophysical Research Letters,* 28**,** 3609-3612.
YUAN, X. & YONEKURA, E. 2011. Decadal variability in the Southern Hemisphere. *Journal of Geophysical Research,* 116**,** D19115.
YUAN, X. J. & LI, C. H. 2008. Climate modes in southern high latitudes and their impacts on Antarctic sea ice. *Journal of Geophysical Research - Oceans,* 113.
ZACHOS, J. C. 1996. High-resolution (104 years) deep-sea foraminiferal stable isotope records of the Eocene-Oligocene. *Paleoceanography,* 100**,** 251-266.
ZIELINSKI, U. 1993. Quantitative estimation of palaeoenvironmental parameters of the Antarctic surface water in the Late Quaternary using transfer functions with diatoms. *Berichte zur Polarforschung,* 126**,** 1–148.
ZIELINSKI, U. & GERSONDE, R. 1997. Diatom distribution in Southern Ocean surface sediments (Atlantic sector): Implications for paleoenvironmental reconstructions. *Palaeogeography, Palaeoclimatology, Palaeoecology,* 129**,** 213-250.
ZONNEVELD, K.; VERSTEEGH, G.; KASTEN, S.; EGLINTON, T. I.; EMEIS, K. C.; HUGUET, C.; KOCH, B.; DE LANGE, G. J.; DE LEEUW, J. & MIDDELBURG, J. J. 2010. Selective preservation of organic matter in marine environments; processes and impact on the sedimentary record.
ZWALLY, H. J.; COMISO, J. C. & GORDON, A. L. 1985. Antarctic offshore leads and polynyas and oceanographic effects. *Oceanology of the Antarctic Continental Shelf, Antarct. Res. Ser,* 43**,** 203-226.

Appendix 1. Diatom plates

This appendix contains plates presenting light microscope and SEM photographs of key diatom taxa from this study.

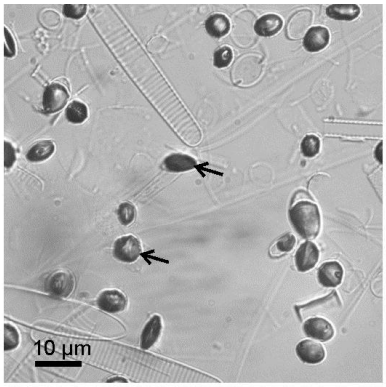

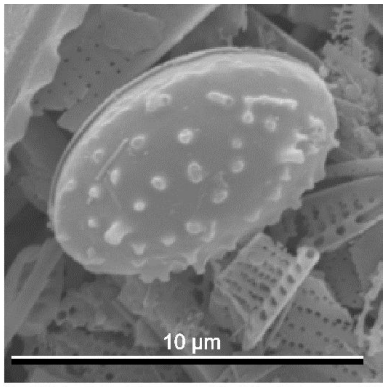

Hyalochaete Chaetoceros spp. - resting spores

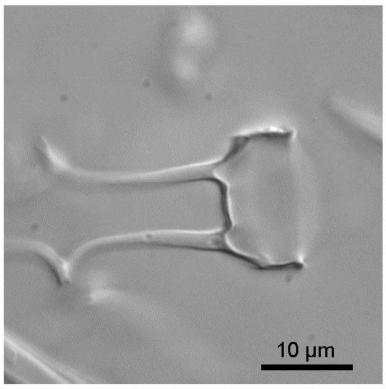

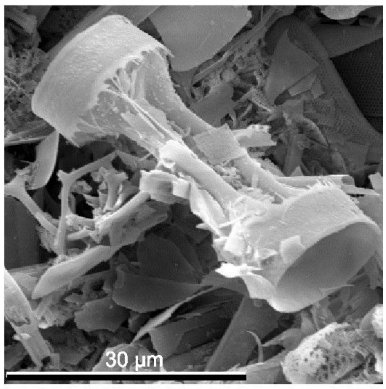

Phaeoceros Chaetoceros dichaeta Ehrenberg

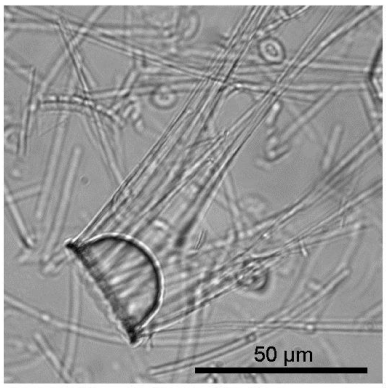

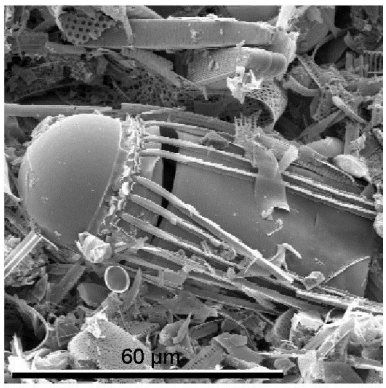

Corethron pennatum (Grunow) Ostenfeld

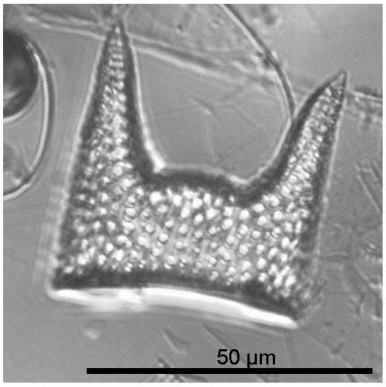

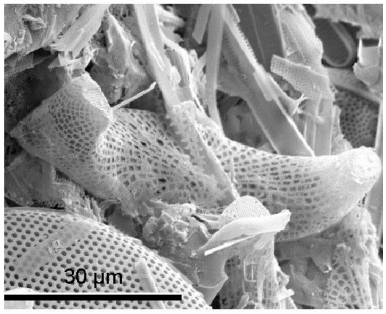

Eucampia antarctica (Castracane) Mangin - resting spore

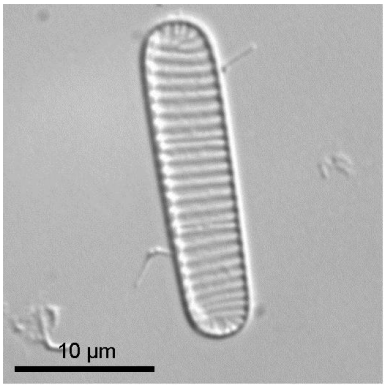

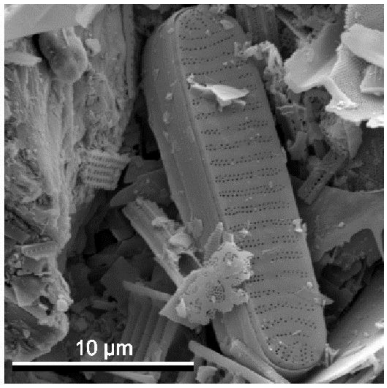

Fragilariopsis curta (Van Heurck) Hustedt

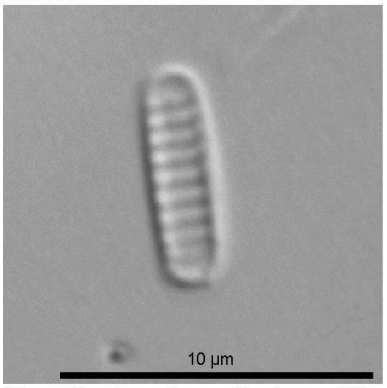

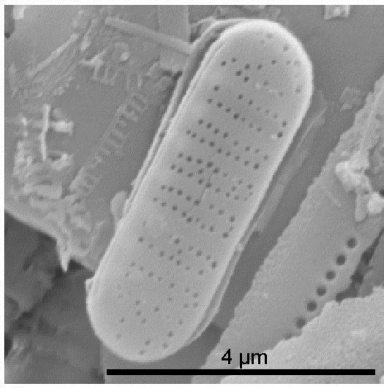

Fragilariopsis cylindrus (Grunow) Krieger

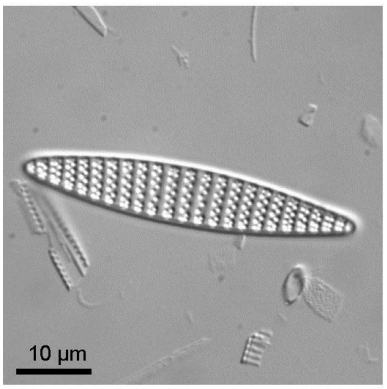

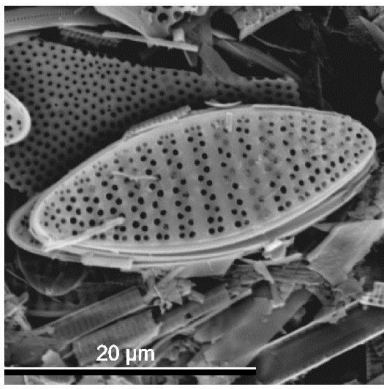

Fragilariopsis kerguelensis (O'Meara) Hustedt

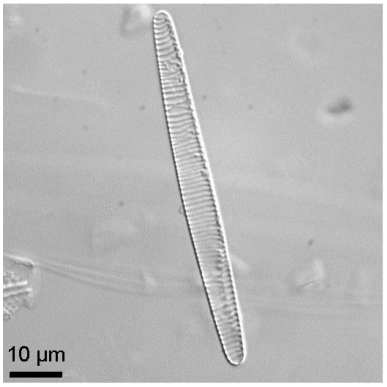

Fragilariopsis obliquecostata (Van Heurck) Heiden

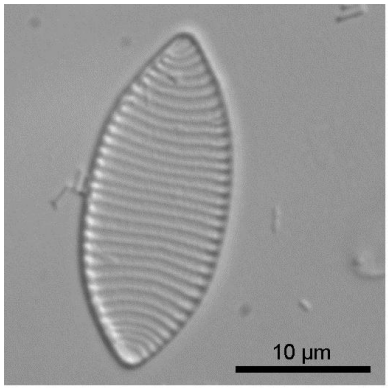

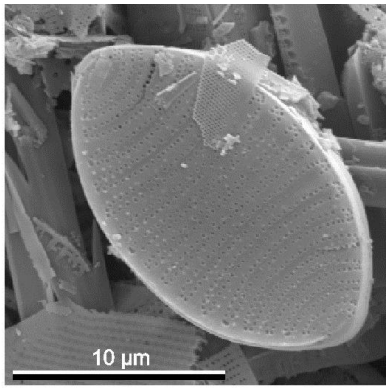

Fragilariopsis rhombica (O'Meara) Hustedt

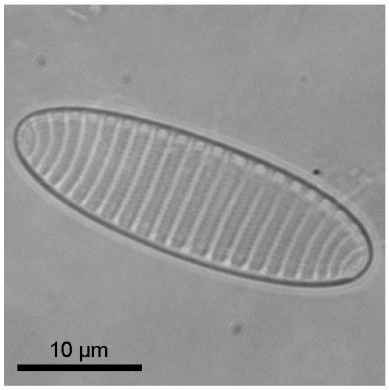

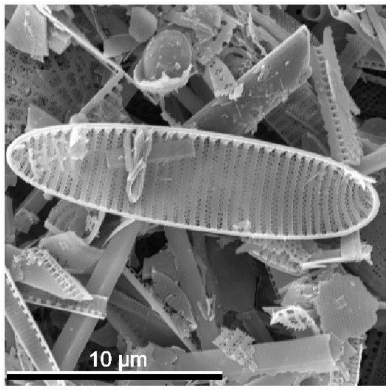

Fragilariopsis ritscheri (Hustedt) Hasle

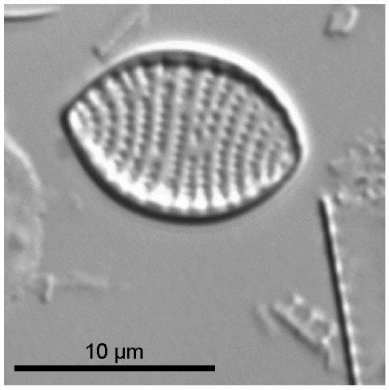

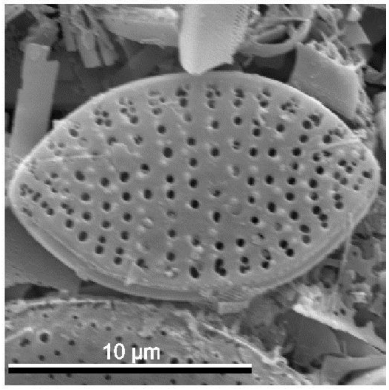

Fragilariopsis separanda Hustedt

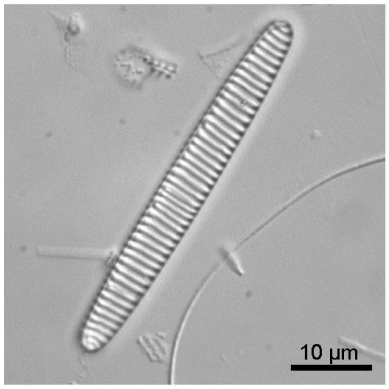

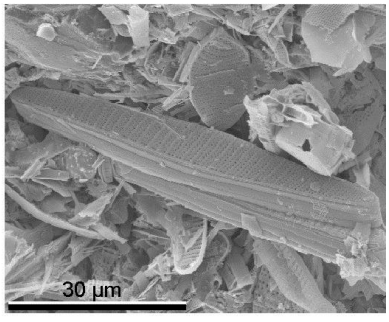

Fragilariopsis sublinearis (van Heurck) Heiden

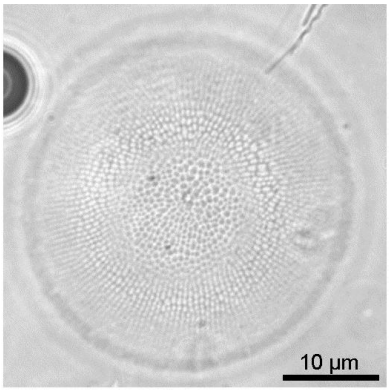

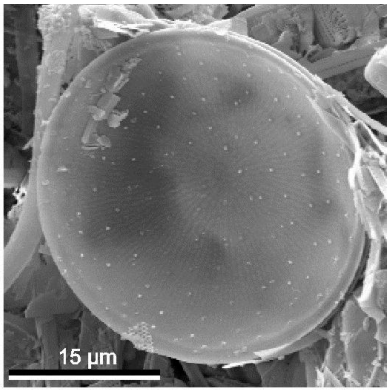

Porosira glacialis (Grunow) Jørgensen - resting spore

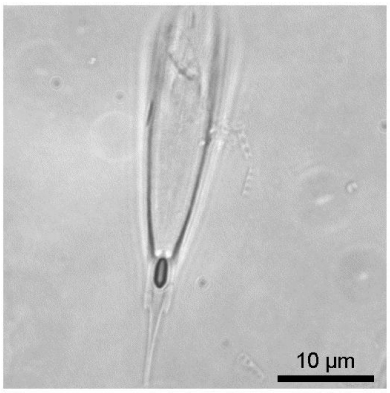

Rhizosolenia antennata (Ehrenberg) f. *semispina* Sundström

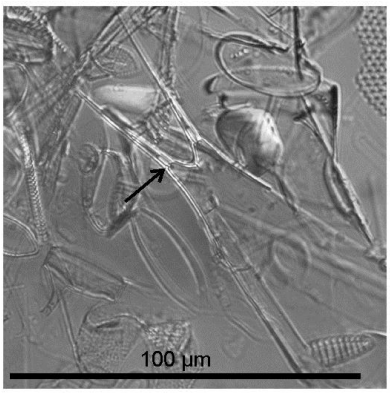

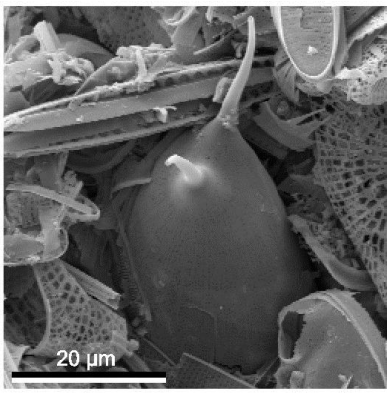

Rhizosolenia antennata (Ehrenberg) f. *antennata* Sundström

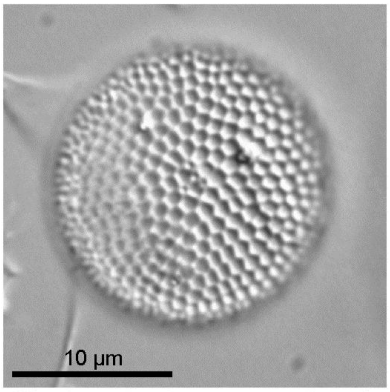

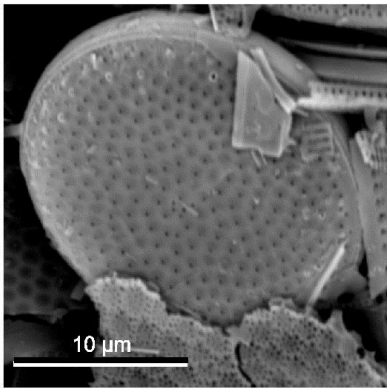

Thalassiosira antarctica Comber

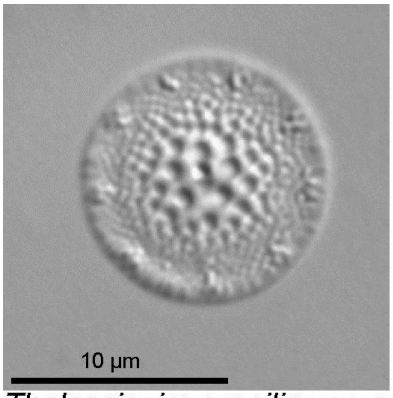

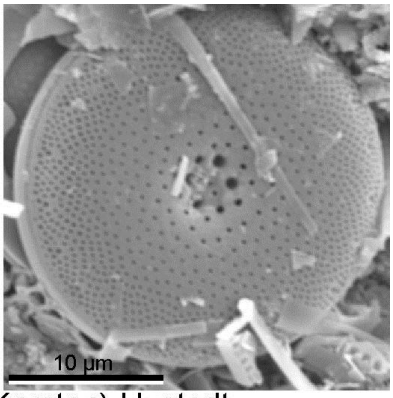

Thalassiosira gracilis var. *gracilis* (Karsten) Hustedt

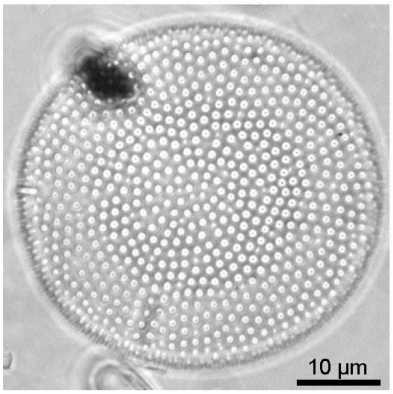

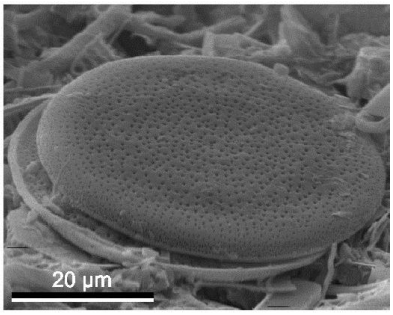

Thalassiosira lentiginosa (Janisch) Fryxell

Appendix 2. Lamina thicknesses

This appendix presents lamina thickness data for all laminae from cores MD03-2601 and IODP-318-U1367B. Lamina numbers were arbitrarily prescribed during data collection and reflect the thin section the lamina occurs on. Year number for each initial lamina within a given sequence is also indicated. The data is presented in five tables: A2.01 – A2.04 contain the data for MD03-2601; A2.05 contains the lamina data for IODP-318-U1357B.

Table A2.01. Lamina thickness measurements (T1 – T5) and mean values for all laminae recorded in core MDO3-2601 section III.

Lamina number	Year in sequence	Lamina type	Lamina thickness (mm)					
			T1	T2	T3	T4	T5	Mean
1305-0		E2	1.83	2.58	3.33	3.87	4.51	3.22
1305-1		D2	4.40	4.51	4.51	4.51	4.72	4.53
1305-2	4	A2	3.65	3.33	3.22	3.01	2.90	3.22
1305-3		D2	6.12	6.23	6.12	6.44	6.66	6.31
1305-4	3	A2	3.01	3.11	3.22	2.68	2.47	2.90
1305-5		D2	3.01	2.47	2.36	2.79	3.76	2.88
1305-6	2	A2	3.76	3.87	3.87	3.76	2.79	3.61
1305-7		D2	4.29	4.29	4.40	4.51	4.40	4.38
1305-8	1	B2	8.16	8.05	7.84	7.73	7.62	7.88
1337-0	Bioturbated	Bio	95.51	96.30	96.69	97.44	97.34	96.65
1337-1		D2	17.62	17.62	17.40	16.84	18.74	17.64
1338-0		Bio	37.76	37.77	38.82	39.61	37.79	38.35
1351-0		A2	12.28	10.17	9.63	8.15	8.08	9.66
1352-0		Bio	38.26	41.13	42.92	45.24	45.27	42.56
1352-1		C2	16.04	16.55	17.15	17.66	17.76	17.03
1352-2		D2	1.51	1.51	2.22	2.12	2.22	1.92
1354-0	1	C2	11.71	11.65	10.75	10.66	10.17	10.99
1361-0	Bioturbated	Bio	62.43	62.49	61.68	59.07	58.89	60.91
1361-1		B2	10.34	11.68	12.68	14.12	14.12	12.59
1362-0		Bio	28.08	27.89	27.97	28.61	29.02	28.31
1362-2		A2	10.58	9.69	9.20	8.41	8.60	9.30
1321-0		D2	24.37	24.46	25.14	23.67	22.78	24.08
1321-1	5	C2	1.96	1.96	2.05	2.15	2.84	2.19
1321-2		D2	1.17	1.47	0.98	1.56	1.56	1.35
1321-3	4	B2	4.99	5.09	5.38	4.79	4.79	5.01
1322-0		D2	13.33	12.71	13.11	13.77	14.03	13.39
1322-1	3	B2	3.08	3.24	3.48	3.81	4.05	3.53
1322-2		D2	3.57	3.57	3.81	3.81	3.81	3.71
1327-0	2	B2	26.35	25.95	26.19	26.01	25.92	26.08
1327-1		D2	5.18	5.37	5.75	5.46	4.90	5.33
1327-2	1	A2	15.35	14.98	14.88	15.63	14.60	15.09
1328-0	Bioturbated	Bio	21.43	21.25	20.33	20.37	22.52	21.18
1328-2		D2	12.61	12.29	12.40	12.29	12.50	12.42
1328-3	11	A2	1.27	1.48	1.91	2.23	1.91	1.76
1309-0		D2	6.10	5.75	5.10	4.45	4.12	5.10
1309-1	10	A2	9.06	9.62	10.29	10.18	9.96	9.82
1309-2		D2	2.68	2.57	2.46	2.80	3.24	2.75
1309-3	9	B2	11.30	10.96	10.74	10.85	11.07	10.98
1309-5		D2	1.90	1.90	2.01	2.01	2.13	1.99
1309-6	8	A2	7.27	7.16	6.71	6.04	5.70	6.58
1310-0		D2	10.13	10.05	9.68	8.27	8.27	9.28

Lamina number	Year in sequence	Lamina type	Lamina thickness (mm)					
			T1	T2	T3	T4	T5	Mean
1310-1	7	A2	1.77	1.58	2.36	1.77	1.97	1.89
1310-2		D2	2.56	2.56	1.97	3.84	3.15	2.82
1310-3	6	A2	3.65	3.94	4.53	4.93	5.71	4.55
1310-4		D2	2.56	2.86	3.05	3.05	3.45	3.00
1310-5	5	C2	4.93	4.34	3.84	3.55	3.05	3.94
1310-6		D2	2.66	2.86	3.05	3.05	3.45	3.01
1310-7	4	B2	2.27	1.97	1.77	1.58	1.08	1.73
1319-0		D2	7.73	8.75	9.87	9.84	10.23	9.28
1319-1		B2	4.98	4.30	3.85	4.30	3.74	4.24
1319-2	3	A2	6.46	5.78	4.76	3.63	3.40	4.80
1319-3		D2	8.84	7.36	10.65	10.42	9.97	9.45
1319-4	2	B2	3.85	3.63	2.49	2.61	2.83	3.08
1320-0		D2	11.52	13.25	13.93	14.73	15.42	13.77
1320-1	1	B2	5.58	4.10	3.58	3.16	3.05	3.89
1323-0	Bioturbated	Bio	27.43	27.20	26.91	26.87	26.82	27.04
1323-1		E2	3.79	3.60	3.42	2.96	2.96	3.34
1323-2		D2	4.25	4.80	4.99	5.36	5.08	4.90
1323-3	4	A2	3.88	3.42	2.96	2.96	4.25	3.49
1323-4		D2	2.40	2.77	3.51	4.16	3.79	3.33
1323-5	3	C2	1.16	1.53	2.27	2.92	2.55	2.09
1324-0		D2	18.53	18.05	17.97	17.79	17.06	17.88
1324-1	2	B2	3.18	3.59	3.79	3.79	3.59	3.59
1339-0		D2	24.23	24.22	23.79	23.56	23.76	23.91
1339-1	1	B2	5.52	5.63	5.73	5.84	6.37	5.82
1339-2		Bio	26.12	26.66	27.08	27.61	27.82	27.06
1340-0	Bioturbated	C2	2.32	1.42	2.27	2.11	2.77	2.18
1340-1		D2	7.43	6.89	6.71	6.71	6.98	6.94
1340-2	9	B2	1.54	1.81	1.81	1.99	2.18	1.87
1340-3		D2	11.11	11.59	9.97	8.43	7.93	9.81
1340-4	8	B2	1.94	1.64	1.54	1.99	1.59	1.74
1333-0		D2	7.99	7.88	7.74	7.69	7.06	14.84
1333-1	7	A2	6.74	8.69	10.63	10.73	13.18	9.99
1333-2		D2	9.50	7.15	4.80	3.27	2.35	5.42
1333-3	6	A2	6.74	8.69	10.53	11.75	13.18	10.18
1333-4		D2	5.12	7.06	8.80	9.72	7.88	7.72
1333-5	5	C2	2.19	4.14	5.87	6.79	4.95	4.79
1334-0		E2	3.19	3.19	2.59	2.30	2.61	2.77
1334-1		D2	5.88	6.27	6.47	6.67	6.96	6.45
1334-2	4	A2	8.04	7.35	6.86	6.47	6.37	7.02
1334-3		D2	15.00	14.70	15.29	15.29	15.00	15.06
1334-4	3	C2	2.45	2.84	2.45	2.55	2.84	2.63
1334-5		D2	5.01	4.89	4.76	3.90	2.91	4.30
1329-0	2	A2	6.89	6.78	6.65	5.78	4.80	6.18

Lamina number	Year in sequence	Lamina type	Lamina thickness (mm)					
			T1	T2	T3	T4	T5	Mean
1329-1		E2	1.80	1.80	1.72	1.96	2.29	1.91
1330-0		D2	12.82	12.48	12.28	11.81	11.94	12.27
1330-1	1	A2	3.62	3.62	4.30	4.75	4.98	4.26
1330-2	Bioturbated	Bio	27.62	28.07	28.07	28.52	28.75	28.21
1303-0	8	D2	9.87	11.70	11.91	11.62	11.80	11.38
1303-1		C2	3.57	2.02	2.12	2.31	2.22	2.45
1303-2		D2	2.12	2.12	2.02	1.93	2.02	2.04
1303-3	7	C2	1.45	1.83	1.35	1.35	1.54	1.50
1303-4		D2	4.82	4.63	4.53	4.43	4.43	4.57
1303-5	6	C2	4.63	4.43	4.34	4.24	3.95	4.32
1303-6		D2	8.09	8.58	8.96	9.15	6.65	8.29
1303-7	5	B2	5.01	4.43	3.66	3.18	3.08	3.87
1304-0		D2	8.94	9.44	10.62	11.33	11.92	10.45
1304-1	4	A2	4.30	4.41	4.41	3.69	3.18	4.00
1304-2		D2	7.89	7.48	7.17	7.27	8.09	7.58
1304-3	3	A2	4.00	4.10	4.30	4.41	4.41	4.24
1365-0		D2	10.60	10.70	11.81	13.43	13.83	12.08
1365-2	2	A2	10.66	10.46	10.36	9.24	9.34	10.01
1365-3		D2	9.85	9.55	8.73	7.62	6.81	8.51
1365-4	1	B2	3.76	4.16	5.08	5.89	5.99	4.98
1347-0	Bioturbated	Bio	75.87	69.33	68.58	68.79	68.82	70.28
1347-1		D2	5.93	6.33	6.43	6.63	6.43	6.35
1347-2	4	B2	2.67	2.67	2.57	2.18	1.98	2.41
1347-3		D2	1.58	0.89	0.30	0.00	0.00	0.55
1348-0	3	B2	0.00	0.00	0.54	1.29	2.04	0.77
1348-1		D2	8.36	8.25	7.61	7.08	6.54	7.57
1348-2	2	A2	4.50	4.93	5.68	6.22	6.75	5.62
1348-3		D2	5.25	6.86	6.75	6.00	6.22	6.22
1348-4	1	A2	5.47	2.68	2.14	3.97	4.07	3.67
1395-0	Bioturbated	Bio	43.59	43.52	42.81	42.42	42.38	42.95
1395-1		A2	2.53	2.33	2.14	1.85	1.36	2.04
1307-0		Bio	68.83	69.67	70.71	71.85	73.44	70.90
1308-0		A2	16.77	17.06	18.25	19.28	18.46	17.96
1301-0		D2	31.76	31.04	29.53	28.51	28.82	29.93
1301-1	2	A2	4.69	4.88	4.88	6.35	6.72	5.50
1302-0		D2	22.14	21.71	21.38	17.54	15.72	19.70
1302-1	1	A2	11.33	10.77	10.66	12.68	13.24	11.74
1376-0	Bioturbated	Bio	77.36	78.22	79.51	80.53	80.40	79.20
1393-0		D2	7.41	7.86	7.16	7.48	7.07	7.39
1393-1	1	A2	4.07	3.09	2.39	2.21	2.48	2.85
1394-0		Bio	45.39	45.92	45.97	46.58	46.79	46.13
1392-0	Bioturbated	A2	8.04	7.50	6.03	5.49	5.23	6.46
1392-1		Bio	15.14	15.48	16.48	16.75	16.75	16.12

Table A2.02. Lamina thickness measurements (T1 – T5) and mean values for all laminae recorded in core MDO3-2601 section VIII.

Lamina number	Year in sequence	Lamina type	Lamina thickness (mm)					
			T1	T2	T3	T4	T5	Mean
326-0	Bioturbated	Bio	44.21	44.00	43.79	44.13	45.34	44.29
326-1		B1	1.42	1.09	1.53	1.20	0.76	1.20
356-0		Bio	33.60	34.47	34.17	33.59	33.54	33.87
356-1		B1	0.69	0.30	1.29	1.49	1.59	1.07
373-0		Bio	60.88	60.73	59.49	59.40	58.76	59.85
373-1		A2	0.50	0.70	0.70	0.90	1.20	0.80
373-2		D1	4.60	4.60	4.70	4.60	3.80	4.46
373-3	43	A2	2.60	2.90	3.20	3.50	3.40	3.12
373-4		D1	1.60	1.20	1.10	1.10	1.10	1.22
373-5	42	B1	7.10	7.20	7.20	7.30	7.40	7.24
373-6		D1	4.10	4.10	4.10	4.00	3.90	4.04
373-7	41	B1	1.70	1.50	1.50	1.30	0.90	1.38
373-8		D1	4.40	5.20	5.40	5.50	6.10	5.32
374-0	40	B1	6.56	6.26	5.94	5.41	5.80	5.99
374-1		D1	6.10	5.48	5.68	5.68	4.44	5.48
374-2	39	B1	1.76	1.65	1.65	1.14	1.76	1.59
374-3		D1	6.20	6.92	7.34	7.75	7.34	7.11
374-4	38	C2	2.48	2.38	2.17	1.96	1.45	2.09
385-0		D1	18.45	17.64	17.54	17.55	17.95	17.83
385-1	37	B1	3.73	4.01	4.01	3.92	3.64	3.86
385-2		D1	3.68	3.96	3.96	3.86	3.58	3.81
385-3		B1	5.27	5.55	5.55	5.46	5.18	5.40
385-4	36	A2	3.71	3.71	3.62	3.62	3.62	3.66
386-0		D1	7.06	7.08	6.46	5.69	6.06	6.47
386-1		B1	1.49	2.33	3.35	3.26	2.97	2.68
386-2	35	A2	0.57	0.69	0.91	1.60	0.91	0.94
386-3		E1	7.20	6.97	6.40	6.74	4.80	6.42
386-4		D1	4.68	4.91	5.03	4.80	4.80	4.84
386-5	34	A1	1.60	1.37	1.48	1.60	1.48	1.51
386-6		D1	9.14	8.79	7.88	7.42	6.85	8.02
386-7	33	A2	0.91	1.03	1.37	1.71	2.40	1.48
386-8		D1	10.74	11.42	12.11	12.22	12.33	11.76
341-0	32	A2	4.62	7.26	8.07	8.85	9.44	7.65
341-1		D1	8.31	8.45	8.45	8.60	8.60	8.48
341-2	31	B1	2.48	2.33	2.19	1.89	2.19	2.21
341-3		D1	1.75	2.48	2.91	3.35	3.64	2.83
341-4		B1	4.08	3.50	3.64	3.64	3.50	3.67
341-5	30	C1	5.97	6.56	7.58	7.87	7.72	7.14
341-6		D1	7.72	7.29	6.12	5.97	6.12	6.64
341-7		E1	5.10	4.81	4.37	3.93	3.64	4.37
342-1	29	B1	4.78	4.46	4.13	4.24	4.24	4.37

Lamina number	Year in sequence	Lamina type	Lamina thickness (mm)					
			T1	T2	T3	T4	T5	Mean
342-2		D1	4.24	4.35	4.78	4.89	4.35	4.52
342-3	28	C2	13.48	13.48	13.37	12.94	12.61	13.18
387-0		D1	15.99	17.33	18.92	19.83	19.83	18.38
387-1		B1	1.04	1.27	1.04	1.50	2.42	1.45
387-2	27	A2	3.45	3.45	3.57	3.22	2.42	3.22
387-3		D1	1.15	0.81	0.69	0.69	0.58	0.78
387-4	26	B1	8.52	9.10	9.33	9.44	9.79	9.24
387-5		D1	2.19	2.30	2.42	2.42	2.42	2.35
387-6	25	C2	1.84	1.84	1.84	1.96	1.84	1.87
387-7		D1	1.27	0.92	0.92	0.92	1.27	1.06
387-8	24	A2	2.19	1.96	1.84	1.84	1.61	1.89
387-9		D1	4.84	4.84	4.61	4.49	4.26	4.61
387-10	23	C2	1.61	1.61	1.61	1.50	1.73	1.61
387-11		D1	2.65	2.30	2.07	2.19	1.84	2.21
387-12	22	B1	1.27	1.38	1.61	1.04	2.30	1.52
388-0		D1	11.87	11.15	8.98	7.93	5.25	9.04
388-1		C2	2.84	2.52	0.74	0.74	0.53	1.47
388-2	21	A2	1.89	0.95	3.05	1.58	1.47	1.79
388-3		D1	5.57	7.04	6.93	7.77	8.61	7.18
388-4	20	A2	2.42	2.52	4.20	2.21	2.31	2.73
388-5		D1	7.98	6.62	6.09	7.98	8.19	7.37
388-6	19	B1	3.26	4.73	4.31	4.41	5.57	4.45
388-7		D1	4.52	4.83	5.99	6.20	4.62	5.23
307-1	18	A2	6.44	5.88	5.69	5.88	6.44	6.07
307-2		D1	11.18	10.99	11.37	11.75	10.90	11.24
308-0	17	C2	8.92	8.97	8.53	7.98	8.26	8.53
308-1		D1	7.63	7.85	7.74	7.96	8.50	7.94
308-2		B1	10.47	10.90	11.01	11.12	11.12	10.92
308-3	16	C2	6.43	5.67	6.00	6.00	5.67	5.95
308-4		D1	1.16	0.72	1.05	3.67	4.86	2.29
308-5	15	C1	0.24	-0.20	0.13	2.75	3.95	1.37
308-6		E1	2.94	3.82	3.16	1.31	0.65	2.38
308-7		D1	1.09	1.64	2.83	2.40	2.29	2.05
308-8	14	A2	0.76	2.07	1.20	0.76	0.98	1.16
379-0		D1	4.44	2.06	3.69	2.94	2.73	3.17
379-1	13	B1	1.50	1.29	1.40	2.16	1.52	1.57
379-2		D1	7.13	5.39	6.70	6.17	6.06	6.29
379-3		C2	2.36	2.58	3.22	3.76	4.08	3.20
379-4	12	B1	3.76	3.98	4.19	3.98	3.76	3.93
349-5		D1	5.05	4.41	3.87	4.30	3.87	4.30
379-6		E1	1.40	1.72	2.36	2.26	2.36	2.02
379-7		D1	4.84	5.05	5.16	5.37	6.23	5.33
379-8	11	B1	2.04	1.93	1.93	1.83	1.72	1.89

Lamina number	Year in sequence	Lamina type	Lamina thickness (mm)					
			T1	T2	T3	T4	T5	Mean
380-0		D1	8.75	8.75	9.07	8.32	8.75	8.73
380-1	10	B1	2.38	2.59	2.70	2.81	2.92	2.68
380-2		D1	5.08	4.75	4.32	3.89	3.35	4.28
380-3	9	B1	7.56	7.56	7.56	7.56	8.10	7.67
380-4		D1	3.57	3.35	3.35	3.24	2.59	3.22
380-5	8	B1	4.65	4.65	4.65	4.75	4.75	4.69
380-6		D1	5.08	5.19	4.97	5.08	4.54	4.97
311-0	7	B1	2.59	2.38	2.48	3.11	4.68	3.05
311-1		D1	2.42	3.05	3.68	2.94	1.47	2.71
311-2		E1	0.53	0.42	0.53	0.95	1.16	0.71
311-3		D1	11.03	10.72	11.45	12.08	12.19	11.49
311-4	6	B1	1.37	1.37	1.05	0.95	1.26	1.20
311-5		D1	15.65	15.55	15.55	15.23	14.92	15.38
312-0		C2	6.01	6.33	6.87	7.09	7.00	6.66
312-1		D1	3.09	3.94	3.73	2.66	1.38	2.96
312-2	5	A1	2.87	1.81	1.81	2.45	4.15	2.62
312-3		D1	9.26	9.15	8.94	8.73	8.09	8.83
312-4		B1	3.73	3.94	4.15	4.36	5.11	4.26
312-5	4	A2	2.77	2.77	2.66	2.13	1.49	2.36
393-0		D1	5.91	6.54	7.38	9.38	10.86	8.02
393-1	3	B1	9.99	10.10	8.84	7.47	6.63	8.60
393-2		D1	6.63	6.63	6.52	6.21	6.31	6.46
393-3	2	A2	0.74	0.84	0.95	0.95	1.05	0.90
393-4		D1	8.52	8.42	8.21	7.68	6.63	7.89
393-5	1	A2	3.05	2.95	2.95	2.95	3.47	3.07
394-0	Bioturbated	Bio	27.95	28.04	28.34	28.55	28.65	28.31
381-0		B1	15.32	16.50	17.04	18.31	19.15	17.26
381-1		D1	6.16	6.47	7.72	7.52	7.83	7.14
381-2	7	A2	11.38	11.27	10.86	10.86	10.96	11.07
382-0		D1	9.87	8.71	9.24	8.61	7.98	8.88
382-1	6	A2	6.85	6.32	6.32	6.74	7.69	6.79
382-2		D1	10.22	10.75	10.85	10.33	9.80	10.39
313-0	5	C2	16.77	15.72	14.38	14.44	14.48	15.16
313-1		D1	3.98	3.88	4.79	5.96	6.32	4.99
313-2		C2	6.78	6.69	6.23	5.51	5.24	6.09
313-3	4	A2	4.97	5.15	5.51	5.24	4.43	5.06
313-4		D1	7.77	7.77	7.59	7.41	7.50	7.61
313-5	3	A2	2.26	2.17	1.99	2.44	3.16	2.40
313-6		D1	2.08	2.44	2.71	2.35	2.71	2.46
314-0	2	C1	7.84	7.90	7.32	5.77	5.57	6.88
314-1		D1	10.04	10.26	10.69	10.69	11.02	10.54
314-2	1	C1	6.59	6.80	6.80	6.91	7.45	6.91
370-0	Bioturbated	Bio	54.58	54.51	55.27	54.99	54.12	54.69

Lamina number	Year in sequence	Lamina type	Lamina thickness (mm)					
			T1	T2	T3	T4	T5	Mean
370-1		D1	3.97	3.63	3.51	3.40	3.29	3.56
370-2	15	A1	1.36	1.36	1.70	2.04	2.04	1.70
370-3		D1	7.03	7.25	7.25	7.25	7.37	7.23
370-4	14	C1	2.95	2.61	2.27	2.27	2.04	2.43
370-5		D1	5.78	6.23	6.57	6.01	6.12	6.14
370-6		B1	9.29	9.07	9.18	9.52	9.63	9.34
370-7		A1	2.04	2.15	2.04	2.27	2.27	2.15
331-0	13	B1	3.86	3.97	4.08	4.49	4.69	4.22
331-1		D1	8.99	8.36	7.73	6.69	5.23	7.40
332-0	12	B1	24.26	23.55	23.55	24.06	24.37	23.96
332-1		D1	8.10	8.10	8.10	8.20	8.41	8.18
332-2		C1	2.97	3.18	2.87	2.77	2.56	2.87
332-3	11	A1	7.89	8.30	8.82	9.43	9.33	8.75
332-4		D1	6.25	6.56	6.77	6.36	5.84	6.36
371-0	10	A1	4.61	4.77	4.77	5.41	6.34	5.18
371-1		D1	16.87	16.65	16.19	14.84	14.04	15.72
371-2	9	A1	5.78	5.55	5.32	5.89	7.25	5.96
372-0		D1	14.84	14.84	15.52	16.34	14.32	15.17
372-1		C1	0.23	2.66	3.82	3.82	3.82	2.87
371-2	8	A1	3.13	3.36	3.47	3.36	3.36	3.33
371-3		D1	10.68	10.80	10.68	10.80	10.91	10.77
371-4	7	B1	3.35	3.46	3.35	3.46	3.58	3.44
371-5		E1	13.66	13.43	13.08	12.85	12.85	13.17
377-1		D1	11.63	11.72	11.72	10.87	10.21	11.23
377-2		A1	2.93	3.03	3.03	3.50	3.12	3.12
377-3		D1	1.23	1.13	1.42	1.70	1.80	1.46
377-4	6	C1	0.57	0.57	0.66	0.66	0.76	0.64
378-0		D1	17.99	18.45	16.22	16.55	16.84	17.21
378-1	5	A1	28.85	29.39	29.39	28.42	28.31	28.87
392-1		D1	24.62	24.51	24.05	22.90	22.32	23.68
391-0	4	A1	4.40	3.87	3.90	4.37	5.18	4.34
391-1		D1	3.00	2.90	2.90	2.80	2.90	2.90
391-2	3	B1	14.19	13.79	13.69	13.79	13.49	13.79
391-3		D1	8.70	9.40	9.79	9.79	9.79	9.50
391-4	2	A1	2.60	1.90	1.40	1.00	0.90	1.56
391-5		E1	1.30	1.30	1.50	1.40	1.30	1.36
391-6		D1	6.50	7.20	7.90	7.90	8.10	7.52
343-0	1	A1	2.84	2.52	2.94	4.87	6.31	3.89
343-1	Bioturbated	Bio	26.47	27.10	27.00	27.21	26.47	26.85
343-2		A1	2.31	2.63	2.84	3.57	3.36	2.94
359-0		Bio	36.77	40.72	40.38	39.83	38.79	39.30
359-1		A1	3.91	3.62	4.40	5.18	6.75	4.77
359-2		D1	7.04	6.06	4.89	4.40	4.50	5.38

Lamina number	Year in sequence	Lamina type	Lamina thickness (mm)					
			T1	T2	T3	T4	T5	Mean
359-3	3	A1	2.25	2.25	2.84	2.54	2.93	2.56
359-4		D1	14.87	15.06	15.45	15.84	15.75	15.39
360-0	2	A1	3.32	3.56	4.24	2.40	2.99	3.30
360-1		D1	8.93	9.02	9.64	8.49	8.22	8.86
360-2	1	A1	6.45	6.45	6.37	6.45	6.72	6.49
318-0	Bioturbated	Bio	58.86	60.79	62.30	64.45	66.22	62.52
318-1		D1	7.79	7.20	6.91	6.52	6.04	6.89
318-2		E1	0.58	0.68	0.78	0.58	0.58	0.64
383-0		D1	11.89	12.06	11.51	13.79	14.20	12.69
383-1	6	A1	11.87	11.75	11.64	11.17	10.81	11.45
383-2		D1	3.41	3.76	3.88	4.47	5.29	4.16
384-0		C1	14.45	14.04	14.61	14.71	14.51	14.46
384-1	5	A1	11.23	10.46	9.48	9.26	9.37	9.96
315-0		D1	22.27	23.17	23.55	23.36	22.83	23.03
315-1	4	C1	5.19	5.46	5.86	5.79	5.39	5.54
316-0		D1	10.19	11.74	11.67	11.65	11.43	11.34
316-1	3	B1	8.00	6.15	5.64	4.46	4.38	5.73
316-2		D1	10.45	9.94	10.19	11.20	11.29	10.61
316-3	2	B1	4.30	3.79	3.62	3.45	3.03	3.64
350-0		D1	7.55	6.86	6.50	6.49	6.74	6.83
350-1		B1	1.06	0.98	0.98	0.90	0.73	0.93
350-2	1	A1	2.04	1.71	1.31	0.73	0.41	1.24
350-3		D1	21.38	22.28	22.19	23.09	23.09	22.41

Table A2.03. Lamina thickness measurements (T1 – T5) and mean values for all laminae recorded in core MDO3-2601 section IX.

Lamina number	Year in sequence	Lamina type	Lamina thickness (mm)					
			T1	T2	T3	T4	T5	Mean
1345-1		D1	3.23	3.74	4.14	4.54	4.75	4.08
1345-2	6	A1	2.22	2.32	2.32	2.52	2.52	2.38
1345-3		D1	3.33	3.23	3.03	2.63	2.93	3.03
1345-4	5	A1	1.51	1.62	1.92	2.32	2.52	1.98
1345-5		D1	7.88	7.88	7.98	7.98	7.37	7.82
1345-6	4	A1	5.15	4.85	4.85	4.95	5.35	5.03
1345-7		D1	5.05	5.25	5.25	5.15	4.75	5.09
1345-8	3	A1	1.11	1.11	1.01	0.91	1.01	1.03
1345-9		D1	6.97	7.07	6.97	6.87	6.67	6.91
1346-0	2	A1	6.91	5.69	5.28	6.91	6.09	6.18
1346-1		D1	9.85	10.66	11.48	10.06	11.07	10.62
1346-2	1	A1	4.77	4.88	4.77	4.98	5.18	4.92
1385-0	Bioturbated	Bio	44.05	44.90	45.22	44.58	43.51	44.45
1385-1		D1	5.35	6.09	6.41	6.09	5.88	5.97
1385-2	4	A1	1.67	1.67	1.36	1.15	1.36	1.44
1386-1		D1	16.60	16.39	15.97	15.14	14.61	15.74
1386-2	3	A1	6.58	6.05	6.05	6.37	6.47	6.31
1386-3		D1	4.07	4.07	3.76	3.76	3.97	3.93
1386-4	2	A1	0.63	0.73	0.84	1.04	1.25	0.90
1379-0		D1	27.54	28.84	30.04	31.06	31.62	29.82
1379-1	1	A1	2.41	2.32	2.50	3.34	3.52	2.82
1325-0	Bioturbated	Bio	85.77	86.69	87.18	87.43	86.88	86.79
1325-1		A1	2.23	2.23	1.88	3.06	3.53	2.59
1325-2		D1	1.29	1.18	1.53	0.82	1.41	1.25
1325-3		E1	0.82	0.71	0.47	0.59	0.35	0.59
1325-4	8	A1	3.53	3.88	4.00	3.88	3.53	3.76
1325-5		D1	3.53	4.23	4.82	4.94	5.76	4.66
1326-0	7	A1	7.30	5.73	4.88	4.89	4.36	5.43
1326-0a		D1	3.54	3.64	3.64	3.75	3.32	3.58
1326-1	6	A1	3.14	3.14	3.14	3.14	3.14	3.14
1326-2		D1	2.15	1.83	2.47	3.01	3.23	2.54
1326-3	5	A1	2.90	3.01	2.37	3.12	2.80	2.84
1326-4		D1	3.77	3.98	3.98	3.12	2.69	3.51
1326-5	4	A1	2.58	2.15	1.72	1.72	1.83	2.00
1326-6		D1	3.98	5.06	5.92	6.35	8.07	5.87
1326-7	3	A1	4.30	4.41	6.02	5.16	5.16	5.01
1326-8		D1	7.21	6.67	6.02	4.52	4.30	5.75
1326-9	2	A1	3.12	2.58	2.47	1.61	1.51	2.26
1356-0		D1	7.63	8.30	8.40	9.37	9.75	8.69
1356-1		B1	8.11	7.92	7.82	8.30	9.17	8.26
1356-2		D1	0.87	1.26	1.45	1.35	1.16	1.22

Lamina number	Year in sequence	Lamina type	Lamina thickness (mm)					
			T1	T2	T3	T4	T5	Mean
1356-3	1	B1	4.92	5.21	5.31	5.41	5.60	5.29
1355-0	Bioturbated	Bio	39.14	39.03	39.03	38.37	37.59	38.63
1355-1		D1	7.12	6.56	5.89	5.45	5.00	6.01
1315-0	15	A1	3.87	3.87	4.19	4.29	3.65	3.97
1315-1		D1	5.37	5.15	4.94	4.19	4.40	4.81
1315-2		E1	3.01	3.11	3.11	2.90	2.15	2.86
1315-3	14	A1	2.58	2.58	2.36	2.25	1.93	2.34
1315-4		D1	8.80	8.80	9.13	9.66	9.88	9.26
1315-5	13	A1	1.61	1.50	1.50	1.93	2.47	1.80
1315-6		D1	6.55	6.33	6.23	6.12	5.26	6.10
1316-0	12	A1	10.42	10.71	10.90	11.28	11.76	11.01
1316-1		D1	3.92	3.82	3.82	3.82	3.54	3.79
1316-2	11	A1	2.39	2.20	2.20	2.10	1.82	2.14
1316-3		D1	2.10	2.10	1.82	2.20	2.39	2.12
1316-4	10	A1	0.76	0.76	0.67	0.29	0.29	0.55
1316-5		D1	7.74	7.46	7.55	7.84	7.65	7.65
1316-6	9	A1	1.24	2.01	2.01	1.72	1.53	1.70
1316-7		D1	2.20	2.01	2.29	2.68	2.96	2.43
1316-8	8	A1	0.57	0.48	0.48	0.67	0.76	0.59
1316-9		D1	2.96	2.58	2.39	2.01	1.53	2.29
1316-10	7	A1	0.96	1.63	1.53	1.05	1.15	1.26
1371-0		D1	7.11	8.99	8.89	9.27	9.92	8.84
1371-1	6	A1	1.31	1.50	1.50	1.40	1.03	1.35
1371-2		D1	1.12	1.03	0.84	0.84	1.03	0.97
1371-3		A1	1.97	2.53	2.90	2.90	2.81	2.62
1371-4		D1	0.75	0.75	0.56	0.66	0.66	0.67
1371-5	5	A1	0.84	0.66	0.75	0.84	0.66	0.75
1371-6		D1	5.43	4.96	4.40	4.21	4.59	4.72
1371-7	4	A1	4.68	4.87	5.62	5.71	5.15	5.20
1371-8		D1	5.99	5.80	5.52	5.52	6.18	5.80
1371-9		E1	1.31	1.31	1.31	1.31	1.31	1.31
1372-0		D1	11.30	10.80	10.21	6.44	6.05	8.96
1372-1	3	A1	6.05	6.74	7.14	7.63	7.83	7.08
1372-2		D1	2.18	2.38	2.58	2.87	2.97	2.60
1372-3	2	A1	1.09	1.09	1.09	1.19	1.19	1.13
1372-4		D1	6.64	6.24	5.95	5.95	5.95	6.15
1372-5	1	A1	0.79	1.49	1.98	1.78	1.19	1.45
1349-0	Bioturbated	Bio	62.93	62.43	62.50	63.04	63.67	62.91
1367-0		D1	13.68	13.99	13.99	14.29	15.22	14.23
1367-1	11	A1	2.88	3.08	2.88	2.57	2.98	2.88
1367-2		D1	7.10	6.99	7.30	7.51	7.30	7.24
1367-3	10	B1	8.33	8.33	8.33	8.43	8.74	8.43
1367-4		D1	5.55	5.66	5.55	5.55	4.83	5.43

Lamina number	Year in sequence	Lamina type	Lamina thickness (mm)					
			T1	T2	T3	T4	T5	Mean
1367-5	9	A1	4.11	3.91	4.42	5.14	5.24	4.57
1368-0		D1	2.92	2.83	2.83	2.50	2.50	2.72
1368-1	8	A1	0.33	0.33	0.33	0.42	0.50	0.38
1368-2		D1	6.09	5.75	5.34	4.92	4.50	5.32
1368-3	7	C1	3.92	4.09	4.42	4.84	5.00	4.45
1368-4		D1	6.00	6.00	6.00	5.92	5.75	5.94
1368-5	6	A1	0.58	0.50	0.67	0.42	0.50	0.53
1368-6		D1	3.17	3.25	3.25	3.59	3.67	3.39
1357-0	5	A1	15.85	15.63	15.63	15.51	15.74	15.67
1357-1		D1	10.42	9.74	9.17	8.72	8.49	9.31
1357-2	4	A1	4.42	4.64	5.21	5.66	6.23	5.23
1357-3		D1	8.04	8.72	8.49	8.15	7.70	8.22
1358-0	3	A1	4.14	3.50	3.29	3.72	5.41	4.01
1358-1		D1	18.58	18.15	17.84	17.41	15.50	17.50
1358-2	2	A1	6.26	6.26	6.48	6.69	6.90	6.52
1313-0		D1	16.88	17.53	16.88	16.77	16.99	17.01
1313-1	1	A1	8.06	7.84	7.08	6.32	5.88	7.03
1390-0		Bio	98.37	99.22	99.54	101.49	101.69	100.06
1389-0		C1	10.97	8.84	8.02	7.31	7.11	8.45
1377-0	Bioturbated	Bio	42.39	42.72	43.92	45.12	45.56	43.94
1377-1		A1	11.80	11.58	11.36	10.93	10.71	11.27
1378-0		Bio	46.76	46.43	45.12	45.23	45.01	45.71
1335-0		D1	18.26	18.46	19.15	19.25	19.15	18.85
1335-1	30	A1	2.58	2.58	2.48	2.28	2.48	2.48
1335-2		D1	10.32	11.21	11.31	11.51	11.61	11.19
1335-3	29	A1	1.49	1.79	1.89	1.59	0.99	1.55
1335-4		D1	7.58	7.47	7.35	7.13	7.24	7.35
1336-1	28	A1	9.84	9.95	10.29	10.52	10.97	10.32
1336-2		D1	3.28	2.94	2.26	2.38	2.94	2.76
1336-3	27	A1	0.90	1.24	1.24	1.36	0.90	1.13
1336-4		D1	5.66	5.66	5.54	4.64	3.85	5.07
1336-5		A1	2.26	2.15	2.83	3.17	3.05	2.69
1336-6		D1	1.47	1.81	1.36	1.24	1.81	1.54
1336-7	26	A1	0.68	1.02	0.68	0.90	0.68	0.79
1336-8		E1	0.68	0.45	0.90	0.90	0.90	0.77
1336-9		D1	0.90	1.02	1.13	1.13	1.36	1.11
1311-0	25	A1	8.06	8.56	8.31	8.43	8.18	8.31
1311-1		D1	0.74	0.62	1.49	2.11	2.36	1.46
1311-2	24	A1	2.60	2.73	2.11	1.86	1.98	2.26
1311-3		D1	2.23	2.23	2.23	2.48	2.85	2.41
1311-4	23	A1	3.10	3.10	2.73	2.60	2.85	2.88
1311-5		D1	3.60	4.71	5.33	4.96	4.46	4.61
1311-6	22	A1	4.22	2.85	2.36	2.48	2.48	2.88

Lamina number	Year in sequence	Lamina type	Lamina thickness (mm)					
			T1	T2	T3	T4	T5	Mean
1311-7		D1	15.50	15.13	15.00	15.25	15.25	15.23
1311-9	21	A1	0.99	0.87	0.99	0.99	0.87	0.94
1311-10		D1	0.74	0.74	0.87	0.99	0.87	0.84
1312-0	20	A1	12.36	13.66	14.46	14.76	14.46	13.94
1312-1		D1	2.99	3.19	3.29	3.49	3.49	3.29
1312-2	19	A1	3.69	3.39	2.99	2.79	2.99	3.17
1312-3		D1	1.99	2.19	2.59	2.69	2.29	2.35
1312-4	18	A1	2.69	2.69	2.59	2.39	3.09	2.69
1312-5		D1	2.89	2.89	2.89	2.99	2.09	2.75
1312-6	17	A1	0.70	0.70	0.70	1.00	0.40	0.70
1312-7		D1	12.66	12.55	12.09	11.63	12.32	12.25
1381-1	16	A1	5.47	5.59	5.59	5.59	5.47	5.54
1381-2		D1	10.72	10.26	10.26	10.38	10.38	10.40
1381-3	15	A1	2.40	2.40	2.51	2.62	2.62	2.51
1381-4		D1	9.69	9.47	9.24	8.90	8.55	9.17
1382-0	14	A1	5.18	5.07	4.86	4.97	5.39	5.09
1382-1		D1	5.39	5.49	5.49	5.60	5.49	5.49
1382-3	13	A1	4.02	4.12	4.12	3.80	3.38	3.89
1382-3		D1	3.06	2.96	2.54	2.75	3.06	2.87
1382-4	12	A1	2.01	2.11	2.22	2.22	1.90	2.09
1359-0		D1	18.22	18.05	18.57	18.91	19.08	18.57
1359-1	11	B1	6.27	6.45	6.53	6.62	6.62	6.50
1359-2		D1	5.59	6.10	6.36	6.45	6.45	6.19
1359-3		E1	1.12	1.20	1.12	1.29	1.80	1.31
1359-4		D1	6.19	6.62	6.27	5.50	4.90	5.90
1359-5	10	A1	3.60	3.50	3.89	4.67	5.16	4.16
1360-2		D1	12.45	12.26	12.06	11.77	11.38	11.98
1360-3	9	A1	3.89	3.79	3.99	3.70	3.40	3.75
1360-4		D1	5.93	5.84	5.45	6.03	6.61	5.97
1387-0	8	A1	4.94	6.29	5.81	4.84	4.26	5.23
1387-1		D1	13.26	13.75	14.23	14.81	16.07	14.43
1387-2	7	B1	3.58	3.87	4.07	4.07	3.29	3.78
1388-0		D1	14.45	17.55	17.04	16.86	16.78	16.54
1388-1	6	A1	2.93	3.01	3.10	3.10	3.27	3.08
1388-2		D1	7.40	7.92	8.17	8.26	8.17	7.98
1388-3	5	A1	3.87	3.61	3.53	3.61	3.70	3.67
1388-4		D1	11.03	11.36	11.69	12.13	12.13	11.67
1369-1	4	A1	5.57	5.57	5.35	5.35	5.35	5.44
1369-2		D1	10.93	10.60	10.82	10.71	10.60	10.73
1369-3	3	A1	1.53	1.20	1.20	1.20	1.64	1.35
1369-4		D1	1.53	2.73	3.28	3.71	3.82	3.02
1369-5	2	A1	2.40	2.19	1.97	2.08	2.08	2.14
1369-6		D1	5.46	5.90	6.45	6.56	6.34	6.14

Lamina number	Year in sequence	Lamina type	Lamina thickness (mm)					
			T1	T2	T3	T4	T5	Mean
1370-0	1	A1	6.20	6.11	5.29	5.02	5.29	5.58
1370-1	Bioturbated	Bio	29.27	29.00	29.27	29.64	29.82	29.40
1331-0	3	A1	3.28	3.28	3.28	3.47	3.93	3.45
1331-1		D1	6.93	6.65	6.37	6.18	5.43	6.31
1331-2	2	A1	4.78	4.31	4.21	4.12	4.50	4.38
1331-3		D1	8.62	8.90	8.99	8.90	8.99	8.88
1331-4		E1	0.94	1.22	1.31	1.40	1.22	1.22
1331-5		D1	2.53	2.53	2.24	2.04	1.85	2.24
1332-0	1	C1	10.50	10.31	9.92	9.34	10.21	10.06
1332-1	Bioturbated	Bio	22.76	22.95	23.73	24.60	23.53	23.51
1383-0		B1	8.74	7.37	7.37	8.22	7.90	7.92
1383-2		D1	26.44	27.60	27.39	26.97	26.44	26.97
1383-3	2	A1	1.58	1.58	1.69	3.37	3.16	2.28
1384-0		D1	7.55	7.64	7.55	7.21	7.47	7.48
1384-1	1	A1	9.87	8.67	8.24	7.98	7.55	8.46
1384-2	Bioturbated	Bio	19.23	19.31	19.31	19.31	19.48	19.33
1343-2	3	A1	4.53	5.13	5.13	5.30	5.21	5.06
1344-0		D1	14.55	14.46	14.12	14.55	15.24	14.58
1344-1	2	A1	14.72	15.06	15.58	16.10	16.79	15.65
1373-0		D1	19.42	19.14	19.14	19.21	19.28	19.24
1373-1	1	C1	5.77	5.63	5.42	5.35	5.35	5.50
1373-2	Bioturbated	Bio	10.77	10.77	10.91	10.77	10.70	10.78

Table A2.04. Lamina thickness measurements (T1 – T5) and mean values for all laminae recorded in core MDO3-2601 section XVII.

Lamina number	Year in sequence	Lamina type	Lamina thickness (mm) T1	T2	T3	T4	T5	Mean
319-0	Bioturbated	Bio	22.36	22.36	22.36	21.84	21.63	22.11
319-1		A1	1.45	0.93	0.72	0.72	0.72	0.91
319-2		D1	8.28	8.49	8.80	9.11	9.00	8.74
319-3	2	A1	1.66	1.76	1.76	1.76	1.66	1.72
320-0		D1	9.86	9.34	9.72	9.49	9.03	9.49
320-1	1	A1	3.05	3.17	2.56	2.93	3.66	3.08
365-0	Bioturbated	Bio	41.90	41.42	40.56	39.41	38.03	40.27
365-1		C1	0.84	0.84	0.84	0.95	1.05	0.90
365-2		D1	4.00	3.79	3.26	2.31	1.79	3.03
365-3	57	A1	10.20	10.41	10.73	11.36	11.78	10.89
365-4		E1	1.05	1.16	1.26	1.37	1.37	1.24
366-0		D1	19.07	19.18	18.99	18.98	19.20	19.08
366-1	56	A1	4.44	4.44	4.14	4.34	4.44	4.36
366-2		D1	18.68	18.28	19.39	19.19	18.99	18.90
321-0	55	A1	1.98	1.56	2.35	3.76	5.28	2.99
321-1		D1	6.27	6.06	5.54	5.01	8.15	6.21
321-2		C1	1.36	1.36	1.36	1.15	1.04	1.25
321-3		D1	1.57	1.78	1.88	1.88	2.09	1.84
321-4	54	A1	7.31	7.00	6.48	6.27	6.06	6.62
321-5		D2	7.02	7.23	7.75	7.96	8.38	7.67
321-6	53	A2	2.76	2.97	3.49	3.70	4.12	3.41
322-0		E1	12.98	13.29	13.40	13.41	12.59	13.14
322-1		D1	7.75	7.13	7.03	6.72	6.51	7.03
322-2	52	A1	7.75	7.75	8.47	9.51	10.23	8.74
395-0		D1	23.52	23.81	22.41	21.86	19.55	22.23
395-1	51	A1	3.14	3.14	3.47	3.59	3.92	3.45
395-2		D1	2.35	2.24	1.91	1.68	1.68	1.97
395-3	50	A1	1.35	1.35	1.68	1.91	2.13	1.68
395-4		D1	6.39	6.50	6.17	5.72	5.38	6.03
395-5	49	A1	2.13	2.24	2.35	2.47	2.47	2.33
395-6		D1	6.39	6.28	6.05	5.83	5.72	6.05
396-0	48	A1	7.69	7.70	7.95	7.60	7.53	7.69
396-1		D1	1.83	2.02	2.41	2.41	2.41	2.22
396-2	47	C1	1.64	1.35	1.16	1.45	1.64	1.45
396-3		D1	4.53	4.53	4.53	4.53	4.63	4.55
396-4		A1	5.40	5.40	5.40	5.30	5.11	5.32
396-5		C1	3.18	3.28	3.47	3.37	3.47	3.35
396-6	46	A1	1.93	1.35	1.54	1.73	1.83	1.68
396-7		D1	3.08	3.95	3.76	3.47	3.37	3.53
396-8	45	A1	4.72	5.20	5.69	5.88	6.75	5.65
396-9		D1	3.20	3.07	2.04	2.79	1.93	2.60

Lamina number	Year in sequence	Lamina type	Lamina thickness (mm) T1	T2	T3	T4	T5	Mean
396-10	44	A1	5.05	4.09	3.98	3.52	2.42	3.81
636-0		D1	8.96	8.96	8.96	8.42	7.88	8.64
363-1	43	A1	4.54	4.00	2.92	3.02	3.56	3.61
363-2		D1	10.58	11.23	12.31	12.85	13.07	12.01
363-3	42	A1	0.86	0.76	0.76	1.19	0.97	0.91
364-0		D1	8.17	8.27	8.61	8.05	7.93	8.21
364-1	41	A1	5.77	5.47	5.28	5.08	4.89	5.30
364-2		D1	2.93	3.13	3.13	3.03	2.35	2.91
364-3	40	A1	1.37	0.98	0.88	1.08	2.64	1.39
364-4		D1	2.15	2.74	3.23	3.23	2.64	2.80
364-5	39	A1	2.74	2.25	1.86	1.17	0.98	1.80
364-6		C1	5.77	5.57	5.47	5.38	4.99	5.44
364-7		D1	0.98	1.17	1.17	1.17	1.17	1.13
303-0	38	A1	12.16	11.77	12.16	12.74	13.02	12.37
303-1		D1	10.62	10.41	10.41	10.73	11.27	10.69
303-2	37	A1	1.52	1.63	1.73	1.63	1.84	1.67
303-3		D1	6.72	6.72	6.72	6.18	5.74	6.42
303-4	36	A1	2.82	3.79	4.55	5.09	5.20	4.29
303-x		D1	14.48	13.85	13.76	14.09	14.02	14.04
304-0	35	A1	3.42	2.79	2.70	3.03	2.95	2.98
304-1		D1	8.82	8.92	8.72	8.41	8.41	8.65
304-2	34	A1	4.51	2.67	1.95	1.64	2.05	2.56
351-0		D1	7.10	7.32	7.29	6.98	6.56	7.05
351-1	33	A1	5.35	5.68	5.85	6.10	6.18	5.83
351-2		D1	1.59	1.50	1.75	1.59	1.59	1.60
351-3		C1	8.52	8.35	7.77	7.77	8.10	8.10
351-4	32	B1	3.67	3.67	3.67	3.76	3.67	3.69
351-5		D1	0.67	0.67	0.67	0.84	0.67	0.70
351-6	31	C1	2.67	2.42	2.09	1.67	1.42	2.05
351-7		D1	2.26	2.76	2.92	2.92	2.42	2.66
352-1		C1	6.89	7.08	7.14	7.56	7.72	7.28
352-2	30	A1	2.12	2.12	2.12	2.12	2.01	2.10
352-3		D1	2.12	2.12	2.01	2.01	2.01	2.06
352-4	29	A1	2.24	2.24	2.24	2.12	2.12	2.19
352-5		D1	3.58	3.46	3.69	3.91	4.02	3.73
352-6	28	A1	5.70	5.81	5.92	5.70	5.36	5.70
352-7		D1	5.81	5.48	5.25	5.14	5.14	5.36
352-8	27	A1	2.24	3.13	4.47	5.03	5.25	4.02
329-0		D1	10.31	10.09	9.33	8.75	8.90	9.48
329-1	26	A1	5.23	4.92	4.61	4.20	4.00	4.59
329-2		D1	2.97	3.38	3.69	4.10	4.20	3.67
329-3	25	A1	2.97	2.25	2.05	2.05	2.25	2.32
329-4		D1	3.28	3.89	4.10	4.10	4.00	3.87

Lamina number	Year in sequence	Lamina type	Lamina thickness (mm) T1	T2	T3	T4	T5	Mean
330-0	24	A1	8.85	7.45	7.45	7.11	6.99	7.57
330-1		D1	3.96	4.51	4.73	5.50	5.83	4.91
330-2	23	A1	0.33	0.55	0.55	0.66	0.66	0.55
330-3		D1	3.63	2.86	2.31	2.42	3.19	2.88
330-4	22	A1	1.98	2.53	2.86	2.53	1.32	2.24
330-5		D1	3.63	3.85	3.96	3.74	4.07	3.85
330-6	21	A1	1.21	0.88	0.66	1.10	1.54	1.08
330-7		D1	3.85	3.63	3.63	3.63	3.96	3.74
330-8	20	A1	1.76	1.43	1.10	0.99	0.88	1.23
330-9		D1	0.99	1.10	1.43	1.76	1.43	1.34
330-10	19	A1	3.52	3.63	3.19	2.31	1.65	2.86
330-11		D1	4.95	4.62	4.95	4.95	4.62	4.82
330-12	18	A1	2.09	2.31	2.09	2.20	2.53	2.24
330-13		D1	2.20	2.86	3.74	4.29	4.62	3.54
337-0	17	A1	3.06	2.11	1.48	0.85	0.00	1.50
337-1		D1	5.15	5.78	6.31	6.20	4.94	5.68
337-2	16	A1	2.84	2.10	1.47	1.68	2.63	2.15
337-3		D1	1.68	1.68	1.79	2.00	1.89	1.81
337-4	15	A1	1.47	1.79	1.89	1.79	1.68	1.72
337-5		C1	3.16	2.73	2.42	2.10	2.21	2.52
337-6		D1	1.79	2.21	0.21	2.21	2.21	1.72
337-7	14	A1	1.68	1.37	1.16	1.16	1.79	1.43
337-8		D1	1.16	1.16	1.37	1.58	0.84	1.22
337-9	13	A1	0.63	0.53	0.42	0.32	0.32	0.44
337-10		D1	2.42	2.52	2.73	2.94	3.16	2.76
338-0	12	A1	16.12	17.59	18.22	19.59	20.01	18.31
338-1		D1	1.59	1.59	1.69	1.37	1.37	1.52
338-3	11	A1	5.28	5.28	5.49	6.02	6.02	5.62
338-4		D1	4.23	4.54	4.54	4.02	3.59	4.18
338-5	10	A1	11.31	11.10	11.10	11.20	11.94	11.33
338-6		D1	2.85	4.23	4.54	4.54	4.33	4.10
354-0	9	A1	7.09	6.25	5.83	5.72	5.83	6.14
354-1		D1	6.98	6.66	6.55	6.44	6.55	6.64
354-2	8	A1	3.44	3.87	4.19	4.08	4.08	3.93
354-3		D1	7.95	8.16	8.05	8.27	8.37	8.16
353-0	7	A1	18.13	18.73	18.91	18.22	17.50	18.30
353-1		D1	4.54	5.36	5.83	5.94	5.94	5.52
353-2	6	A1	8.16	8.51	8.39	7.81	7.81	8.13
353-3		D1	13.40	13.40	13.63	14.45	14.92	13.96
347-0	5	A1	6.09	6.65	6.74	7.31	6.94	6.75
347-1		D1	5.79	5.43	4.34	3.98	3.62	4.63
347-2	4	A1	1.81	1.93	1.81	1.33	0.84	1.54
347-4		D1	10.73	11.09	12.30	13.26	13.75	12.23

Lamina number	Year in sequence	Lamina type	Lamina thickness (mm)					
			T1	T2	T3	T4	T5	Mean
347-5		C1	3.01	3.38	3.38	3.62	3.62	3.40
347-6	3	A1	8.20	7.48	6.51	5.31	4.58	6.41
348-0		D1	11.41	12.33	13.46	14.18	14.64	13.21
348-1	2	C1	8.33	8.43	8.54	8.54	8.64	8.49
348-2		D1	6.96	6.74	6.53	6.43	6.11	6.55
348-3	1	C1	2.00	1.90	2.00	1.58	1.79	1.85
309-0	Bioturbated	Bio	95.23	96.03	96.05	96.66	97.05	96.20
309-1		A1	3.06	2.95	2.74	2.63	2.53	2.78
309-2		D1	3.16	3.16	2.74	2.63	2.63	2.87
310-0	50	A1	8.12	8.14	8.39	7.91	7.34	7.98
310-1		D1	3.17	2.97	2.68	2.68	2.48	2.80
310-2	49	A1	3.07	2.97	2.68	2.58	2.68	2.80
310-3		D1	1.98	2.18	2.58	2.58	2.28	2.32
310-4		E1	0.59	0.50	0.30	0.30	0.40	0.42
310-5		D1	8.42	8.92	9.02	8.72	8.42	8.70
310-6	48	A1	1.19	1.19	1.49	2.18	2.38	1.68
310-7		E1	4.36	4.26	3.96	3.96	4.16	4.14
310-8		D1	3.96	3.27	2.48	1.59	1.09	2.48
310-9	47	C1	0.99	1.19	0.99	0.50	0.69	0.87
310-10		D1	7.43	8.52	9.52	10.80	11.30	9.52
335-0	46	A1	1.50	0.90	1.31	2.33	2.72	1.75
335-1		D1	7.02	7.63	6.61	4.78	4.27	6.06
335-2	45	A1	4.37	3.76	4.37	5.19	5.39	4.62
335-3		E1	4.98	5.09	4.78	4.37	4.07	4.66
335-4		D1	1.02	0.92	1.02	1.22	1.02	1.04
335-5	44	A1	3.25	3.46	3.66	3.25	3.25	3.38
335-6		E1	2.64	2.34	2.14	2.95	3.05	2.62
336-0		D1	10.45	10.34	10.24	9.69	7.97	9.74
336-1	43	A1	6.33	5.75	5.64	5.75	6.10	5.91
336-2		D1	4.60	4.49	4.14	3.80	3.34	4.07
336-3	42	A1	4.49	4.72	4.49	4.37	4.95	4.60
363-4		D1	3.95	5.10	4.76	3.95	3.26	4.21
363-5	41	C1	3.27	4.42	4.08	3.27	2.58	3.53
357-0		D1	15.86	14.78	14.85	16.09	16.62	15.64
357-1		A1	1.07	1.43	1.07	0.48	0.95	1.00
357-2	40	C1	3.94	3.46	3.10	3.46	4.06	3.60
357-3		D1	0.84	1.91	2.27	1.31	0.48	1.36
357-4	39	A1	1.79	2.51	3.10	4.65	4.77	3.36
357-5		D1	2.62	2.62	2.39	1.31	1.31	2.05
357-6	38	A1	1.19	1.31	0.95	1.79	1.79	1.41
357-7		D1	5.97	5.73	6.20	6.68	6.68	6.25
357-8	37	A1	2.03	2.27	2.15	2.27	2.51	2.24
357-9		D1	6.44	6.56	6.68	6.20	5.49	6.28

Lamina number	Year in sequence	Lamina type	Lamina thickness (mm) T1	T2	T3	T4	T5	Mean
357-10	36	C1	0.84	1.07	1.19	1.19	1.67	1.19
358-0		D1	8.52	8.27	8.01	8.46	8.94	8.44
358-2	35	A1	4.58	4.88	4.98	4.88	4.48	4.76
358-3		D1	14.44	15.05	15.16	15.46	15.36	15.09
358-4	34	A1	0.51	0.51	0.41	0.51	0.81	0.55
361-0		D1	11.57	12.47	12.88	12.68	12.68	12.46
361-1		E1	1.69	1.69	1.79	1.58	1.26	1.60
361-2		D1	2.53	2.63	2.11	2.00	2.11	2.28
361-3	33	A1	1.37	1.58	1.69	1.58	1.37	1.52
361-4		D1	7.59	6.74	6.53	6.43	5.90	6.64
361-5	32	A1	1.16	1.26	0.95	0.74	0.84	0.99
361-6		D1	3.48	3.69	4.22	4.64	4.85	4.17
361-7	31	A1	3.27	3.37	3.27	3.16	3.16	3.25
361-8		D1	5.27	5.48	5.69	5.90	6.32	5.73
361-9	30	A1	1.26	1.26	1.26	1.48	1.58	1.37
361-10		D1	1.05	1.16	1.16	1.05	0.95	1.07
362-0	29	A1	2.57	2.64	1.54	0.55	0.33	1.53
362-1		D1	2.91	3.01	3.86	4.70	4.59	3.81
362-2	28	A1	2.75	2.64	2.64	2.41	2.41	2.57
362-3		D1	1.91	2.35	2.69	3.14	3.36	2.69
362-4	27	A1	2.35	1.46	1.57	1.68	1.35	1.68
362-5		D1	5.16	5.60	5.04	4.71	5.04	5.11
362-6	26	A1	3.40	2.95	2.73	2.84	2.95	2.97
362-7		D1	1.23	1.46	1.57	1.57	2.02	1.57
362-8	25	A1	2.69	2.69	2.35	2.13	1.68	2.31
362-9		C1	2.02	1.68	1.68	2.02	1.91	1.86
362-10		D1	2.13	2.24	2.13	2.02	1.91	2.08
362-11	24	A1	1.91	1.68	1.79	1.35	1.68	1.68
362-12		D1	1.79	2.24	2.47	2.69	2.24	2.29
362-13	23	A1	1.23	1.01	0.90	1.12	1.23	1.10
362-14		D1	3.14	3.25	3.14	3.14	3.03	3.14
339-0	22	A1	4.59	3.71	3.39	2.67	2.22	3.32
339-1		D1	0.45	1.08	1.37	1.37	1.78	1.21
339-2	21	A1	0.63	0.63	0.74	1.30	2.16	1.09
339-3		D1	1.90	2.08	2.35	2.08	1.72	2.02
339-4	20	A1	0.81	0.72	0.81	0.81	0.81	0.80
339-5		D1	2.26	2.62	2.71	2.71	2.71	2.60
339-6	19	A1	3.88	3.52	2.80	2.53	2.89	3.13
339-7		D1	5.78	5.96	6.59	7.14	6.78	6.45
340-0	18	A1	3.78	3.77	3.66	3.17	3.23	3.52
340-1		D1	1.56	1.35	1.25	1.15	0.83	1.23
340-2		E1	0.83	0.94	0.94	0.94	0.94	0.92
340-3		D1	1.35	1.15	1.04	1.56	1.88	1.40

Lamina number	Year in sequence	Lamina type	Lamina thickness (mm) T1	T2	T3	T4	T5	Mean
340-4	17	A1	6.98	6.98	6.56	6.36	6.56	6.69
340-5		D1	3.23	3.33	3.33	3.44	4.69	3.61
340-6	16	A1	1.56	1.67	1.98	1.98	1.88	1.81
340-7		D1	2.40	2.29	2.08	1.77	1.56	2.02
340-9	15	A1	2.81	2.81	2.81	2.81	3.33	2.92
340-10		D1	4.58	5.00	5.73	6.15	6.25	5.54
340-11		E1	2.29	2.19	1.88	1.88	1.98	2.04
340-12		D1	5.31	5.94	6.25	6.36	5.83	5.94
305-0	14	A1	4.35	3.30	3.12	2.29	2.60	3.13
305-1		D1	1.54	1.42	2.01	2.79	2.80	2.11
305-2	13	C1	9.48	9.00	8.05	7.34	7.58	8.29
305-3		D1	9.83	10.30	10.90	11.84	10.78	10.73
305-4	12	A1	6.16	4.62	3.79	3.43	3.79	4.36
305-5		D1	5.09	6.04	6.51	6.16	4.86	5.73
305-6	11	A1	0.83	0.95	1.07	1.18	1.42	1.09
306-0		D1	8.75	10.20	11.67	12.76	13.44	11.36
306-1	10	A1	5.76	4.51	4.03	3.55	3.75	4.32
301-0		D1	17.20	18.47	18.96	18.47	18.92	18.40
301-1	9	A1	1.64	0.62	0.62	0.72	0.62	0.84
301-2		D1	9.54	10.05	9.54	9.33	9.84	9.66
301-3	8	A1	6.05	5.84	5.95	6.05	6.05	5.99
301-4		D1	11.59	10.87	10.66	10.36	10.46	10.79
302-0	7	A1	2.69	4.63	5.85	6.87	7.69	5.55
302-1		D1	6.22	5.68	5.03	4.28	3.42	4.93
302-2	6	A1	2.94	2.40	1.76	1.01	0.15	1.65
302-3		E1	0.64	0.75	0.75	0.54	0.54	0.64
302-4		D1	2.36	2.04	1.72	1.72	1.83	1.93
302-5	5	B1	4.19	4.19	4.30	4.40	4.30	4.27
302-6		D1	7.19	7.52	7.62	7.41	7.30	7.41
302-7	4	A1	0.75	0.86	0.75	0.54	1.07	0.79
302-8		D1	1.50	1.18	0.97	0.64	1.07	1.07
302-9	3	A1	3.97	4.08	4.19	4.40	5.05	4.34
302-10		E1	1.18	1.07	1.18	1.40	0.86	1.14
302-11		D1	0.97	2.79	2.15	1.72	1.93	1.91
333-1	2	A1	10.23	11.12	11.08	11.24	11.15	10.96
333-2		E1	1.29	0.99	0.99	0.99	1.09	1.07
333-3		D1	3.96	3.86	3.57	2.97	2.28	3.33
333-4	1	A1	4.26	3.96	3.76	3.57	3.17	3.74
334-0	Bioturbated	Bio	41.85	42.34	39.77	40.56	42.05	41.31
334-1		C1	2.44	2.55	2.34	2.14	2.65	2.42
345-0		D1	13.88	15.19	16.80	16.46	15.09	15.48
345-1	8	C1	6.79	6.58	6.58	6.58	6.68	6.64
345-2		E1	4.14	3.61	3.18	2.76	3.08	3.35

Lamina number	Year in sequence	Lamina type	Lamina thickness (mm)					
			T1	T2	T3	T4	T5	Mean
345-3		D1	9.12	9.86	10.50	11.14	11.35	10.39
345-4	7	A1	4.67	4.18	3.37	2.86	3.18	3.65
346-1		D1	2.81	3.17	2.92	3.39	3.29	3.12
346-2	6	A1	0.90	0.90	2.10	3.19	3.02	2.02
346-3		D1	3.26	3.47	3.68	3.75	3.75	3.58
346-4	5	A1	1.18	1.87	1.94	1.81	1.94	1.75
375-0		D1	13.89	13.33	13.51	14.28	13.95	13.79
375-1	4	A1	5.40	5.31	5.31	5.40	6.24	5.53
375-2		D1	7.93	7.84	7.67	7.42	6.41	7.45
375-3	3	A1	2.45	2.36	2.19	1.86	1.77	2.12
375-4		D1	6.66	6.75	7.17	7.50	7.76	7.17
375-5	2	A1	0.93	0.84	0.84	0.67	0.59	0.78
376-0		D1	0.83	0.93	1.69	2.36	3.20	1.80
376-1	1	C1	1.81	1.56	0.25	0.00	0.00	0.72
376-3	Bioturbated	Bio	20.45	20.78	21.11	21.03	20.20	20.71
323-0		D1	9.40	8.16	6.78	5.63	3.52	6.70
323-1	1	A1	9.07	8.88	8.79	8.98	9.45	9.03
323-2	Bioturbated	Bio	20.05	20.34	20.72	21.58	21.39	20.82

Table A2.05. Lamina thickness measurements (T1 – T5) and mean values for all laminae recorded in sediments from core IODP-318-U1357B sections -4H, -5H and -6H.

Lamina number	Year in sequence	Lamina type	Lamina thickness (mm)					
			T1	T2	T3	T4	T5	Mean
77-1		A3	1.93	2.04	2.14	1.93	1.82	1.97
77-2	Year end	D3	17.46	17.25	17.36	17.57	17.79	17.49
77-3		C3	5.25	5.57	5.57	5.68	5.79	5.57
77-4		B3	3.32	3.11	2.79	2.57	2.14	2.79
77-5	73	A3	4.07	4.07	4.39	4.18	4.29	4.20
77-6		E3	1.71	1.61	1.50	1.61	1.50	1.59
78-0		D3	9.97	10.02	10.55	10.69	11.19	10.48
78-1	72	C3	3.69	3.69	3.60	3.60	3.69	3.65
78-2		D3	10.15	10.52	10.61	10.52	10.33	10.43
78-3		C3	1.75	1.85	1.85	2.03	1.85	1.86
78-4		D3	1.75	1.75	1.66	1.38	1.66	1.64
78-6		C3	7.01	7.10	7.38	7.38	7.47	7.27
133-0	71	A3	9.83	9.64	9.29	8.16	7.25	8.83
133-1		D3	1.84	2.01	2.26	2.51	2.76	2.28
133-2		C3	3.01	2.85	2.93	2.85	2.76	2.88
133-3		A3	2.01	1.76	1.51	1.42	2.09	1.76
133-4		C3	6.86	6.95	7.20	7.20	7.03	7.05
134-0	70	A3	12.06	12.33	12.63	13.26	13.43	12.74
134-1		E3	2.72	2.81	2.72	2.16	2.06	2.49
134-2		D3	19.22	18.75	18.56	17.91	18.19	18.53
134-3	69	A3	0.84	0.84	0.66	0.75	1.03	0.83
69-1		D3	4.50	4.82	5.57	5.36	4.93	5.04
69-2		C3	7.39	7.50	6.96	7.07	7.39	7.26
69-3		A3	3.11	2.89	2.57	2.36	2.36	2.66
69-4		C3	3.00	2.68	2.57	2.68	3.00	2.79
69-5	68	A3	12.43	12.54	12.32	11.57	11.04	11.98
70-0		E3	9.11	9.78	10.45	11.71	11.92	10.59
70-1		D3	14.90	16.06	16.55	16.65	16.65	16.16
70-2		C3	3.39	3.19	3.10	3.19	3.29	3.23
70-3		B3	5.90	6.10	6.19	6.29	6.29	6.15
70-4	67	A3	1.74	1.55	1.55	1.55	1.55	1.59
70-5		D3	2.42	2.52	2.42	2.32	2.23	2.38
73-1	66	A3	18.49	17.83	17.83	18.19	18.20	18.11
73-2		C3	1.19	1.37	1.46	1.65	1.65	1.46
73-3		D3	2.19	2.01	1.83	1.74	1.65	1.88
73-4		A3	1.10	0.91	0.82	0.64	0.91	0.88
73-5		D3	7.22	7.31	7.68	7.86	7.77	7.57
73-6	65	A3	3.47	3.38	3.20	3.02	2.93	3.20
74-0		D3	5.85	6.87	6.81	6.87	6.45	6.57
74-1		E3	2.61	3.12	3.02	2.51	2.31	2.72
74-2		D3	10.76	10.26	10.66	10.96	10.96	10.72

Lamina number	Year in sequence	Lamina type	Lamina thickness (mm) T1	T2	T3	T4	T5	Mean
74-3		C3	4.32	4.53	4.43	4.73	5.33	4.67
74-4	64	A3	6.64	7.14	7.24	7.74	7.84	7.32
45-1		E3	21.09	21.73	21.73	20.91	17.82	20.65
46-0		D3	13.56	13.39	11.91	11.69	13.66	12.84
67-0	63	A3	35.78	37.38	39.75	41.31	42.34	39.31
67-1		D3	19.73	19.53	18.91	18.09	17.58	18.77
68-0		A3	14.55	14.23	13.82	13.72	12.89	13.84
68-1		D3	4.28	5.54	5.74	5.25	4.76	5.11
68-2		A3	2.53	2.33	2.53	2.33	2.24	2.39
68-3		D3	2.04	2.04	2.14	2.92	3.79	2.59
68-4		A3	5.54	4.86	4.38	4.28	4.86	4.78
68-5		D3	3.21	3.50	4.28	4.38	3.60	3.79
41-0		A3	14.95	16.12	15.65	14.58	15.85	15.43
41-1		C3	9.58	9.85	9.76	9.85	9.58	9.72
41-2	62	A3	5.23	5.15	4.88	4.88	5.23	5.07
41-3		E3	2.31	2.75	3.10	3.19	2.84	2.84
42-0		D3	7.05	6.02	6.18	5.59	5.62	6.09
42-1		B3	0.66	0.66	0.66	0.66	0.99	0.73
42-2		D3	2.98	2.90	2.73	2.90	2.56	2.81
42-3		C3	19.69	20.35	20.76	20.85	21.01	20.53
43-0		A3	4.63	5.33	5.82	6.04	5.94	5.55
43-2		C3	5.81	5.91	5.91	6.11	5.71	5.89
43-5	61	A3	11.01	11.11	11.01	11.21	11.21	11.11
43-6		E3	5.61	5.50	5.61	5.71	5.91	5.67
44-0		D3	15.36	15.15	14.95	14.93	14.91	15.06
44-1		C3	3.91	4.00	4.00	4.10	4.19	4.04
44-2	60	A3	1.14	1.24	1.43	1.81	1.91	1.51
44-3		D3	2.38	2.29	2.10	1.72	1.52	2.00
44-4		A3	4.38	4.38	4.38	4.57	4.67	4.48
44-5		D3	3.81	3.72	3.72	3.62	3.33	3.64
44-7	59	A3	5.43	5.43	5.72	6.10	6.48	5.83
375-0		D3	15.46	16.21	16.39	16.20	15.27	15.91
375-1		A3	1.86	1.86	1.33	1.15	1.24	1.49
375-2		C3	0.80	0.97	1.24	1.06	1.15	1.04
375-3		A3	3.62	3.89	3.98	3.98	3.71	3.84
375-4		D3	0.80	0.80	0.71	0.80	0.62	0.74
375-5		A3	3.18	3.54	3.27	3.54	3.89	3.48
375-6		D3	0.35	0.53	0.80	0.71	0.62	0.60
375-7	58	A3	1.50	1.77	1.68	2.30	2.65	1.98
6-0		D3	51.97	51.33	50.34	50.23	50.02	50.78
23-1		C3	18.35	18.63	18.55	18.59	18.99	18.62
23-2		D3	2.48	2.55	2.55	2.18	1.95	2.34
23-3		C3	2.10	2.18	2.25	2.25	2.10	2.18

Lamina number	Year in sequence	Lamina type	Lamina thickness (mm)					
			T1	T2	T3	T4	T5	Mean
23-4	57	A3	0.67	0.90	0.75	0.75	0.75	0.76
23-5		E3	3.68	3.15	3.08	3.38	3.83	3.42
23-6		D3	4.88	4.88	4.95	4.88	4.65	4.85
24-0		C3	8.58	8.50	8.19	7.89	7.74	8.18
24-1		B3	0.89	0.82	0.97	1.26	1.64	1.12
332-0		C3	18.33	18.09	17.94	18.03	18.58	18.19
332-1		A3	2.55	2.39	2.23	2.31	2.39	2.37
332-2		E3	0.88	0.95	1.03	1.03	0.88	0.95
332-3		C3	1.11	0.95	1.03	1.11	1.11	1.07
332-4	56	A3	1.83	2.94	3.10	2.71	2.39	2.59
332-5		E3	5.25	5.17	5.17	4.93	6.45	5.40
331-0		D3	5.97	4.94	4.72	4.90	8.83	5.87
331-1		C3	4.21	5.04	5.12	5.12	4.79	4.85
331-2		A3	0.66	0.50	0.41	0.50	0.74	0.56
331-3		D3	0.50	0.50	0.50	0.58	0.58	0.53
331-4		C3	3.22	2.97	2.81	2.48	2.31	2.76
331-5	55	A3	0.74	0.74	0.83	0.99	1.07	0.87
331-6		D3	6.03	6.44	6.85	6.85	6.85	6.60
331-7		C3	1.16	1.24	1.16	1.40	1.73	1.34
331-8		D3	1.16	1.16	0.99	0.91	0.91	1.02
331-9	54	A3	1.24	1.16	1.16	1.07	1.16	1.16
336-0		E3	9.99	8.34	8.10	8.07	7.87	8.47
336-1		D3	14.91	15.79	17.28	17.01	16.58	16.31
336-3		C3	11.49	10.79	10.44	10.35	10.35	10.68
335-0	53	A3	3.16	3.26	3.26	3.71	3.72	3.42
335-1		D3	3.82	3.55	3.27	3.09	3.00	3.35
335-2		A3	3.18	3.18	3.27	3.36	3.55	3.31
335-3		D3	10.09	9.91	9.45	9.82	10.27	9.91
374-1		C3	13.32	14.37	15.45	15.98	16.91	15.21
374-2	52	A3	1.58	1.27	1.08	1.20	1.46	1.32
374-3		D3	3.36	3.48	3.55	3.42	3.10	3.38
374-4		B3	0.76	0.76	0.70	0.63	0.63	0.70
374-5		D3	7.79	7.85	7.92	7.60	7.35	7.70
326-1	51	A3	1.14	1.45	1.24	0.93	1.24	1.20
326-2		D3	9.21	9.31	10.03	11.17	12.00	10.34
326-3		C3	1.34	1.34	1.24	1.24	1.03	1.24
326-4		D3	3.83	4.03	4.14	4.34	4.45	4.16
326-5		B3	1.76	1.66	1.55	1.55	1.45	1.59
326-6		C3	3.41	3.62	3.83	3.83	4.14	3.77
325-0	50	A3	16.88	15.52	14.69	13.86	11.51	14.49
325-2		D3	4.59	4.18	4.01	3.93	3.60	4.06
325-3		A3	0.49	0.82	0.82	0.66	0.98	0.75
325-4		D3	6.31	5.81	5.08	4.67	4.42	5.26

Lamina number	Year in sequence	Lamina type	Lamina thickness (mm)					
			T1	T2	T3	T4	T5	Mean
325-5		C3	1.80	1.64	1.97	2.29	1.72	1.88
325-6		D3	0.90	0.90	0.90	1.06	0.82	0.92
325-7		C3	3.19	3.85	3.85	3.68	4.09	3.73
325-8		A3	0.90	0.74	0.74	0.66	0.74	0.75
325-9		D3	0.49	0.49	0.41	0.49	0.66	0.51
325-10		C3	3.03	3.11	3.52	3.85	4.01	3.50
328-0	49	A3	10.97	11.13	11.20	12.48	12.63	11.68
328-1		E3	4.53	4.44	4.09	4.18	4.53	4.36
328-2		D3	6.97	7.75	7.84	7.84	7.58	7.60
328-3		C3	1.66	0.87	0.87	1.39	1.74	1.31
328-4		A3	3.05	3.05	3.05	2.53	2.35	2.81
327-0		C3	13.21	13.41	14.01	14.88	15.77	14.25
327-1	48	A3	1.16	1.26	1.45	1.55	1.65	1.41
327-2		D3	3.97	3.68	3.29	2.90	2.52	3.27
327-3		C3	6.68	7.26	8.03	8.81	9.48	8.05
327-4		A3	3.10	2.71	2.52	2.32	2.52	2.63
327-5		C3	0.97	1.45	1.74	1.94	1.74	1.57
327-6		D3	7.16	6.58	5.71	5.52	5.13	6.02
314-1		A3	0.93	0.65	0.56	1.02	1.86	1.01
314-2		D3	3.63	3.72	3.72	3.63	3.44	3.63
314-3		C3	10.42	10.61	10.42	9.86	9.21	10.11
314-4	47	A3	4.19	3.91	3.91	4.00	4.28	4.06
314-5		D3	2.70	2.79	2.88	3.07	3.44	2.98
314-6		E3	3.16	3.26	3.26	3.26	2.88	3.16
313-0		D3	5.66	5.70	6.09	5.97	6.21	5.93
313-1		C3	5.28	5.11	4.77	4.94	5.20	5.06
313-2		B3	5.71	5.54	5.20	4.85	4.51	5.16
313-3		C3	1.96	2.04	2.21	2.47	2.64	2.27
313-4	46	A3	2.64	2.55	2.38	2.47	2.55	2.52
313-5		E3	2.47	2.64	2.81	2.64	2.55	2.62
313-6		D3	2.81	3.07	3.07	3.49	3.49	3.19
313-7		A3	0.43	0.60	0.51	0.43	0.43	0.48
316-0		D3	7.25	7.87	7.65	7.93	8.44	7.83
316-1		A3	0.88	0.68	0.97	0.78	0.97	0.86
316-2		D3	8.94	8.94	8.65	8.56	8.75	8.77
316-3		A3	1.17	1.17	0.97	0.88	0.68	0.97
316-4		D3	4.96	5.54	5.93	5.74	5.44	5.52
316-5		C3	6.81	6.51	6.51	7.10	7.97	6.98
316-6		D3	0.39	0.39	0.49	0.39	0.39	0.41
316-7		B3	2.04	1.75	1.65	1.56	1.36	1.67
316-8		D3	0.58	0.68	0.68	0.68	0.88	0.70
316-9	45	A3	0.88	1.17	1.17	1.17	1.26	1.13
316-10		E3	0.97	0.88	0.78	0.78	0.88	0.86

Lamina number	Year in sequence	Lamina type	Lamina thickness (mm)					
			T1	T2	T3	T4	T5	Mean
316-11		D3	4.18	4.47	4.76	4.67	3.89	4.39
315-0		C3	4.23	3.75	4.07	3.11	3.12	3.66
315-1		D3	1.61	1.61	1.51	1.51	1.61	1.57
315-2		B3	1.61	1.51	1.81	2.01	2.31	1.85
315-3		C3	2.82	2.51	2.92	3.32	3.62	3.04
315-4		B3	4.12	4.53	4.43	3.82	3.32	4.04
315-5		C3	6.03	5.43	5.43	5.63	5.73	5.65
315-6	44	B3	4.12	3.72	2.61	2.61	2.72	3.16
315-7		D3	3.12	3.22	3.92	3.92	3.32	3.50
315-8		C3	1.21	1.21	1.21	1.31	1.31	1.25
315-9		D3	2.61	2.92	3.12	3.32	3.72	3.14
371-0	43	A3	11.78	13.29	12.78	12.58	12.89	12.66
371-1		D3	9.78	9.78	10.08	10.59	10.99	10.25
371-2		C3	12.50	12.71	12.71	12.61	12.61	12.63
306-0	42	A3	9.52	9.27	9.36	9.73	8.36	9.25
306-1		C3	3.06	2.91	2.83	2.69	2.69	2.83
306-2		E3	2.09	1.79	1.49	1.27	1.04	1.54
306-3		D3	5.59	5.37	5.52	5.22	5.07	5.36
306-4		C3	5.07	5.67	5.97	6.12	6.19	5.80
306-5		A3	1.49	1.57	1.42	1.19	1.19	1.37
305-0		C3	4.83	4.27	3.94	3.40	3.85	4.06
305-1	41	A3	1.22	1.54	1.62	1.38	0.97	1.35
305-2		D3	5.28	5.36	5.52	5.60	5.93	5.54
305-3		C3	1.70	1.38	1.38	1.46	1.62	1.51
305-4		A3	1.62	1.62	1.46	1.54	1.46	1.54
305-5		E3	4.14	4.55	4.87	4.87	4.79	4.64
312-0		D3	13.07	14.60	12.81	12.87	12.87	13.25
312-1		C3	3.88	3.88	3.88	3.96	4.11	3.94
312-2	40	B3	2.89	2.74	2.74	2.51	2.36	2.65
312-3		D3	5.48	5.33	5.41	5.56	5.79	5.51
311-0		C3	11.44	11.45	11.62	10.87	11.22	11.32
311-2	39	A3	4.89	4.74	4.74	5.05	4.66	4.82
311-3		E3	4.97	5.05	4.89	4.89	4.89	4.94
311-4		C3	8.45	8.29	8.53	8.68	8.68	8.53
370-1		A3	2.06	1.96	2.48	2.37	2.37	2.25
370-2		C3	8.77	8.87	7.94	7.73	7.73	8.21
370-3		D3	2.27	2.27	2.17	1.96	1.96	2.12
370-4		C3	6.60	6.70	7.01	7.12	7.32	6.95
370-5	38	A3	1.65	1.75	2.17	2.58	2.68	2.17
369-0		D3	15.02	13.99	13.37	12.54	12.23	13.43
369-1		C3	10.36	10.87	11.18	11.38	11.38	11.03
372-0		A3	40.68	40.86	41.35	41.73	42.11	41.35
372-1		C3	1.84	1.84	1.94	1.84	1.65	1.82

Lamina number	Year in sequence	Lamina type	Lamina thickness (mm)					
			T1	T2	T3	T4	T5	Mean
372-2	37	A3	2.23	2.13	2.13	2.13	2.52	2.23
506-0		D3	20.59	20.83	20.71	20.97	20.69	20.76
506-1		C3	5.84	5.77	5.77	5.77	5.84	5.80
506-2	36	A3	3.06	3.06	3.21	3.14	3.06	3.11
359-1		D3	5.87	5.97	5.68	5.87	5.87	5.85
359-2		C3	5.01	5.58	5.97	6.06	5.97	5.72
368-0		A3	3.31	2.99	3.68	3.75	3.91	3.53
368-1		D3	4.41	4.15	3.71	3.71	3.71	3.94
368-2		C3	2.21	2.12	2.38	2.65	2.82	2.44
368-3	35	A3	3.00	3.88	4.24	4.32	4.32	3.95
368-4		D3	10.59	10.50	10.32	9.97	9.97	10.27
368-6	34	A3	7.32	7.32	7.15	7.15	7.41	7.27
367-0		D3	12.35	12.24	11.97	12.20	11.99	12.15
350-0		A3	26.19	25.61	25.48	25.32	24.13	25.35
350-2	33	C3	13.68	10.29	10.29	9.70	9.82	10.75
350-3		D3	3.74	4.32	6.55	6.19	5.14	5.19
350-4		E3	8.88	9.00	9.35	9.82	8.42	9.09
350-5		D3	6.43	6.43	6.43	6.08	5.73	6.22
355-1		A3	0.91	1.37	1.46	1.82	2.37	1.59
355-2		D3	19.34	19.25	19.62	19.98	19.98	19.64
355-3	32	A3	5.84	5.75	5.57	5.57	6.39	5.82
356-0		D3	11.82	10.31	11.46	11.96	11.62	11.44
356-3		A3	2.38	1.99	2.08	1.89	2.28	2.12
356-4		D3	10.22	9.93	9.63	9.13	8.64	9.51
356-5	31	C3	6.35	6.45	6.65	7.44	8.34	7.05
356-6		E3	1.79	1.89	1.99	1.69	1.19	1.71
360-0		D3	16.29	16.97	17.89	17.74	16.69	17.12
360-1		C3	5.14	4.22	3.65	4.11	5.25	4.47
360-2	30	A3	6.28	6.16	6.16	6.05	6.16	6.16
360-3		E3	0.80	0.91	0.91	1.03	1.14	0.96
346-0		D3	11.64	11.92	12.24	12.55	12.44	12.16
346-1		C3	16.68	16.77	17.20	17.37	19.17	17.44
345-0	29	A3	6.98	6.77	6.27	5.38	5.50	6.18
345-1		D3	10.59	10.31	11.04	12.23	12.60	11.35
345-2		C3	4.11	4.20	3.56	2.10	1.83	3.16
345-3		A3	8.76	9.13	9.58	9.58	9.31	9.27
345-4		C3	5.29	4.56	4.75	4.75	5.20	4.91
349-3	28	A3	19.52	19.43	19.26	19.35	19.77	19.47
511-1		D3	1.68	1.76	1.91	1.99	0.23	1.51
523-0		E3	3.35	2.60	2.38	2.86	2.57	2.75
523-1		D3	14.20	14.44	14.28	13.88	14.12	14.19
523-2	27	A3	8.27	8.35	8.91	9.63	10.67	9.16
389-1		D3	26.75	27.82	28.77	29.52	29.52	28.47

Lamina number	Year in sequence	Lamina type	Lamina thickness (mm)					
			T1	T2	T3	T4	T5	Mean
390-1	26	A3	9.70	10.29	8.46	7.55	8.23	8.85
390-2		E3	2.32	2.42	2.52	2.42	2.32	2.40
390-3		D3	7.65	6.87	7.35	7.16	6.97	7.20
390-4	25	C3	6.68	6.97	6.97	7.16	7.35	7.03
344-0		D3	24.97	24.68	24.97	25.35	25.26	25.05
344-1		C3	11.61	11.81	11.90	12.29	12.58	12.04
344-2	24	A3	3.29	3.29	3.29	3.48	3.39	3.35
344-3		E3	4.35	4.65	4.45	4.16	3.97	4.32
343-0		D3	6.57	6.52	6.66	5.92	5.86	6.30
343-1		C3	3.65	3.95	3.65	3.14	2.94	3.47
385-1		D3	0.51	0.41	0.61	0.61	0.41	0.51
385-2		A3	0.51	0.61	0.71	0.71	0.82	0.67
385-3		D3	1.43	1.43	1.22	1.12	0.82	1.20
385-4		C3	8.16	8.06	8.06	8.16	8.36	8.16
385-5		A3	1.53	1.53	1.73	1.84	2.04	1.73
385-7		C3	11.93	12.34	12.75	12.85	13.26	12.63
385-8		A3	3.26	3.16	3.37	3.77	3.98	3.51
388-2		C3	15.11	16.58	16.96	16.64	17.48	16.55
388-3		A3	1.05	1.05	1.37	1.37	1.21	1.21
387-0		C3	33.25	34.17	34.36	34.13	34.06	34.00
387-1	23	A3	16.20	16.20	16.03	15.94	15.86	16.05
381-1		D3	6.27	5.36	4.45	4.91	4.36	5.07
381-2		A3	4.00	3.73	3.36	3.36	3.18	3.53
381-3		D3	5.91	6.27	6.91	7.55	8.64	7.05
381-4		B3	10.73	10.45	10.09	9.55	9.18	10.00
381-5	22	C3	2.45	1.91	2.27	3.00	3.45	2.62
384-0		D3	16.52	16.98	17.34	17.29	17.43	17.11
384-1	21	C3	7.48	7.48	7.59	7.91	8.12	7.72
348-2		D3	6.32	6.32	6.32	6.22	6.11	6.26
384-3		C3	5.06	5.48	4.74	4.53	4.64	4.89
383-0		B3	14.83	14.89	14.84	14.48	14.40	14.69
383-1	20	A3	1.88	1.79	1.88	1.69	1.79	1.81
383-2		E3	2.07	2.07	2.16	1.98	1.79	2.01
383-3		D3	3.10	3.01	2.63	2.16	2.07	2.60
383-4		A3	1.22	1.22	1.32	1.98	1.88	1.52
383-5		D3	4.42	4.52	4.52	4.23	4.05	4.35
383-6	19	A3	6.02	6.02	5.83	5.74	6.21	5.97
383-7		C3	3.29	3.29	3.86	4.14	3.58	3.63
386-0		D3	2.54	3.04	3.51	4.19	4.39	3.54
386-1	18	B3	9.86	9.92	9.07	8.12	8.02	9.00
386-2		D3	3.08	2.97	2.86	2.86	2.97	2.95
386-z		Ash	1.10	1.43	1.76	2.09	2.64	1.80
386-3		C3	3.74	3.63	3.63	3.74	3.41	3.63

Lamina number	Year in sequence	Lamina type	Lamina thickness (mm)					
			T1	T2	T3	T4	T5	Mean
386-5	17	A3	10.11	10.11	9.56	9.23	8.79	9.56
386-6		D3	4.73	4.62	4.62	4.62	4.18	4.55
401-2	16	A3	20.77	21.12	20.65	21.67	23.27	21.50
401-3		D3	9.77	9.43	9.17	8.82	7.44	8.93
380-0		C3	5.94	6.29	6.37	5.68	4.99	5.86
380-1		A3	4.73	4.90	5.08	5.42	5.85	5.20
380-2		D3	3.87	4.90	5.51	6.11	5.59	5.20
380-3		C3	8.26	8.17	8.09	8.00	8.26	8.15
380-4	15	A3	1.20	1.20	1.12	1.46	1.20	1.24
379-0		D3	25.57	26.49	27.27	28.06	28.54	27.18
379-1	14	C3	7.57	6.41	8.20	8.62	8.62	7.88
379-2		D3	12.62	12.41	12.09	7.46	6.20	10.16
382-2	13	A3	14.40	14.40	15.14	16.08	16.40	15.28
382-3		D3	15.87	16.19	16.29	16.19	16.08	16.12
382-4		A3	1.05	0.95	0.74	0.84	0.84	0.88
405-4		C3	25.14	25.72	26.02	25.72	25.82	25.68
404-0		A3	1.90	2.30	2.69	1.85	2.57	2.26
404-2		C3	9.67	8.77	9.89	10.48	9.52	9.67
404-3		A3	3.42	3.49	2.75	2.83	3.64	3.23
404-5		C3	10.26	10.19	9.89	9.52	9.82	9.93
403-0		A3	4.12	4.19	4.36	4.65	4.76	4.42
403-2		C3	11.68	11.41	11.23	11.41	11.59	11.46
403-3		D3	0.45	0.45	0.53	0.62	0.98	0.61
403-4	12	C3	4.19	4.37	4.28	3.92	3.74	4.10
403-5		D3	2.50	2.50	2.58	2.67	2.41	2.53
403-6		C3	1.60	1.52	1.60	1.52	1.60	1.57
403-7		A3	3.03	3.12	2.50	2.58	2.76	2.80
403-8		D3	6.60	7.04	7.13	7.04	6.60	6.88
402-1		C3	8.45	8.91	9.38	9.32	9.67	9.15
402-2		D3	0.84	1.13	1.13	1.13	1.03	1.05
409-0	11	C3	40.56	40.86	40.86	42.37	41.52	41.24
409-1		D3	11.11	11.31	11.82	11.82	10.80	11.37
408-0		A3	10.97	10.94	11.75	12.58	12.78	11.80
408-1		C3	1.76	1.76	1.67	1.48	1.39	1.61
408-2		A3	4.17	4.17	4.26	4.26	4.54	4.28
408-3		C3	12.41	11.94	11.57	11.20	10.83	11.59
407-1		A3	13.95	15.09	15.70	15.96	15.24	15.19
407-2		C3	10.26	10.46	10.86	11.36	9.76	10.54
407-3	10	A3	3.92	3.52	3.12	3.52	4.02	3.62
407-4		D3	8.55	8.75	9.05	9.25	9.15	8.95
407-5		B3	3.42	3.02	3.02	2.92	2.92	3.06
407-6		A3	1.31	1.31	1.11	1.01	0.91	1.13
406-0		D3	5.39	6.06	6.21	6.89	7.25	6.36

Lamina number	Year in sequence	Lamina type	Lamina thickness (mm)					
			T1	T2	T3	T4	T5	Mean
406-1		B3	5.40	5.62	4.86	4.43	5.73	5.21
406-2		D3	3.56	3.89	3.56	3.35	2.38	3.35
413-0	9	A3	24.01	27.75	27.49	28.29	28.18	27.14
413-1		D3	3.28	3.08	2.88	2.75	2.62	2.92
413-2		C3	11.93	12.98	13.31	13.57	13.77	13.11
413-4		A3	2.36	2.23	2.16	2.23	2.16	2.23
412-0		B3	3.57	3.38	3.45	2.56	3.84	3.36
412-1		A3	2.76	3.06	3.16	3.06	3.16	3.04
412-2	8	B3	1.09	0.79	0.79	0.69	0.49	0.77
412-3		D3	19.24	19.24	19.24	18.85	18.45	19.01
412-4		C3	0.89	0.59	0.79	0.79	1.48	0.91
412-5		D3	4.74	4.44	4.14	4.14	3.55	4.20
411-0		C3	9.29	9.57	10.14	9.24	10.51	9.75
411-1	7	A3	2.34	2.06	1.97	1.78	1.69	1.97
411-2		D3	16.88	17.44	17.44	17.63	17.34	17.34
410-0	6	A3	10.59	10.13	11.67	10.75	11.87	11.00
410-1		D3	0.00	0.54	1.18	1.94	2.26	1.18
410-z		Ash	2.26	2.37	1.94	0.97	1.08	1.72
410-3		D3	3.45	3.66	4.31	5.38	5.38	4.44
410-4		C3	6.14	6.46	6.78	7.22	6.78	6.68
410-5	5	A3	3.12	3.66	3.34	2.37	2.15	2.93
410-6		D3	3.55	2.91	2.91	2.80	2.58	2.95
410-7		C3	6.46	6.03	5.60	5.92	6.57	6.12
410-9	4	A3	4.74	4.52	4.42	4.20	3.98	4.37
416-0		D3	11.62	12.29	12.45	12.05	12.09	12.10
416-1		C3	12.72	13.08	13.17	13.35	13.35	13.13
415-0	3	A3	7.99	6.99	6.43	5.84	5.49	6.55
415-1		D3	3.74	3.82	3.82	3.50	3.50	3.68
415-2		C3	3.98	3.98	4.30	4.46	4.38	4.22
415-3		A3	2.94	2.47	2.07	1.91	1.91	2.26
415-5		C3	8.91	9.71	10.03	10.19	10.19	9.80
415-6	2	A3	1.27	1.27	1.35	1.75	2.23	1.58
415-7		E3	1.03	1.27	1.11	1.03	1.03	1.10
415-8		D3	5.57	4.93	4.62	4.54	4.14	4.76
415-9		A3	0.72	0.80	0.80	0.56	0.40	0.65
414-0		D3	6.00	6.10	6.36	6.53	7.03	6.40
414-1		C3	9.26	9.35	9.43	9.51	9.60	9.43
414-2		A3	3.81	3.47	3.31	3.14	3.14	3.38
414-3		C3	5.21	5.29	5.38	5.29	5.13	5.26
414-4	1	A3	4.80	4.38	3.97	3.56	3.31	4.00
414-5		D3	1.65	1.99	2.23	1.90	2.15	1.99

Appendix 3. Quantitative diatom counts

This appendix presents the results of quantitative diatom assemblage counts from cores MD03-2601 (Table A3.01) and IODP-318-U1357B (Table A3.02).

Table A3.01. Table showing the distribution by sample of all diatom species in core MD03-2601 from discrete samples of laminae described using BSEI. Diatom species abundances are given as % of total assemblage, and those included in PCA are in bold. The area of the settling beaker is 7854 mm^2 and the area of the field of view is 0.00018 mm^2. Abbreviations used in species list are: rs – resting spores; veg. – vegetative cells.

Species	Depth (cmbsf)	2367.7	2369.1	2376.6	2389.5	2397.5	423.5	431.2	349	323	318	1196.8	1143.5
	Lamina	A1	A1	A1	A1	A1	A2	A2	A2	A2	A2	B1	B1
	Total valves	519	508	519	516	511	508	516	503	505	509	505	504
	Fields of view	45	108	45	76	87	52	153	66	80	86	44	60
	Dry mass (g)	0.0027	0.0017	0.0021	0.0025	0.0012	0.0031	0.0013	0.0031	0.0027	0.0025	0.0027	0.0027
Actinocylus actinochilus		0.2	0.4	0.0	0.0	0.2	0.2	0.0	0.4	0.4	0.2	0.2	0.0
Asterompahlus parvulus		0.0	0.0	0.0	0.0	0.4	0.0	0.0	0.0	0.0	0.0	0.0	0.0
Actinocyclus curvatulus		0.0	0.0	0.0	0.0	0.0	0.0	0.2	0.0	0.0	0.0	0.0	0.0
Asteromphalus hookeri		0.0	0.0	0.0	0.0	0.0	0.4	0.2	0.2	0.6	0.2	0.2	0.0
Asteromphalus hyalinus		0.0	0.0	0.0	0.0	0.0	0.0	0.2	0.0	0.0	0.0	0.0	0.2
Asteromphalus spp.		0.0	0.0	0.2	0.0	0.2	0.0	0.0	0.0	0.0	0.0	0.0	0.0
Azpeitia tabularis		1.1	0.0	0.0	0.0	0.2	0.0	0.0	0.0	0.0	0.0	0.0	0.0
***Hyalochaete Chaetoceros* spp.**		**0.0**	**0.0**	**2.1**	**0.0**	**0.2**	**0.0**	**0.0**	**0.0**	**0.0**	**0.0**	**0.0**	**0.0**
***Phaeoceros Chaetoceros* spp.**		**1.2**	**0.0**	**1.5**	**1.0**	**0.4**	**6.7**	**3.3**	**1.8**	**2.8**	**1.8**	**1.0**	**4.8**
***Chaetoceros* rs**		**41.6**	**41.3**	**45.1**	**42.4**	**42.1**	**5.1**	**17.6**	**21.9**	**18.6**	**14.3**	**52.5**	**46.8**
Cocconeis spp. large		0.0	0.0	0.0	0.0	0.0	0.2	0.2	0.6	0.0	0.2	0.2	0.0
Cocconeis spp. small		0.9	0.0	1.0	0.0	0.8	0.0	0.0	0.0	0.0	0.0	0.0	0.0
Corethron pennatum		**0.0**	**0.0**	**0.0**	**0.6**	**0.0**	**0.4**	**0.2**	**0.6**	**0.4**	**0.0**	**1.6**	**2.2**
Coscinodiscus bouvet		0.0	0.2	0.0	0.0	0.2	0.0	0.0	0.0	0.0	0.0	0.0	0.0
Coscinodiscus radiatus		0.5	0.0	0.0	0.0	0.0	0.0	0.0	0.0	0.0	0.0	0.0	0.0
Coscinodiscus spp.		1.1	0.0	0.2	0.2	0.6	0.0	0.2	0.0	0.0	0.2	0.2	0.2
Eucampia antarctica rs		0.2	0.2	0.0	0.2	0.0	0.2	1.0	0.4	0.2	1.0	1.0	0.0
Eucampia antarctica veg.		0.5	0.0	1.0	0.6	0.2	0.0	0.2	0.2	0.2	0.4	0.2	0.2
Fragilariopsis curta		**8.5**	**10.6**	**6.6**	**7.0**	**7.0**	**53.1**	**32.9**	**40.2**	**39.4**	**39.1**	**9.5**	**11.1**
Fragilariopsis cylindrus		**0.7**	**0.2**	**6.0**	**0.2**	**1.6**	**6.1**	**4.1**	**5.0**	**1.0**	**4.1**	**0.0**	**0.6**
Fragilariopsis kerguelensis		**11.8**	**12.8**	**6.4**	**18.0**	**9.6**	**4.7**	**8.1**	**7.4**	**11.1**	**11.0**	**10.1**	**11.5**
Fragilariopsis obliquecostata		**1.1**	**1.4**	**1.3**	**2.3**	**1.4**	**3.3**	**2.7**	**3.4**	**5.5**	**4.9**	**2.0**	**0.4**
Fragilariopsis pseudonana		0.0	0.0	0.0	0.0	0.0	0.0	0.2	0.0	0.0	0.0	0.0	0.2
Fragilariopsis rhombica		**11.3**	**13.2**	**4.2**	**10.5**	**8.0**	**2.8**	**7.0**	**4.0**	**3.8**	**6.3**	**9.5**	**11.3**
Fragilariopsis ritscheri		**5.5**	**4.1**	**3.1**	**3.9**	**6.5**	**5.3**	**2.5**	**2.8**	**1.8**	**2.0**	**2.8**	**3.0**
Fragilariopsis separanda		**2.3**	**3.7**	**3.9**	**2.9**	**1.8**	**2.6**	**7.6**	**2.8**	**5.1**	**6.1**	**1.6**	**1.2**
Fragilariopsis spp.		0.9	0.0	0.2	0.4	0.4	0.0	1.0	1.0	0.0	0.0	0.0	0.0
Fragilariopsis sublinearis		**0.4**	**0.2**	**0.4**	**0.6**	**0.4**	**0.8**	**0.2**	**0.8**	**0.6**	**0.0**	**0.6**	**0.4**
Fragilariopsis vanheurckii		0.0	0.0	0.4	0.0	0.0	0.6	0.4	0.4	0.2	0.0	0.0	0.0
Licmophora spp.		0.0	0.0	0.0	0.0	0.0	0.0	0.0	0.0	0.0	0.0	0.0	0.0
Navicula spp.		0.2	0.0	0.4	0.0	0.6	0.2	0.8	0.8	0.6	1.2	0.0	0.0
Nitzschia spp.		0.2	0.0	0.8	0.2	0.2	0.0	0.0	0.0	0.2	0.0	0.0	0.0
Odontella litigiosa		0.0	0.0	0.0	0.0	0.0	0.2	0.0	0.0	0.0	0.0	0.0	0.0
***Porosira glacialis* rs**		**0.2**	**0.0**	**0.0**	**0.0**	**0.2**	**0.2**	**1.4**	**1.2**	**1.4**	**1.2**	**0.0**	**0.0**
Porosira pseudodenticula		0.0	0.2	0.0	0.0	0.4	0.0	0.2	0.0	0.0	0.0	0.0	0.0
Proboscia inermis		**0.0**	**0.0**	**0.2**	**0.0**	**0.0**	**0.6**	**0.8**	**0.4**	**0.6**	**0.8**	**0.2**	**0.2**
Proboscia truncata		0.0	0.0	0.0	0.2	0.0	0.6	0.4	0.2	0.2	0.2	0.0	0.0
***Pseudonitzschia* spp.**		**0.4**	**0.0**	**1.5**	**0.0**	**1.4**	**0.4**	**0.2**	**0.2**	**0.6**	**1.0**	**0.0**	**0.0**
Rhizosolenia antennata f. antennata		**0.0**	**0.2**	**0.0**	**0.0**	**0.0**	**0.0**	**0.0**	**0.0**	**0.0**	**0.0**	**0.0**	**0.0**
Rhizosolenia antennata f. semispina		**0.4**	**0.2**	**0.2**	**0.0**	**0.8**	**0.2**	**1.4**	**0.4**	**0.6**	**0.2**	**0.4**	**0.2**
Rhizosolenia simplex		0.0	0.0	0.0	0.0	0.0	0.0	0.4	0.2	0.0	0.0	0.2	0.0
Stellarima microtrias		0.0	0.2	0.2	0.0	0.2	0.0	0.0	0.0	0.2	0.0	0.0	0.2
Thalassionema nitzschioides		0.0	0.0	3.1	0.0	0.0	0.0	0.0	0.0	0.0	0.0	0.0	0.0
Thalassiosira ambigua		0.0	0.0	0.0	0.2	0.0	0.0	0.0	0.0	0.0	0.0	0.0	0.4
***Thalassiosira antarctica* rs (cold)**		**2.3**	**3.0**	**1.7**	**1.6**	**2.0**	**1.0**	**1.2**	**0.4**	**0.8**	**0.8**	**3.4**	**1.6**
Thalassiosira antarctica rs warm)		0.4	0.0	0.4	0.0	0.0	0.0	0.0	0.0	0.0	0.0	0.0	0.0
Thalassiosira antarctica veg.		0.5	0.0	1.3	0.0	0.2	0.0	0.0	0.0	0.0	0.2	0.0	0.0
Thalassiosira gracilis v. expecta		0.4	0.0	0.2	0.0	0.2	0.0	0.0	0.0	0.0	0.0	0.0	0.0
Thalassiosira gracilis v. gracilis		**1.6**	**1.4**	**0.6**	**1.4**	**2.0**	**2.2**	**1.0**	**0.8**	**0.8**	**1.4**	**0.2**	**0.6**
Thalassiosira lentiginosa		**0.4**	**3.0**	**0.6**	**3.3**	**1.6**	**0.6**	**0.4**	**0.0**	**0.6**	**0.6**	**1.6**	**1.0**
Thalassiosira oestrupii		0.2	0.4	0.2	0.0	0.0	0.0	0.0	0.0	0.2	0.0	0.0	0.0
Thalassiosira oliveriana		0.2	0.6	0.0	0.0	0.0	0.0	0.0	0.0	0.0	0.0	0.0	0.0
Thalassiosira ritscheria		0.0	0.0	0.0	0.0	0.0	0.0	0.0	0.0	0.0	0.0	0.0	0.0
Thalassiosira spp.		0.9	0.8	1.9	0.4	3.9	0.0	0.6	0.2	0.6	0.0	0.0	0.0
Thalassiosira tealata		0.0	0.0	0.0	0.0	0.0	0.4	0.0	0.0	0.0	0.0	0.0	0.0
Thalassiosira trifulta		**0.0**	**1.0**	**1.0**	**0.8**	**2.3**	**0.2**	**0.6**	**0.8**	**0.0**	**0.0**	**0.6**	**0.0**
Thalassiosira tumida		0.2	0.4	0.2	0.0	0.0	0.2	0.4	0.0	0.2	0.4	0.4	1.8
Thalassiothrix antarctica		**0.5**	**0.0**	**0.8**	**0.4**	**0.4**	**0.2**	**0.2**	**0.2**	**0.2**	**0.2**	**0.0**	**0.0**
Thalassiothrix/nema/toxon		0.0	0.0	0.0	0.0	0.0	0.0	0.0	0.0	0.0	0.0	0.0	0.0
Trichotoxon reinboldii		0.5	0.0	0.2	0.4	0.2	0.4	0.4	0.4	0.6	0.2	0.0	0.0
Unidentified centrics		1.1	0.4	1.0	0.6	1.6	0.0	0.0	0.2	0.0	0.0	0.0	0.0
Unidentified pennates		0.2	0.0	0.2	0.0	0.0	0.0	0.0	0.0	0.0	0.0	0.0	0.0

Table A3.01 continued.

Species	Depth (cmbsf)	1142	1140	315.6	345.7	355.6	395	2276.2	2297.6	2332.6	2386.8	2069.6	341.4
	Lamina	B1	B1	B2	B2	B2	B2	C1	C1	C1	C1	C2	C2
	Valves counted	510	503	502	507	506	500	502	513	510	511	508	504
	Fields of view	56	113	68	108	85	118	44	57	75	55	76	95
	Dry mass (g)	0.0022	0.0016	0.003	0.002	0.002	0.0011	0.0022	0.0025	0.0021	0.0025	0.0025	0.0021
Actinocylus actinochilus		0.0	0.0	0.0	0.0	0.0	0.2	0.2	0.0	0.0	0.2	0.2	0.0
Asterompahlus parvulus		0.0	0.0	0.0	0.0	0.0	0.0	0.4	0.0	0.0	0.0	0.0	0.0
Actinocyclus curvatulus		0.0	0.0	0.0	0.0	0.0	0.0	0.0	0.0	0.0	0.2	0.0	0.0
Asteromphalus hookeri		0.0	0.2	0.6	0.0	0.0	0.4	0.2	0.0	0.0	0.0	0.0	0.2
Asteromphalus hyalinus		0.0	0.0	0.0	0.0	0.0	0.0	0.0	0.0	0.0	0.2	0.0	0.0
Asteromphalus spp.		0.0	0.0	0.0	0.0	0.0	0.0	0.0	0.0	0.2	0.0	0.0	0.0
Azpeitia tabularis		0.0	0.0	0.0	0.2	0.0	0.0	0.0	0.0	1.0	0.6	0.0	0.0
***Hyalochaete Chaetoceros* spp.**		**0.0**	**0.0**	**0.0**	**0.6**	**0.4**	**0.0**	**0.6**	**0.2**	**0.0**	**0.0**	**0.0**	**0.2**
***Phaeoceros Chaetoceros* spp.**		**2.2**	**3.2**	**2.4**	**4.5**	**16.0**	**5.4**	**10.0**	**3.1**	**2.2**	**6.8**	**4.1**	**1.4**
***Chaetoceros* rs**		**49.8**	**50.1**	**23.7**	**25.6**	**22.1**	**30.0**	**31.1**	**38.0**	**30.2**	**36.0**	**35.8**	**35.3**
Cocconeis spp. large		0.2	0.0	0.2	0.0	0.0	0.0	0.0	0.0	0.0	0.0	0.0	0.0
Cocconeis spp. small		0.0	0.0	0.6	0.6	0.0	0.0	0.0	0.0	0.6	0.8	0.0	0.0
Corethron pennatum		**1.4**	**2.0**	**0.2**	**3.2**	**2.0**	**3.8**	**0.2**	**1.0**	**0.2**	**0.2**	**0.8**	**1.0**
Coscinodiscus bouvet		0.0	0.0	0.0	0.0	0.0	0.0	0.0	0.2	0.0	0.0	0.0	0.0
Coscinodiscus radiatus		0.0	0.0	0.0	0.0	0.0	0.0	0.0	0.0	0.2	0.2	0.0	0.0
Coscinodiscus spp.		0.2	0.0	0.0	0.0	0.0	0.0	0.0	0.0	0.6	0.6	0.0	0.2
Eucampia antarctica rs		0.8	0.6	0.8	0.4	0.4	0.2	0.2	1.0	0.4	0.2	0.2	0.4
Eucampia antarctica veg		0.4	0.2	0.2	0.2	1.0	0.2	0.2	0.0	0.2	0.8	0.2	0.8
Fragilariopsis curta		**10.4**	**8.5**	**24.9**	**18.3**	**17.8**	**21.6**	**10.0**	**7.4**	**6.5**	**6.1**	**34.1**	**23.2**
Fragilariopsis cylindrus		**0.2**	**0.6**	**4.8**	**1.2**	**3.2**	**4.0**	**1.0**	**1.2**	**3.9**	**1.2**	**0.8**	**0.6**
Fragilariopsis kerguelensis		**11.0**	**8.9**	**10.8**	**8.9**	**5.3**	**5.0**	**8.8**	**15.3**	**10.2**	**9.4**	**3.5**	**8.9**
Fragilariopsis obliquecostata		**1.8**	**1.2**	**6.0**	**11.4**	**10.1**	**4.0**	**0.2**	**2.3**	**2.2**	**1.6**	**2.2**	**1.8**
Fragilariopsis pseudonana		0.0	0.0	0.0	0.0	0.4	0.4	0.0	0.0	0.0	0.0	0.0	0.0
Fragilariopsis rhombica		**10.0**	**7.6**	**4.6**	**6.3**	**7.1**	**11.6**	**6.2**	**8.8**	**5.7**	**7.4**	**7.7**	**9.5**
Fragilariopsis ritscheri		**3.1**	**4.2**	**4.8**	**2.8**	**1.2**	**2.2**	**8.8**	**4.1**	**6.3**	**4.3**	**1.8**	**3.6**
Fragilariopsis separanda		**2.2**	**3.4**	**4.6**	**3.6**	**2.6**	**2.2**	**4.2**	**6.8**	**5.3**	**6.3**	**1.2**	**0.8**
Fragilariopsis spp.		0.2	0.0	0.6	1.0	0.2	0.2	0.8	0.0	0.8	1.8	0.2	0.4
Fragilariopsis sublinearis		**0.4**	**0.0**	**0.8**	**3.0**	**0.8**	**1.4**	**0.0**	**0.2**	**0.4**	**0.0**	**2.0**	**1.0**
Fragilariopsis vanheurckii		0.2	0.0	0.8	0.2	0.0	0.2	0.2	0.0	0.2	0.0	0.0	0.0
Licmophora spp.		0.0	0.0	0.0	0.0	0.0	0.2	0.0	0.0	0.0	0.0	0.0	0.0
Navicula spp.		0.0	0.0	0.4	0.4	0.4	1.2	0.4	0.6	0.4	0.8	0.2	0.0
Nitzschia spp.		0.0	0.0	0.0	0.0	0.0	0.0	0.4	0.0	0.8	0.2	0.2	0.0
Odontella litigiosa		0.0	0.0	0.0	0.0	0.0	0.0	0.0	0.0	0.0	0.0	0.0	0.0
***Porosira glacialis* rs**		**0.0**	**0.0**	**0.8**	**1.2**	**1.2**	**0.4**	**0.0**	**0.0**	**0.0**	**0.2**	**0.2**	**1.4**
Porosira pseudodenticula		0.0	0.0	0.0	0.0	0.0	0.0	0.0	0.2	0.4	0.4	0.2	0.4
Proboscia inermis		**0.4**	**0.8**	**0.6**	**0.2**	**0.6**	**1.2**	**0.2**	**0.0**	**0.6**	**0.4**	**0.4**	**1.0**
Proboscia truncata		0.0	0.4	0.2	0.0	1.0	0.0	0.2	0.2	0.2	0.0	0.0	1.0
***Pseudonitzschia* spp.**		**0.0**	**0.4**	**1.0**	**0.8**	**1.4**	**0.2**	**0.0**	**1.0**	**1.0**	**1.4**	**0.0**	**0.0**
Rhizosolenia antennata f. antennata		**0.2**	**0.0**	**0.2**	**0.2**	**0.0**	**0.0**	**0.0**	**0.0**	**0.0**	**0.0**	**0.0**	**0.0**
Rhizosolenia antennata f. semispina		**1.0**	**1.4**	**1.4**	**0.2**	**0.0**	**0.8**	**2.6**	**0.4**	**0.4**	**0.8**	**0.8**	**1.2**
Rhizosolenia simplex		**0.0**	**0.2**	**0.6**	**0.2**	**0.0**	**0.0**	**0.2**	**0.0**	**0.2**	**0.6**	**0.0**	**0.4**
Stellarima microtrias		0.0	0.0	0.0	0.0	0.0	0.2	0.4	0.0	0.4	0.0	0.0	0.0
Thalassionema nitzschioides		0.0	0.0	0.0	0.0	0.0	0.0	0.0	0.0	0.2	0.0	0.0	0.0
Thalassiosira ambigua		0.2	0.6	0.0	0.0	0.0	0.0	0.0	0.0	0.0	0.0	0.2	0.0
***Thalassiosira antarctica* rs (cold)**		**2.0**	**2.4**	**0.8**	**1.6**	**1.0**	**0.4**	**2.6**	**1.2**	**4.3**	**4.1**	**1.2**	**1.0**
Thalassiosira antarctica rs (warm)		0.0	0.2	0.0	0.0	0.0	0.0	1.8	0.0	0.4	0.2	0.0	0.0
Thalassiosira antarctica veg.		0.0	0.0	0.0	0.0	0.2	0.0	0.4	0.2	0.8	0.0	0.0	0.0
Thalassiosira gracilis v. expecta		0.0	0.2	0.0	0.0	0.0	0.0	0.4	0.0	0.2	0.2	0.0	0.2
Thalassiosira gracilis v. gracilis		**0.4**	**0.8**	**1.2**	**1.2**	**1.6**	**0.6**	**0.6**	**2.0**	**2.0**	**1.6**	**0.2**	**0.8**
Thalassiosira lentiginosa		**0.6**	**1.2**	**0.4**	**0.8**	**0.6**	**0.6**	**1.0**	**1.8**	**1.4**	**0.2**	**1.8**	**2.0**
Thalassiosira oestrupii		0.0	0.0	0.0	0.2	0.0	0.0	0.6	0.6	1.0	0.0	0.0	0.0
Thalassiosira oliveriana		0.0	0.0	0.0	0.0	0.0	0.0	0.2	0.0	0.0	0.0	0.0	0.0
Thalassiosira ritscheria		0.2	0.0	0.0	0.0	0.0	0.0	0.0	0.0	0.0	0.0	0.0	0.0
Thalassiosira spp.		0.0	0.0	0.0	0.2	0.0	0.0	0.2	1.4	2.2	2.0	0.0	0.0
Thalassiosira tealata		0.0	0.0	0.0	0.0	0.0	0.0	0.0	0.0	0.0	0.0	0.0	0.0
Thalassiosira trifulta		**0.4**	**0.2**	**0.2**	**0.2**	**0.2**	**0.2**	**0.4**	**0.4**	**3.7**	**0.0**	**0.0**	**0.4**
Thalassiosira tumida		0.0	0.0	0.4	0.6	0.6	0.4	0.2	0.4	0.8	0.4	0.0	0.6
Thalassiothrix antarctica		**0.2**	**0.4**	**0.4**	**0.2**	**0.2**	**0.4**	**3.0**	**0.0**	**0.4**	**0.2**	**0.0**	**0.4**
Thalassiothrix/nema/toxon		0.0	0.0	0.0	0.0	0.0	0.0	0.0	0.0	0.0	0.0	0.0	0.0
Trichotoxon reinboldii		0.2	0.2	0.0	0.0	0.0	0.2	0.6	0.2	0.4	0.2	0.0	0.0
Unidentified centrics		0.0	0.0	0.2	0.0	0.6	0.0	0.2	0.0	0.8	1.2	0.0	0.0
Unidentified pennates		0.0	0.0	0.0	0.0	0.0	0.0	0.4	0.0	0.2	0.4	0.0	0.0

Table A3.01 continued.

Species	Depth (cmbsf)	357.9	385.8	394.6	2380.9	2390.8	2373	2354.1	2376.5	C330	337	340	354.2
	Lamina	C2	C2	C2	D1	D1	D1	D1	D1	D2	D2	D2	D2
	Valves counted	509	516	519	505	535	512	525	513	504	509	506	505
	Fields of view	57	67	90	52	49	64	44	109	92	58	101	87
	Dry mass (g)	0.0033	0.0033	0.0027	0.0029	0.0025	0.0021	0.0032	0.0018	0.0027	0.0024	0.002	0.0033
Actinocylus actinochilus		0.0	0.0	0.2	0.1	0.2	0.6	0.2	0.2	0.0	0.8	0.0	0.0
Asterompahlus parvulus		0.0	0.0	0.0	0.2	0.0	0.4	0.2	0.2	0.0	0.0	0.0	0.0
Actinocyclus curvatulus		0.0	0.0	0.0	0.0	0.0	0.0	0.0	0.2	0.0	0.0	0.0	0.0
Asteromphalus hookeri		0.4	0.0	0.4	0.0	0.2	0.0	0.2	0.0	0.4	0.0	0.0	0.0
Asteromphalus hyalinus		0.0	0.0	0.0	0.0	0.0	0.0	0.0	0.0	0.2	0.0	0.0	0.0
Asteromphalus spp.		0.0	0.0	0.0	0.0	0.0	0.0	0.0	0.2	0.0	0.2	0.0	0.0
Azpeitia tabularis		0.0	0.0	0.0	0.0	0.4	0.0	0.0	1.0	0.0	0.0	0.0	0.0
***Hyalochaete Chaetoceros* spp.**		**0.6**	**0.0**	**0.0**	**0.1**	**0.0**	**0.0**	**0.0**	**0.0**	**0.0**	**0.0**	**0.0**	**0.6**
***Phaeoceros Chaetoceros* spp.**		**5.9**	**3.1**	**2.7**	**0.3**	**0.2**	**0.0**	**0.8**	**2.7**	**2.2**	**4.5**	**1.6**	**8.1**
***Chaetoceros* rs**		**35.4**	**45.3**	**31.0**	**42.9**	**41.9**	**35.4**	**49.5**	**29.8**	**31.9**	**43.2**	**35.4**	**34.5**
Cocconeis spp. large		0.0	0.0	0.0	0.0	0.0	0.0	0.2	0.2	0.0	0.0	0.2	0.2
Cocconeis spp. small		0.0	0.0	0.0	0.0	0.4	0.2	0.6	0.0	0.2	0.2	0.2	0.0
Corethron pennatum		**0.6**	**0.2**	**1.7**	**0.1**	**0.0**	**0.2**	**0.0**	**0.0**	**0.6**	**1.8**	**0.8**	**0.2**
Coscinodiscus bouvet		0.0	0.0	0.0	0.0	0.0	0.2	0.0	0.0	0.0	0.0	0.0	0.0
Coscinodiscus radiatus		0.0	0.2	0.0	0.0	0.0	0.0	0.0	0.2	0.0	0.0	0.0	0.0
Coscinodiscus spp.		0.0	0.0	0.0	0.0	0.8	0.6	1.0	0.2	0.2	0.8	0.0	0.0
Eucampia antarctica rs		0.0	0.6	0.2	0.3	0.2	1.2	0.4	1.0	0.4	0.0	0.2	1.0
Eucampia antarctica veg		0.8	0.0	0.2	0.1	0.4	0.4	0.2	0.6	0.2	0.8	0.6	0.2
Fragilariopsis curta		**29.5**	**17.0**	**28.5**	**6.3**	**6.2**	**8.0**	**5.5**	**7.8**	**17.9**	**12.6**	**16.4**	**13.5**
Fragilariopsis cylindrus		**1.0**	**0.0**	**0.6**	**0.7**	**0.4**	**0.6**	**1.0**	**1.2**	**1.8**	**4.1**	**1.2**	**1.4**
Fragilariopsis kerguelensis		**4.3**	**8.7**	**5.2**	**15.1**	**10.8**	**15.4**	**10.9**	**11.9**	**6.2**	**6.7**	**9.1**	**8.9**
Fragilariopsis obliquecostata		**3.1**	**2.7**	**2.7**	**0.9**	**1.5**	**1.8**	**1.9**	**2.5**	**11.5**	**8.6**	**9.7**	**9.5**
Fragilariopsis pseudonana		0.0	0.2	0.0	0.0	0.0	0.0	0.0	0.0	0.0	0.2	0.0	0.0
Fragilariopsis rhombica		**7.9**	**10.0**	**14.5**	**2.8**	**5.8**	**6.6**	**5.0**	**7.0**	**8.3**	**4.1**	**6.3**	**5.0**
Fragilariopsis ritscheri		**2.4**	**1.5**	**2.3**	**4.7**	**8.1**	**7.4**	**5.5**	**9.7**	**4.0**	**1.2**	**2.8**	**2.2**
Fragilariopsis separanda		**0.4**	**1.5**	**2.3**	**9.6**	**5.8**	**5.9**	**5.7**	**7.4**	**3.0**	**2.0**	**4.3**	**4.8**
Fragilariopsis spp.		0.0	0.2	0.2	0.9	1.9	1.8	1.0	2.7	0.0	0.0	0.6	0.2
Fragilariopsis sublinearis		**1.8**	**0.8**	**1.4**	**0.1**	**0.0**	**0.2**	**0.0**	**0.4**	**0.8**	**1.0**	**1.0**	**0.8**
Fragilariopsis vanheurckii		**0.0**	**0.0**	**0.0**	**0.0**	**0.0**	**0.0**	**0.0**	**1.0**	**0.0**	**0.0**	**0.0**	**0.2**
Licmophora spp.		0.0	0.0	0.2	0.0	0.0	0.0	0.0	0.0	0.0	0.0	0.0	0.0
Navicula spp.		0.0	0.2	0.2	0.1	0.0	0.2	0.2	0.0	0.0	0.6	0.0	0.4
Nitzschia spp.		0.0	0.0	0.0	0.1	0.0	0.0	0.2	0.0	0.6	0.2	0.0	0.0
Odontella litigiosa		0.0	0.0	0.0	0.0	0.0	0.0	0.0	0.0	0.0	0.0	0.0	0.0
***Porosira glacialis* rs**		**0.6**	**1.2**	**0.4**	**0.0**	**0.2**	**0.0**	**0.0**	**0.0**	**2.6**	**0.6**	**1.6**	**2.0**
Porosira pseudodenticula		0.0	0.2	0.0	0.1	0.4	0.0	0.2	0.0	0.2	0.2	0.2	0.0
Proboscia inermis		**0.4**	**0.2**	**0.6**	**0.4**	**0.4**	**0.4**	**0.2**	**0.0**	**0.0**	**0.2**	**0.2**	**0.2**
Proboscia truncata		0.4	0.6	0.6	0.1	0.0	0.0	0.0	0.0	0.0	0.2	0.0	0.2
***Pseudonitzschia* spp.**		**0.0**	**0.0**	**0.0**	**0.0**	**0.4**	**0.2**	**1.0**	**0.4**	**0.0**	**2.4**	**0.4**	**0.4**
Rhizosolenia antennata f. antennata		**0.0**	**0.8**	**0.0**	**0.0**	**0.0**	**0.0**	**0.0**	**0.0**	**0.0**	**0.0**	**0.0**	**0.0**
Rhizosolenia antennata f. semispina		**1.2**	**0.0**	**1.4**	**0.2**	**0.2**	**0.6**	**0.0**	**0.6**	**0.2**	**0.2**	**0.4**	**0.4**
Rhizosolenia simplex		**0.0**	**0.0**	**0.2**	**0.3**	**0.2**	**0.0**	**0.0**	**0.2**	**0.6**	**0.0**	**0.2**	**0.6**
Stellarima microtrias		0.0	0.0	0.0	0.1	0.2	0.4	0.0	0.0	0.0	0.0	0.0	0.0
Thalassionema nitzschioides		0.0	0.0	0.0	0.0	0.0	0.0	0.0	0.0	0.0	0.0	0.0	0.0
Thalassiosira ambigua		0.2	0.2	0.2	0.0	0.0	0.0	0.0	0.0	0.0	0.0	0.0	0.0
***Thalassiosira antarctica* rs (cold)**		**1.4**	**1.0**	**0.4**	**7.0**	**0.8**	**2.3**	**0.6**	**2.9**	**1.6**	**1.4**	**1.4**	**0.8**
Thalassiosira antarctica rs (warm)		0.0	0.0	0.0	0.8	0.0	0.0	0.0	0.6	0.0	0.0	0.0	0.0
Thalassiosira antarctica veg.		0.0	0.0	0.0	0.5	0.4	0.2	0.2	0.0	0.0	0.0	0.0	0.0
Thalassiosira gracilis v. expecta		0.0	0.2	0.0	0.2	0.2	0.0	0.2	0.2	0.0	0.0	0.0	0.0
Thalassiosira gracilis v. gracilis		**0.8**	**0.8**	**0.2**	**1.2**	**1.2**	**1.6**	**1.7**	**1.8**	**2.4**	**0.4**	**2.4**	**0.8**
Thalassiosira lentiginosa		**0.6**	**0.6**	**1.2**	**1.6**	**0.8**	**0.8**	**1.9**	**0.2**	**1.6**	**0.4**	**0.8**	**0.8**
Thalassiosira oestrupii		0.0	0.4	0.0	0.1	0.0	0.6	0.2	0.4	0.0	0.0	0.0	0.0
Thalassiosira oliveriana		0.0	0.0	0.0	0.0	0.2	0.0	0.0	0.2	0.0	0.0	0.0	0.0
Thalassiosira ritscheria		0.0	0.0	0.0	0.0	0.0	0.0	0.0	0.0	0.0	0.0	0.0	0.0
Thalassiosira spp.		0.0	0.0	0.0	0.1	4.0	1.2	2.3	0.8	0.0	0.2	1.0	0.0
Thalassiosira tealata		0.0	0.0	0.0	0.0	0.0	0.0	0.0	0.0	0.0	0.0	0.0	0.0
Thalassiosira trifulta		**0.2**	**0.4**	**0.0**	**0.1**	**3.1**	**4.1**	**1.1**	**0.6**	**0.0**	**0.0**	**0.2**	**0.8**
Thalassiosira tumida		0.4	0.6	0.4	0.4	0.0	0.2	0.0	0.8	0.0	0.2	0.4	0.4
Thalassiothrix antarctica		**0.0**	**0.4**	**0.0**	**1.0**	**0.4**	**0.4**	**0.4**	**1.2**	**0.2**	**0.0**	**0.4**	**0.0**
Thalassiothrix/nema/toxon		0.0	0.0	0.0	0.0	0.0	0.0	0.0	0.0	0.0	0.0	0.0	0.0
Trichotoxon reinboldii		0.0	0.2	0.0	0.4	0.4	0.0	0.0	0.2	0.4	0.2	0.2	0.4
Unidentified centrics		0.0	0.4	0.0	0.1	1.5	0.2	0.2	0.8	0.0	0.0	0.0	0.8
Unidentified pennates		0.0	0.0	0.0	0.0	0.2	0.0	0.0	0.0	0.0	0.0	0.0	0.0

Table A3.01 continued.

Species	Depth (cmbsf)	398.5	2336.3	2340.8	2363.8	2387.5	300.3	370	383.5	388.6
	Lamina	D2	E1	E1	E1	E1	E2	E2	E2	E2
	Valves counted	504	521	524	540	543	502	508	505	512
	Fields of view	91	68	104	66	59	71	80	83	72
	Dry mass	0.0025	0.0015	0.0018	0.0024	0.0023	0.0029	0.0028	0.003	0.003
Actinocylus actinochilus		0.4	0.0	0.2	0.0	0.4	0.2	0.4	0.2	0.0
Asterompahlus parvulus		0.0	0.0	0.0	0.0	0.0	0.0	0.0	0.0	0.0
Actinocyclus curvatulus		0.0	0.0	0.0	0.0	0.0	0.0	0.0	0.0	0.0
Asteromphalus hookeri		0.0	0.0	0.2	0.0	0.2	0.4	0.2	0.4	0.2
Asteromphalus hyalinus		0.2	0.0	0.0	0.0	0.0	0.0	0.0	0.0	0.0
Asteromphalus spp.		0.0	0.0	0.0	0.0	0.2	0.0	0.0	0.0	0.0
Azpeitia tabularis		0.0	0.0	0.0	0.0	0.0	0.0	0.0	0.0	0.0
***Hyalochaete Chaetoceros* spp.**		**0.0**	**0.0**	**0.0**	**0.0**	**0.0**	**0.0**	**0.0**	**0.2**	**0.0**
***Phaeoceros Chaetoceros* spp.**		**2.6**	**0.0**	**2.5**	**0.7**	**1.8**	**4.4**	**2.2**	**3.0**	**4.3**
***Chaetoceros* rs**		**23.2**	**40.5**	**38.2**	**30.4**	**37.6**	**40.8**	**37.0**	**40.0**	**39.1**
Cocconeis spp. large		0.0	0.0	0.2	0.0	0.0	0.0	0.0	0.2	0.0
Cocconeis spp. small		0.0	0.0	0.8	0.0	0.6	0.2	0.0	0.0	0.0
Corethron pennatum		**0.4**	**0.0**	**0.2**	**0.2**	**0.6**	**0.0**	**0.6**	**0.0**	**0.2**
Coscinodiscus bouvet		0.0	0.0	0.0	0.4	0.0	0.0	0.2	0.2	0.0
Coscinodiscus radiatus		0.0	0.0	0.0	0.6	0.2	0.0	0.0	0.0	0.0
Coscinodiscus spp.		0.4	0.6	0.0	0.0	0.0	0.0	0.0	0.0	0.0
Eucampia antarctica rs		0.6	0.4	0.4	0.6	0.4	0.4	0.2	0.0	0.2
Eucampia antarctica veg		0.0	0.0	0.6	0.6	0.2	0.2	0.2	0.4	0.2
Fragilariopsis curta		**16.9**	**6.5**	**6.5**	**12.4**	**7.9**	**11.8**	**17.5**	**14.5**	**12.1**
Fragilariopsis cylindrus		**1.0**	**0.6**	**1.1**	**0.7**	**0.4**	**1.0**	**0.2**	**0.8**	**2.1**
Fragilariopsis kerguelensis		**8.3**	**12.7**	**13.5**	**14.4**	**12.3**	**11.2**	**8.3**	**9.3**	**7.8**
Fragilariopsis obliquecostata		**9.1**	**1.2**	**0.8**	**4.3**	**1.1**	**7.2**	**10.0**	**6.9**	**7.2**
Fragilariopsis pseudonana		0.0	0.0	0.0	0.0	0.0	0.0	0.0	0.2	0.0
Fragilariopsis rhombica		**14.3**	**8.1**	**5.9**	**7.6**	**5.7**	**2.2**	**2.4**	**3.6**	**3.9**
Fragilariopsis ritscheri		**3.4**	**6.1**	**5.7**	**6.3**	**5.3**	**0.6**	**3.0**	**1.2**	**2.1**
Fragilariopsis separanda		**8.7**	**7.1**	**4.4**	**4.4**	**5.7**	**5.0**	**6.1**	**6.7**	**5.3**
Fragilariopsis spp.		0.8	0.6	0.6	0.0	0.9	0.0	0.4	0.6	0.0
Fragilariopsis sublinearis		**0.4**	**0.0**	**0.4**	**1.9**	**0.2**	**0.6**	**1.0**	**0.6**	**0.8**
Fragilariopsis vanheurckii		0.0	0.0	1.0	0.2	0.2	0.0	0.0	0.2	0.0
Licmophora spp.		0.0	0.0	0.0	0.0	0.0	0.0	0.0	0.0	0.0
Navicula spp.		0.6	0.0	0.4	0.2	0.4	0.0	0.4	0.2	0.4
Nitzschia spp.		0.0	0.0	0.0	0.0	0.0	0.4	0.4	0.0	0.2
Odontella litigiosa		0.0	0.0	0.2	0.0	0.0	0.0	0.0	0.0	0.0
***Porosira glacialis* rs**		**1.2**	**0.6**	**0.2**	**0.4**	**0.6**	**5.0**	**3.1**	**4.8**	**5.5**
Porosira pseudodenticula		0.0	0.0	0.0	0.2	0.0	0.0	0.0	0.0	0.2
Proboscia inermis		**0.6**	**0.6**	**0.4**	**0.0**	**0.7**	**0.0**	**0.0**	**0.0**	**0.4**
Proboscia truncata		0.6	0.0	0.2	0.4	0.0	0.0	0.2	0.0	0.4
***Pseudonitzschia* spp.**		**1.0**	**0.0**	**0.0**	**0.2**	**0.0**	**0.6**	**0.0**	**0.6**	**0.6**
Rhizosolenia antennata f. antennata		**0.0**	**0.0**	**0.0**	**0.2**	**0.0**	**0.0**	**0.0**	**0.0**	**0.0**
Rhizosolenia antennata f. semispina		**0.4**	**0.6**	**0.2**	**0.4**	**0.4**	**0.4**	**0.8**	**0.4**	**0.6**
Rhizosolenia simplex		**0.0**	**0.0**	**0.2**	**0.2**	**0.2**	**0.2**	**0.0**	**0.8**	**0.4**
Stellarima microtrias		0.0	0.0	0.4	0.0	0.2	0.8	0.2	0.0	0.2
Thalassionema nitzschioides		0.0	0.0	0.0	0.0	0.0	0.0	0.0	0.0	0.0
Thalassiosira ambigua		0.0	0.0	0.0	0.0	0.0	0.0	0.0	0.0	0.0
***Thalassiosira antarctica* rs (cold)**		**0.6**	**9.8**	**7.1**	**8.5**	**9.9**	**2.2**	**2.0**	**1.4**	**2.0**
Thalassiosira antarctica rs warm)		0.0	0.2	0.2	0.2	0.0	0.0	0.0	0.0	0.0
Thalassiosira antarctica veg.		0.0	1.0	0.4	0.0	0.7	0.0	0.0	0.0	0.0
Thalassiosira gracilis v. expecta		*0.0*	*0.0*	*0.2*	*0.0*	*0.2*	*0.0*	*0.0*	*0.0*	*0.0*
Thalassiosira gracilis v. gracilis		***1.6***	***0.2***	***1.9***	***1.3***	***1.5***	***1.6***	***0.6***	***1.4***	***1.4***
Thalassiosira lentiginosa		***0.8***	***0.4***	***1.7***	***0.4***	***1.7***	***1.0***	***1.2***	***0.6***	***1.0***
Thalassiosira oestrupii		*0.0*	*0.4*	*0.0*	*0.2*	*0.0*	*0.0*	*0.0*	*0.0*	*0.0*
Thalassiosira oliveriana		*0.0*	*0.0*	*0.0*	*0.4*	*0.0*	*0.2*	*0.2*	*0.0*	*0.2*
Thalassiosira ritscheria		*0.0*	*0.0*	*0.0*	*0.0*	*0.0*	*0.0*	*0.0*	*0.0*	*0.0*
Thalassiosira spp.		0.4	0.4	1.7	0.9	0.4	0.2	0.0	0.0	0.4
Thalassiosira tealata		0.0	0.0	0.0	0.0	0.0	0.0	0.0	0.0	0.0
Thalassiosira trifulta		**0.0**	**0.2**	**0.0**	**0.0**	**0.0**	**0.2**	**0.4**	**0.2**	**0.4**
Thalassiosira tumida		0.4	0.6	0.2	0.4	0.4	0.6	0.4	0.4	0.2
Thalassiothrix antarctica		**0.6**	**0.2**	**0.8**	**0.0**	**0.4**	**0.2**	**0.2**	**0.2**	**0.2**
Thalassiothrix/nema/toxon		0.0	0.0	0.2	0.0	0.2	0.0	0.0	0.0	0.0
Trichotoxon reinboldii		0.6	0.2	0.6	0.2	0.2	0.4	0.2	0.0	0.0
Unidentified centrics		0.0	0.6	0.0	0.0	0.2	0.0	0.0	0.0	0.0
Unidentified pennates		0.0	0.0	0.0	0.0	0.2	0.0	0.0	0.0	0.0

Table A3.02. Table showing the distribution by sample of all diatom species in core IODP-318-U1357B from discrete samples of laminae described using BSEI. Diatom species abundances are given as % of CRS-free total assemblage, and those included in PCA are in bold. The area of the settling beaker is 7854 mm^2 and the area of the field of view is 0.00018 mm^2. Abbreviations used in species list are: rs – resting spores; veg. – vegetative cells.

CRS-free species abundance	Core section	5H	5H	5H	5H	5H	5H	6H	5H	5H
	Depth in section (cm)	45	57	121.5	134.5	113.7	126	56	44.3	133
	Lamina type	A3	A3	A3	A3	A3	A3	A3	B3	B3
	FOV	69	42	65	57	50	36	28	50	62
	Dry mass (g)	0.0029	0.0024	0.0026	0.003	0.0029	0.003	0.0029	0.0025	0.0024
	No. valves total	510	739	508	501	500	515	612	501	517
	CRS valves	193	486	245	201	228	118	358	171	113
	% CRS	37.84	65.76	48.22	40.11	45.6	22.91	58.49	34.13	21.85
Actinocylus actinochilus		0.32	0.00	0.00	0.00	0.00	0.00	0.00	0.30	0.00
Asteromphalus heptactis		0.00	0.00	0.00	0.00	0.00	0.00	0.00	0.00	0.00
Asteromphalus hookeri		0.32	0.00	0.38	0.00	0.00	0.00	0.00	0.61	0.50
Asteromphalus hyalinus		0.00	0.00	0.00	0.00	0.00	0.00	0.00	0.00	0.00
Asteromphalus parvulus		0.00	0.00	0.00	0.00	0.00	0.00	0.00	0.00	0.00
Azpeitia tabularis		0.00	0.00	0.00	0.00	0.00	0.00	0.00	0.00	0.25
Chaetoceros - Hyalochaete		2.21	3.56	0.00	0.67	0.74	0.50	0.39	4.55	1.49
Chaetoceros - Phaeoceros		**13.56**	**8.70**	**6.84**	**11.67**	**8.46**	**18.14**	**3.94**	**25.45**	**23.51**
Cocconeis spp. Large		0.00	0.00	0.00	0.00	0.00	0.00	0.00	0.00	0.00
Corethron pennatum		**0.00**	**1.19**	**1.14**	**0.33**	**2.57**	**1.26**	**1.57**	**1.21**	**5.45**
Coscinodiscus bouvet		0.32	0.00	0.00	0.00	0.00	0.00	0.00	0.00	0.00
***Eucampia antarctica* rs**		**0.32**	**0.00**	**0.38**	**0.00**	**0.00**	**0.50**	**0.00**	**0.61**	**0.50**
Eucampia antarctica veg		0.63	1.19	1.14	0.33	0.37	1.01	1.18	0.61	0.74
Fragilariopsis curta		**37.54**	**30.04**	**29.66**	**29.67**	**29.41**	**34.26**	**43.70**	**27.88**	**28.47**
Fragilariopsis cylindrus		**11.99**	**10.67**	**3.42**	**19.33**	**16.91**	**5.04**	**13.39**	**8.18**	**5.69**
Fragilariopsis kerguelensis		**3.47**	**9.09**	**9.13**	**6.67**	**6.25**	**3.78**	**7.87**	**4.55**	**4.95**
Fragilariopsis obliquecostata		**1.89**	**2.37**	**3.80**	**1.33**	**1.47**	**0.25**	**1.18**	**0.30**	**2.97**
Fragilariopsis pseudonana		0.32	0.00	0.00	0.00	0.00	0.00	0.00	0.30	0.25
Fragilariopsis rhombica		**9.15**	**11.46**	**23.57**	**16.00**	**15.81**	**25.19**	**12.60**	**8.79**	**13.61**
Fragilariopsis ritscheri		**2.52**	**1.98**	**2.66**	**3.33**	**1.84**	**2.02**	**0.79**	**1.52**	**0.50**
Fragilariopsis separanda		**0.63**	**0.00**	**1.52**	**0.33**	**0.74**	**0.76**	**0.00**	**0.00**	**0.25**
Fragilariopsis spp.		0.00	0.00	0.00	0.00	0.00	0.00	0.00	0.00	0.00
Fragilariopsis sublinearis		**4.10**	**3.56**	**3.80**	**2.33**	**4.04**	**2.02**	**2.76**	**3.64**	**2.72**
Fragilariopsis vanheurckii		0.00	0.79	0.00	0.33	0.00	0.00	0.00	0.00	0.00
Haslea spp.		0.00	0.00	0.00	0.00	0.00	0.00	0.00	0.00	0.00
Licmophora spp.		0.63	0.00	0.00	0.00	0.00	0.00	0.00	0.00	0.00
Navicula spp.		0.63	1.58	1.90	1.00	1.84	0.00	0.39	0.30	0.00
Nitzschia spp.		0.32	0.00	0.38	0.00	0.00	0.00	0.00	0.30	0.00
***Porosira glacialis* rs**		**1.89**	**0.40**	**2.66**	**0.33**	**2.21**	**0.76**	**0.79**	**1.52**	**1.73**
Porosira pseudodenticula		0.32	0.00	0.38	0.00	0.00	0.00	0.00	0.00	0.00
Proboscia inermis		**0.95**	**0.40**	**0.38**	**0.33**	**0.37**	**0.25**	**0.00**	**0.30**	**1.98**
Proboscia truncata		0.32	0.00	0.38	1.00	0.00	0.76	0.79	0.91	0.50
Pseudonitzschia spp.		1.26	8.70	1.14	1.00	2.57	1.76	5.51	5.76	1.24
Rhizosolenia simplex		0.32	0.00	0.00	0.00	0.00	0.00	0.00	0.00	0.00
Rhizosolenia antennata* f. *semispina		**0.95**	**0.00**	**0.00**	**0.67**	**0.00**	**0.00**	**0.00**	**0.91**	**0.50**
Rhizosolenia antennata f. *antennata*		0.00	0.00	0.00	0.00	0.00	0.00	0.00	0.00	0.00
Stellarima microtrias		0.00	0.00	0.00	0.00	0.00	0.00	0.00	0.00	0.25
Thalassiosira ambigua		0.32	0.40	0.38	0.00	1.10	0.00	0.79	0.00	0.50
***Thalassiosira antarctica* rs (cold)**		**0.95**	**0.40**	**1.90**	**1.33**	**0.37**	**0.25**	**1.18**	**0.30**	**0.25**
Thalassiosira antarctica rs (warm)		0.00	0.00	0.00	0.00	0.00	0.00	0.00	0.00	0.00
Thalassiosira antarctica veg.		0.00	0.40	0.00	0.00	0.00	0.00	0.00	0.00	0.00
Thalassiosira frenguellii		0.00	0.00	0.00	0.00	0.00	0.00	0.00	0.30	0.00
Thalassiosira gracilis v. *expecta*		0.00	0.00	0.00	0.00	0.00	0.00	0.00	0.00	0.00
Thalassiosira gracilis* v. *gracilis		**0.63**	**0.00**	**0.76**	**0.67**	**1.10**	**0.50**	**0.00**	**0.00**	**0.25**
Thalassiosira lentiginosa		**0.63**	**0.00**	**1.52**	**1.00**	**0.74**	**0.00**	**0.79**	**0.91**	**0.25**
Thalassiosira lineata		0.00	0.00	0.00	0.00	0.00	0.00	0.00	0.00	0.00
Thalassiosira longissima		0.00	0.00	0.00	0.00	0.00	0.00	0.00	0.00	0.00
Thalassiosira oestrupii		0.00	0.00	0.00	0.00	0.00	0.00	0.00	0.00	0.00
Thalassiosira oliveriana		0.00	0.00	0.00	0.00	0.00	0.00	0.00	0.00	0.00
Thalassiosira perpusilla		0.00	0.00	0.00	0.00	0.00	0.00	0.00	0.00	0.00
Thalassiosira ritscheria		0.00	0.00	0.00	0.00	0.00	0.00	0.00	0.00	0.00
Thalassiosira spp.		0.00	0.00	0.00	0.00	0.00	0.00	0.00	0.00	0.00
Thalassiosira trifulata		0.00	0.00	0.00	0.33	0.37	0.00	0.00	0.00	0.25
Thalassiosira tumida		0.00	0.00	0.00	0.00	0.37	1.01	0.39	0.00	0.25
Thalassiothrix antarctica		0.32	0.40	0.38	0.00	0.00	0.00	0.00	0.00	0.00
Trichotoxon reinboldii		0.00	0.00	0.38	0.00	0.00	0.00	0.00	0.00	0.25
Unidentified centrics		0.32	0.00	0.00	0.00	0.37	0.00	0.00	0.00	0.00

Table A3.02 continued.

CRS-free species abundance	Core section	5H	5H	7H	5H	5H	5H	6H	6H	5H
	Depth in section (cm)	136.5	142.8	1.5	40	59.5	112.5	1.5	118	53.7
	Lamina type	B3	B3	B3	C3	C3	C3	C3	C3	D3
	FOV	59	30	41	59	40	70	65	82	52
	Dry mass (g)	0.0029	0.0029	0.003	0.0025	0.003	0.0027	0.0026	0.003	0.003
	No. valves total	520	512	508	537	525	500	550	531	601
	CRS valves	195	316	145	281	166	185	288	162	348
	% CRS	37.5	61.71	28.54	52.32	31.61	37	52.36	30.50	57.90
Actinocylus actinochilus		0.31	0.00	0.00	0.39	0.00	0.00	0.00	0.54	0.40
Asteromphalus heptactis		0.00	0.00	0.00	0.00	0.00	0.00	0.00	0.00	0.00
Asteromphalus hookeri		0.00	1.02	0.00	0.39	0.00	0.32	0.00	0.54	0.79
Asteromphalus hyalinus		0.00	0.00	0.00	0.00	0.00	0.00	0.00	0.00	0.00
Asteromphalus parvulus		0.00	0.00	0.00	0.39	0.00	0.00	0.38	0.00	0.00
Azpeitia tabularis		0.00	0.00	0.00	0.00	0.00	0.00	0.38	0.00	0.00
Chaetoceros - Hyalochaete		1.23	3.57	1.65	5.08	0.56	0.32	0.00	1.90	2.37
Chaetoceros - Phaeoceros		**23.69**	**25.51**	**29.48**	**11.33**	**11.70**	**8.25**	**12.98**	**12.20**	**9.88**
Cocconeis spp. Large		0.00	0.00	0.00	0.00	0.28	0.00	0.00	0.00	0.00
Corethron pennatum		**1.54**	**2.04**	**0.83**	**0.78**	**0.28**	**5.08**	**0.38**	**0.00**	**0.00**
Coscinodiscus bouvet		0.31	0.00	0.00	0.00	0.00	0.00	0.00	0.00	0.00
***Eucampia antarctica* rs**		**0.00**	**0.51**	**0.00**	**1.17**	**0.56**	**0.00**	**0.76**	**0.00**	**0.79**
Eucampia antarctica veg		0.00	1.02	0.00	0.00	0.56	1.27	1.15	1.36	0.40
Fragilariopsis curta		**17.23**	**34.18**	**23.97**	**30.86**	**37.33**	**32.06**	**27.86**	**24.39**	**27.27**
Fragilariopsis cylindrus		**6.77**	**8.67**	**11.29**	**5.47**	**1.11**	**11.43**	**4.20**	**8.67**	**2.77**
Fragilariopsis kerguelensis		**7.38**	**4.08**	**1.93**	**5.86**	**13.09**	**8.89**	**12.98**	**8.94**	**15.81**
Fragilariopsis obliquecostata		**1.23**	**1.02**	**0.83**	**0.78**	**1.11**	**1.27**	**0.76**	**0.00**	**2.77**
Fragilariopsis pseudonana		0.62	0.00	1.38	0.00	0.00	0.00	0.38	0.27	0.00
Fragilariopsis rhombica		**20.00**	**4.08**	**12.67**	**11.33**	**19.50**	**18.73**	**12.21**	**16.53**	**17.39**
Fragilariopsis ritscheri		**3.38**	**1.53**	**1.10**	**3.13**	**0.56**	**0.95**	**6.11**	**2.44**	**3.16**
Fragilariopsis separanda		**0.92**	**0.00**	**0.55**	**0.00**	**0.84**	**0.95**	**0.38**	**3.25**	**0.40**
Fragilariopsis spp.		0.00	0.00	0.55	0.00	0.00	0.00	0.00	0.00	0.00
Fragilariopsis sublinearis		**4.00**	**3.57**	**1.38**	**3.91**	**2.51**	**3.81**	**4.58**	**4.34**	**2.37**
Fragilariopsis vanheurckii		0.31	1.02	0.83	0.39	0.00	0.00	1.15	0.54	0.00
Haslea spp.		0.00	0.00	0.00	0.00	0.56	0.00	0.00	0.00	0.00
Licmophora spp.		0.00	0.00	0.00	0.00	0.00	0.00	0.00	0.00	0.00
Navicula spp.		0.62	0.51	0.55	0.00	0.84	0.63	0.76	1.36	0.79
Nitzschia spp.		0.00	0.00	0.00	1.17	0.00	0.00	0.00	0.00	0.00
***Porosira glacialis* rs**		**4.00**	**0.00**	**0.55**	**4.69**	**1.11**	**0.32**	**1.15**	**0.00**	**5.53**
Porosira pseudodenticula		0.62	0.00	0.00	0.39	0.00	0.32	0.00	0.27	0.40
Proboscia inermis		**0.92**	**1.02**	**3.31**	**1.17**	**0.84**	**0.32**	**0.38**	**1.36**	**0.40**
Proboscia truncata		0.00	0.00	1.65	0.00	0.84	0.00	0.38	1.36	0.00
Pseudonitzschia spp.		1.54	2.55	3.31	5.86	1.39	1.59	2.29	4.34	2.77
Rhizosolenia simplex		0.00	0.00	0.55	0.00	0.00	0.00	0.00	0.00	0.00
Rhizosolenia antennata* f. *semispina		**0.31**	**0.00**	**0.55**	**0.78**	**0.56**	**0.63**	**2.67**	**1.08**	**0.00**
Rhizosolenia antennata f. *antennata*		0.00	0.00	0.00	0.00	0.00	0.00	0.00	0.00	0.00
Stellarima microtrias		0.00	0.00	0.00	0.39	0.00	0.00	0.00	0.00	0.00
Thalassiosira ambigua		0.00	0.00	0.00	0.39	0.28	0.00	0.76	0.00	0.40
***Thalassiosira antarctica* rs (cold)**		**0.31**	**1.53**	**0.00**	**0.39**	**0.28**	**0.63**	**0.76**	**1.36**	**1.19**
Thalassiosira antarctica rs (warm)		0.00	0.00	0.00	0.00	0.00	0.00	0.00	0.27	0.00
Thalassiosira antarctica veg.		0.00	0.00	0.00	0.78	0.00	0.00	0.00	0.00	0.00
Thalassiosira frenguellii		0.00	0.00	0.00	0.00	0.56	0.00	0.38	0.00	0.00
Thalassiosira gracilis v. *expecta*		0.00	0.00	0.00	0.00	0.28	0.00	0.00	0.00	0.00
Thalassiosira gracilis* v. *gracilis		**1.23**	**1.02**	**0.00**	**0.78**	**0.84**	**0.63**	**0.76**	**1.36**	**1.19**
Thalassiosira lentiginosa		**0.62**	**0.51**	**0.00**	**0.39**	**0.28**	**0.32**	**1.15**	**0.54**	**0.00**
Thalassiosira lineata		0.00	0.00	0.28	0.00	0.00	0.00	0.00	0.00	0.00
Thalassiosira longissima		0.00	0.00	0.00	0.00	0.00	0.00	0.00	0.00	0.00
Thalassiosira oestrupii		0.00	0.00	0.00	0.00	0.00	0.00	0.00	0.00	0.00
Thalassiosira oliveriana		0.00	0.00	0.00	0.00	0.00	0.00	0.76	0.00	0.00
Thalassiosira perpusilla		0.00	0.00	0.00	0.00	0.00	0.00	0.00	0.00	0.00
Thalassiosira ritscheria		0.00	0.00	0.00	0.00	0.00	0.00	0.00	0.00	0.00
Thalassiosira spp.		0.00	0.00	0.55	0.39	0.00	0.00	0.00	0.00	0.40
Thalassiosira trifulata		0.31	0.51	0.00	0.00	0.28	0.32	0.38	0.54	0.00
Thalassiosira tumida		0.00	0.00	0.00	0.78	0.28	0.32	0.00	0.00	0.00
Thalassiothrix antarctica		0.31	0.51	0.28	0.00	0.28	0.32	0.38	0.00	0.00
Trichotoxon reinboldii		0.31	0.00	0.00	0.39	0.56	0.32	0.38	0.27	0.40
Unidentified centrics		0.00	0.00	0.00	0.00	0.00	0.00	0.00	0.00	0.00

Table A3.02 continued.

CRS-free species abundance	Core section	5H	5H	5H	5H	5H	5H	5H	5H	5H
	Depth in section (cm)	60	70	81	99.5	135.6	52.5	64	85.5	106.6
	Lamina type	D3	D3	D3	D3	D3	E3	E3	E3	E3
	FOV	41	63	49	43	68	66	55	56	53
	Dry mass (g)	0.0029	0.0026	0.0023	0.003	0.0029	0.0026	0.0026	0.0026	0.0027
	No. valves total	508	1147	550	568	515	1009	596	500	1334
	CRS valves	257	895	297	314	263	759	345	230	1080
	% CRS	50.59	78.03	54	55.28	51.07	75.22	57.89	46.00	80.96
Actinocylus actinochilus		0.00	0.00	0.40	0.00	0.79	0.00	0.00	0.37	0.79
Asteromphalus heptactis		0.00	0.00	0.00	0.00	0.00	0.00	0.00	0.00	0.00
Asteromphalus hookeri		0.80	0.00	0.40	0.79	0.40	0.00	0.40	0.00	0.00
Asteromphalus hyalinus		0.00	0.00	0.00	0.00	0.00	0.00	0.00	0.00	0.39
Asteromphalus parvulus		0.00	0.00	0.00	0.00	0.40	0.40	0.00	0.74	0.00
Azpeitia tabularis		0.40	0.40	0.00	0.00	0.00	0.00	0.00	0.74	0.00
Chaetoceros - Hyalochaete		2.39	0.79	0.40	1.18	0.79	2.00	4.38	0.00	2.36
Chaetoceros - Phaeoceros		**7.97**	**17.06**	**6.72**	**6.30**	**9.52**	**6.80**	**9.56**	**3.70**	**11.02**
Cocconeis spp. Large		0.00	0.00	0.40	0.00	0.00	0.00	0.00	0.00	0.00
Corethron pennatum		**0.40**	**0.00**	**0.40**	**1.57**	**1.98**	**0.80**	**0.80**	**0.37**	**1.18**
Coscinodiscus bouvet		0.40	0.40	0.00	0.00	0.00	0.00	0.00	0.00	0.39
***Eucampia antarctica* rs**		**0.00**	**0.40**	**0.00**	**0.79**	**0.00**	**0.00**	**0.00**	**0.74**	**0.00**
Eucampia antarctica veg		3.19	2.78	0.79	2.76	1.59	1.60	1.20	1.11	4.33
Fragilariopsis curta		**15.54**	**17.86**	**30.43**	**15.35**	**10.71**	**14.40**	**15.14**	**13.70**	**14.57**
Fragilariopsis cylindrus		**10.36**	**5.56**	**5.14**	**2.36**	**12.70**	**7.60**	**8.76**	**4.07**	**9.06**
Fragilariopsis kerguelensis		**15.94**	**14.29**	**9.09**	**14.17**	**9.52**	**6.40**	**6.37**	**5.19**	**8.27**
Fragilariopsis obliquecostata		**5.58**	**3.97**	**2.37**	**1.18**	**1.59**	**2.00**	**0.80**	**2.96**	**0.39**
Fragilariopsis pseudonana		0.00	0.40	1.19	0.79	0.00	0.00	0.00	0.00	0.00
Fragilariopsis rhombica		**13.55**	**7.94**	**14.62**	**22.83**	**24.60**	**12.40**	**8.76**	**9.26**	**6.69**
Fragilariopsis ritscheri		**1.99**	**1.19**	**1.98**	**2.76**	**2.78**	**1.60**	**0.00**	**0.74**	**1.97**
Fragilariopsis separanda		**1.20**	**0.40**	**1.19**	**3.15**	**0.79**	**0.80**	**0.80**	**2.22**	**2.36**
Fragilariopsis spp.		0.00	0.00	0.00	0.00	1.19	0.00	0.00	0.74	0.00
Fragilariopsis sublinearis		**3.59**	**1.59**	**7.51**	**3.94**	**3.57**	**4.80**	**3.19**	**1.11**	**5.91**
Fragilariopsis vanheurckii		0.00	0.00	0.40	0.79	0.00	0.80	0.00	0.74	0.00
Haslea spp.		0.00	0.00	0.00	0.00	0.00	0.00	0.00	0.00	0.00
Licmophora spp.		0.40	0.00	0.00	0.00	0.00	0.00	0.00	0.00	0.00
Navicula spp.		1.20	0.79	0.79	0.00	0.00	0.80	0.80	0.00	1.18
Nitzschia spp.		0.00	0.40	0.40	0.39	0.79	0.00	0.80	0.00	0.79
***Porosira glacialis* rs**		**3.98**	**2.78**	**2.77**	**3.54**	**5.16**	**18.80**	**23.51**	**39.26**	**13.39**
Porosira pseudodenticula		0.40	0.40	0.00	0.79	1.19	0.40	1.20	0.00	0.00
Proboscia inermis		**0.00**	**1.19**	**3.16**	**1.57**	**0.40**	**1.60**	**0.40**	**0.00**	**1.97**
Proboscia truncata		0.40	0.79	1.19	0.39	0.00	0.40	0.40	0.00	0.79
Pseudonitzschia spp.		2.39	7.94	1.58	6.69	4.37	8.00	6.77	1.48	5.12
Rhizosolenia simplex		0.00	0.00	0.00	0.00	0.00	0.80	0.00	0.00	0.00
Rhizosolenia antennata* f. *semispina		**0.80**	**0.79**	**3.16**	**1.18**	**0.00**	**0.80**	**0.80**	**0.00**	**0.39**
Rhizosolenia antennata f. *antennata*		0.00	0.00	0.00	0.00	0.00	0.00	0.00	0.00	0.79
Stellarima microtrias		0.00	0.40	0.00	0.00	0.00	0.40	0.40	1.11	0.79
Thalassiosira ambigua		0.00	0.40	0.00	0.00	1.19	0.00	0.00	0.37	0.39
***Thalassiosira antarctica* rs (cold)**		**2.39**	**2.38**	**0.79**	**1.18**	**1.59**	**3.20**	**1.20**	**3.33**	**3.54**
Thalassiosira antarctica rs (warm)		0.00	0.00	0.00	0.00	0.00	0.00	0.00	0.00	0.00
Thalassiosira antarctica veg.		0.00	0.00	0.00	0.39	0.00	0.40	0.00	0.37	0.39
Thalassiosira frenguellii		0.00	0.00	0.40	0.00	0.40	0.00	0.00	1.85	0.00
Thalassiosira gracilis v. *expecta*		0.00	0.00	0.00	0.00	0.00	0.00	0.00	0.00	0.00
Thalassiosira gracilis* v. *gracilis		**2.39**	**0.79**	**1.19**	**0.79**	**0.40**	**0.00**	**1.59**	**1.11**	**0.00**
Thalassiosira lentiginosa		**0.40**	**3.57**	**0.00**	**1.97**	**1.19**	**0.40**	**0.80**	**0.00**	**0.00**
Thalassiosira lineata		0.00	0.00	0.00	0.00	0.00	0.00	0.00	0.00	0.00
Thalassiosira longissima		0.00	0.00	0.00	0.00	0.00	0.00	0.00	0.00	0.00
Thalassiosira oestrupii		0.00	0.00	0.00	0.00	0.00	0.00	0.00	0.00	0.00
Thalassiosira oliveriana		0.00	0.00	0.00	0.00	0.00	0.00	0.00	0.00	0.00
Thalassiosira perpusilla		0.00	0.00	0.00	0.00	0.00	0.00	0.00	0.00	0.00
Thalassiosira ritscheria		0.00	0.00	0.00	0.00	0.00	0.00	0.00	0.00	0.00
Thalassiosira spp.		0.40	0.00	0.00	0.00	0.00	0.00	0.00	1.48	0.00
Thalassiosira trifulata		0.80	0.79	0.79	0.39	0.00	0.40	0.40	0.00	0.00
Thalassiosira tumida		0.40	1.19	0.00	0.00	0.00	0.40	0.00	0.00	0.00
Thalassiothrix antarctica		0.40	0.00	0.00	0.00	0.00	0.40	0.40	0.00	0.79
Trichotoxon reinboldii		0.00	0.40	0.00	0.00	0.40	0.40	0.40	0.00	0.00
Unidentified centrics		0.00	0.00	0.40	0.00	0.00	0.00	0.00	1.11	0.00

Appendix 4. Wavelet analyses of lamina based time series.

This appendix presents additional wavelet analyses of lamina- and annual-time series that were not presented in the main text. The wavelet analysis was found to typically perform badly on the relatively short time series presented in this study and produces spectral power bands that, despite statistical significance in the wavelet analysis, may not present a realistic assessment of the data, particularly for the datasets in which there are a large number of zero values. For instance, in Figure A4.04 (a) and (b) an approximately 11-year cyclicity is evident at >95% significance; however, both of these can be seen in both instances to result from two large peaks in the data that are ~11-years apart and do not represent an actual trend in the data.

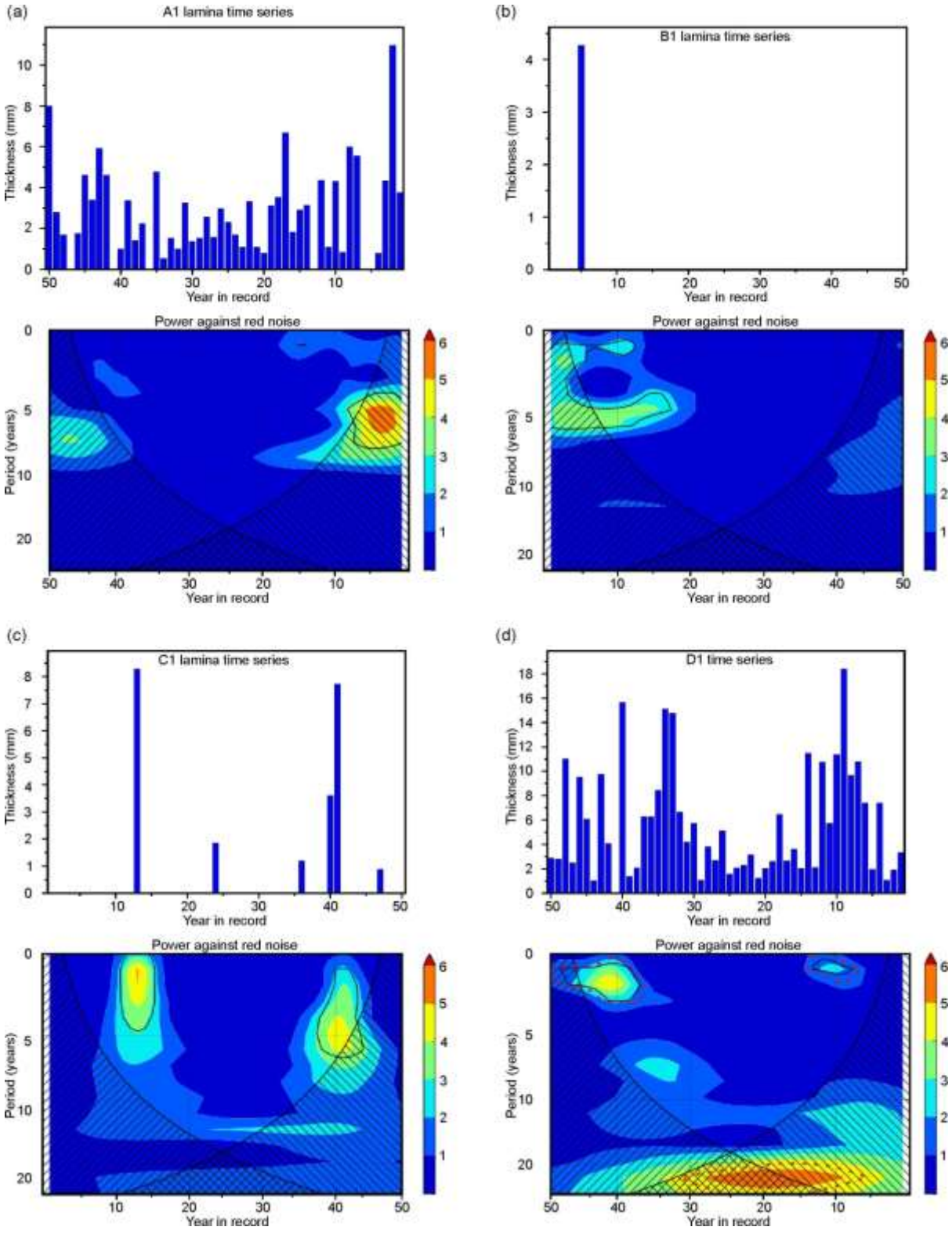

Figure A4.01. Wavelet time series analysis of the continuously laminated 50-year record in core MD03-2601 section XVII (Hypsithermal) relative to a red noise model. (a) A1 lamina time series; (b) B1 lamina time series; (c) C1 lamina time series; (d) D1 lamina time series; (e) E1 lamina time series (next page). Cross hatching indicates regions outside the cone of influence (COI), outside of which attenuation of the signal may occur due to edge effects of the dataset. Black lines indicate spectral power >95% confidence, red dashed line indicates spectral power >90% confidence.

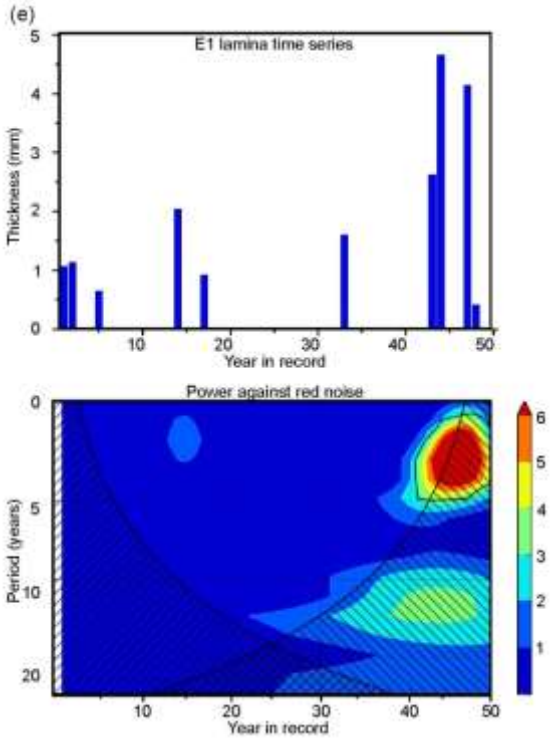

Figure A4.01 continued.

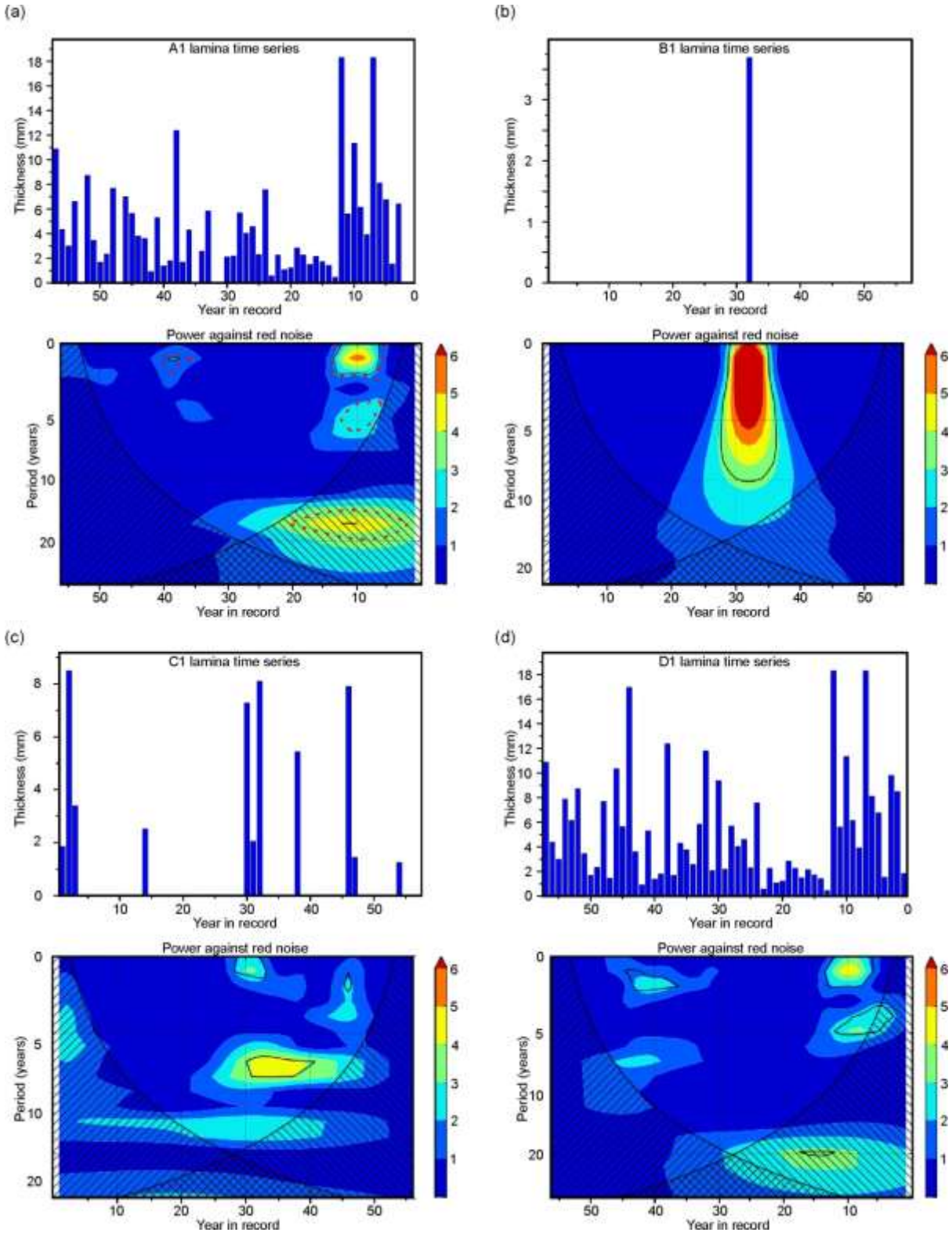

Figure A4.02. Wavelet time series analysis of the continuously laminated 57-year record in core MD03-2601 section XVII (Hypsithermal) relative to a red noise model. (a) A1 lamina time series; (b) B1 lamina time series; (c) C1 lamina time series; (d) D1 lamina time series; (e) E1 lamina time series (next page). Cross hatching indicates regions outside the cone of influence (COI), outside of which attenuation of the signal may occur due to edge effects of the dataset. Black lines indicate spectral power >95% confidence, red dashed line indicates spectral power >90% confidence.

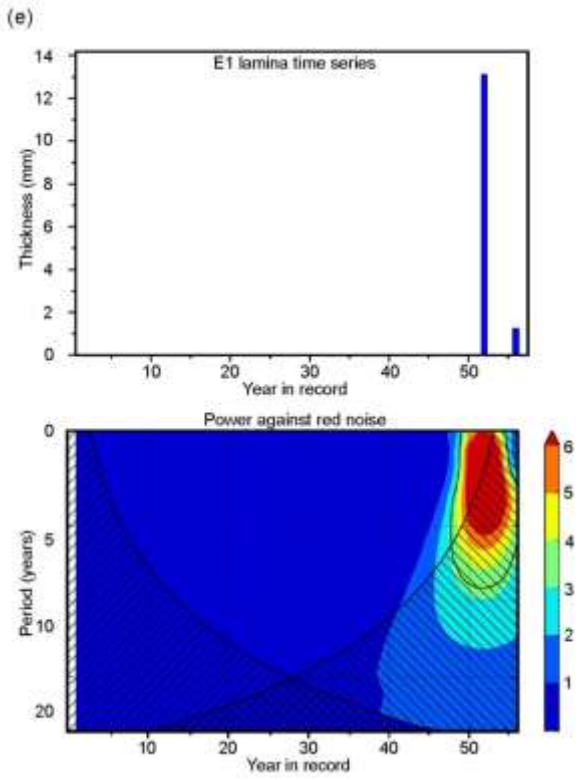

Figure A4.02 continued.

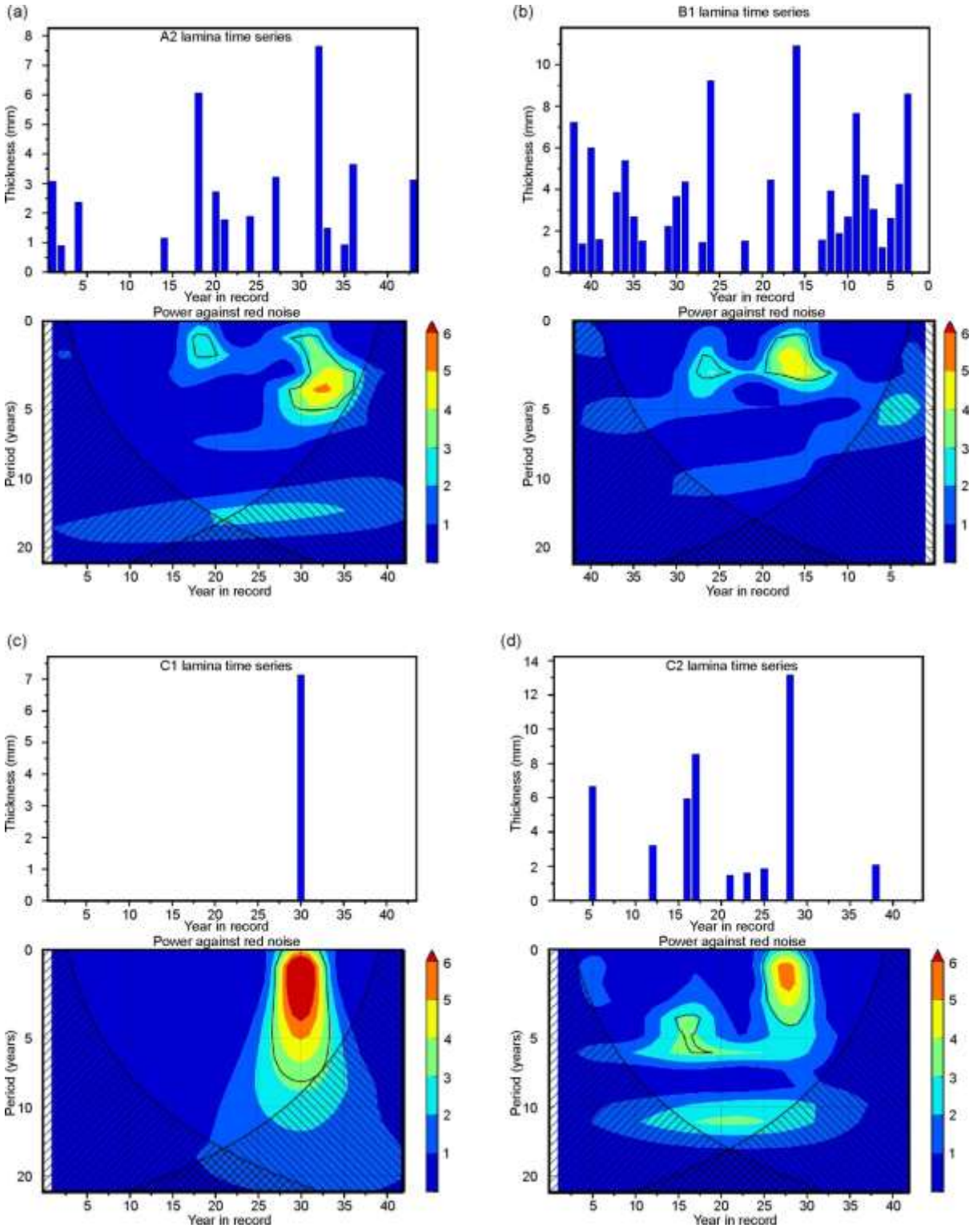

Figure A4.03. Wavelet time series analysis of the continuously laminated 43-year record in core MD03-2601 section VIII (early Neoglacial interval) relative to a red noise model. (a) A2 lamina time series; (b) B1 lamina time series; (c) C1 lamina time series; (d) C2 lamina time series; (e) E1 lamina time series (next page). Cross hatching indicates regions outside the cone of influence (COI), outside of which attenuation of the signal may occur due to edge effects of the dataset. Black lines indicate spectral power >95% confidence.

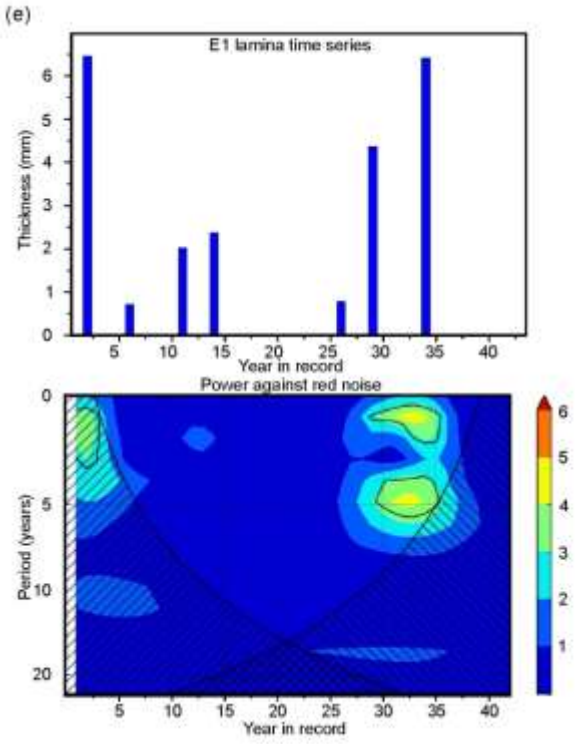

Figure A4.03 continued.

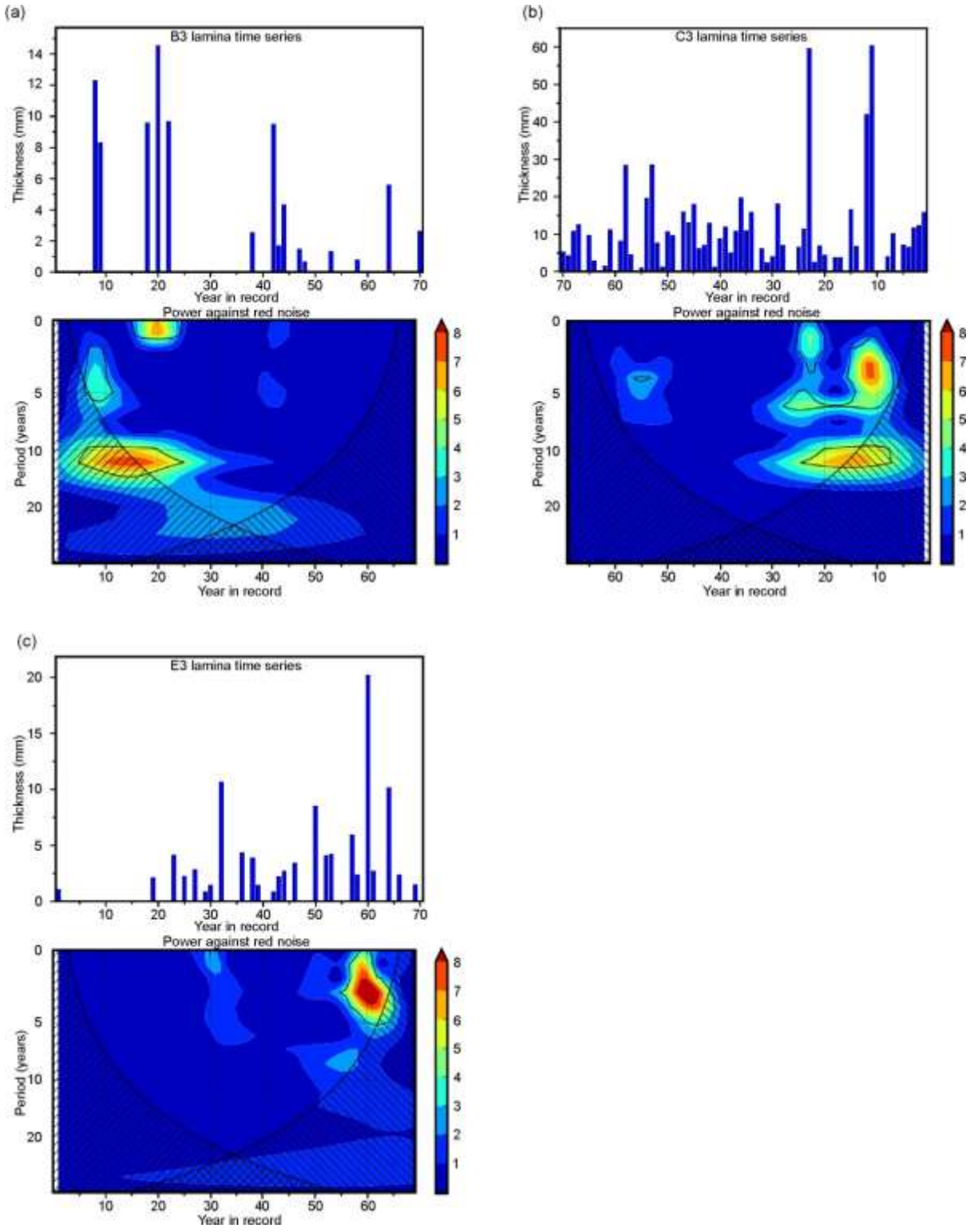

Figure A4.04. Wavelet time series analysis of the continuously laminated 73-year record in core IODP-318-U1357B (Neoglacial) relative to a red noise model. (a) B3 laminae time series; (b) C3 lamina time series; (c) E3 lamina time series. Cross hatching indicates regions outside the cone of influence (COI), outside of which attenuation of the signal may occur due to edge effects of the dataset. Black lines indicate spectral power >95% confidence.

Appendix 5. HBI data

This appendix contains the primary HBI concentration data presented in Chapter 6 (section A5.1), data from attempts at lamina-scale analysis (section A5.2) and measurements of the offset between continuously sampled HBI data and lamina position used for producing the graphic logs presented in Chapter 6.

A5.1 HBI data from continuous 1 cm resolution sampling

Table A5.01. HBI concentrations in all samples from MD03-2601 core section III. Blank values indicate samples which were processed but failed to run properly on the GC-MS.

End depth (cmbsf)	HBI diene concentration	HBI triene concentration
300	0.0	49.5
301	5.2	112.7
302	8.6	153.7
303	5.2	145.3
304	0.0	103.4
305	0.0	0.0
306	0.0	74.6
307	0.0	54.5
308	4.5	57.8
309	3.0	38.2
310	4.0	32.8
311	0.0	47.5
312	0.0	59.8
313	2.3	54.6
314	3.2	58.2
315	0.0	49.4
316		
317	5.5	65.9
318	4.9	73.1
319	5.0	30.2
320	0.0	80.3
321	4.4	64.1
322		
323	0.0	52.0
324	5.9	26.8
325	0.0	52.6
326	0.0	57.2
327	5.4	51.6
328	5.9	77.2
329	2.8	43.5
330	4.1	42.6
331	4.6	51.3
332	2.5	38.0
333	4.3	51.6
334	1.6	38.5
335	0.0	32.6
336	5.7	37.6
337	0.0	45.3
338		
339	4.3	29.0

End depth (cmbsf)	HBI diene concentration	HBI triene concentration
340	5.2	50.9
341	2.6	21.8
342	3.5	30.0
343	0.0	38.8
344	0.0	27.4
345	5.9	44.1
346	4.8	27.9
347	7.4	30.4
348		
349	3.6	20.6
350	0.0	58.7
351	0.0	42.5
352	0.0	68.9
353	3.7	58.9
354	2.9	48.4
355	6.0	71.0
356	5.4	83.2
357	0.0	68.7
358	0.0	79.5
359	0.0	53.2
360	0.0	55.4
361	20.0	48.6
362	20.4	67.4
363	20.0	48.0
364	0.0	49.0
365	0.0	41.8
366	3.1	45.0
367	3.0	36.0
368	0.0	47.1
369	0.0	60.1
370	0.0	61.1
371	4.9	46.8
372	6.6	37.2
373	3.4	39.8
374	4.0	37.2
375	3.4	49.5
376	0.0	44.5
377	1.7	23.0
378	4.2	53.6
379	0.0	49.0
380	4.2	41.6
381	3.8	42.8
382	4.2	64.2
383	4.5	41.3

End depth (cmbsf)	HBI diene concentration	HBI triene concentration
384	3.5	46.4
385	0.0	40.7
386	0.0	38.1
387	0.0	39.4
388	2.5	60.4
389	0.0	70.1
390	0.0	71.3
391	0.0	58.3
392	3.1	51.5
393	3.9	69.3
394	6.2	85.6
395	7.9	59.2
396	7.7	34.1
397	13.2	26.5
398	6.0	20.1
399	7.4	41.0
400	14.7	64.8
401	11.5	71.6
402	3.7	31.9
403	0.0	27.4
404	0.0	32.7
405	5.4	69.2
406	9.4	69.7
407	10.5	89.5
408	5.9	99.9
409	5.7	143.3
410	2.8	88.8
411	5.2	52.0
412	7.7	31.6
413	4.4	26.3
414	7.0	47.6
415	6.9	35.7
416	3.1	51.1
417	2.6	38.9
418	0.0	36.6
419	3.9	38.5
420	0.0	33.9
421	2.1	50.2
422	5.1	47.9
423	4.5	56.5
424	10.9	42.9
425	6.2	39.6
426	5.7	44.1
427	3.2	36.5

End depth (cmbsf)	HBI diene concentration	HBI triene concentration
428	7.2	53.7
429	0.0	48.1
430	7.2	61.6
431	5.3	58.8
432	0.0	43.3
433	0.0	39.5
434	9.9	184.1
435	0.0	0.0
436	0.0	54.9
437	4.0	48.7
438	1.7	13.8
439		
440	7.5	45.8
441	5.5	42.2
442	0.0	46.6
443	0.0	51.6
444	1.5	34.4
445	5.1	35.8
446	2.8	37.1
447	9.9	28.6

Table A5.02. HBI concentrations in all samples from MD03-2601 core section VIII. Blank values indicate samples which were processed but failed to run properly on the GC-MS.

End depth (cmbsf)	HBI diene concentration	HBI triene concentration
1050	2.1	10.6
1051	3.4	20.0
1052	0.0	25.9
1053	3.0	19.3
1054	1.8	14.5
1055	2.5	21.7
1056	2.8	20.9
1057	2.9	13.5
1058		
1059	2.6	14.3
1060	2.9	11.3
1061	1.9	8.7
1062		
1063	0.2	16.9
1064	0.8	14.2
1065	0.0	25.7
1066	1.9	33.4
1067	0.6	35.3
1068	2.3	27.2
1069	0.8	21.0
1070	1.0	18.9
1071	1.8	17.9
1072	2.1	17.3
1073	1.0	7.4
1074	1.1	23.4
1075	0.4	9.1
1076	0.9	14.0
1077	0.3	16.5
1078	0.5	19.0
1079	0.4	21.1
1080	0.5	18.4
1081	0.5	17.3
1082	0.4	33.1
1083	1.8	19.0
1084	3.6	26.7
1085	2.5	13.6
1086		
1087	0.6	19.2
1088	1.2	15.6
1089	1.9	16.4
1090	3.5	16.8
1091	1.9	17.8

End depth (cmbsf)	HBI diene concentration	HBI triene concentration
1092	0.5	9.5
1093	1.9	27.8
1094	1.0	12.5
1095	0.7	19.4
1096	0.9	17.4
1097	0.3	21.4
1098	0.6	21.3
1099	1.0	16.5
1100	0.8	10.8
1101	0.5	13.3
1102	1.3	26.2
1103	1.1	16.8
1104	3.1	20.8
1105	2.2	11.9
1106	6.2	16.7
1107	1.5	16.1
1108	0.4	14.3
1109	0.9	26.2
1110	0.6	21.5
1111	0.3	12.2
1112	0.4	34.4
1113	0.4	30.4
1114	0.1	20.0
1115	0.0	18.2
1116	0.2	16.5
1117	0.3	13.3
1118	0.4	29.1
1119	0.6	21.4
1120	0.0	8.9
1121	0.0	10.8
1122	0.5	16.0
1123	0.0	16.7
1124	0.0	19.9
1125	0.0	16.7
1126	0.3	14.2
1127		
1128	0.0	11.2
1129	2.0	19.6
1130	0.6	8.8
1131	0.5	12.8
1132	0.0	15.0
1133	0.1	20.0
1134	0.5	12.6
1135	0.1	10.7

End depth (cmbsf)	HBI diene concentration	HBI triene concentration
1136		
1137	0.3	6.4
1138	0.3	20.9
1139	0.0	32.0
1140	0.0	28.8
1141	1.3	30.7
1142	0.4	33.2
1143	0.3	31.7
1144	2.3	17.6
1145	0.5	22.6
1146	0.8	33.4
1147	0.8	28.2
1148	0.0	13.8
1149	0.1	10.6
1150	0.0	19.1
1151	0.5	14.4
1152	0.3	16.8
1153	0.5	11.3
1154	1.4	18.5
1155	0.2	14.6
1156	0.7	16.6
1157	0.5	14.4
1158	0.0	12.8
1159	0.0	16.7
1160	0.6	13.5
1161	0.8	21.2
1162	0.4	16.1
1163	0.8	10.4
1164	0.0	14.6
1165	0.6	9.8
1166	0.8	12.1
1167	0.7	16.6
1168	0.4	13.9
1169	0.2	8.9
1170	0.0	10.8
1171	0.2	11.0
1172	0.2	20.6
1173	0.3	11.4
1174	0.0	22.7
1175	0.2	18.6
1176	0.1	15.3
1177	0.0	22.2
1178	0.3	23.8
1179		

End depth (cmbsf)	HBI diene concentration	HBI triene concentration
1180	0.0	14.2
1181	0.2	11.4
1182	0.3	21.0
1183	0.1	15.2
1184	0.2	15.3
1185	1.5	26.0
1186	0.5	11.0
1187	0.3	8.7
1188	0.5	18.6
1189	0.3	18.8
1190	0.0	19.9
1191	0.3	12.2
1192	0.5	26.1
1193	0.1	18.2
1194	0.0	21.0
1195	0.0	43.4
1196	0.9	30.0
1197	1.1	26.4
1198	0.5	15.3

Table A5.03. HBI concentrations in all samples from MD03-2601 core section XVII. Blank values indicate samples which were processed but failed to run properly on the GC-MS.

End depth (cmbsf)	HBI diene concentration	HBI triene concentration
2250	0.0	15.1
2251	0.0	17.2
2252	0.0	3.2
2253	0.0	22.2
2254	0.0	6.8
2255	0.0	16.0
2256	0.0	18.7
2257	0.0	15.9
2258	0.0	15.9
2259	0.0	28.6
2260	0.0	4.2
2261	0.0	16.7
2262	0.0	11.7
2263	0.0	16.2
2264	0.0	14.0
2265	0.0	9.6
2266	0.0	11.7
2267	0.0	20.8
2268	0.0	13.0
2269	0.0	12.8
2270	0.0	19.8
2271	0.0	26.1
2272	0.0	26.5
2273	0.0	8.7
2274	0.0	13.8
2275	0.0	24.5
2276	0.0	23.7
2277	0.0	24.5
2278	0.0	13.4
2279	0.0	12.5
2280	0.0	17.6
2281	0.0	13.3
2282	0.0	6.2
2283	0.0	11.3
2284	0.0	22.9
2285	0.0	8.7
2286	0.0	11.1
2287	0.0	6.7
2288	0.0	11.7
2289	0.0	7.0
2290	0.0	9.0
2291	0.0	16.6

End depth (cmbsf)	HBI diene concentration	HBI triene concentration
2292		
2293	0.0	23.1
2294	0.0	26.6
2295	0.0	24.7
2296	0.0	1.5
2297	0.0	4.1
2298	0.0	18.0
2299	0.0	14.8
2300	0.0	13.6
2301	0.0	16.3
2302	0.0	12.4
2303	0.0	3.5
2304	0.0	33.8
2305	0.0	24.2
2306	0.0	10.5
2307	0.0	9.2
2308	0.0	13.3
2309	0.0	17.3
2310	0.0	4.8
2311	0.0	21.0
2312	0.0	11.4
2313		
2314	0.0	12.2
2315	0.0	10.4
2316	0.0	8.6
2317	0.0	9.6
2318	0.0	2.8
2319	0.0	13.3
2320	0.0	11.3
2321	0.0	16.2
2322	0.0	16.7
2323	0.0	7.4
2324	0.0	10.3
2325	0.0	14.3
2326	0.0	10.4
2327	0.0	8.1
2328	0.0	12.6
2329	0.0	8.7
2330	0.0	8.7
2331	0.0	10.0
2332	0.0	15.2
2333	0.0	15.2
2334	0.0	11.3
2335	0.0	15.3

End depth (cmbsf)	HBI diene concentration	HBI triene concentration
2336	0.0	16.3
2337	0.0	22.8
2338	0.0	17.4
2339	0.0	11.4
2340	0.0	8.5
2341		
2342	0.0	13.5
2343	0.0	2.2
2344	0.0	14.2
2345	0.0	12.2
2346	0.0	10.8
2347	0.0	16.7
2348	0.0	8.9
2349		
2350	0.0	4.8
2351	0.0	6.2
2352	0.0	7.7
2353	0.0	12.9
2354	2.0	10.1
2355	0.0	17.1
2356	0.0	14.1
2357	0.0	25.3
2358	0.0	21.0
2359	0.0	16.9
2360	0.0	12.3
2361	0.0	16.6
2362	0.0	19.6
2363	0.0	21.2
2364	0.0	19.3
2365	0.0	18.0
2366	0.0	10.7
2367	0.0	11.1
2368	0.0	13.0
2369	0.0	16.5
2370	0.0	12.2
2371	0.0	8.6
2372	0.0	6.0
2373	0.0	9.0
2374	0.0	10.6
2375	0.0	2.0
2376		
2377	0.0	9.0
2378	0.0	12.5
2379	0.0	19.9

End depth (cmbsf)	HBI diene concentration	HBI triene concentration
2380	0.0	12.2
2381	0.0	10.6
2382	0.0	13.4
2383		
2384	0.0	20.0
2385	0.0	18.7
2386	0.0	22.1
2387	0.0	12.9
2388	0.0	14.0
2389	0.0	17.9
2390	0.0	3.5
2391	0.0	8.2
2392	0.0	10.5
2393	0.0	10.7
2394	0.0	13.5
2395	19.1	2.1
2396	7.6	10.0

A5.2 Lamina scale HBI data

Table A5.04. HBI diene and triene relative abdundances in lamina targeted samples from MD03-2601 core section III. Corresponding lamina types are indicated in Figure A5.01 to Figure A5.03.

Start depth (cmbsf)	End depth (cmbsf)	HBI diene concentration	HBI triene concentration
346.4	344.4	0.1	2.9
348.4	346.4	0.1	2.9
349.4	348.4	0.8	13.7
350	349.4	0.6	14.4
352.2	350	0.5	11.3
352.5	352.2	0.4	6.4
353.5	352.5	0.4	8.2
354.5	353.5	1.3	17.8
355.5	354.5	0.8	9.4
356.5	355.5	0.8	8.7
357	356.5	1.0	7.9
358	357	0.9	6.6
382.5	380	0.4	6.1
384	382.5	0.5	8.0
384.5	384	0.3	5.4
385.5	384.5	0.7	9.8
386	385.5	0.4	5.9
386.5	386	0.2	11.4
387.5	386.5	0.2	6.8
393.5	392	1.4	16.9
394	393.5	0.9	4.8
394.5	394	2.7	8.5
395	394.5	1.7	6.7
395.5	395	0.9	9.8
396.5	395.5	0.6	7.3
397.5	396.5	0.8	7.8
398	397.5	1.2	10.7
399.5	398	0.6	5.0
400	399.5	1.5	10.8
400.5	400	1.8	6.8
401	400.5	0.8	9.2
402	401	0.9	11.4

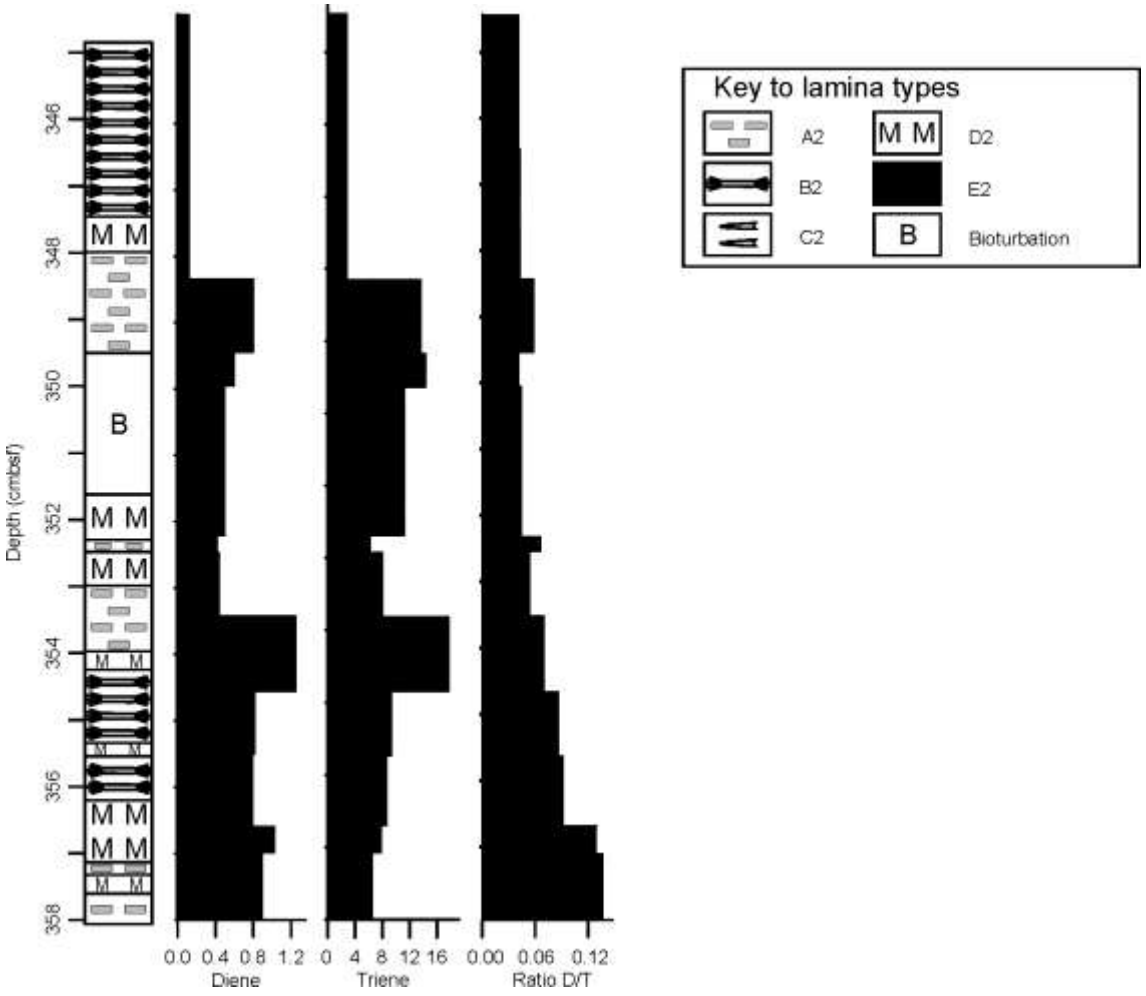

Figure A5.01. HBI diene and triene relative abundances and the ratio D/T between 345 and 358 cm, compared to lamina distribution.

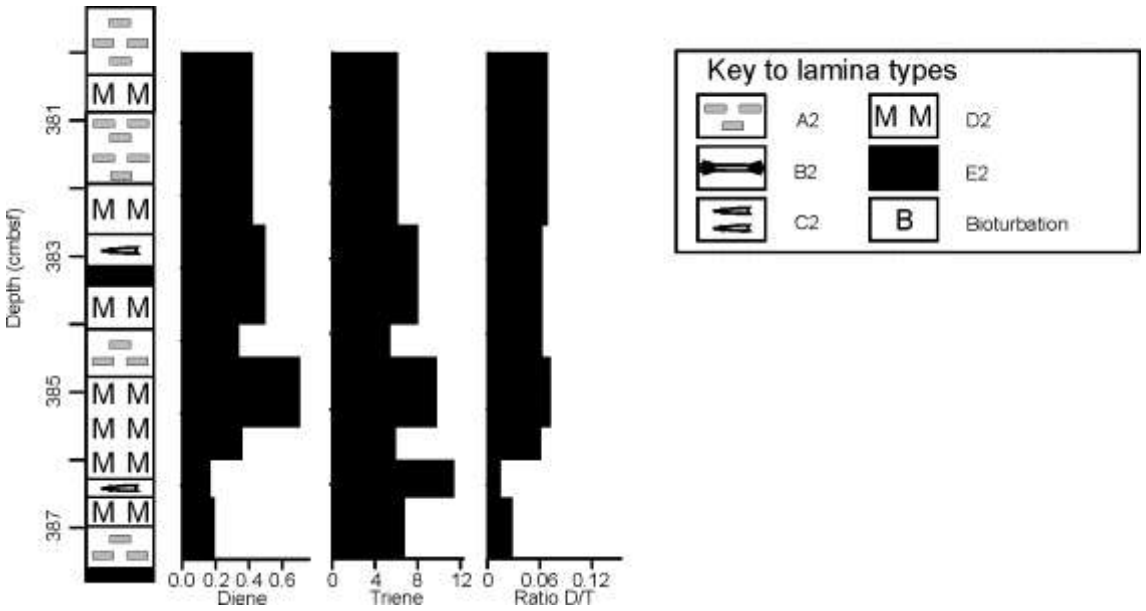

Figure A5.02. HBI diene and triene relative abundances and the ratio D/T between 380 and 387.5 cm, compared to lamina distribution.

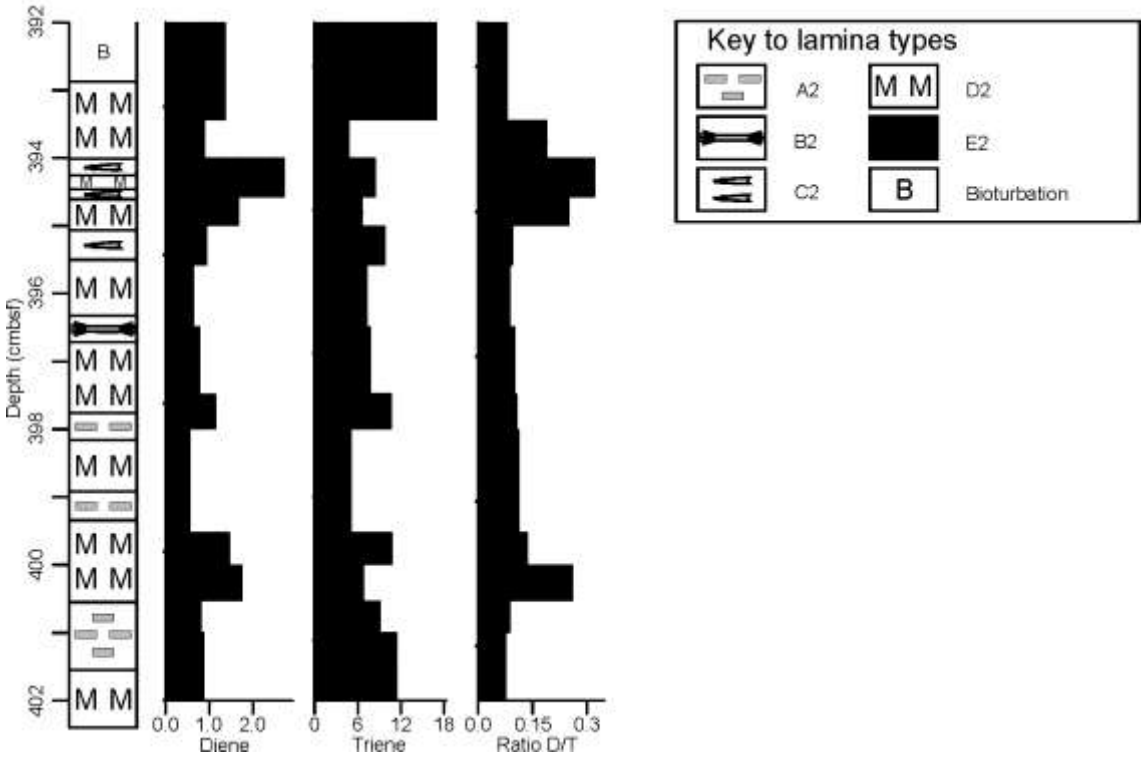

Figure A5.03. HBI diene and triene relative abundances and the ratio D/T between 392 and 402 cm, compared to lamina distribution.

Table A5.05. HBI diene and triene relative abdundances in lamina targeted samples from MD03-2601 core section VIII. Corresponding lamina types are indicated in Figure A5.04 to Figure A5.07.

Start depth (cmbsf)	End depth (cmbsf)	HBI diene concentration	HBI triene concentration
1068.2	1067.7	0.2	4.3
1069.7	1068.2	0.2	4.9
1070	1069.7	0.2	3.8
1071	1070	0.6	5.5
1072	1071	0.3	4.2
1073	1072	1.2	3.9
1075	1073	0.2	4.2
1077	1075	0.2	3.6
1078.7	1077	0.1	6.8
1079.7	1078.7	0.1	6.7
1080	1079.7	0.3	8.9
1081	1080	0.2	6.2
1081.5	1081	0.7	19.8
1082	1081.5	0.1	3.4
1083	1082	0.6	4.6
1084	1083	1.9	6.7
1085	1084	0.2	4.9
1086	1085	0.65	6.8
1087	1086	0.1	1.7
1111.5	1110.8	0	7.8
1111.8	1111.5	0	10.1
1113.3	1111.8	0.1	2.9
1114.8	1113.3	0.1	6.113733
1116.5	1114.8	<0.1	3.0
1117.2	1116.5	0	7.3
1118.2	1117.2	0	6.4
1119	1118.2	1.0	6.2
1120	1119	0	4.8
1129.5	1128.5	0	5.3
1131	1129.5	0.1	4.5
1133.5	1131	0.2	4.0
1135	1133.5	0.1	3.5
1136.5	1135	0.069467	3.0
1137.5	1136.5	0	5.5
1138	1137.5	0	3.2
1139	1138	0	8.7
1140	1139	0	11.8
1141	1140	0.2	14.1
1186.9	1184.9	0	2.5
1188.9	1186.9	0.1	5.7
1189.1	1188.9	<0.1	5.3

Start depth (cmbsf)	End depth (cmbsf)	HBI diene concentration	HBI triene concentration
1190.9	1189.1	0.1	4.8
1192.9	1190.9	0.1	5.8
1194.9	1192.9	0.1	7.5
1195.3	1194.9	0	3.2
1196.3	1195.3	0.1	9.0

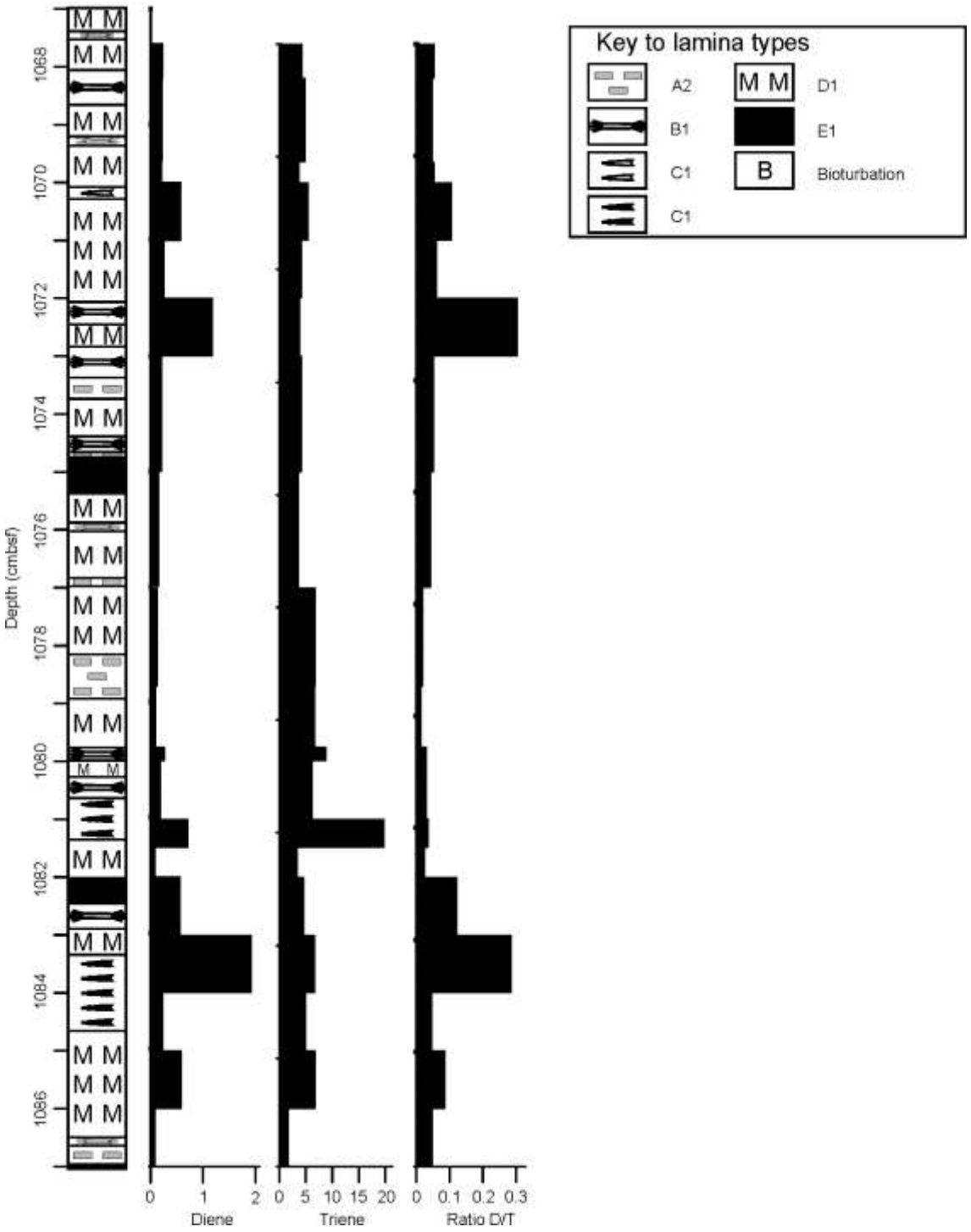

Figure A5.04. HBI diene and triene relative abundances and the ratio D/T between 1067 and 1085 cm, compared to lamina distribution.

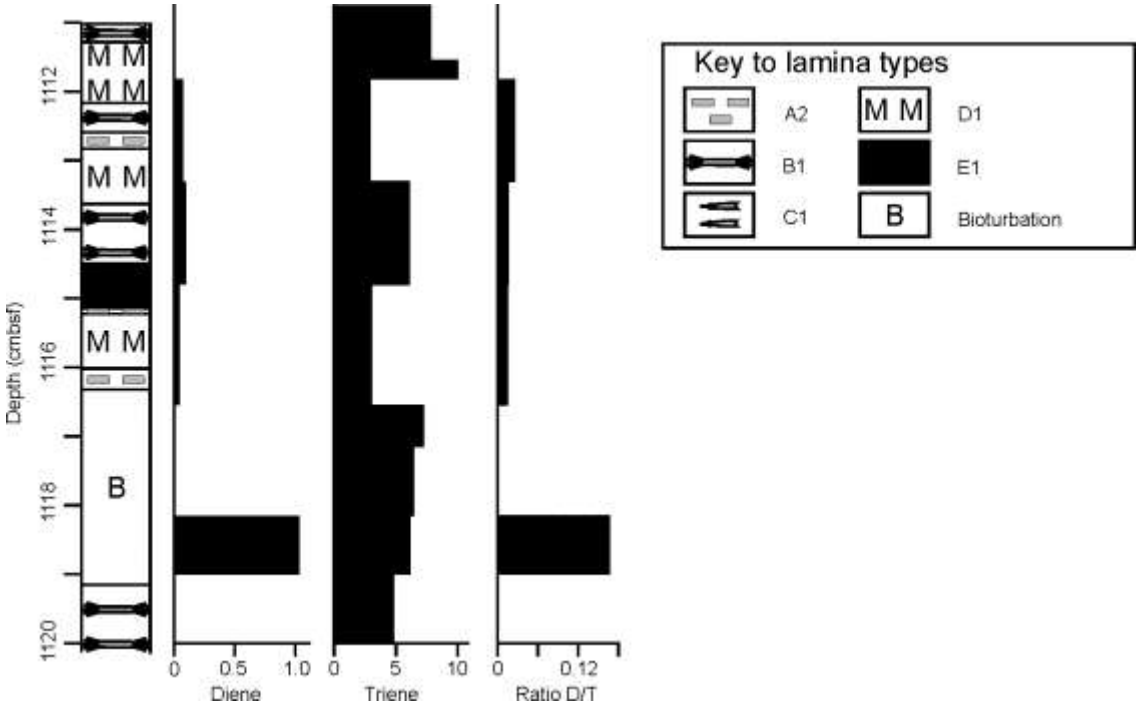

Figure A5.05. HBI diene and triene relative abundances and the ratio D/T between 1111 and 1120 cm, compared to lamina distribution.

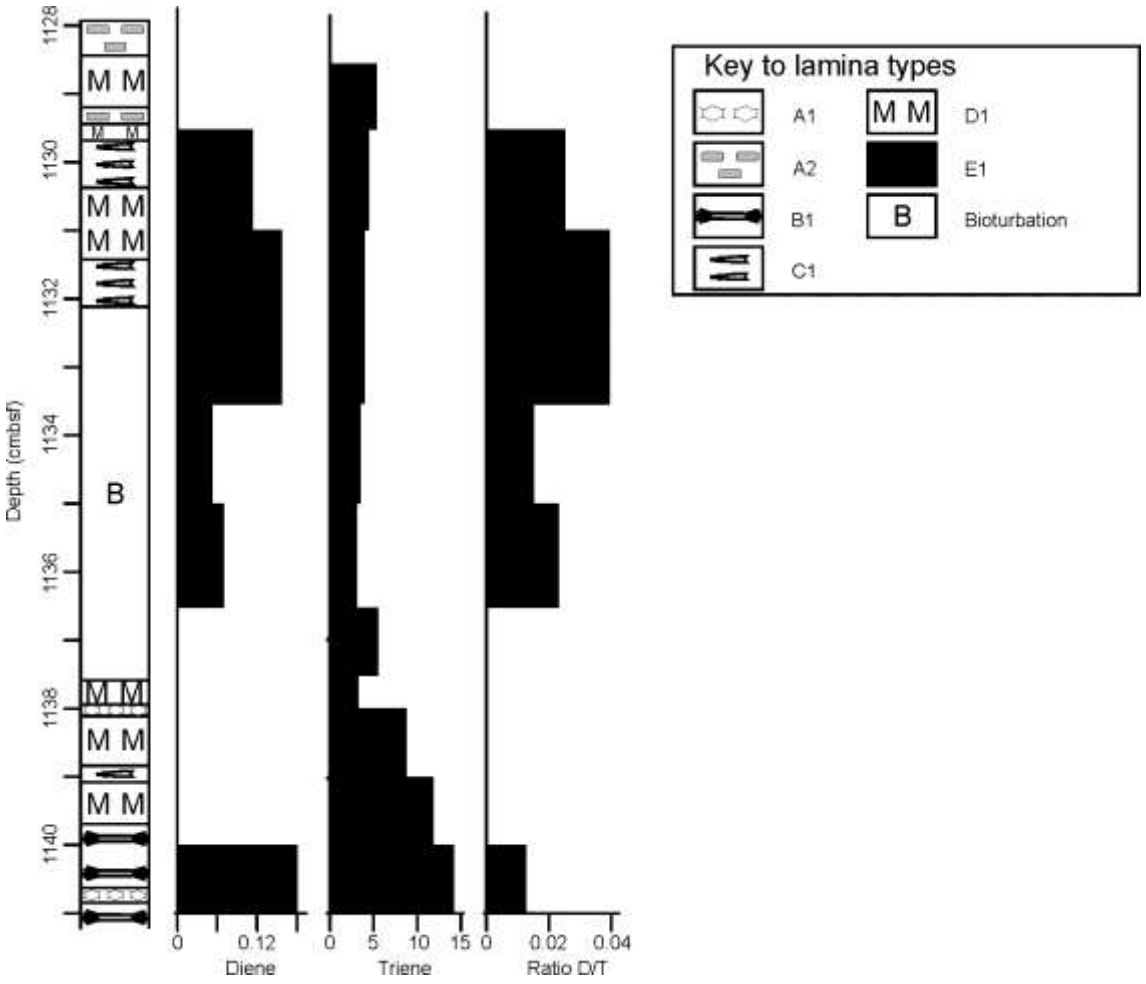

Figure A5.06. HBI diene and triene relative abundances and the ratio D/T between 1128 and 1141 cm, compared to lamina distribution.

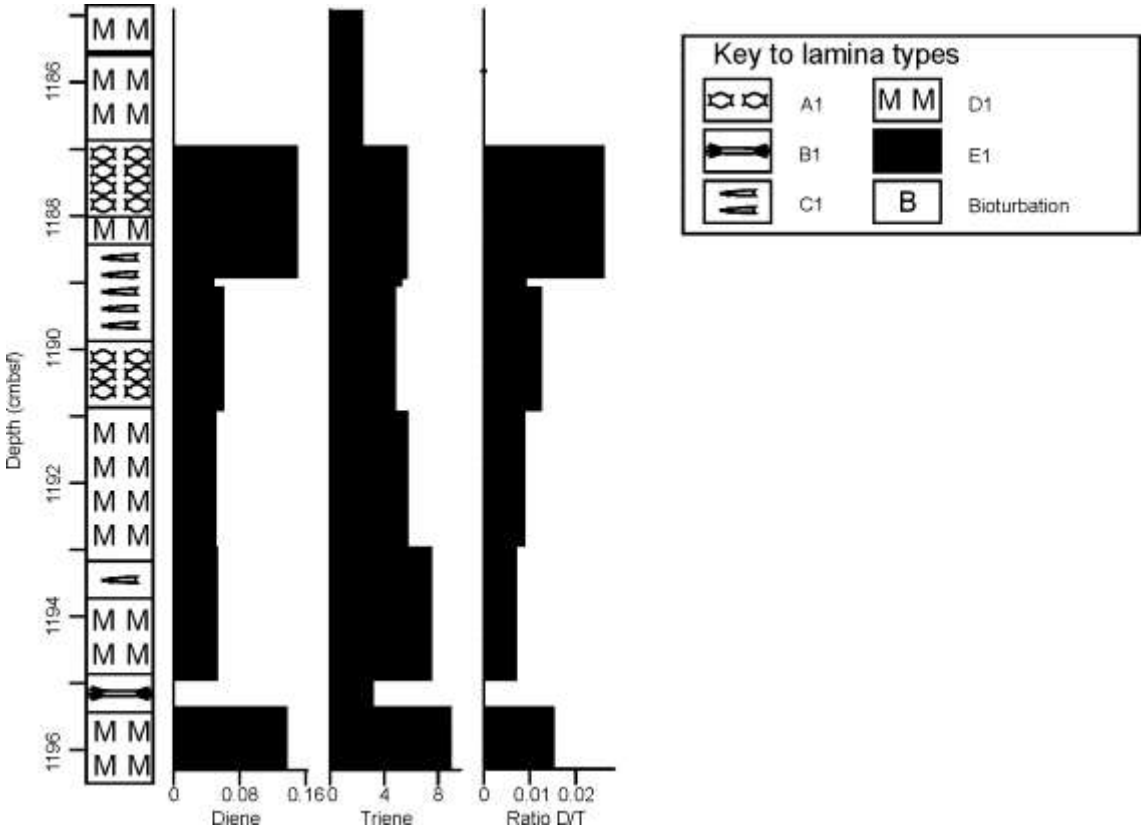

Figure A5.07. HBI diene and triene relative abundances and the ratio D/T between 1185 and 1196 cm, compared to lamina distribution.

Table A5.06. HBI diene and triene relative abdundances in lamina targeted samples from MD03-2601 core section VIII. Corresponding lamina types are indicated in Figure A5.08 to Figure A5.13.

Start depth (cmbsf)	End depth (cmbsf)	HBI diene concentration	HBI triene concentration
2279	2278	0.0	3.1
2280	2279	0.0	3.9
2281	2280	0.0	1.4
2282	2281	0.0	2.9
2283	2282	0.1	2.4
2306	2305.5	0.0	3.0
2306b	2306	0.0	2.0
2308	2306.5	0.0	2.9
2308.5	2308	0.0	0.4
2340	2339	0.1	0.2
2340.5	2340b	0.0	0.7
2341	2340.5	0.0	0.9
2341.5	2341	0.0	4.5
2347	2346.5	0.1	0.0
2348	2347	0.1	1.2
2349	2348	0.0	0.1
2350	2349	0.0	0.4
2353.5	2353	0.0	0.2
2354	2353.5	0.0	1.0
2354.5	2354	0.0	1.6
2355	2354.5	0.0	0.1
2355.5	2355	0.0	0.8
2385	2384.5	0.0	1.0
2385.5	2385	0.0	5.1
2386	2385.5	0.0	3.6
2386.5	2386	0.0	2.9
2387	2386.5	0.0	0.8
2387.5	2387	0.0	2.4
2388	2387.5	0.1	1.3
2398	2388	0.0	1.2
2399	2398	0.1	0.9

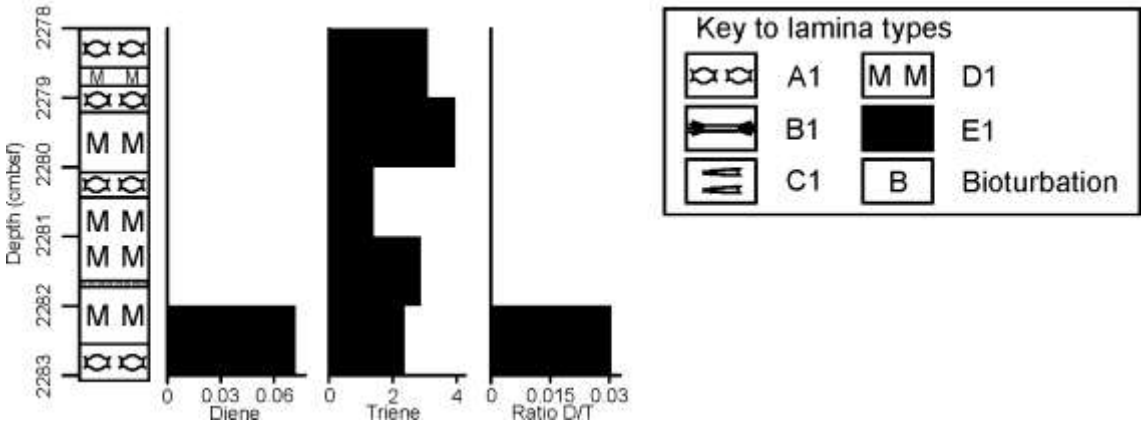

Figure A5.08. HBI diene and triene relative abundances and the ratio D/T between 2278 and 2283 cm, compared to lamina distribution.

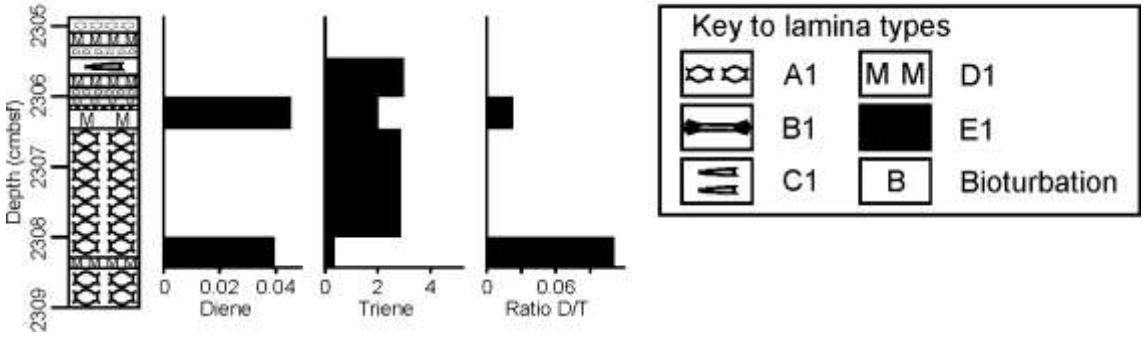

Figure A5.09. HBI diene and triene relative abundances and the ratio D/T between 2306 and 2309 cm, compared to lamina distribution.

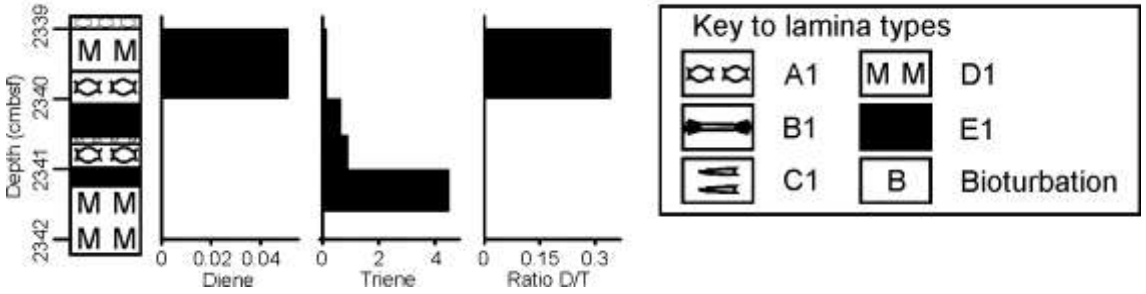

Figure A5.10. HBI diene and triene relative abundances and the ratio D/T between 2339 and 2342 cm, compared to lamina distribution.

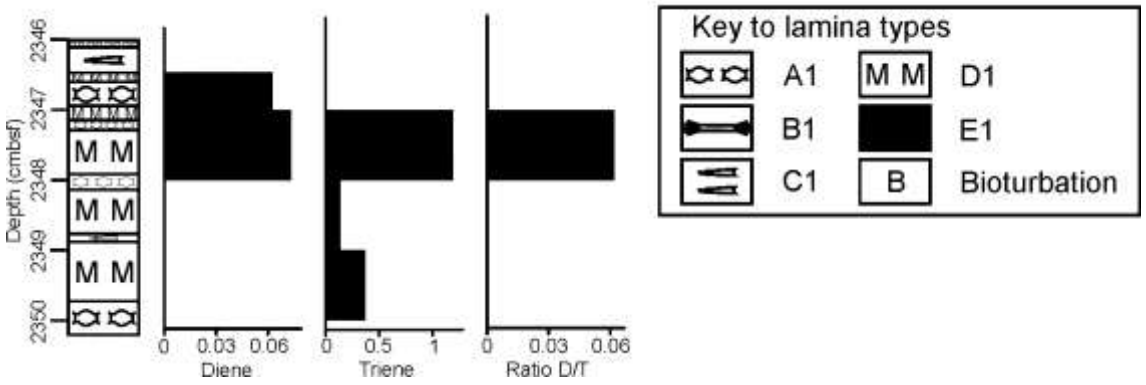

Figure A5.11. HBI diene and triene relative abundances and the ratio D/T between 2346 and 2350 cm, compared to lamina distribution.

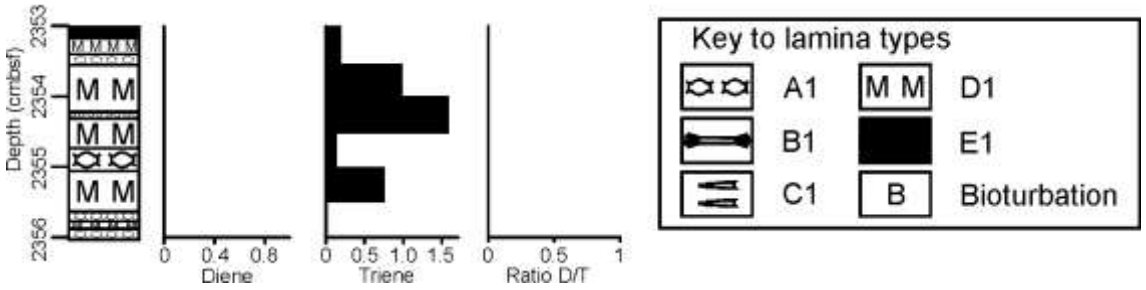

Figure A5.12. HBI diene and triene relative abundances and the ratio D/T between 2353 and 2356 cm, compared to lamina distribution.

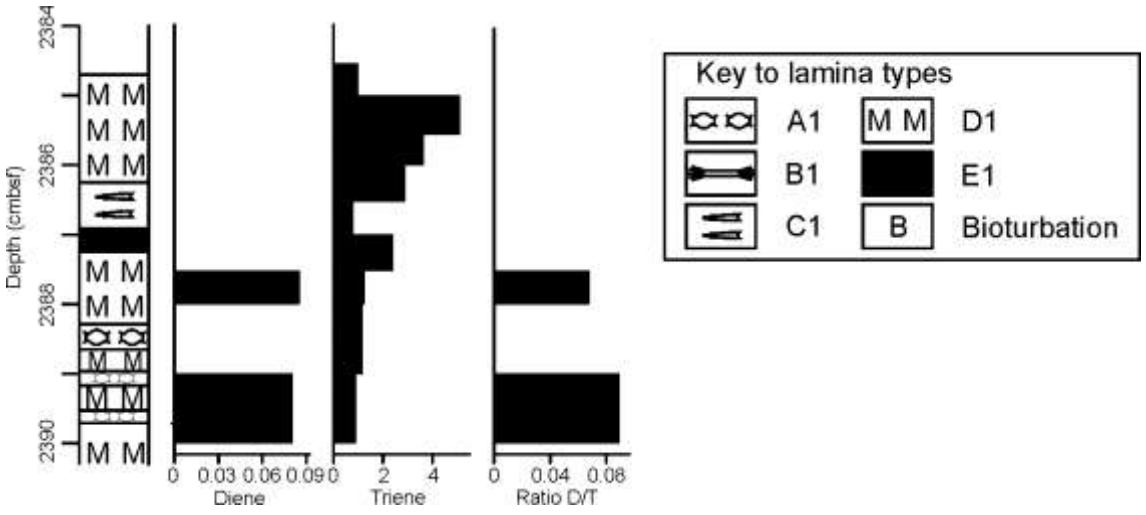

Figure A5.13. HBI diene and triene relative abundances and the ratio D/T between 2384 and 2390 cm, compared to lamina distribution.

A5.3 Lamina versus HBI offset data

As the laminae in core MD03-2601 are not horizontally aligned an offset exists between the depth below sea floor at which the lamina thicknesses have been measured and the depth at which corresponding HBI samples were taken for the continuously sampled data presented in Chapter 6 (Figure A5.14). To compensate for this, a mean of ten measurements (Table A5.07) of the offset between the mean sampling track for thin section sampling and the mean sampling track for HBI sampling was taken for each core section. This difference was then added to the sample depth before plotting the graphic logs in Chapter 6.

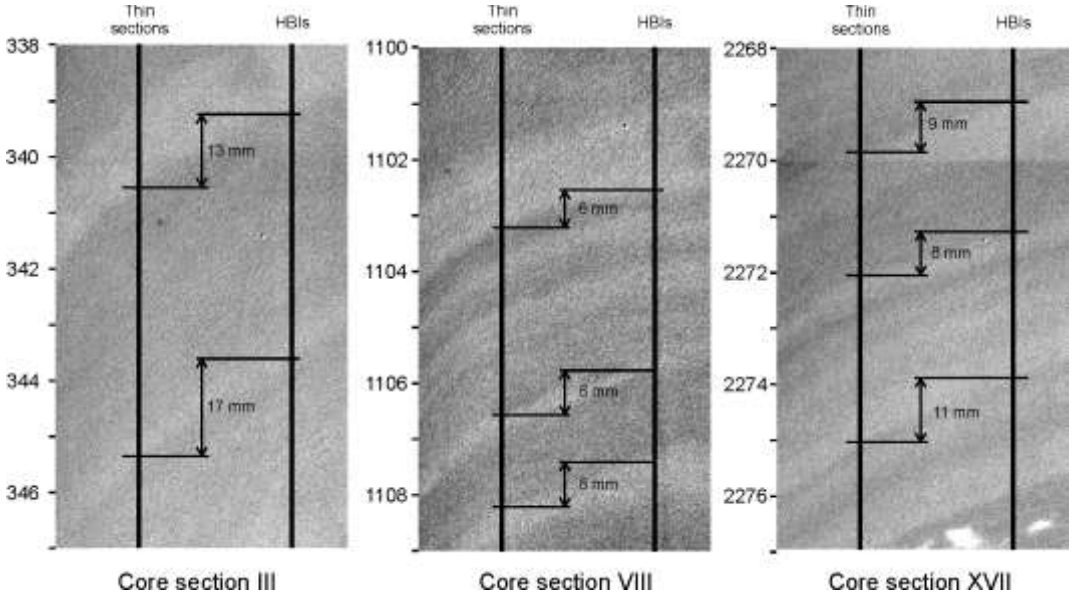

Figure A5.14. Examples of how offsets between the mean sampling track for HBI analysis and mean sampling track for thin section production were calculated from positive X-ray images of core MD03-2601.

Table A5.07. Measured offsets between laminae and HBI samples.

	Section III	Section VIII	Section XVII
Measured offset (mm)	13	6	9
	17	8	8
	13	8	11
	18	10	9
	17	11	12
	23	8	10
	18	9	7
	5	10	8
	24	11	10
	16	8	8
Mean (mm)	**16.4**	**8.9**	**9.2**